Inhibitors of the Plasminogen/Plasmin system for the treatment of Traumatic Brain Injury

Oriol Bosch Sanz

http://hdl.handle.net/10803/688137

Data de defensa: 19-04-2023

DOCTORAL THESIS

Title	Inhibitors of the Plasminogen/Plasmin system for the treatment of Traumatic Brain Injury
Presented by	Oriol Bosch Sanz
Centre	IQS School of Engineering
Department	Bioengineering
Directed by	Dra. Mercedes Balcells Camps Dr. David Sánchez García

Acknowledgements

A la Dra. Mercedes Balcells, per ser la meva guia i mentora tot aquest temps que hem treballant junts, ja durant el màster i ara a la tesi doctoral. Amb l'energia i determinació que demostres a diari m'has ensenyat a no rendir-me per gran que sigui el repte. Gràcies per tot, Merche.

Al Dr. David Sanchez, per ser part fonamental d'aquesta tesi. No tan sols per tot el que m'has ensenyat al laboratori, sinó per ser-hi present en els bons i els mals moments. Sense tu, aquesta tesi no hauria tirat endavant.

Al Dr. Jordi Martorell, per ser una font de suport constant durant tot el procés i saber guiar-me tant a nivell científic com personal. Tot i no ser oficial, per mi ets el tercer director d'aquesta tesi.

Al Dr. Xevi Biarnés, per ajudar-me de forma imprescindible en tota la feina computacional, i per estar sempre disponible davant qualsevol dubte.

Al Dr. Javier Pedreño, por dar comienzo a este proyecto y transmitirme la pasión para embarcarme en él. Gracias también por todos los conocimientos y consejos que me has dado.

To Prof. Elazer Edelman, for opening the doors of your lab and giving me countless resources to do my research. I will always cherish this amazing opportunity that has been granted to me.

To all the people at the Edelman Lab, it was a joy to be there for the last period of my thesis. Thank you for making my experience better by your presence, and I hope we can meet again someday.

A la gent de Supra: Iris, Andrea, Marta, Gabi. Hem compartit espai de treball durant molt de temps, alguns més que altres. Gràcies per ser sempre una font de suport. Se us trobarà a faltar.

A la Ivet, gràcies per la teva predisposició i la feina tan ben feta. Vas ser un exemple de saber-se adaptar i aprendre ràpidament. Ha sigut un plaer treballar junts.

A la gent d'Aortyx, amb la qual hem compartit tant. Àlex, Noe, Pau, Carlota, Paquito, Juan, Laura, Germán, i tota la resta de l'equip. Gràcies per tots els bons moments compartits, tant dins com fora d'IQS. Heu fet que tota aquesta etapa sembli més curta del que realment ha sigut. Espero que ara que s'acaba no ens distanciem, i ens seguim veient habitualment.

A Brigada, sou els millors amics que una persona podria desitjar. Moltes gràcies per fer la meva vida millor amb la vostra presència, per alegrar-me els bons i els mals moments. Sou amics per tota la vida, i no us canviaria per res.

A la meva família, gràcies infinites per ser el meu suport en tot moment, per aguantar-me quan estava estressat, per entendre que no volgués parlar de la tesi gairebé mai. En definitiva, gràcies per transmetre'm sempre la calma que necessitava per tal de portar aquest projecte a bon port. Bé, gràcies per això i per les mil i una coses que feu a diari i que heu fet sempre per mi.

Y finalmente a ti, Ainhoa, por impulsarme cada día a intentar ser un poquito mejor y a no conformarme. Lo mejor que me ha pasado en esta etapa ha sido conocerte. Ahora empieza una etapa nueva en mi vida, y no puedo más que ilusionarme por saber que la voy a vivir contigo.

Abstract

Plasmin is a proteolytic enzyme responsible for the degradation of fibrin, the structural protein of blood clots. It is activated from the zymogen plasminogen by tissue plasminogen activator (tPA). The degradation of fibrin, or fibrinolysis, is a natural process which constitutes a control mechanism for hemostasis and helps to ensure blood fluidity. However, there are situations in which the fibrinolytic system is dysregulated, which can result into excessive blood loss and other complications. During traumatic brain injury (TBI), an excessive activation of plasmin has been linked to an increased permeability of the blood-brain barrier (BBB). The inhibition of plasmin or plasmin activation is therefore an interesting strategy to minimize the damage to the BBB under these hyperfibrinolytic conditions during TBI.

A novel compound named LTI-6 with high antifibrinolytic activity was discovered in collaboration with the start-up company Alxerion Biotech. This compound combined a piperidine, a 1,2,3-triazole and a 1,3,4-oxadiazolone ring. Blood and plasma assays confirmed its antifibrinolytic activity, with an equivalent potency to the gold standard tranexamic acid (TXA). After studying affinity towards different possible targets, the proposed mechanism of action for LTI-6 is an interaction with the lysine binding sites of plasminogen, hindering its activation into plasmin.

After proposing different chemical modifications, a total of ten new compounds were synthesized and studied both *in vitro* and *in silico*. Substitution of the piperidine for linear amines hindered the overall activity. In contrast, substituting the 1,3,4-oxadiazolone for a 1,2,4-oxadiazole improved the activity due to a higher number of H-bonds. In addition, modifying the 1,2,3-triazole for a 1,2,4-triazole provided molecules with no detectable activity.

The compounds with higher antifibrinolytic activity were studied in a hyperfibrinolytic BBB *in vitro* model. High concentrations of plasminogen and tPA caused an increased permeability, as well as a reduction of tight junction protein expression. The presence of the new compounds proved to have a protective effect, partially reducing the damage to the BBB.

This work opens the door to develop future drugs based on these 1,2,3-triazole derivatives for two purposes: as a novel antifibrinolytic agent to substitute TXA, and as a potential BBB protective agent during TBI.

Resumen

La plasmina es una encima proteolítica responsable de la degradación de la fibrina, la proteína estructural de los coágulos sanguíneos. Es activada a partir del zimógeno plasminógeno por el activador de tisular del plasminógeno (tPA). La degradación de fibrina, o fibrinolisis, es un proceso natural que actúa como mecanismo de control para la hemostasis y ayuda a mantener la adecuada fluidez de la sangre. Sin embargo, hay situaciones en que la fibrinolisis se ve alterada, lo que puede resultar en excesivo sangrado y otras complicaciones. Durante un traumatismo cerebral, se puede producir una excesiva activación de plasmina que está correlacionada con un incremento en la permeabilidad de la barrera hematoencefálica (BHE). La inhibición de la plasmina o de su activación es en consecuencia una estrategia interesante para minimizar los daños a la BHE bajo dichas condiciones hiperfibrinolíticas.

Un nuevo compuesto llamado LTI-6 con alta actividad antifibrinolítica fue descubierto en colaboración con la empresa Alxerion Biotech. Este compuesto combina una piperidina, un 1,2,3-triazol y una 1,3,4-oxadiazolona. Ensayos en sangre y en plasma confirmaron su actividad antifibrinolítica, con una potencia equivalente al ácido tranexámico (TXA). Tras estudiar su afinidad hacia posibles receptores biológicos, el mecanismo de acción propuesto para LTI-6 es la interacción con los centros de unión a lisina presentes en el plasminógeno.

Tras propuesta de varias modificaciones estructurales, un total de diez nuevos compuestos fueron sintetizados i estudiados tanto *in vitro* como *in silico*. Sustituir la piperidina por aminas lineales disminuyó la actividad global. Por el contrario, la sustitución de la 1,3,4-oxadiazolona por 1,2,4-oxadiazolona mejoró la actividad debido a un mayor número de puentes de hidrógeno. Además, modificar el 1,2,3-triazol por un 1,2,4-triazol generó moléculas sin actividad detectable.

Los compuestos con mayor actividad antifibrinolítica fueron estudiados en un modelo in vitro de BHE bajo condiciones hiperfibrinolíticas. Concentraciones elevadas de plasminógeno y tPA incrementaron la permeabilidad, además de reducir la expresión de proteínas de unión estrecha. La presencia de los nuevos compuestos demostró tener un efecto protector, ya que amortiguó parcialmente el daño a la BHE.

Este trabajo abre la puerta a desarrollar futuros fármacos basados en estos derivados de 1,2,3-triazol para dos aplicaciones: como nuevo compuesto antifibrinolítico que sustituta al TXA, y como agente protector de la BHE durante un traumatismo cerebral.

Resum

La plasmina és un enzim proteolític responsable de la degradació de la fibrina, la proteïna estructural dels coàguls sanguinis. És activada a partir del zimogen plasminogen per l'activador tissular del plasminogen (tPA). La degradació de fibrina, o fibrinòlisi, és un procés natural que actua com a mecanisme de control per la hemostàsia i ajuda a mantenir la adequada fluïdesa de la sang. No obstant, hi ha situacions en que la fibrinòlisi es veu afectada, el que pot resultar en un sagnat excessiu, a més d'altres complicacions. Durant un traumatisme cerebral, es pot produir una activació excessiva de plasmina, que està correlacionada amb un increment en la permeabilitat de la barrera Hematoencefàlica (BHE). La inhibició de la plasmina o de la seva activació és per tant una estratègia interessant per minimitzar els danys a la BHE sota aquestes condicions hiperfibrinolítiques.

Un nou compost anomenat LTI-6 amb elevada activitat antifibrinolítica va ser descobert en col·laboració amb l'empresa Alxerion Biotech. Aquest compost combina una piperidina, un 1,2,3-triazol i una 1,3,4-oxadiazolona. Els assaigs en sang i plasma van confirmar la seva activitat antifibrinolítica, amb una potència equivalent a l'àcid tranexàmic (TXA). Després d'estudiar la seva afinitat envers possibles receptors biològics, el mecanisme d'acció proposat per LTI-6 és la interacció amb els centres d'unió a lisina presents al plasminogen.

Després de proposar diverses modificacions estructurals, un total de deu nous compostos vas ser sintetitzats i estudiats tant *in vitro* com *in silico*. La substitució de piperidina per amines lineals va reduir l'activitat global de la molècula. Per contra, substituir la 1,3,4-oxadiazolona per una 1,2,4-oxadiazolona va millorar l'activitat degut a un major nombre de ponts d'hidrogen. A més, modificar el 1,2,3-triazol per un 1,2,4-triazol va produir molècules sense activitat mesurable.

Els compostos amb major activitat antifibrinolítica van ser estudiats en un model *in vitro* de la BHE sota condicions hiperfibrinolítiques. Concentracions elevades de plasminogen i tPA van incrementar la permeabilitat, a més de reduir l'expressió de proteïnes d'unió estreta. La presència dels nous compostos va demostrar tenir un efecte protector, ja que va esmorteir parcialment el dany sobre la BHE.

Aquest treball obra la porta a desenvolupar futurs fàrmacs basats en aquests derivats de 1,2,3-triazol per a dues possibles aplicacions: com a nou fàrmac antifibrinolític que substitueixi al TXA, i com a agent protector de la BHE durant un traumatisme cerebral.

Table of content

List of abbreviations

^{13}C-NMR	Carbon nuclear magnetic resonance	MeOH	Methanol
^{1}H-NMR	Proton nuclear magnetic resonance	MsCl	Methanesulfonyl chloride
A2AP	α2-antiplasmin	PAI	Plasminogen activator inhibitor
ACN	Acetonitrile	PAN	Plasminogen-apple-nematode
ACT	Acute traumatic coagulopathy	PBS	Phosphate buffer saline
BBB	Blood-brain barrier	PFA	Paraformaldehyde
Boc	*tert*-butyloxycarbonyl	Plg	Plasminogen
BSA	Bovine serum albumin	Plm	Plasmin
$CDCl_3$	Deuterated chloroform	SAR	Structure-activity relationship
CDI	Carbonyldiimidazole	sc-tPA	Single chain tPA
CNS	Central nervous system	SP	Serine protease
d_6-DMSO	Deuterated dimethyl sulfoxide	TAFI	Thrombin-activatable fibrinolysis inhibitor

DAPI	4′,6-diamidino-2-phenylindole	TBI	Traumatic brain injury
DBU	1,8-diazabicyclo(5.4.0)undec-7-ene	tc-tPA	Two chain tPA
DCM	Dichloromethane	TEA	Triethylamine
DMF	Dimethylformamide	TF	Tissue factor
EACA	ε-aminocaproic acid	TFAA	Trifluoroacetic acid anhydride
EtOH	Ethanol	THF	Tetrahydrofuran
FDP	Fibrin degradation products	TJ	Tight junctions
Fn	Fibronectin	tPA	Tissue plasminogen activator
GABA	γ-aminobutyric acid	TsCl	4-toluenesulfonyl chloride
$GABA_A$	γ-aminobutyric acid A receptor	TXA	Tranexamic acid
HBMEC	Human brain microvascular endothelial cells	uPA	Urokinase plasminogen activator
K	Kringle	uPAR	uPA receptor
LBS	Lysine binding site		

List of Figures, Schemes and Tables

Figures

Schemes

Tables

Funding

This project was made possible by the funding from the following sources:

- IQS School of Engineering: IQS PhD Scholarship.
- MIT Science and Technology Initiatives: MISTI-Spain grant.
- Ministerio de economía, industria y competitividad: Grant SAF2017-84773-C2-1-R.
- La Caixa Foundation: Health Research Call 2019, "Network of leaders in medicine, science, Technology and entrepreneurs, who work with communities on local heatlh problems with global impact potential".

1.Introduction

1.1. Coagulation and fibrinolysis

Hemostasis is the natural ability of the human body to stop a hemorrhage and prevent major blood loss after a vascular injury[1]. The process is therefore initiated by an injury in the endothelial wall of a blood vessel. Platelets are then activated upon contact with subendothelial matrix proteins, including collagen, von Willebrand factor, and fibronectin[2]. This enables the formation of a cellular plug at the site of injury, constituting what is known as primary hemostasis[3]. Platelet activation also leads to the exposure of cell surface anionic phospholipids, which serve as a nidus for the assembly of procoagulant proteins[3].

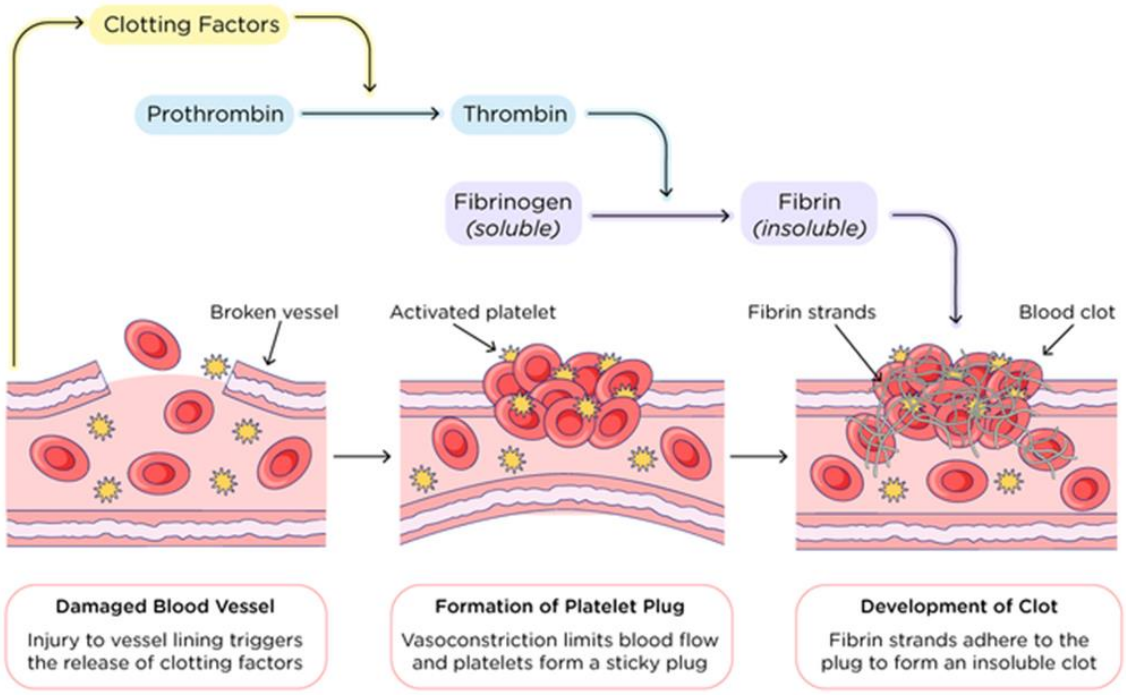

Figure 1. General representation of the main steps of clot formation. Vascular injury initiates the process. Platelets are then activated and form a cellular plug at the site of injury. Finally, the coagulation cascade results in the formation of a fibrin mesh which brings structural stability to the thrombus.[4]

Secondary hemostasis, which occurs in parallel, includes the two major coagulation pathways: extrinsic and intrinsic. The extrinsic pathway is initiated by tissue factor (TF) released by the damaged endothelial cells, as well as the underlying smooth muscle cells. TF then proteolytically cleaves a zymogen form of factor VII and activates it[1,3,5]. The intrinsic pathway is initiated by the activation of factor XII after exposure to sub-endothelial collagen[5–7]. Both pathways initiate a cascade in which different clotting factors are activated by a previously activated clotting factor[5]. These factors, most of which are serine proteases, circulate through the blood stream as inactive zymogens until activated[8]. Both cascades, extrinsic and intrinsic, end in a common pathway that ultimately cleaves fibrinogen into fibrin, which then polymerizes into an insoluble fibrin polymer mesh[9]. This fibrin mesh constitutes the structural base of the blood clot and ensures the stability of the initial platelet cell plug[7]. As the clot forms, circulating red blood cells, white blood cells and platelets become incorporated into the structure. Additionally, fibrin becomes further cross-linked through the action of factor XIIIa, which provides further structural stability[10].

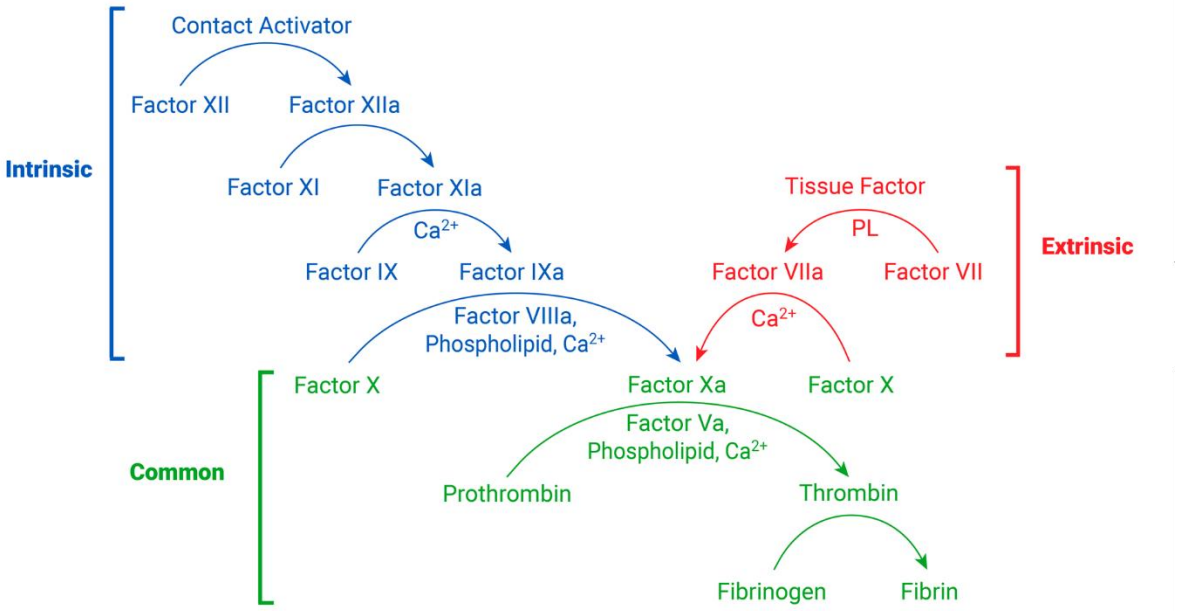

Figure 2. Secondary hemostasis. The coagulation cascade is initiated in parallel through the intrinsic and extrinsic pathways, which then converge into a common pathway. The result is the activation of fibrinogen into fibrin, which is catalyzed by thrombin.[11]

Upon healing of the injured blood vessel, the remaining clot is lysed through the action of the fibrinolytic system[12]. The degradation of fibrin is performed by plasmin (Plm), a serine protease which is activated from its inactive zymogen plasminogen (Plg). Proteolysis of fibrin gives rise to soluble fibrin degradation products (FDPs), some of which have immunomodulatory and chemotactic functions[13]. The coagulation and fibrinolytic systems are highly regulated and inter-related through mechanisms that insure balanced hemostasis. Fibrinolysis can therefore be considered a control mechanism for the hemostatic process.

1.2. The fibrinolytic system

Like the coagulation cascade, fibrinolysis is tightly controlled by a series of cofactors, inhibitors, and receptors[13]. Plasmin (Plm) is the protease able to degrade fibrin, and therefore the key enzyme in fibrinolysis. It is activated from plasminogen (Plg) by either of two primary serine proteases, tissue plasminogen activator (tPA) and urokinase plasminogen activator (uPA). Whereas tPA is synthesized and released by endothelial cells, uPA is produced by monocytes, macrophages, and urinary epithelium[14].

Plg is mainly produced in the liver, and then released into circulation as a single chain in a closed globular conformation, which is resistant to its activation. The concentration of Plg in blood is in the range of 1.1-2.2 μM[15–17]. In its mature form, it contains 791 amino acids and has a molecular weight of 90 kDa[16]. Plg consists of seven domains: an N-terminal plasminogen-apple-nematode (PAN) domain, followed by five kringle domains (K1-K5) and the C-terminal catalytic trypsin-like serine protease (SP) domain[18].

The kringle domains 1, 2, 4, and 5 in human Plg possess lysine binding sites (LBS) that enable the binding of Plg on lysine-rich target surfaces like C-terminal fibrin monomers or other proteins with accessible lysine residues[19,20]. The closed Plg conformation is stabilized by numerous interdomain contacts between the different kringle, PAN and SP domains, partially mediated by chloride ions[15]. Despite the closed Plg conformation, the K1 domain is permanently exposed, allowing the initial binding to Lys residues on target sites like fibrin. Such binding triggers the transition into an open Plg conformation, which allows the subsequent binding of K2, K4 and K5 to additional Lys residues on targets. Additionally, the conformational change exposes Plg to Plg activators such as tPA and uPA. These can then form active Plm, by cleaving Plg between amino acids Arg561 and Val562[21].

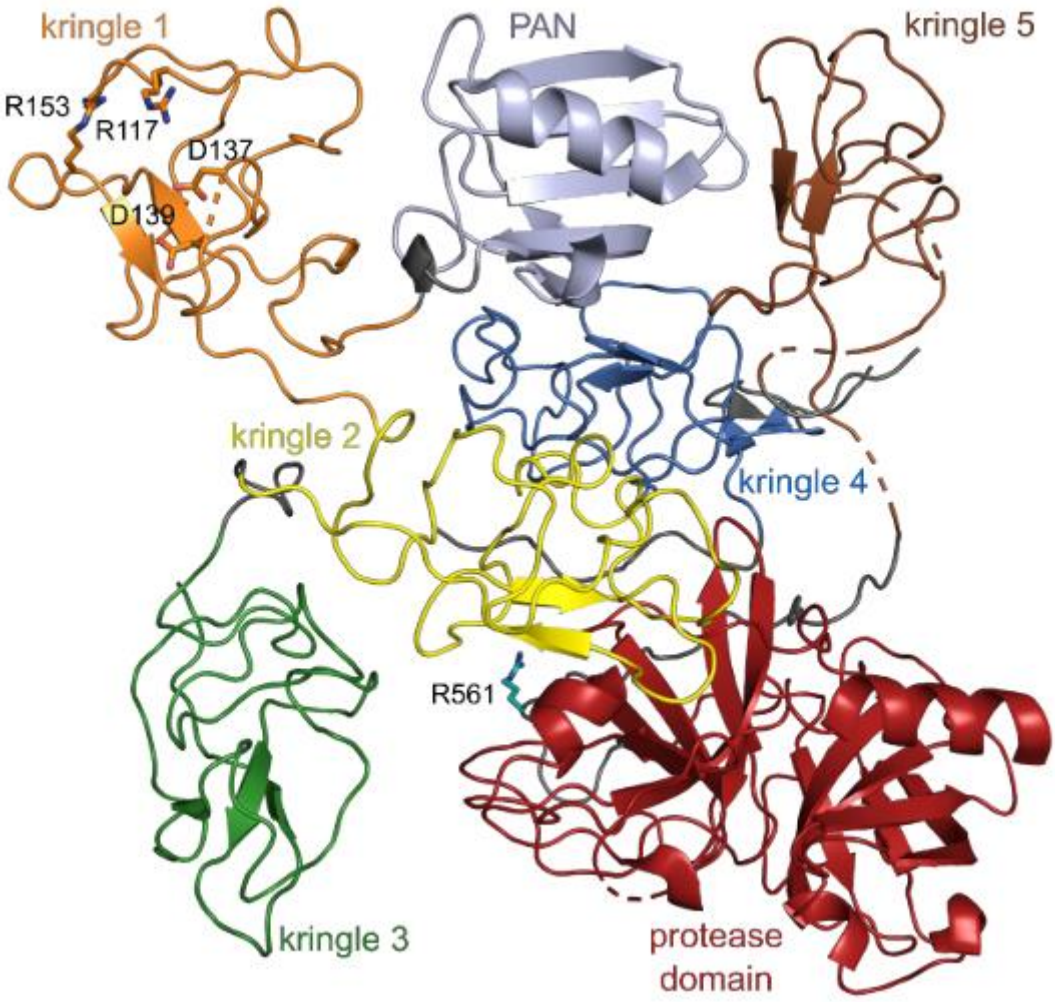

Figure 3. Structure of human type II Plg in the closed conformation (PBD: 4dur)[19]. The LBS on K1, highlighted by the illustrated Asp (R) and Arg (D) side chains of its anionic and cationic centers, is freely accessible and can bind to C-terminal lysine residues on fibrin and other targets. The bound Plg is finally activated by tPA or uPA, which cleaves the activation loop behind the highlighted Arg561 residue.[21]

Depending on the location, Plg activation can be extravascular or intravascular. Extravascular Plg is mainly activated by uPA, which binds to its specific uPA receptor (uPAR) on cell surfaces. Such interaction does not require fibrin as a cofactor[14]. This active Plm mainly contributes to cell

migration and tissue remodeling, not to fibrin clot dissolution[22]. In intravascular fibrinolysis, Plg bound to fibrin is activated by tPA. Stimulated endothelial cells release its zymogen, single-chain tPA (sc-tPA)[21]. In contrast to most other trypsin-like serine proteases, sc-tPA already has considerable proteolytic activity, especially when bound to fibrin. This enables the initial formation of Plm[23]. In a feedback mechanism, the formed Plm activates additional sc-tPA into two-chain tPA (tc-tPA), thereby contributing to the fibrinolytic process[24]. Initially the binding of tPA to fibrin is mediated by its finger domain, which occurs independently from the presence of Lys residues on fibrin[25]. During the progress of Plg activation, the degradation of fibrin exposes C-terminal Lys residues, which enables an additional binding of tPA to fibrin through its own LBS. This allows a faster Plg activation[26,27]. Overall, fibrin surfaces are key activation sites for fibrinolysis that modulate the binding of plasminogen, tPA and active plasmin. In fact, the catalytic efficiency of plasminogen activation has been found to be approximately 500-fold higher for fibrin-bound tPA than for tPA in the fluid phase[26]. Blocking this ternary complex between Plg, tPA and fibrin inhibits the formation of Plm, and therefore provides an antifibrinolytic effect.

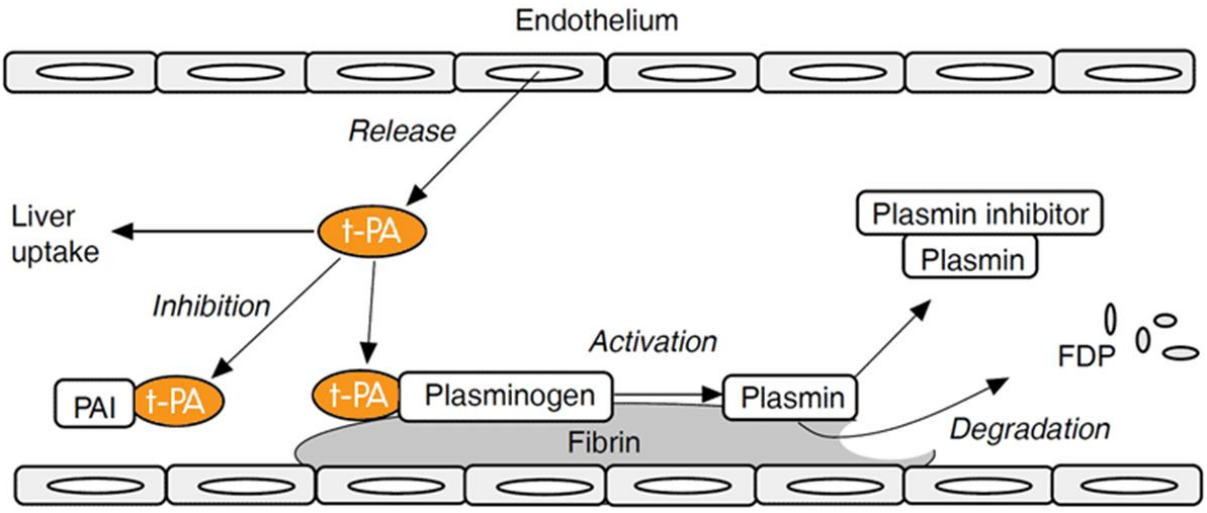

Figure 4. Representation of intravascular fibrinolysis. Plasminogen (Plg) and tissue plasminogen activator (tPA) are colocalized on the surface of fibrin, optimizing contact between them and

therefore accelerating plasmin (Plm) formation. Plm is responsible for fibrin degradation into fibrin degradation products (FDP). Further regulation of the system is provided by Plg activator inhibitor 1 (PAI-1) and plasmin inhibitor α2-antiplasmin. Free tPA, as well as complexed tPA/PAI-1, is cleared from the circulation by receptors in the liver.[28]

The activity of the fibrinolytic proteases is tightly controlled by endogenous inhibitors, which prevent the excess of unregulated plasmin or plasminogen activator activity. Circulating plasmin and plasminogen activators are neutralized by serine protease inhibitors, or serpins, which are present in excess concentrations[29]. Serpins form covalent complexes with their unique target enzymes that are subsequently cleared from the circulation. The three serpins most important in fibrinolysis are plasminogen activator inhibitor-1 (PAI-1), plasminogen activator inhibitor-2 (PAI-2), and α2-antiplasmin (A2AP)[12]. Plasmin and A2AP bind with 1:1 stoichiometry, after which both become inactive. When plasmin is bound to fibrin, however, it is protected from A2AP inhibition, allowing for fibrinolysis to proceed[30]. Similarly, the plasminogen activators tPA and uPA are rapidly inhibited by PAI-1, which is released into the circulation from endothelial cells, platelets, and other cells[31]. PAI-1 is upregulated by a large number of proinflammatory cytokines as well[13]. In pregnancy, PAI-2 is also a major tPA and uPA inhibitor, and its concentrations increase as the pregnancy progresses. Deficiencies in PAI-2 have been associated with adverse pregnancy outcomes[32,33]. Thrombin-activatable fibrinolysis inhibitor (TAFI) is a non-serpin fibrinolysis inhibitor which is activated by thrombin, plasmin, or thrombomodulin-associated thrombin. TAFI is a carboxypeptidase that removes C-terminal lysine residues from fibrin, diminishing the quantity of available plasminogen and tPA binding sites and subsequently attenuating plasmin generation and stabilizing clots[34].

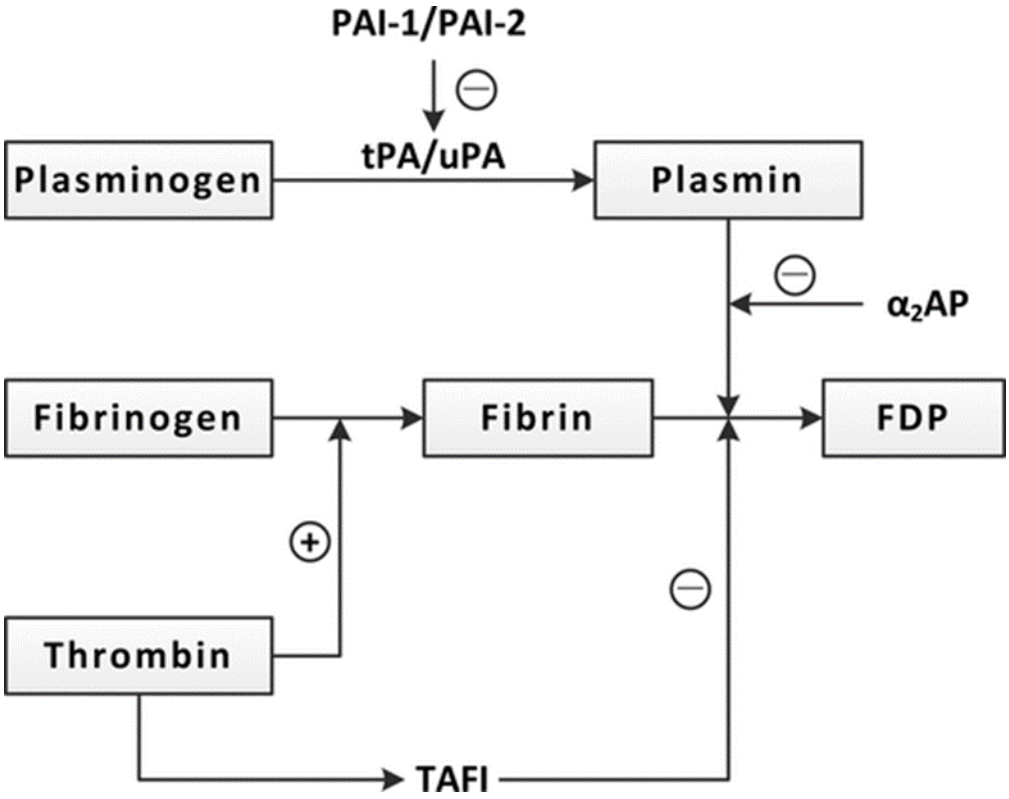

Figure 5. Schematic representation of the fibrinolytic system. Plg is activated by tPA or uPA into Plm. Plm then degrades fibrin into fibrin degradation products. PAI-1 and PAI-2 inhibit the Plg activators, while A2AP inhibits plasmin directly. TAFI, a thrombin-activated inhibitor, also inhibits fibrinolysis by reducing the availability of C-terminal lysine residues.[35]

1.3. Hyperfibrinolysis

Fibrinolysis is a necessary control mechanism to the hemostatic system which ensures the removal of excess fibrin deposits[1,12]. However, there are situations in which the fibrinolytic system is dysregulated, which can result into excessive blood loss and other complications. For example, it has been linked to heavy menstrual bleeding[36], complications during dental surgery for hemophiliac patients[37], as well as excessive post-partum hemorrhage[38]. Medical interventions, such as cardiopulmonary bypass, have been observed to cause hyperfibrinolysis; in this situation, blood contact with non-endothelial cell surfaces appears to initiate thrombin generation, which subsequently stimulates endothelial cell release of tPA, and activation of plasminogen[39–41].

1.3.1. Hyperfibrinolysis in trauma

Trauma is a leading cause of death and disability worldwide[42]. Major bleeding after traumatic events is characterized by the development of coagulopathy, or bleeding disorder[43]. Such major bleeding accounts for 40% of all trauma deaths[44], and control of bleeding is extremely challenging in the presence of an established coagulopathy. The adverse outcomes to this disordered hemostasis are not limited to acute blood loss. Organ dysfunction and multiple organ failure are also potential consequences[45].

Acute traumatic coagulopathy (ATC) is associated to a 4-fold increase in mortality for trauma patients[46,47]. Massive activation of the fibrinolytic system is known to be a common consequence of acute trauma[43]. Such hyperfibrinolytic state is thought to be a consequence of both injury and shock. Injured endothelial cells cause an increase of fibrinolytic activity through the release of tPA[48]. Additionally, trauma induced shock promotes the inhibition of plasminogen activator inhibitor-1 (PAI-1)[49,50]. In consequence, the concentration of available tPA increases dramatically and fibrinolysis becomes exacerbated. The purpose of this hyperfibrinolysis is presumably to limit

clot propagation to the site of vascular injury. With widespread trauma, however, such localization may be lost[51].

Such hyperfibrinolytic state is known to be a major contributor to major bleeding caused by ATC. Existing antifibrinolytic drugs have been proven to reduce mortality in trauma patients in clinical trials, such as the CRASH-2 trial[52,53]. Consequently, antifibrinolytic drugs such as tranexamic acid (TXA) have been adopted into trauma practice guidelines worldwide[54].

1.3.2. Hyperfibrinolysis in traumatic brain injury

1.3.2.1. The blood brain barrier

The Blood-Brain Barrier (BBB) consists of a tight network of blood capillaries in the brain that separate the circulatory system from the central nervous system (CNS). Several roles have been attributed to the BBB. One of the main functions of the BBB is the regulation of the nutrition of the brain. Specific transport systems ensure the appropriate nutrient supply providing the BBB with a low passive permeability to many essential hydrophilic metabolites and nutrients required by the CNS. The BBB also mediates the efflux of waste products from the brain to the blood and protects the brain from the entrance of neurotoxic compounds circulating in the blood. The BBB also helps to keep separate the pools of neurotransmitters and neuroactive agents from central and peripheral nervous systems, allowing their use in both systems independently. Overall, the BBB is an essential barrier for the homeostasis of the brain.[55,56]

Its particular properties are based on the dynamic interaction between cerebral endothelial cells and other surrounding cells such as astrocytes, pericytes, microglia and neurons[57]. One of the hallmarks of the BBB phenotype is the restrictive paracellular pathway, regulated by inter-endothelial tight junctions. These tight junctions consist of protein complexes that are located between endothelial cells, formed by transmembrane proteins (occludin[58], claudin[59]) and

cytoplasmic proteins (zonula occludens). Zonula occludens 1 (ZO-1)[60] is one of the most used protein markers for tight junctions.

Other cell types besides endothelial cells, such as astrocytes or pericytes, are also relevant for the BBB function. Astrocytes are star-shaped glial cells characterized by abundant end-foot processes that come in contact with neuronal synapses and surround the cerebral microvascular endothelium. The purpose of this complex anatomy is thought to be the control of brain water and ionic homeostasis in order to optimize the interstitial space for synaptic transmission[61]. Pericytes are responsible for BBB gene specific expression patterns in brain endothelial cells and induce the polarization of the astrocytic endfoot processes[62].

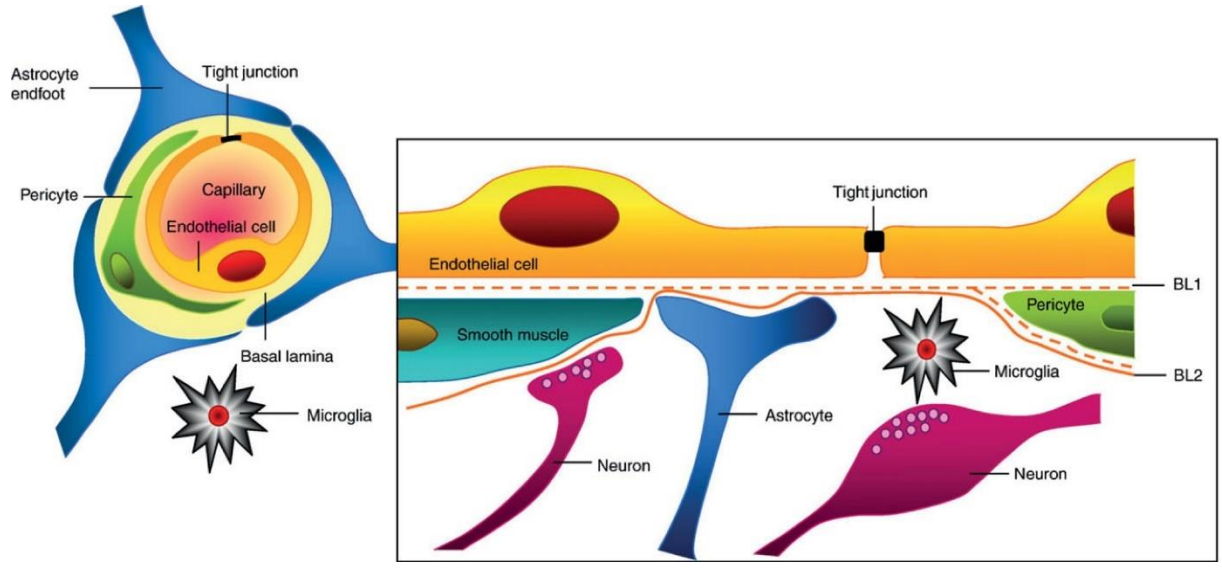

Figure 6. Overview of the neurovascular unit and the main components of the blood-brain barrier (BBB)[63].

1.3.2.2. Traumatic brain injury

Traumatic brain injury is a leading cause of injury-related death and disability[64]. Blood-brain barrier (BBB) disruption in a known consequence of TBI and is associated with poorer outcomes[65,66]. Following the primary impact, BBB disruption contributes to tissue damage, subsequent edema, inflammation, and neural disfunction[67,68]. BBB breakdown also has long-lasting effects, as it is associated with neurodegeneration or other comorbidities such as Alzheimer's disease and epilepsy[69–72].

As mentioned earlier, acute trauma can induce an over expression of tPA due to endothelial injury and shock induced inhibition of PAI-1. In fact, hyperfibrinolysis due to ATC occurs in one of every three patients with TBI[65,73]. Incidentally, there is much data implicating tPA, plasmin, or both in cognitive function, memory, and anxiety. Although direct neurotoxicity of tPA has been proved by some studies[74,75], increased presence of tPA has also been shown to correlate with increased permeability of the neurovascular unit[76–78]. For example, Exogenous tPA was shown to increase BBB permeability via plasmin-mediated cleavage of monocyte chemoattractant protein-1 (MCP-1) *in vitro* and in wild-type mice[79]. Other groups also reported a dependence of plasminogen for exogenous tPA to increase BBB permeability in mouse models of ischemic stroke[80]. It was also shown in a mouse model of hyperfibrinolysis, that transgenic overexpression of tPA in liver (that resulted in an increase in plasma levels of tPA) increased BBB permeability in a plasmin- and bradykinin-dependent mechanism[81]. Other pathways which are not plasmin-dependent have also been reported[76,78].

In conclusion, acute trauma in the brain has been extensively related to increased permeability of the BBB. In addition, the excessive activation of Plg into Plm by tPA has been proposed as a partial mechanism for this permeability increase.

1.4. Fibrinolysis inhibitors

1.4.1. Ligands of lysine binding sites

1.4.1.1. Initial lysine analogues

As previously described, intravascular formation of Plm occurs after the mutual binding of Plg and tPA on fibrin lysine residues[15]. These residues interact with the LBS present on the Kringle domains of both Plg and tPA. In 1948, the Okamoto group initiated a systematic search for synthetic substances for the treatment of bleeding disorders like post-partum hemorrhage (PPH) caused by changes of hemostasis and fibrinolysis during pregnancy[82]. PPH is still a major cause of maternal mortality globally with approximately 86,000 deaths each year, mainly in low-income countries[83].

Initially, a weak antifibrinolytic activity was found for the amino acid lysine. Shortly after, the α-deaminated lysine mimetic ε-aminocaproic acid (EACA) was identified as a stronger fibrinolysis inhibitor, with a 10-fold increase in potency[84,85]. Further efforts led to the discovery of 4-(aminomethyl)cyclohexanecarboxylic acid (AMCHA) in 1962[86]. This compound introduced a ring system which provided a higher rigidity while maintaining, with a similar relative distance, the two key functional groups of EACA: a free amine and a carboxylic group. This rigidification improved the antifibrinolytic effect both *in vitro* and *in vivo*[87]. However, the incorporation of a cyclohexane ring causes the presence of two stereoisomers: cis- and trans-AMCHA. In 1964, trans-AMCHA was found to be the active stereoisomer, which was later named tranexamic acid (TXA)[88]. Nowadays, TXA remains the most widely used antifibrinolytic drug, being the active ingredient of different FDA-approved drugs, such as Cyclokapron™ or Lysteda™. The global antifibrinolytic market, which was valued at $13,593 million in 2018[89], is still dominated by TXA to this day.

During the 1960s, different structurally related compounds were developed. For example, the aromatic TXA analogue 4-aminomethylbenzoic acid (PAMBA)[90,91], which has been approved in some countries including China and Germany. Another case is the bridged TXA derivative 4-aminomethylbicyclo[2.2.2]-ocatne-1-carboxylic acid (AMBOCA), which although exhibiting a higher activity than TXA was not further developed[92,93].

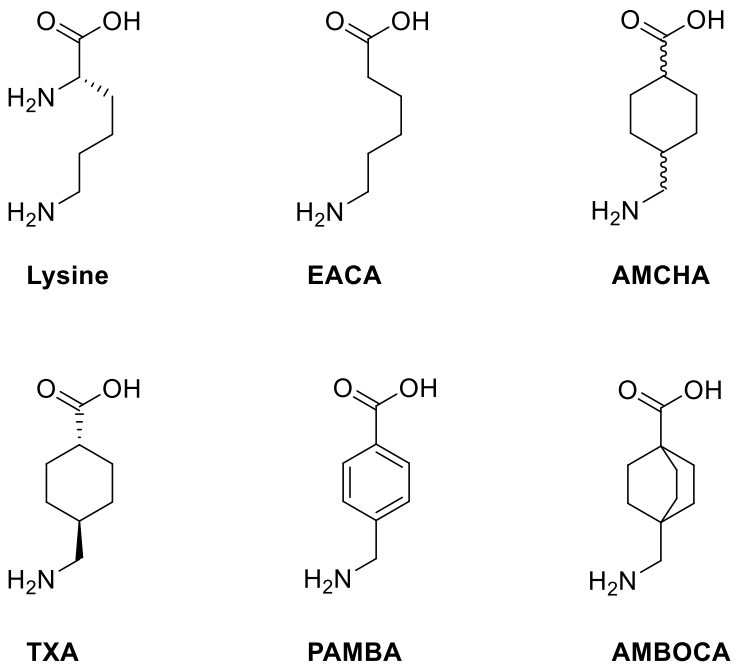

Figure 7. Molecular structure of lysine and its synthetic analogues.

Crystal structure analysis later proved that these derivatives block the LBS present in the Kringle domains of Plg, thereby inhibiting the activation of Plg. Figure 8 shows the crystal structures of TXA and EACA in complex with K1 of Plg[94]. Both ligands present a complementary binding mode to the LBS of K1. They interact with the LBS of K1 with K_D values of 9.0 μM[95] for EACA and 1.1 μM[96] for TXA. The remaining kringle domains, except for K3, can also be blocked by these lysine analogues, although with lower affinities[97]. Furthermore, crystallographic data

concerning the interaction between lysine analogues and the kringle domains are only available for K1[94] and K4[98], which is the second kringle domain with higher affinity.

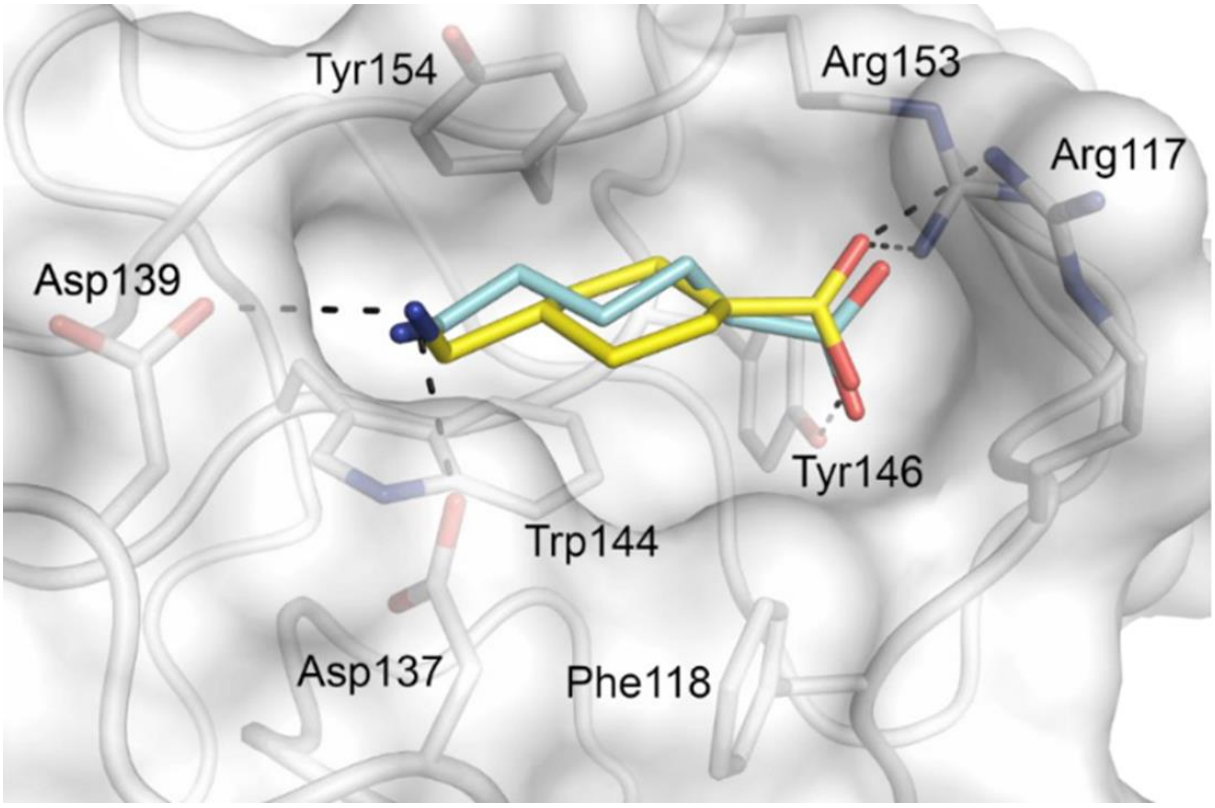

Figure 8. Crystal structure of TXA (yellow carbon atoms) in the LBS of the Plg K1 domain (PDB: 1ceb) superimposed with the structure of EACA (pale blue carbon atoms) from an analogous K1 complex (PDB: 1Cea)[94]. Both compounds form similar salt bridges to K1 residues Asp137 and Asp139 via their amine moiety, while the carboxyl groups interact with the side chains of Arg117, Tyr146 and Arg153. The hydrophobic cyclohexyl core of TXA is stabilized by Van der Waals contacts to Phe118, Trp144, Tyr146 and Tyr154. Residue numbering according to Steinmetzer et al.[21]

The therapeutically active concentration is about 100 µg/mL (~ 0.6 mM) for TXA and 1000 µg/mL (~ 8 mM) for EACA[99]. Therefore, TXA has an antifibrinolytic activity around ten times

higher than EACA. It also presents a more favorable pharmacological profile, while being equally non-toxic[99,100]. Both lysine analogues (TXA and EACA) have proven to be safe and reliable drugs to reduces perioperative bleeding and their pharmaceutical effect has been extensively reviewed[101–103]. However, due to their relatively low affinities, the administration of high doses is required to obtain the desired antifibrinolytic effect. High doses of TXA have been linked to the occurrence of seizures during cardiac surgery, possibly caused by the inhibition of $GABA_A$ receptor[104–106]. Other milder side effects which occur with high frequency are headaches, nasal symptoms, or back, abdominal and muscle pain[36]. Additionally, gastrointestinal discomfort, including nausea, vomiting and diarrhea, occur in 30% of patients treated orally with EACA or TXA[107,108]. Hypotension has also been observed when intravenously administered too rapidly[109]. The need of high doses to obtain sustained effects causes heavy limitations in patients with prior renal malfunctions. Consequently, TXA is contraindicated in patients with severe renal impairment. In cases of mild to moderate renal impairment, the dosage is reduced according to the serum creatinine level[110]. Hence, the development of novel antifibrinolytic agents with increased affinity and selectivity is of high importance.

1.4.1.2. Computationally designed analogues of TXA

To improve the potency and pharmacokinetic properties of the classic lysine analogues, a screening method combined with a computational approach was used to identify molecules that mirror the shape and electrostatic properties of TXA[111]. The result was the discovery of 5-(4-piperidyl)-3-isoxazol (4-PIOL), which was found to be four times more potent than TXA *in vitro*. However, 4-PIOL was found to be a low affinity $GABA_A$ receptor antagonist. This raised concern since some side effects of high dose TXA treatments had been previously linked to its $GABA_A$ antagonistic properties[106]. $GABA_A$ is a ligand-gated receptor present mainly in neuronal tissue. Its

main ligand is γ-aminobutyric acid (GABA), the major inhibitory neurotransmitter in the central nervous system[112].

Substitution of the C2 carbon of the piperidine ring provided derivatives with improved potency and negligible affinity towards $GABA_A$ receptor[113]. These compounds (**d1-d3**) include two stereocenters, which provide 4 possible stereoisomers in each case. It is worth noting that the increase of stereocenters generally increases the complexity of the synthetic pathway. Among the different derivatives, molecule AZD6564 (IC_{50} 0.44 μM in plasma) was found to have the best bioavailability in rats. However, no further development has been announced by AstraZeneca PLC, company which developed the compound.

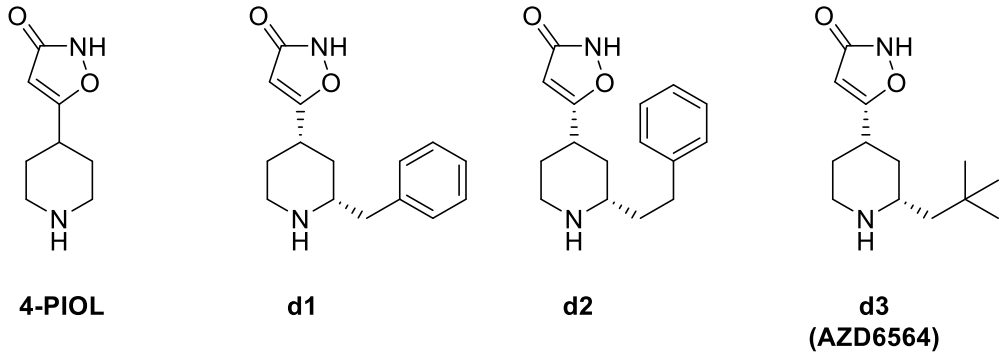

Figure 9. Structures of the computationally designed TXA analogue 4-PIOL and some of its derivatives (d1-d3)[111,113].

The crystal structure of the complex between derivative 1 (**d1**) and K1 of Plg (Figure 10) shows a binding mode similar to that of TXA. The basic nitrogen provided by piperidine interacts similarly to the primary amine in TXA. The same is true for the carbonyl oxygen of derivative d1, which rests in the same position as the carboxyl group of TXA, and therefore equally interacts with the arginine residues.

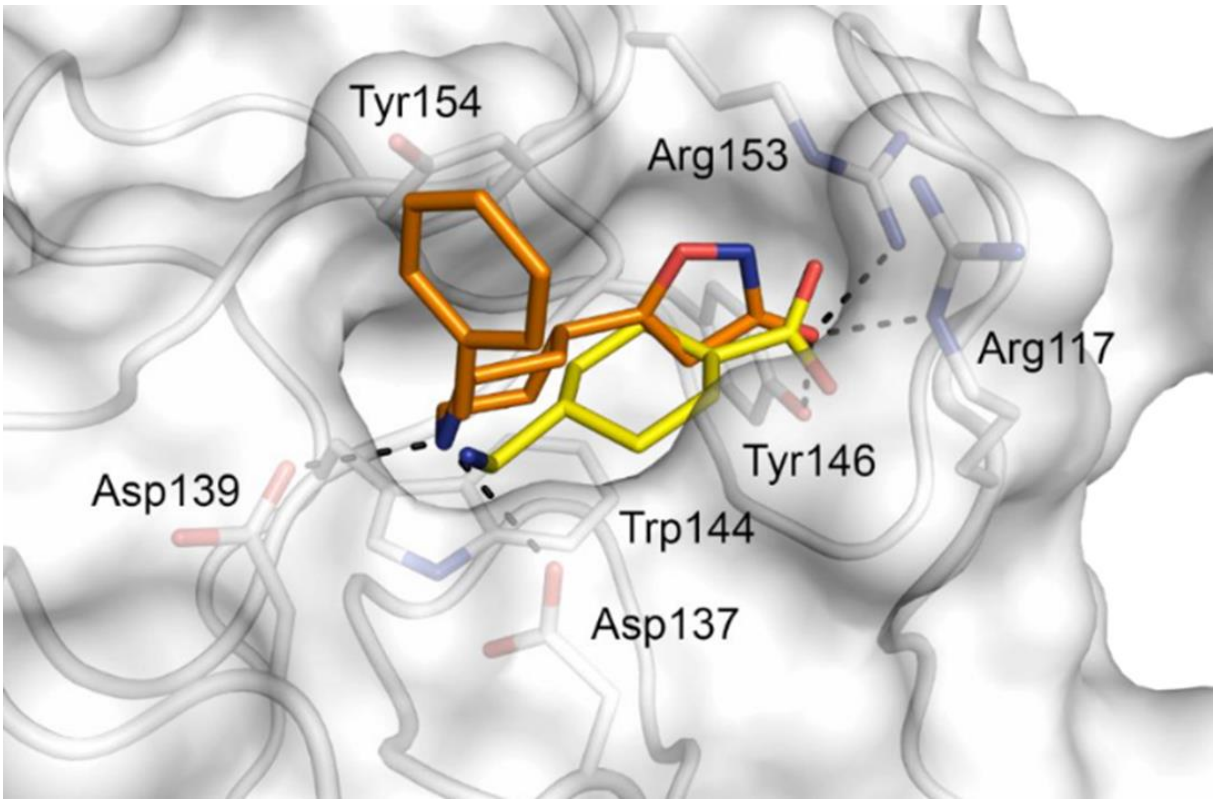

Figure 10. Crystal structure of **d1** (orange carbon atoms) in complex with the K1 domain (PDB: 4cik)[113] superimposed with TXA (yellow carbon atoms) extracted from an analogous K1 complex (PDB: 1ceb)[94]. In analogy to TXA, compound **d1** interacts with Asp137 and Asp139 via its cationic piperidine and with Arg117, Tyr146 and Arg153 via its carbonyl oxygen. Additional Van der Waals contacts are formed between Trp144, Tyr146 and Tyr154 and the hydrophobic core of **d1**. The inhibitor's benzyl group is exposed into the solvent and does not show any interactions with the LBS. Residue numbering according to Steinmetzer et al.[21]

1.4.1.3. Pyrimidinone-derived LBS binders

Some piperidine-derived LBS binders connected to substituted pyrimidoindazolones (**B1**)[114] or pyrazolopyrimidinones (**B2**)[115] were disclosed by Bayer A.G in 2016 (Figure 11). The patent applications reported antifibrinolytic activities with IC_{50} values in the range between 6-15 nM.

These were quantified with an *in vitro* assay using diluted 5% human plasma supplemented with 3 μM fibrinogen. Surface plasmon resonance measurements with immobilized recombinantly expressed K1 suggested that these compounds bind to the LBS of K1. Despite these promising results, no further development has been announced by Bayer A.G. up to this point. It must be noted that these patented compounds required, according to the patents, synthetic routes in the range of 11-15 steps. Such chemical complexity could hinder the scalability of these compound and therefore their actual application as drugs.

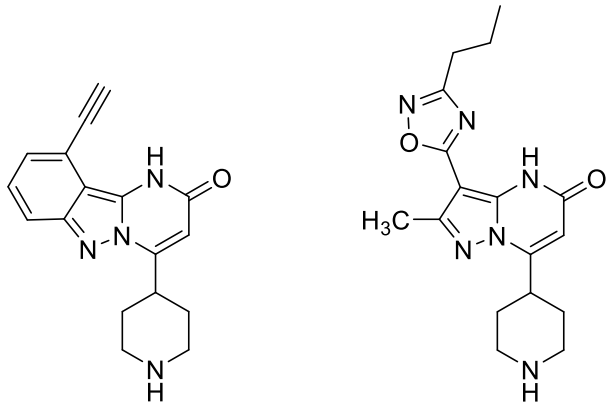

Figure 11. Molecular structure of two examples among the pyrimidoindazolones (**B1**) and pyrazolopyrimidinones (**B2**) derivatives patented by Bayer A.G.[114,115]

1.4.2. Synthetic active site direct inhibitors of plasmin

As previously described, TXA and EACA inhibit fibrinolysis by interacting with the LBS of kringle domains present in Plg (and in Plm). However, it is also well reported that they possess a negligible affinity towards the Plm serine protease domain active site (EACA, Ki = 53 mM; TXA, Ki = 25 mM)[87].

TXA by itself is therefore an extremely poor inhibitor of the active site of Plm. However, the search for Plm direct inhibitors led to the design of different TXA-conjugated compounds. Two

examples are the thoroughly studied alkylated tyrosine derivative YO-2[116] and its close analogue PSI-112[117]. As seen in Figure 12, they combine a TXA residue with a modified tyrosine and an alkyl side chain. The elongation of the tyrosine side chain with heteroaralkyl residues was essential for an improved Plm inhibition, their replacement with hydrogen or a tert-butyl group reduced the affinity 125-fold and 30-fold, respectively.

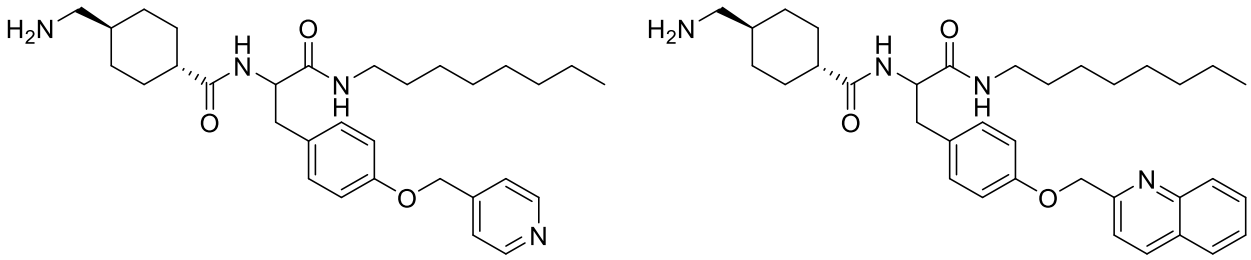

YO-2 **PSI-112**

Figure 12. Structures of TXA-conjugated Plm inhibitors. Both were crystallized in complex with Plm[118].

Other strategies have been followed to develop new Plm synthetic inhibitors[119–122]. However, none of them, including the TXA-conjugated compounds, have led to a fully developed new antifibrinolytic drug.

1.4.3. Kunitz-type inhibitors

Kunitz-type inhibitors comprise a family of stable peptidic protease inhibitors, most of which are from nonhuman origin. The compact structure of the Kunitz-domain is stabilized by an intramolecular hydrogen bond network and three conserved disulfide bonds, providing a rigid multicyclic scaffold. Inhibitors of this type share a canonical recognition loop, which adopts a substrate- like conformation that is further stabilized by a secondary binding loop[123]. Due to their

high stabilities and strong binding affinities, natural Kunitz-type inhibitors provide attractive scaffolds for the development of new serine protease inhibitors.

Aprotinin, also known as BPTI, is a 58-mer Kunitz-type inhibitor isolated from bovine lungs that inhibits numerous trypsin-like serine proteases including Plm (K_i = 0.5 nM), Kallikrein (K_i = 30 nM), and trypsin (K_i < 1 nM)[124,125]. It has been used as an antifibrinolytic drug to reduce perioperative bleeding during surgery and, consequently the need for blood transfusions[126–129]. However, after its application was associated with increased mortality rates in comparison to standard fibrinolytics, its commercial use was suspended in 2008[130–132]. Currently, aprotinin has been reapproved for restricted applications in a few countries.

Other Kunitz-type inhibitors have been described to have relatively high affinity for Plm, such as Textilin-1 and 2[133], isolated from the venom of the Australian common brown snake *Pseudonaja textilis*. They present a highly similar sequence to that of aprotinin, and both textilinins have been proven as potent Plm inhibitors with inhibition constants of 3.5 nM and 2.2 nM, respectively[134]. Although demonstrating an inhibitory effect on fibrinolysis, this was considerably less efficient than that of aprotinin[135]. No other Kunitz type inhibitor has improved the results of aprotinin as a fibrinolysis inhibitor to this day.

1.5. Novel antifibrinolytic compound

In a collaboration of our research group with the start-up company Alxerion Biotech, we discovered a new small molecule with high antifibrinolytic activity through high throughput screening. This compound, named LTI-6, is the combination of three key moieties: a piperidine, a 1,2,3-triazole and a 1,3,4-oxadiazolone ring. This compound had never been described as an antifibrinolytic agent before. However, its synthesis was previously described by Sangshetti et al.[136] in a publication which presents derivatives of this molecule as antifungal agents.

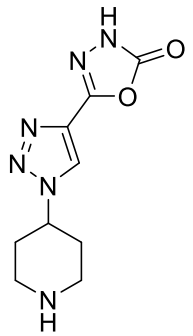

LTI-6

Figure 13. Molecular structure of LTI-6, the new small molecule with high antifibrinolytic activity found through collaboration with Alxerion Biotech.

The mechanism of action of this molecule remained unknown, as well as the real potency as antifibrinolytic agent. Previously described piperidine derivatives, such as 4-PIOL, have been proven to act as inhibitors of the LBS of Plg. This points towards the idea that this newly described piperidine derivative, LTI-6, could be acting through the same mechanism.

However, conjugates of TXA, such as YO-2 or PSI-112, have been described as Plm active site inhibitors. In fact, TXA itself has been reported to present certain Plm direct inhibition, although negligible. This points towards the idea that a compound with a terminal amine, like LTI-6, can potentially be a Plm direct inhibitor with the appropriate structure. Therefore, this possibility could not be discarded.

Although no synthetic compounds have been described to inhibit the active site of tPA, this possibility needed to be also studied.

1.6. Hypothesis and objectives

Severe trauma can induce a hyperfibrinolytic state in which available tPA concentration increases dramatically, and therefore also does the rate of Plm formation. Plm and tPA have been linked to BBB disruption in the specific case of traumatic brain injury (TBI). Although the

mechanism for this disruption is still not fully understood, inhibition of Plm or Plm activation is an interesting approach to limit the damage to the BBB during TBI.

Currently, tranexamic acid (TXA) remains the gold standard among antifibrinolytic drugs. It presents certain limitations due to its low affinity and specificity, which results in a need for a very high dose. However, after more than 50 years since its discovery, no new improved antifibrinolytic drug has reached the market.

LTI-6 presents a novel structure for a compound with antifibrinolytic activity, combining a piperidine, a 1,2,3-triazole and a 1,3,4-oxadiazolone ring. It presents certain similarities to a previously described Plg LBS inhibitor 4-PIOL, which is also a piperidine derivative. Therefore, this is the most likely mechanism of action for LTI-6. However, such mechanism still needs to be established.

In the present thesis, we hypothesize that LTI-6 is an inhibitor of the LBS in Plg, and therefore inhibits its conversion into Plm by tPA. Further modifications of LTI-6 to improve its activity could then render a viable drug candidate to act as a protective agent of the BBB in the hyperfibrinolytic state generated after TBI.

To address these hypotheses, the following objectives are defined:

- To evaluate the potency of LTI-6 and determine the mechanism of action.
- To modify the structure of LTI-6 and study the structure-activity relationship (SAR) to further understand how to improve the activity.
- To study the effect of the most active compound in a hyperfibrinolytic BBB *in vitro* model.

2. Evaluation of activity and mechanism of action of LTI-6

2.1. Chapter introduction

This chapter studies the newly discovered compound LTI-6, both in terms of potency and mechanism. Different hypotheses need to be ruled out or confirmed. First of all, the coagulation and fibrinolytic processes need to be separated in order to assess the effect of LTI-6 on each of them. If the compound is indeed acting as a fibrinolysis inhibitor, the mechanism of action could involve different possible targets: Plg, Plm or tPA. In addition, the compound needs to be evaluated in biological environments (plasma, whole blood) and compared to existing drugs such as tranexamic acid.

2.2. Coagulation in whole blood

Before determining that LTI-6 was acting as an inhibitor of fibrinolysis, it was necessary to rule out the hypothesis that it could be acting on the coagulation process. For example, a compound that accelerated or slowed down the clot formation mechanism would probably affect the quality of the clot itself, for example altering the density of the fibrin mesh. Having a higher or lower fibrin mesh density would then alter the rate of fibrinolysis, without the need for a fibrinolysis inhibitor.

To evaluate the possible effect of LTI-6 on clot formation, an *ex vivo* whole blood clotting test was performed without the addition of exogenous plasminogen activators. Blood was allowed to clot inside a blood extraction tube with the presence of LTI-6 or TXA and compared to a control clot. Since TXA is a known lysine analogue which inhibits fibrinolysis, it was not expected to affect the clotting process.

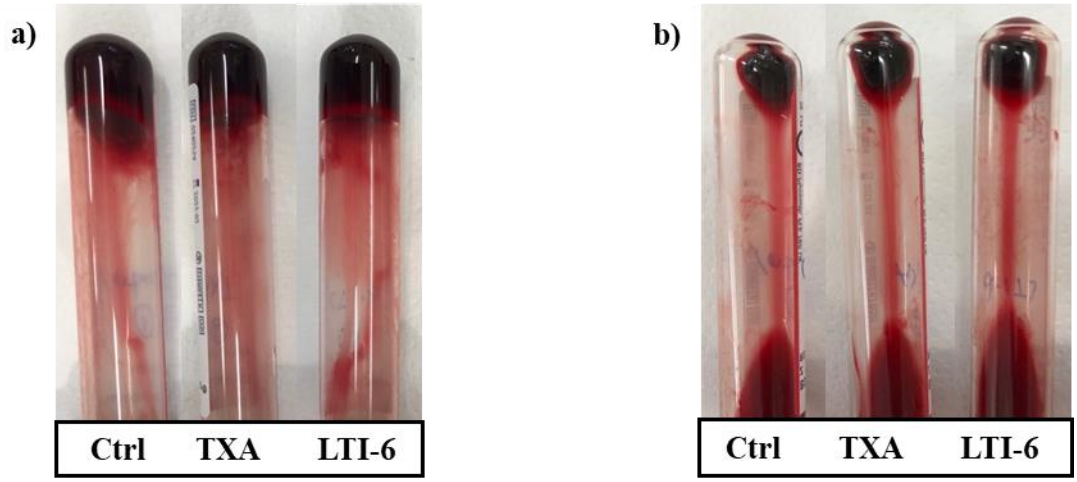

Figure 14. Blood coagulation experiment without the addition of exogenous fibrinolysis activators. a) Photographs of blood clots taken 5 minutes after blood addition to the tubes. b) Photographs of blood clots taken after 24 h of incubation. Tubes were inverted to allow a better differentiation of clots (top) and liquid blood (bottom). TXA and LTI-6 tubes contained 40 μM of each product. Control tubes contained Tris HCl buffer instead.

After the addition of blood to the tubes, blood clots were generated at the same pace for the three different conditions. At minute 5, all three clots were completely formed. Visual differences during clot formation were not observed among the different conditions. Also, all three clots were equal in size and were employing the entirety of the blood contained in the tube. After 24 h of incubation at 37 °C, all three thrombi presented some liquid separation from the clot itself. However, no visual differences were appreciated between the clots containing the studied compounds and the control.

These observations strongly indicate that the structural stability of the clot was unaffected by either TXA or LTI-6. In addition, the observed time of complete coagulation presented no difference between both compounds and the control. Therefore, these results indicate that LTI-6, as well as TXA, does not affect the coagulation process.

2.3. Coagulation-fibrinolysis in plasma

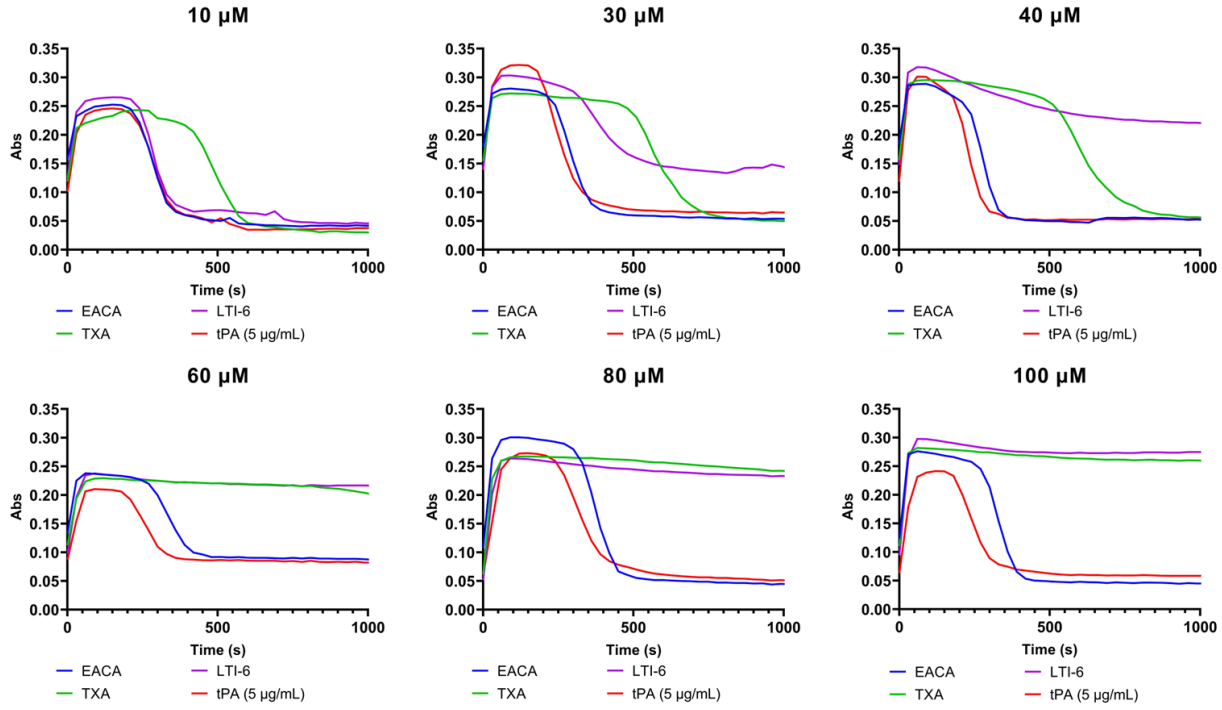

Figure 15. Clot formation-lysis turbidimetry assays in a 96-well plate using human plasma. Clotting was initiated by the addition of tissue factor (TF) and calcium chloride ($CaCl_2$). 5 µg/mL tPA was added to every well. Different concentrations of EACA, TXA and LTI-6 were studied. The formation and lysis of fibrin clots were evaluated by measuring the absorbance of each well through time. Each curve is the average of three replicates. Error bars omitted for visual clarity.

Clot formation-lysis assays were performed to evaluate the effect of LTI-6 on fibrinolysis. As soon as tissue factor and $CaCl_2$ are added, absorbance increases, which indicates the formation of a fibrin clot. With the formation of a fibrin clot, and due to the prior addition of tissue plasminogen activator (tPA), the fibrinolysis process is activated. Consequently, in the assays where this process in not inhibited, a decrease of clot density (absorbance decrease) can be observed. Different concentrations of LTI-6 were evaluated and compared to the same concentrations of currently used

lysine analogues (EACA and TXA). The plots show that at concentrations of 20 μM or lower, LTI-6 was not able to inhibit the degradation of fibrin clots, and therefore fibrin was degraded at the same rate as the tPA control. TXA slightly delayed the clot lysis, although it did not avoid the complete clot dissolution. At 30 μM a slower rate of clot dissolution was already observed for LTI-6, and inhibition of fibrinolysis was almost complete at 40 μM. In the case of TXA, a progressive delay in the clot lysis was observed for 30 μM and 40 μM, although in both cases with a complete clot dissolution. At concentrations of 60 μM or higher, however, both LTI-6 and TXA showed a complete inhibition of the clot dissolution in the plasma assays, since no decrease of absorbance was observed in either case.

These results suggest that both LTI-6 and TXA are inhibiting the clot dissolution at a similar range of concentrations. However, a qualitative difference can be observed at the partial inhibition range (30-40 μM). The curves for TXA show a delayed start of the clot degradation, followed by a steep decline in absorbance. In contrast, the curves for LTI-6 show a slightly faster start of the degradation, but at a slower rate. In fact, in the case of LTI-6 the curves do not return the basal absorbance values, which does occur in the case of TXA. These differences suggest a more stable inhibition of fibrinolysis for LTI-6 than that of TXA.

2.4. Fibrinolysis in plasma pre-formed clots

The protocol mentioned above allowed to study the formation and lysis of clots, which could be occurring simultaneously during some part of the assay. In order to study exclusively the fibrinolytic process, a different assay was performed. In this assay, plasma clots were generated equally for all conditions in a first step, and in a second step the different conditions including tPA and the studied compounds were added on top of each clot. The fibrin degradation in each case was studied by measuring the absorbance, as well as in the coagulation-lysis assays. However, the

lysis process in this case was substantially slower due to the need for tPA and the studied compounds to permeate the previously formed fibrin mesh. To partially compensate for the slower degradation, the concentration of tPA used for this assay was 10 µg/mL, instead of the 5 µg/mL used in the previous assay.

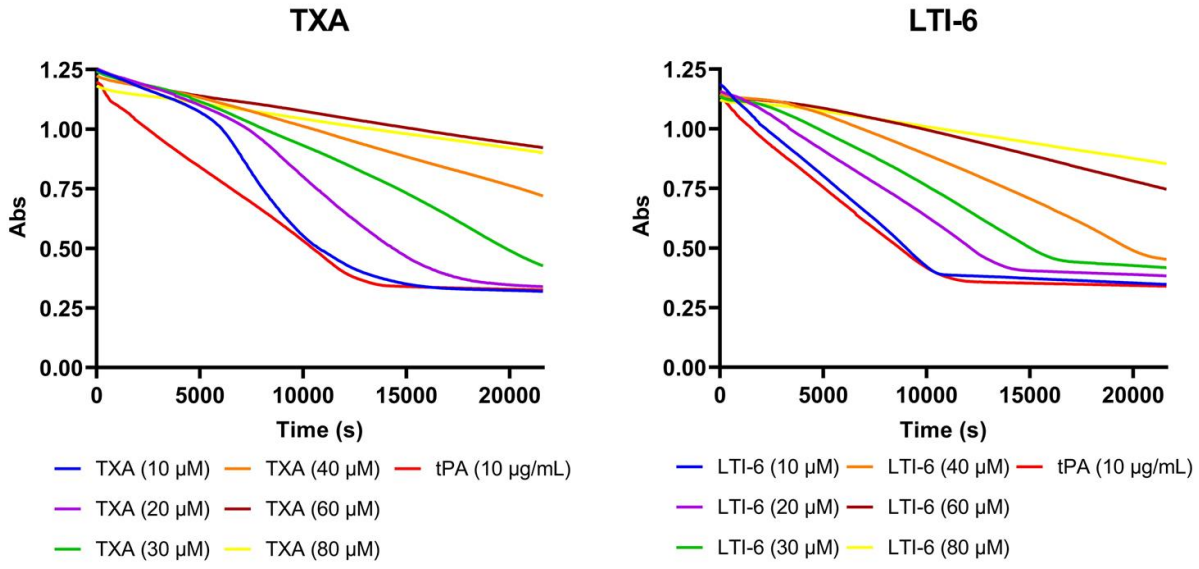

Figure 16. Clot lysis assays with plasma preformed clots for TXA and LTI-6. Fibrinolysis was initiated by adding 10 µg/mL of tPA and the desired concentration of the studied compound. Each curve is the average of three replicates. Error bars omitted for visual clarity.

The results of these experiments (Figure 16) show visual differences between the curves for TXA and LTI-6, especially at the lower concentration range. TXA at 10 µM did not avoid the complete lysis of the clot at a very similar time than that of the tPA control. However, it did cause a visible delay in the start of the degradation. At the early stage of the assay, the curve shows a very low decrease in absorbance, which is then largely accelerated to the point where it compensates for the initial lack of degradation. This acceleration can also be observed, though to

a lesser extent, for the 20 μM concentration of TXA. In the case of LTI-6, the clot degradation happened at a more constant rate, without the presence of any large slope variation.

This difference in the shape of the curves at lower concentrations could also be observed in the plasma coagulation-lysis assays (Figure 15). In both cases, low concentrations of TXA caused a delay in the beginning of fibrinolysis followed by a steep descent in the absorbance. This behavior was not observed for LTI-6, which provided a steadier degradation from the beginning. At higher concentrations, however, both compounds produced a more similar effect, without the presence of any fibrinolysis rate acceleration.

These differences could be interpreted as evidence of a different mechanism of action for both compounds. However, one must consider that the fibrinolytic process is occurring around a fibrin clot, which is a solid mesh of fibrin. Therefore, the capability of a molecule to permeate this mesh can be as important as is binding capacity to a specific binding site. In this regard, it is possible that TXA was permeating the fibrin mesh faster than LTI-6, which would cause and increased inhibition of fibrinolysis in the early stage of the assays for TXA. This effect should be much more relevant in the assays with preformed clots, since tPA and the studied compound were added on top of the fully formed plasma clots. In the case of coagulation-lysis assays, the rate of permeation through the fibrin mesh should be of less importance, since all elements of the assay are mixed homogenously before coagulation starts.

Another possible explanation for the different behavior at lower concentrations could be a less stable interaction of TXA with the target when compared to LTI-6. This would be aligned with the smaller size of TXA and therefore its inherent higher chance of interacting with more nonspecific binding sites.

In order to quantify and compare the activity of each compound, the results with preformed clots were taken into consideration. This assay proved to be more reliable than the one with combined coagulation-fibrinolysis for different reasons. The first, because it isolated the mechanism which we intended to study, fibrinolysis, from coagulation. The second, and equally important, because it showed a much higher accuracy and repeatability. By causing the process to go slower, changes in absorbance were less abrupt, and therefore easier to monitor. From these results, a relative fibrinolysis rate (% fibrinolysis) was calculated by dividing the slope for tPA by the slope for the studied concentration of each compound. The IC_{50} was considered as the concentration at which each compound inhibited 50% of the fibrinolytic activity. The activity-concentration plot (Figure 17) and the calculated IC_{50} values (Table 1) showed no significant difference between the fibrinolytic potency of TXA and LTI-6 in our plasma clot lysis assays.

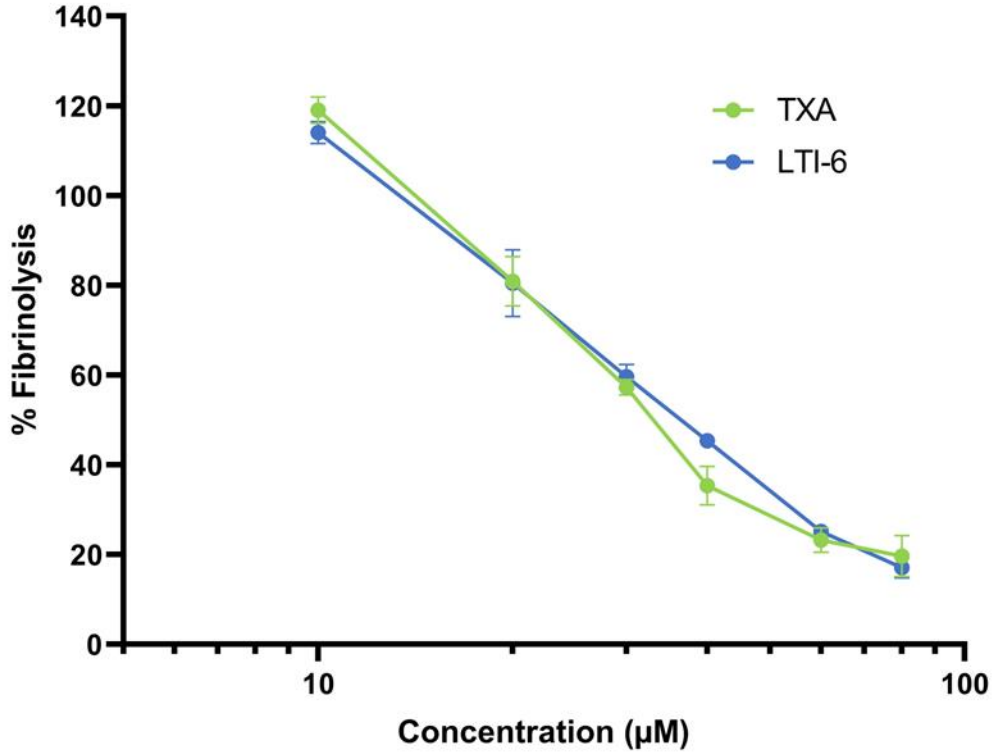

Figure 17. Fibrinolytic activity (%) quantified for each studied concentration of TXA and LTI-6. Each condition was studied in triplicate. The error bar indicates standard deviation.

Table 1. IC_{50} values for TXA and LTI-6. IC_{50} was calculated as the concentration at which each compound provided 50% inhibition of fibrinolysis in our preformed plasma clot lysis assays.

Compound	**IC_{50}**
TXA	33.3
LTI-6	36.8

2.5. Fibrinolysis in whole blood

2.5.1. Qualitative whole blood assay

Once the antifibrinolytic activity of LTI-6 was assessed in plasma, the next step was to study its antifibrinolytic activity in whole blood. Whole blood assays allowed to measure fibrinolysis taking in consideration all circulating cells, which are known to play a major role in thrombolysis and in clot properties and structure.

Since turbidimetric assays are not possible with whole blood due to its inherent opacity, a more qualitative assay was performed. Different concentrations of TXA and LTI-6 were assessed ex vivo in a qualitative whole blood clot lysis assay to determine the effective dosage at which the studied compounds were capable to fully degrade blood clots. A visual representation of clots tested with four different concentrations of each compound is shown in Figure 18. Visual observation of tubes during clotting and fibrinolysis allowed to qualitatively compare the antifibrinolytic capacity of the studied compounds at different concentrations.

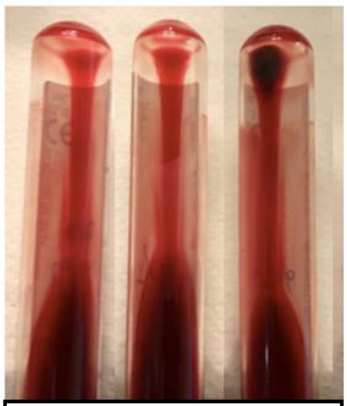

10 µM | Ctrl | TXA | LTI-6

Clot Formation	10’	8’	8’
Clot Lysis	17’	30’	-

20 µM | Ctrl | TXA | LTI-6

Clot Formation	8’	6’	6’
Clot Lysis	18’	26’	-

40 µM | Ctrl | TXA | LTI-6

Clot Formation	7’	6’	6’
Clot Lysis	13’	35’	-

60 µM | Ctrl | TXA | LTI-6

Clot Formation	7’	6’	6’
Clot Lysis	14’	-	-

Figure 18. Coagulation-lysis assays in whole blood. Blood without anticoagulants was allowed to clot inside glass tubes after adding 10 µg /mL tPA and the corresponding concentration of TXA or LTI-6. Coagulation and lysis were visually assessed by slowly tilting each tube every minute. The times of complete coagulation and complete lysis (when present) were recorded. Pictures were

taken with inverted tubes to allow a better differentiation of clots (top) and liquid blood (bottom) after 24 h of incubation.

Blood containing either TXA or LTI-6 clotted at a similar time as the control for each concentration studied. This indicated that neither of them were visibly affecting the coagulation process. However, variations in clot lysis were seen for the three different conditions. Control clots were dissolved in between 13 and 18 minutes after the start of the assay, implying that the fibrinolysis activators present in the tubes triggered fibrinolysis once the clot was formed. Clots containing LTI-6 and TXA had a longer degradation time and after 24 h some conditions had not yet been fully degraded.

Tubes with concentrations of 10, 20 and 40 μM of TXA resulted in a complete degradation of the clot after 24 h, although the lysis time was between 1.5 and 2.5-fold higher than that of the control. In contrast, the same concentrations for LTI-6 did not produce clot dissolution. When concentrations of 60 μM of TXA or LTI-6 were added to each assay, clots were not completely lysed during the assayed time for either condition. Nonetheless, differences in clot size were significant enough to be observed after 24 h, as the clot for TXA was less than halve the size the clot containing LTI-6.

Therefore, LTI-6 showed higher antifibrinolytic activity than TXA, which differs from the results in plasma where TXA showed a slightly higher activity. This could indicate that TXA has a higher probability of interacting with unspecific targets in whole blood, which is a more complex environment than plasma mainly due to the presence of blood cells. These results also point towards the more stable inhibition of LTI-6 when compared to TXA, which was already observed in the plasma assays.

2.5.2. Quantitative whole blood assay

These qualitative results in whole blood showed a higher potency of LTI-6 when compared to TXA than that observed in plasma. Therefore, we decided to perform a more quantitative assay. As mentioned before, turbidimetric methods are not viable in the case of whole blood due to its inherent opacity. Instead of turbidity, we decided to use an ELISA kit to analyze the concentration of D-dimer, a well-known fibrin degradation byproduct. In order to properly compare these results to our results in plasma, preformed blood clots were used for these assays. After allowing the blood to clot and incubating it for 1 hour, the mixture of tPA and the studied compound was added on top, dissolved in Tris HCl buffer. Samples were the extracted at different times to quantify the evolution of D-dimer concentration.

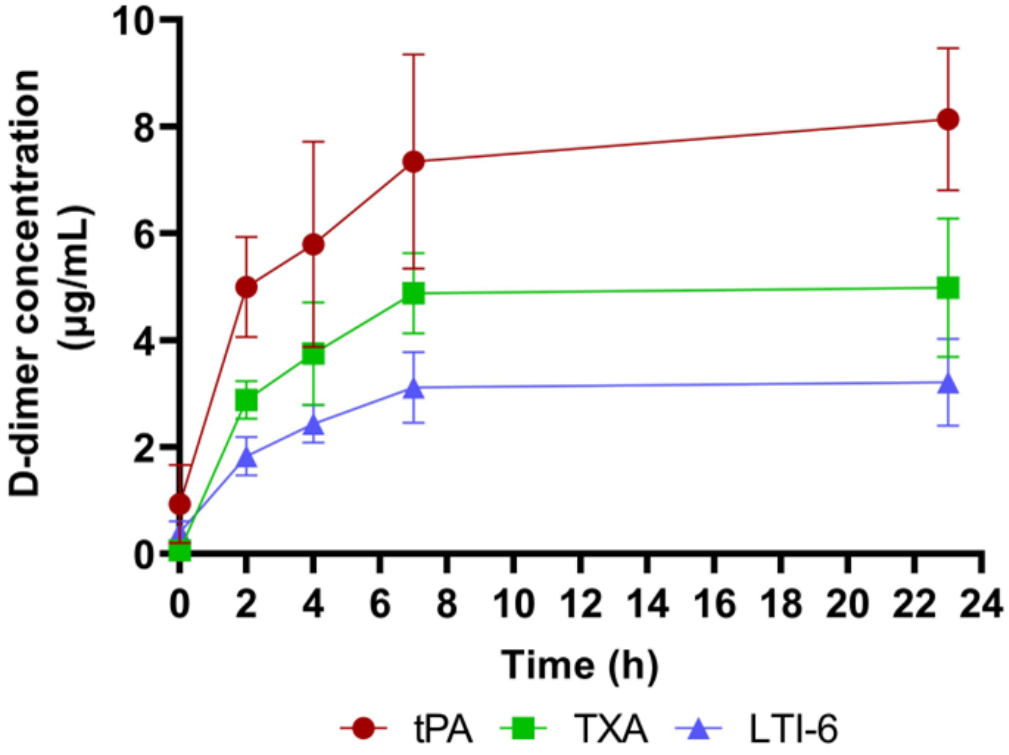

Figure 19. Antifibrinolytic activity of TXA and LTI-6 in whole blood. Concentration of D-dimer was measure with an ELISA kit and evaluated through time. Clots were incubated for 1 h before addition of exogenous tPA and 20 µM of compounds TXA or LTI-6. For the tPA control, Tris HCl Buffer was added. D-dimer concentration was quantified at times 0, 2, 4, 7 and 24 h after the addition of the mixture of tPA and the compounds. Three replicates of each condition were studied.

The concentration of D-dimer increased during the time of the experiment for all three cases, which implies that a certain amount of fibrin degradation occurred for all three conditions. Both compounds, however, reduced both the rate of formation as well as the final concentration of D-dimer. Therefore, they both acted as partial fibrinolysis inhibitors at the studied concentration in whole blood.

When comparing TXA and LTI-6, the latter caused a lower D-dimer formation at every studied time point. The fibrin byproduct concentration was around 2/3 of the control for TXA, while it was less than halve in the case of LTI-6. At the time point of 2 hours, the D-dimer concentration was 1.5 times higher for TXA than for LTI-6, with statistical significance. These results are in accordance with the previous qualitative assessments in whole blood, which already pointed towards a higher potency of LTI-6 than TXA, which was not observed in the plasma assays.

The lower performance of TXA in blood than plasma can be attributed to the presence of circulating cells in blood. Red blood cells, platelets, and white blood cells play an important role in fibrinolysis and they might affect the interaction of TXA with plasminogen. This reinforces the idea that TXA has a higher chance of interacting with unspecific binding sites, the number of which is greatly increase by the presence of cells in the studied system. LTI-6, although presenting a similar potency in plasma, seems to show a higher selectivity in more a more complex biological system such as blood, which translates in a higher potency.

2.6. Interaction with plasmin catalytic domain

Once we had established that LTI-6 was inhibiting fibrinolysis, and that its potency was relevant when compared to the currently used drugs, our goal was to determine the enzymatic target of LTI-6. One possibility was that it was directly binding to the active site of plasmin, which is a mechanism to inhibit fibrinolysis. In fact, lysine analogues such as EACA and TXA, although mainly bind to the lysine binding sites of plasminogen, have also been reported to present a certain affinity towards the active site of plasmin at higher concentrations (mM range).

To test the inhibition capacity of LTI-6, we used an assay in which a fluorophore is released by the cleavage of a specific plasmin substrate. Therefore, the rate of fluorescence increase is proportional to the plasmin activity.

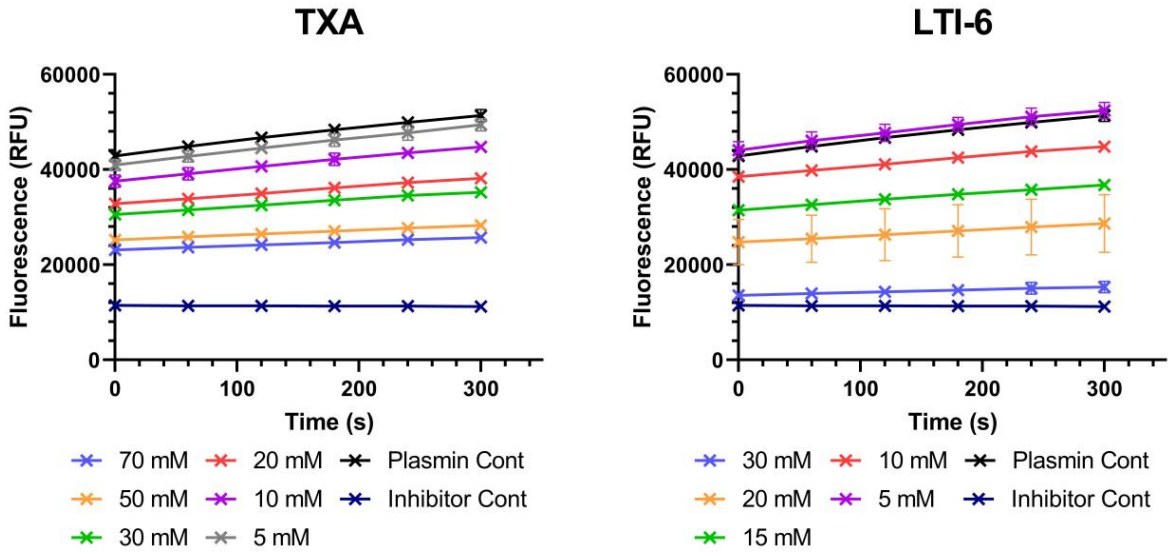

Figure 20. Raw fluorescence results of the plasmin inhibition assays performed for different concentrations of TXA and LTI-6. Fluorescence is generated through the cleavage of a specific substrate by plasmin. Each condition was tested in duplicate.

The fluorescence plots for TXA and LTI-6 (Figure 20) show a steady increase of fluorescence in the studied time frame, which means that plasmin was cleaving the specific substrate and that the conditions of the assay were adequate. The inhibition control consisted of aprotinin, a well-known plasmin inhibitor, at a final concentration of 6 µM . In this case plasmin activity was completely blocked, which caused the fluorescence value to remain constant. The different concentrations of TXA and LTI-6 showed lower fluorescence increase rates than those of the plasmin control, although always higher than that of aprotinin. Therefore, both LTI-6 and TXA proved to partially inhibit the active site of plasmin at the studied concentrations.

To further analyze the inhibition capacity of both molecules, inhibition values were calculated using the fluorescence slope of each condition and standardizing the values with the slope of the plasmin control. The dose response curves (Figure 21) show that both LTI-6 and TXA inhibit the

active site of plasmin in a dose dependent manner. By comparison, the catalytic domain of plasmin was almost twice more susceptible to the inhibition of LTI-6 (IC_{50} 14.9 mM) than to TXA (IC_{50} 26.1 mM).

These values were consistent with the well-known noncompetitive inhibition of plasmin by TXA at high doses (K_i = 25 mM)[87]. LTI-6 also demonstrated to be an inhibitor of the catalytic domain of plasmin, showing a similar activity than TXA. However, both compounds present a much lower potency, less than 1000-fold, than the well-known plasmin inhibitor aprotinin (K_i = 0.5 nM).

In addition, the concentrations needed to observe some inhibition of the catalytic domain of plasmin were 1000 times higher than the concentrations used in our plasma and blood assays. These results, therefore, allowed us to discard the hypothesis that the relevant mechanism of action of LTI-6 is a direct inhibition of plasmin, since its inhibitory function takes place at nontherapeutic doses.

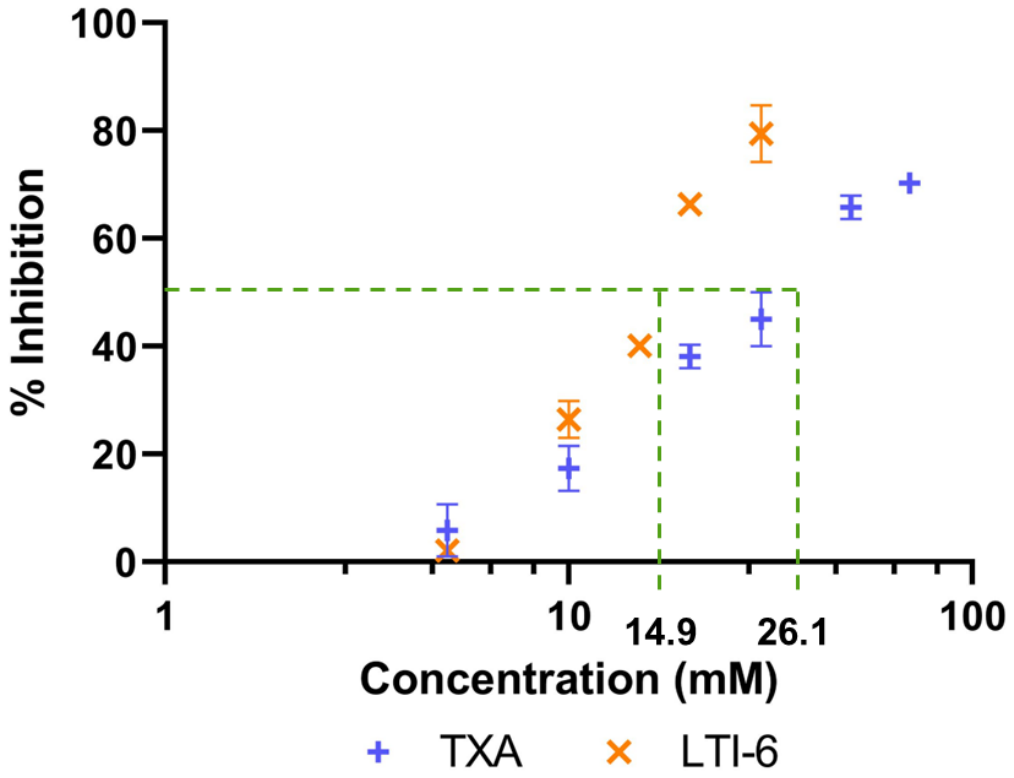

Figure 21. Dose-response curves for TXA and LTI-6. Plasmin inhibition values were determined from the fluorescence slopes of the plasmin activity assay.

2.7. Interaction with tissue plasminogen activator catalytic domain

The antifibrinolytic effect of LTI-6 could also be explained by the direct inhibition of the active site in tissue plasminogen activator. To test this hypothesis, LTI-6 was tested in a purified system with tPA and a synthetic substrate which releases a chromophore after binding with tPA. Therefore, we could quantify the tPA activity by measuring absorbance. LTI-6 was also compared to TXA, of which no activity has been reported on this active site. The positive control consisted in a sample with tPA and chromophore releasing substrate, without the presence of any compound.

The negative control consisted in a sample without the presence of tPA, only with the specific tPA substrate.

The absorbance plots show, for both compounds, a progressive increase in absorbance until reaching saturation (Figure 22). Counterintuitively, high concentrations of LTI-6 and TXA produced an increase in chromophore release. Moreover, no visible reduction of absorbance was observed for any concentration of either compound, showing a lack of inhibitory power for both TXA and LTI-6.

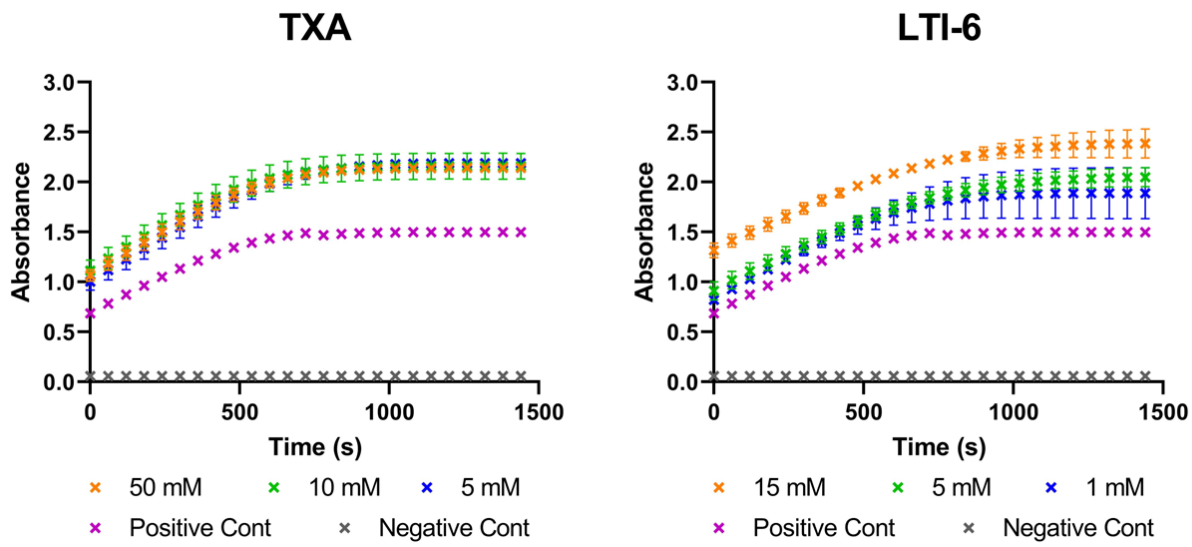

Figure 22. Tissue plasminogen activator enzymatic activity quantified for different concentrations of TXA and LTI-6. Increase of absorbance correlates with tPA activity. All conditions were assayed in duplicate.

The absorbance slopes from the linear range in each case were used to calculate the tPA activity for each concentration studied. The dose-response curve for each compound is presented in Figure 23. Data was presented as activity rate instead if inhibition rate since no clear inhibitory capacity

was observed in the results, even at concentrations almost 1000 times higher than the therapeutic concentrations tested in plasma.

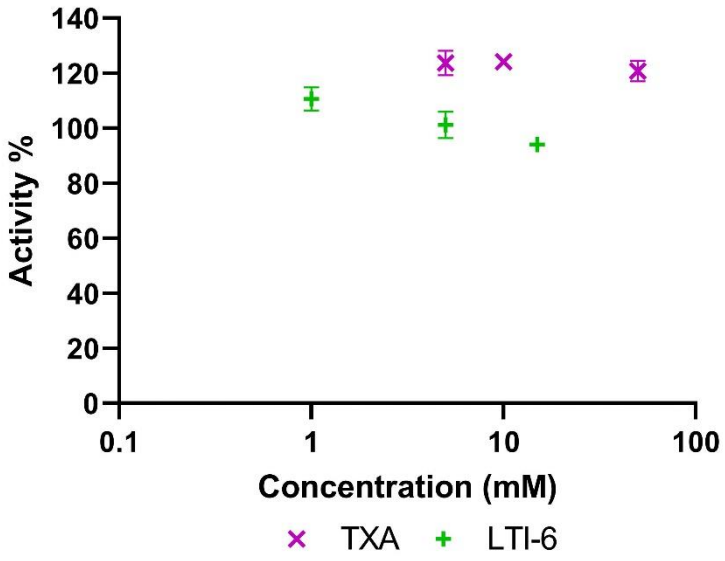

Figure 23. Dose-response curve of TXA and LTI-6 in a tPA purified system. LTI-6 was studied at lower concentrations due to a lower solubility. All conditions were tested in triplicate. Error bars indicate standard deviation.

LTI-6 had similar effects than TXA on the catalytic domain of tPA and increasing concentrations of both molecules did not significantly affect the enzymatic activity. The range of activities tested were significantly higher than those which have shown a clear antifibrinolytic activity in biological environments. Hence, the data allowed us to dismiss the hypothesis that LTI-6 acted as a direct inhibitor of tPA.

2.8. Interaction with Lysine Binding Sites (LBS) of plasminogen

Lysine analogues such as TXA and EACA inhibit fibrinolysis by competitively interacting with the LBS of plasminogen, which reduces its binding capacity to fibrin and therefore its activation

rate into plasmin. To test the hypothesis that LTI-6 was acting through the same mechanism, both TXA and LTI-6 were assessed in a plasminogen-tPA purified system.

Although lysine analogues, as mentioned, are well-known inhibitors of the activation of plasminogen into plasmin, this effect is only true in the presence of fibrin. When fibrin is not present, the opposite effect is observed. The interaction of lysine analogues with the kringle domains of plasminogen triggers a conformational relaxation which facilitates its activation into plasmin[137–139]. This phenomenon becomes irrelevant in the presence of a fibrin clot, since the colocalization of tPA and plasminogen on the surface of the clot becomes the governing mechanism of activation, which occurs at a much faster rate than in the absence of fibrin. However, when studied in a purified system, an increase in plasminogen activation can be attributed to the interaction with LBS in the Kringle domains.

We evaluated different concentrations of TXA and LTI-6 in purified assays with tPA, plasminogen, and a specific substrate that interacts with plasmin releasing a chromophore (Figure 24). Results suggested that, in the absence of fibrin, LTI-6 and TXA were both able to accelerate the conversion of plasminogen into plasmin. For LTI-6, the concentration of 10 μM caused absorbance values to increase faster than the positive control. Furthermore, 1 μM of the same compound generated a moderate raise in the plasminogen activation, whereas concentrations of 0.1 μM or lower did not differ from the control. Regarding TXA, the same effect was observed, but at higher concentrations. At 50 μM a moderate increase in activity was observed, which was progressively more significant at 100, 200 and 1000 μM.

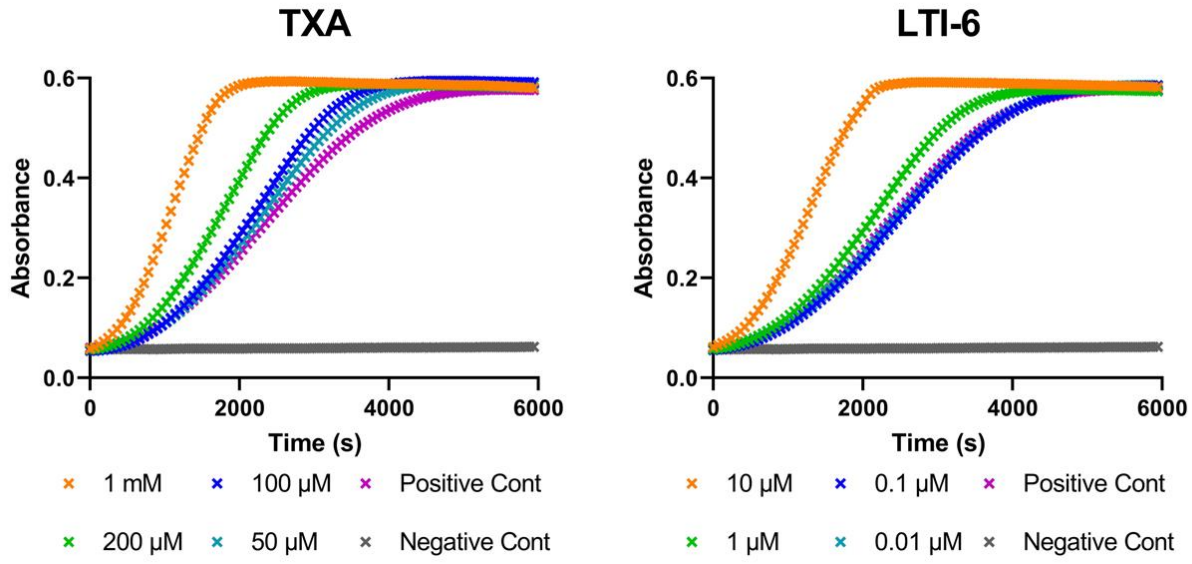

Figure 24. Plasminogen activation by tPA in the presence of different concentrations of TXA and LTI-6. Increase of absorbance correlates with Plasmin formation.

Dose-response curves were calculated using the slopes of the linear range of each curve. The relative increase in activity vs concentration was plotted in this case. Data revealed that LTI-6, as well as TXA, increased the activation rate of plasminogen in a dose-response manner in the absence of fibrin. These findings were consistent with other studies performed for lysine analogues without the presence of fibrin. The dose-response curves show that LTI-6 increased the enzymatic activity at lower concentrations than TXA, therefore indicating a higher affinity towards the target.

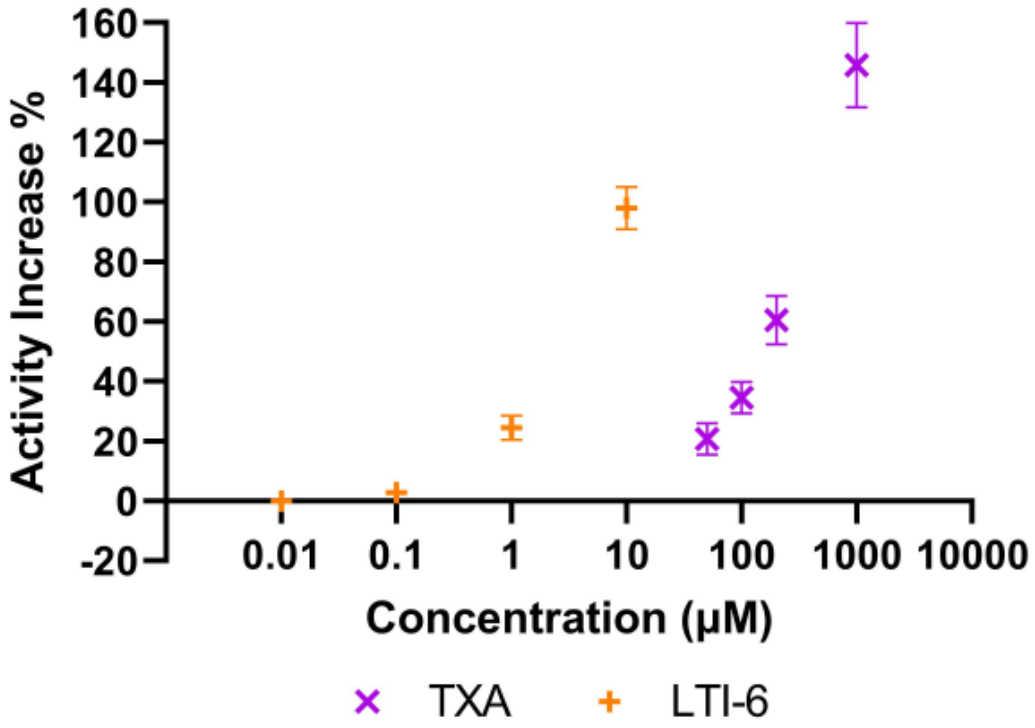

Figure 25. Dose-response curves for TXA and LTI-6 in a purified assay of tPA and plasminogen. The % increase of plasminogen activation relative to the control was plotted. All conditions were tested in triplicate. Error bars indicate standard deviation.

Table 2 details the concentration at which each compound increased plasminogen conversion by 50% in comparison to the control, presented as the EC_{50}. TXA required a concentration of 157 μM to achieve this activity increase, whereas LTI-6 achieved it at 3.6 μM. Therefore, our assays showed more than a 30-fold improvement in activity of LTI-6 over TXA.

Table 2. Concentration values for a 50% increase in plasminogen conversion for TXA and LTI-6 in a plasminogen-tPA purified system. The concentration values of the 50% increase were defined as the concentration at which each compound enhanced tPA's activity by 50%.

Compound	EC_{50} (µM)
TXA	157
LTI-6	3.6

These results validate the hypothesis that LTI-6 shares the same mechanism of action as TXA and other lysine analogues. This implies that LTI-6 binds to the LBS of the Kringle domains of plasminogen and therefore inhibits its conversion to plasmin by displacing plasminogen from the fibrin surface. Furthermore, results from this plasminogen-tPA assay in the absence of fibrin suggest that LTI-6 has a higher affinity for the LBS of plasminogen than TXA.

2.9. Chapter conclusions

The results of this chapter allowed to derive three main conclusions. The first conclusion is that LTI-6 has no noticeable effect on coagulation.

The second conclusion is that LTI-6 inhibits the fibrinolytic process. The activity in plasma resulted equivalent to that of TXA, with no statistically significant difference between them. However, the effect on whole blood did show differences. In this case, the lysis of fibrin occurred at a rate 1.5 times faster for TXA that for LTI-6 at the same concentration. Therefore, LTI-6 presents an overall antifibrinolytic potency equal or higher to that of TXA.

Finally, the third conclusion is that LTI-6 inhibits fibrinolysis by interacting with the LBS of plasminogen, in an analogous mechanism to lysine analogues. At micromolar range, LTI-6 increased the rate of activation of plasminogen to plasmin in the absence of fibrin. The

enhancement of plasminogen activation was around 40-fold higher than that of TXA, the most widely used antifibrinolytic drug. A certain inhibition of the active site of plasmin was observed for LTI-6, as well as for TXA. However, this inhibition occurs at the millimolar range for both compounds, at concentrations around 500-fold higher than their therapeutic doses in plasma.

3. Structure-Activity Relationship of family of compounds

3.1. Chapter introduction

As mentioned in the introduction, lysine analogues inhibit fibrinolysis by competitively interacting with the lysine binding sites (LBS) of Kringle domains in Plg. In the previous chapter, the mechanism of LTI-6 was proposed to be homologous to that of TXA, the most widely used lysine analogue nowadays. In order to further improve the activity of LTI-6 many different modifications can be made to its chemical structure. This chapter explains the proposal of a number of chemical modifications, and the subsequent synthesis of the proposed compounds. The activity for all these compounds was then quantified through a reproducible clot lysis assay. In addition, different computational techniques were used to study the interactions of each of the studied compounds with the LBS of Kringle 1 domain, which is the Kringle domain with higher affinity towards lysine analogues. This allowed to study the structure-activity relationship (SAR) of this family of compounds.

Selectivity can be equally important to activity when considering the adequacy of a candidate drug. In this regard, TXA and other recently discovered inhibitors of Plg activation have been proven to possess a certain undesired affinity towards the $GABA_A$ receptor. Such interaction is related to some of the secondary effects caused by TXA at high doses, such as the occurrence of seizures during cardiac surgery. Therefore, the goal of this chapter is also to study computationally the possible interaction of the developed compounds with $GABA_A$ receptor.

3.2. Structure modifications

A number of structural modifications were proposed in order to determine their effect on activity, as well as to further study the structure-activity relationship of this family of compounds (Figure 26).

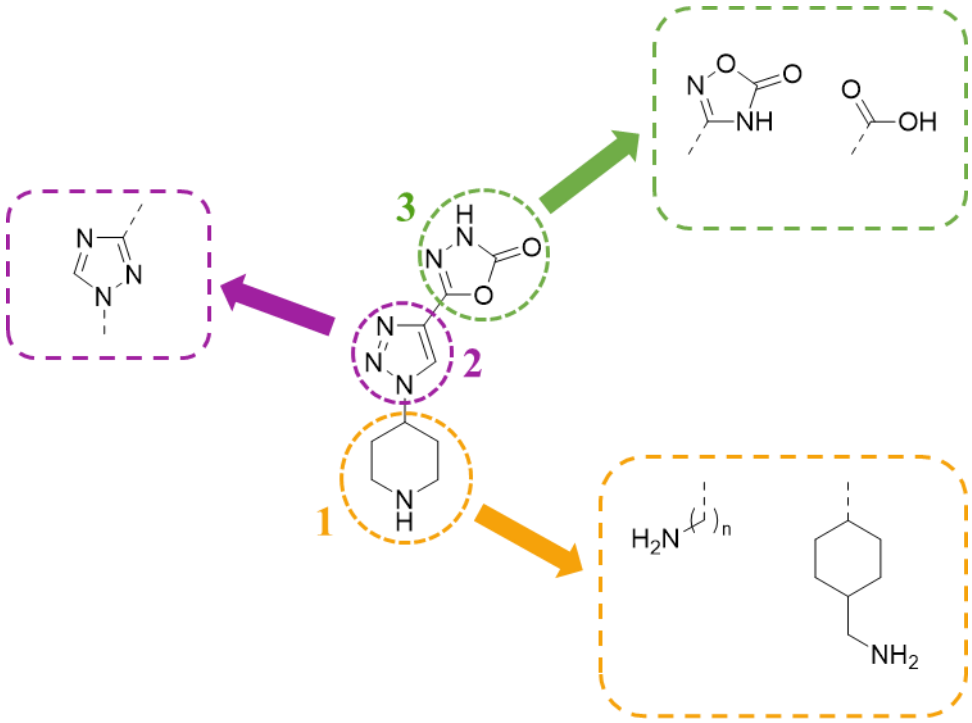

Figure 26. Chemical modifications proposed for the different moieties of the initial hit molecule LTI-6: (1) piperidine, (2) 1,2,3-triazole ring, and (3) 1,3,4-oxadiazolone.

Considering that LTI-6 combines three different key moieties (Figure 26), specific chemical modifications were proposed for each of them to further study their role on the overall activity. Primary amines with different chain lengths (n=2-4) were proposed instead of the piperidine ring. These changes allowed to confer a certain flexibility to basic region of the molecule, as well as to test different distances between the triazole and the amine. A cyclohexyl methanamine was also proposed, since it is the moiety present in tranexamic acid. A 1,2,4-triazole ring instead of the original 1,2,3-triazol was also proposed, as well as eliminating the moiety altogether. Finally, the 1,3,4-oxadiazolone ring was proposed to be substituted for a carboxyl group and a 1,2,4-oxadiazolone ring. All these modifications were then combined into a total of 11 compounds which were studied *in vitro* and *in silico* (Figure 27).

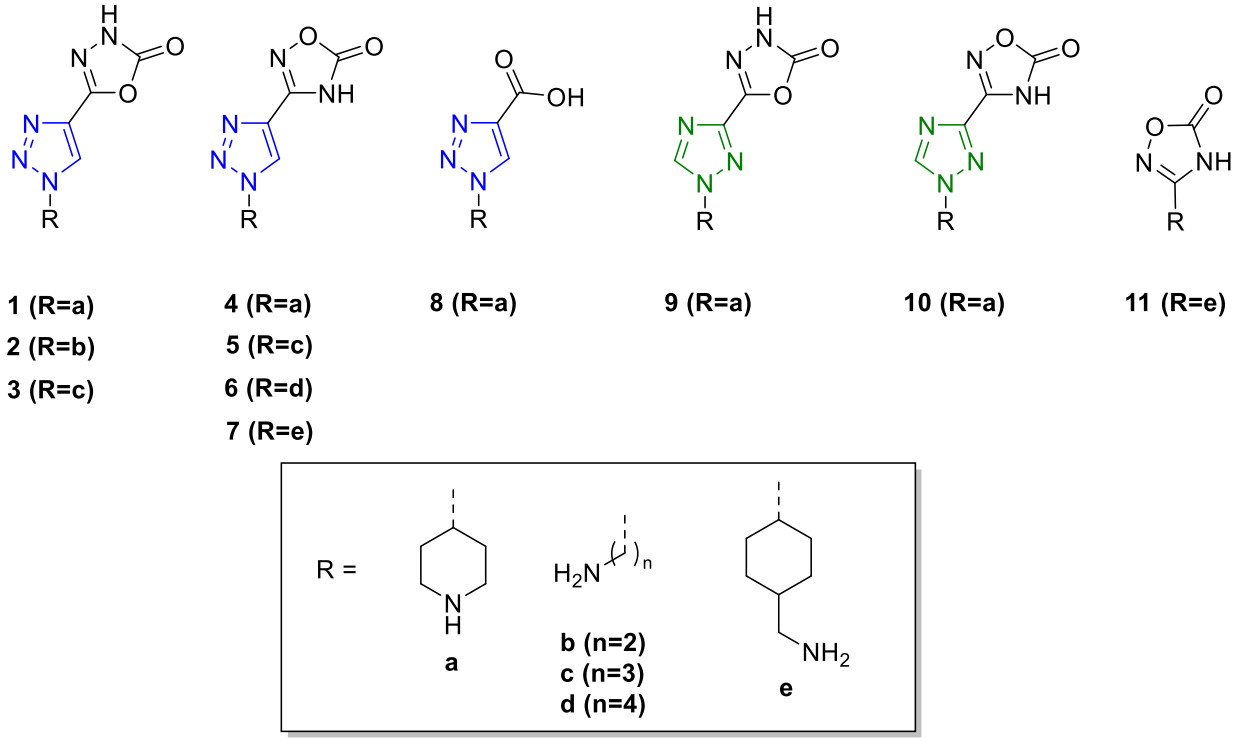

Figure 27. Proposed compounds to study their activity and structure-activity relationship.

3.3. Synthetic routes

After a bibliographic search of all the proposed compounds, compound **8** was found to be available from commercial sources. The remaining molecules, however, were not available and therefore were synthesized for the purpose of this work. Among them, the synthesis of compound **4** had been previously described by Sangshetti et al.[136] as an intermediate of an antifungal agent. All other synthesized molecules were not described in the literature.

Two different types of triazole derivatives were synthesized: 1,2,3-triazole and 1,2,4-triazole. Position 4 (1,2,3-disposition) or 3 (1,2,4-disposition) were substituted for a 1,3,4-oxadiazolone (**1-3**, **10**) or a 1,2,4-oxadiazolone (**4-7**, **10**). 1,2,4-triazole derivatives were only synthesized with piperidine as their terminal amine. In the case of the 1,2,3-triazole family, however, other different

terminal amines were used, as well as piperidine. An additional compound with no presence of triazole (**11**) was synthesized combining a 1,2,4-oxadiazolone and a cyclohexyl methanamine.

3.3.1. Derivatives of 1,2,3-triazole

1,2,3-triazole derivatives were synthesized by a Huisgen cycloaddition catalyzed by copper (I), in which the 1,3-dipolar azide group was reacted with a dipolarophile, ethyl propiolate. Such reaction between the alkyne and azide lead to the formation the 1,2,3-triazole ring. The presence of copper (I) as catalyst allowed for a regioselective reaction in which only the 1,4-disubstituted 1,2,3-triazole compound was synthesized. The mechanism of this reaction, described by Worell et al. in 2013[140], suggests that two equivalents of copper participate in activating the reactivity of each alkyne molecule towards azide. Such activated alkyne consists in a copper acetylide bearing an additional π-bound copper atom. This intermediate then coordinates the azide as shown in Figure 28, forming a six-membered copper metallacycle. Ring contraction to a triazolyl-copper derivative is followed by protonolysis, which delivers the final triazole product and closes the catalytic cycle.

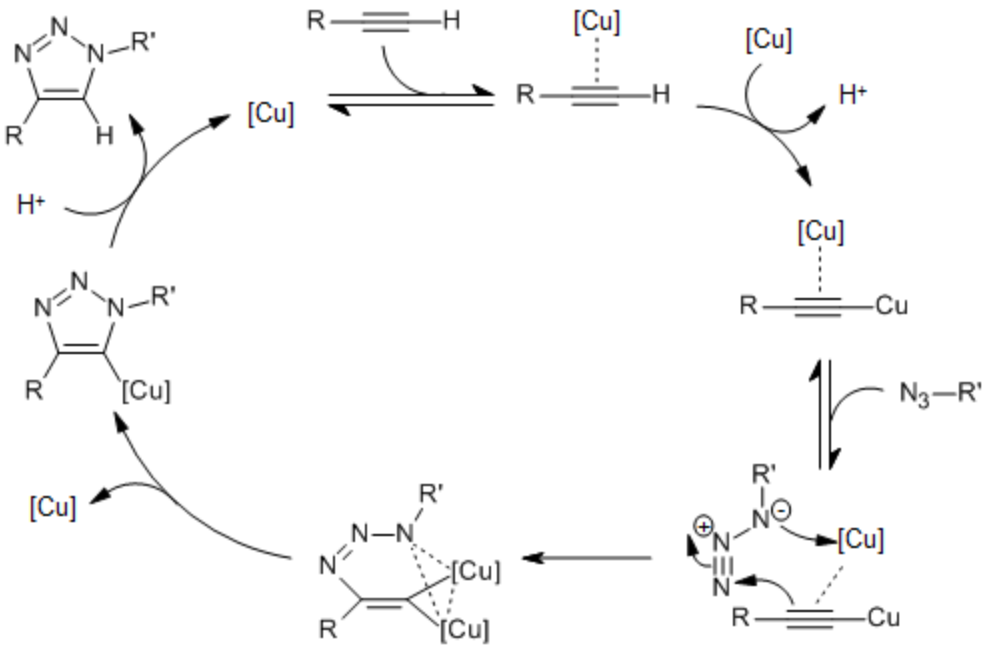

Figure 28. Mechanism of copper (I) catalyzed azide-alkyne cycloaddition.[140]

Their azide precursor was obtained through two different methods. For compounds based on linear amines, their respective bromide derivatives were transformed directly into azide by treatment with NaN_3 (Scheme 1). For the piperidine and cyclohexyl methanamine derivatives, hydroxyl groups were activated into mesylates by treatment with methanesulfonyl chloride in DCM. Subsequently, the mesylate groups were converted into azide by treatment with NaN_3.

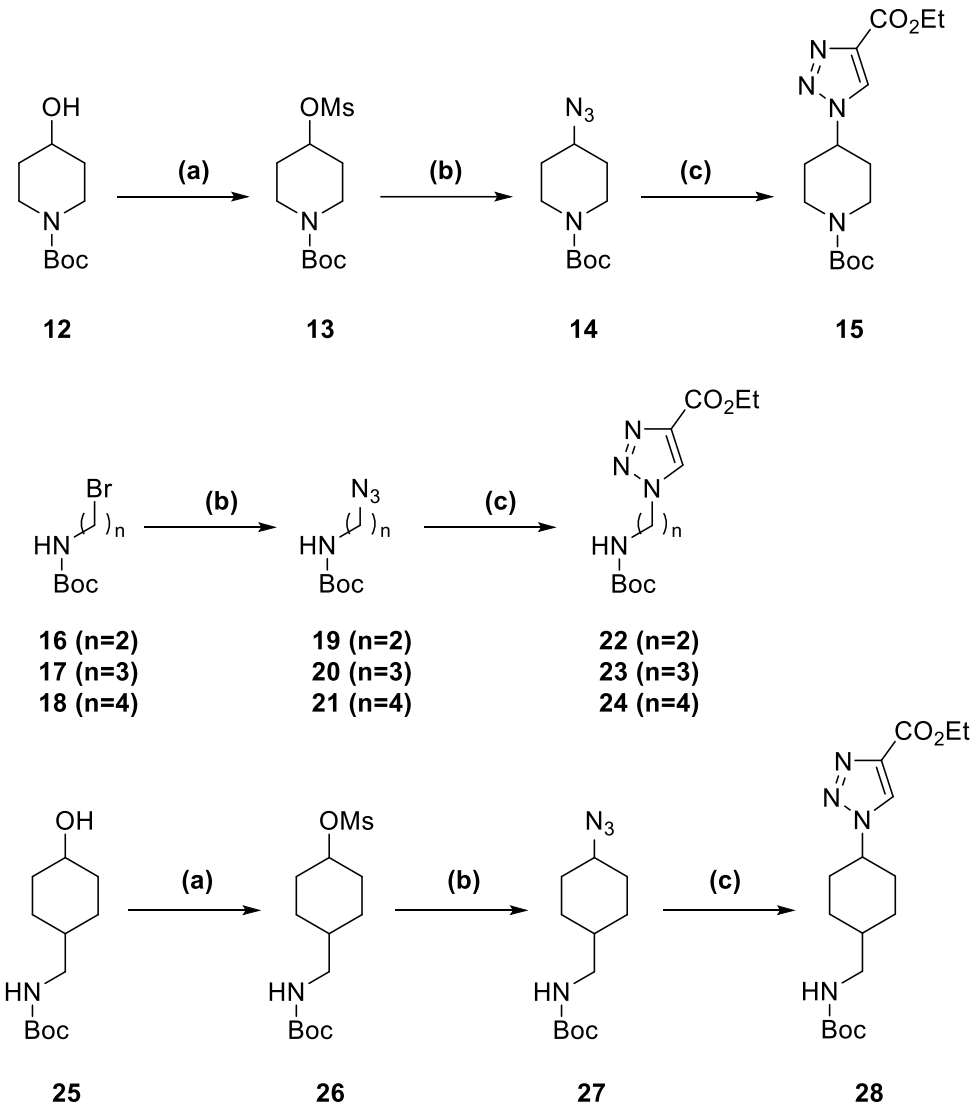

Scheme 1. 1,2,3-triazole formation. (a) TEA, MsCl, DCM, 0-5 °C to 23 °C, 2 h. (b) NaN_3, DMF, 80 °C, 8 h. (c) Ethyl propiolate, CuI, ACN, 23 °C, 12 h.

To obtain the final 1,3,4-oxadiazolone derivatives (compounds **1**, **2**, **3**), ester groups were first transformed into the corresponding hydrazides by treatment with hydrazine hydrate in refluxing *n*-butanol (Scheme 2). This methodology was adapted from a similar reaction described by Jansen et al.[112] The hydrazide served as the precursor to form the oxadiazolone ring. Alternatively, to obtain the 1,2,4-oxadiazolone derivatives (compounds **4**, **5**, **6**, **7**), the methodology was inspired in

the work by Sangshetti et al.[136] In this case, the ester groups were transformed into their corresponding amide by treatment with methanolic ammonia at room temperature. The amide was later dehydrated in the presence of TFAA to provide the corresponding nitrile. Subsequent reflux with hydroxylamine hydrochloride and sodium bicarbonate in MeOH yielded the corresponding hydroxylamine (Scheme 2), precursor of the oxadiazolone ring. Finally, the oxadiazolone ring in both cases was formed by reaction with CDI, using TEA or DBU as the base. Final compounds (Figure 27) were always obtained in the form of hydrochloride salts, after treating their protected precursors with methanolic HCl at room temperature for 2 h.

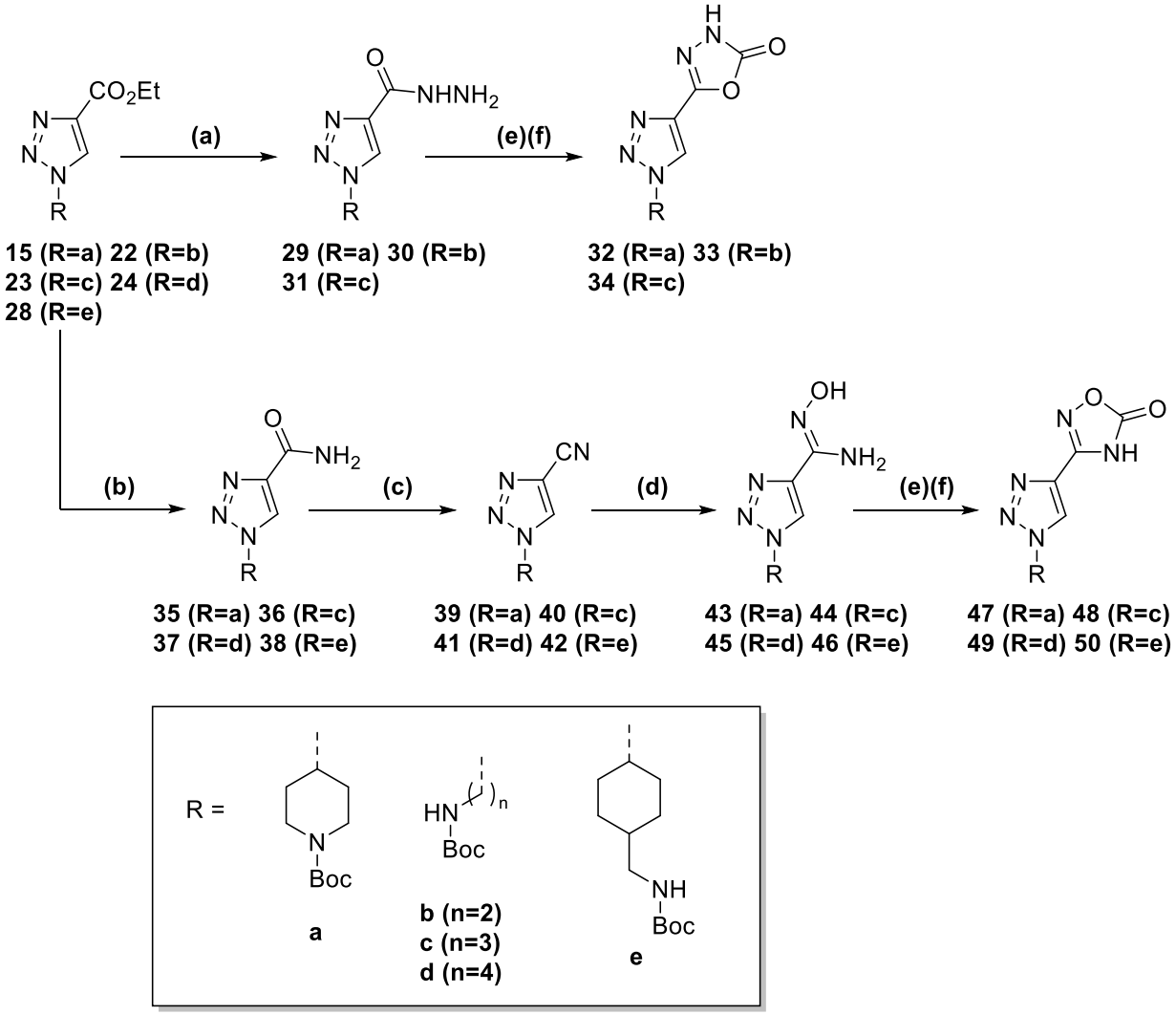

Scheme 2. Oxadiazolone precursors synthesis for 1,2,3-triazole derivatives. (a) Hydrazine hydrate, *n*-butanol, reflux, 3 h. (b) NH_3, MeOH, 23 °C, 12 h. (c) TEA, TFAA, DCM, 0-5 °C to 23 °C, 5 h. (d) $NH_2OH \cdot HCl$, $NaHCO_3$, MeOH, reflux, 14 h. (e) CDI, TEA, THF-DMF 10:1, reflux 15 h. (f) CDI, DBU, ACN, reflux, 15 h.

3.3.2. Derivatives of 1,2,4-triazole

For the 1,2,4-triazole derivatives, the ester-triazole compound **51** was obtained through alkylation in DMF at 70 °C during 48 h, using NaH as a base (Scheme 3). The following steps, both for the final 1,3,4-oxadiazolone (compound **9**) and 1,2,4-oxadiazolone derivatives (compound **10**), were identical to the ones described for 1,2,3-triazole derivatives (Scheme 2). Final compounds (Figure 27) were always obtained in the form of hydrochloride salts, after treating their protected precursors with methanolic HCl at room temperature for 2 h.

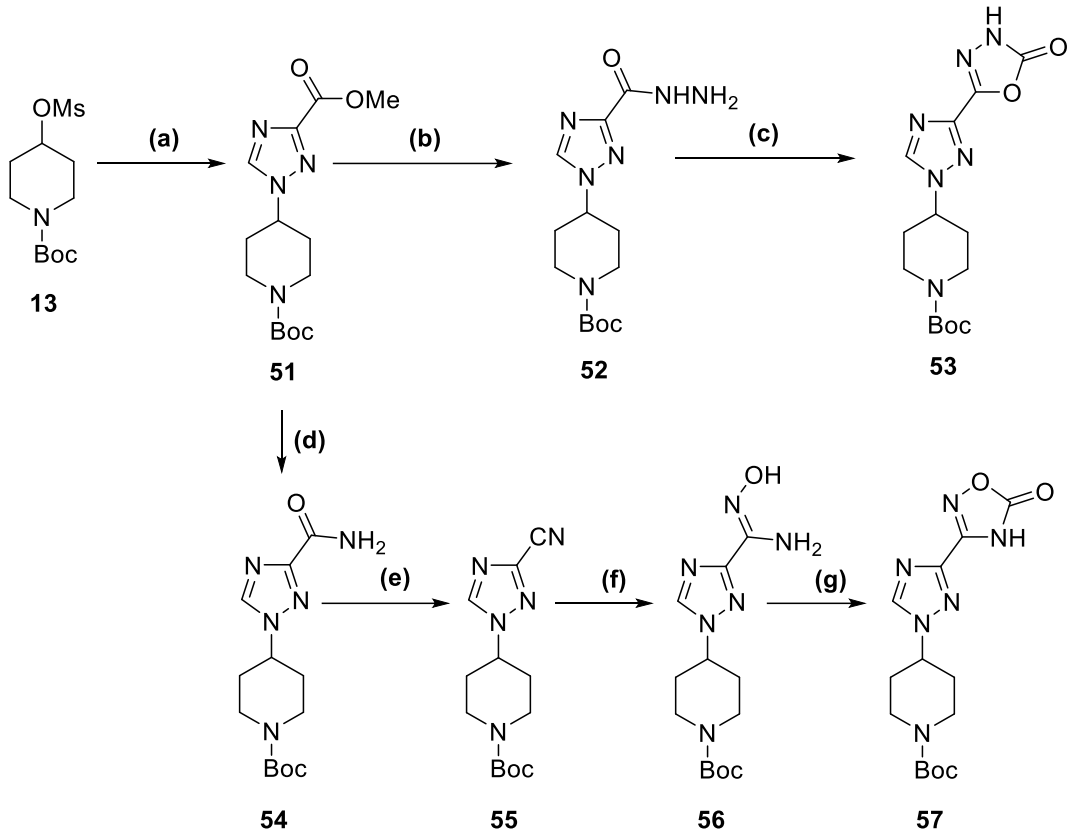

Scheme 3. 1,2,4-triazole derivatives complete synthetic pathway. (a) methyl 1*H*,1,2,4-triazole-3-carboxylate, NaH, DMF, 70 °C, 48 h. (b) Hydrazine hydrate, *n*-butanol, reflux, 3 h. (c) CDI, DBU, ACN, reflux, 15 h. (d) NH3, MeOH, 23 °C, 12 h. (e) TEA, TFAA, DCM, 0-5 °C to 23 °C, 5 h. (f) $NH_2OH{\cdot}HCl$, $NaHCO_3$, MeOH, reflux, 14 h. (g) CDI, TEA, THF-DMF 10:1, reflux 15 h.

3.3.3. Tranexamic acid derivative

Compound **11** was synthesized using tranexamic acid as starting material (Scheme 4). First it was treated with thionyl chloride in ethanol to provide the ester. Subsequently, the terminal amine was protected with a Boc group. The conversion of ester to amide was achieved by treatment of the corresponding ester with methanolic ammonia at 85 °C during 5 days inside an autoclave. The following steps were again identical to those explained for 1,2,3-triazole (Scheme 2) and 1,2,4-

triazole (Scheme 3) derivatives. Final compound **11** was obtained as a hydrochloride salt, after treating its protected precursor with methanolic HCl at room temperature for 2 h.

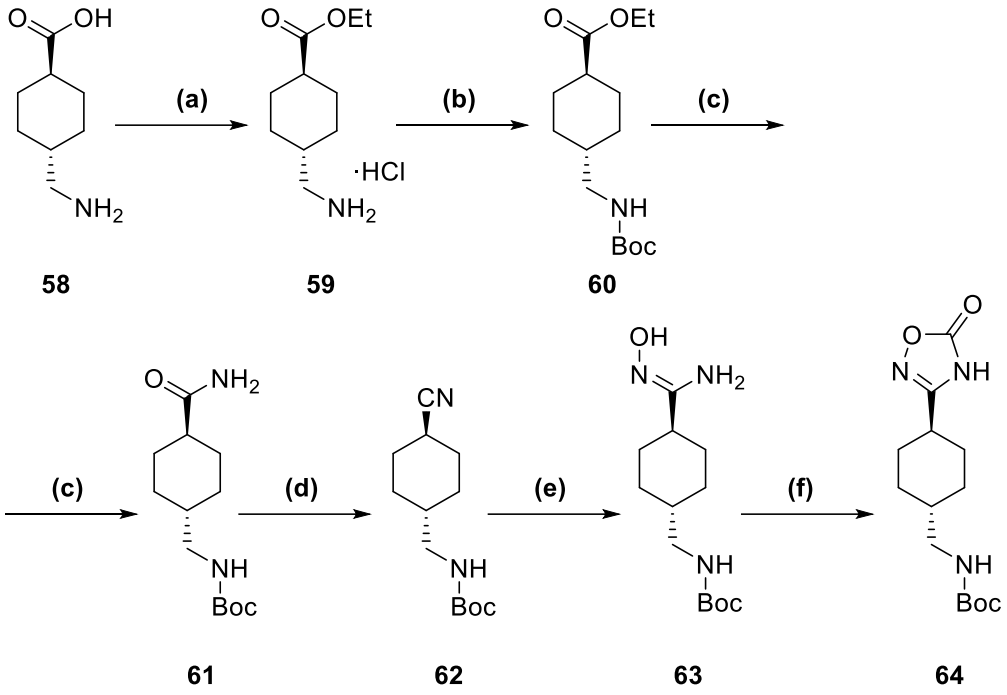

Scheme 4. Tranexamic acid derivative complete synthetic pathway. (a) TsCl, EtOH, reflux, 2 h. (b) Boc_2O, TEA, MeOH, 23 °C, 8 h. (c) NH_3, MeOH, 85 °C (sealed vial), 5 days. (d) TEA, TFAA, DCM, 0-5 °C to 23 °C, 5 h. (e) $NH_2OH{\cdot}HCl$, $NaHCO_3$, MeOH, reflux, 14 h. (f) CDI, DBU, ACN, reflux, 15 h.

3.4. Chemical reactions

3.4.1. Azide derivative synthesis

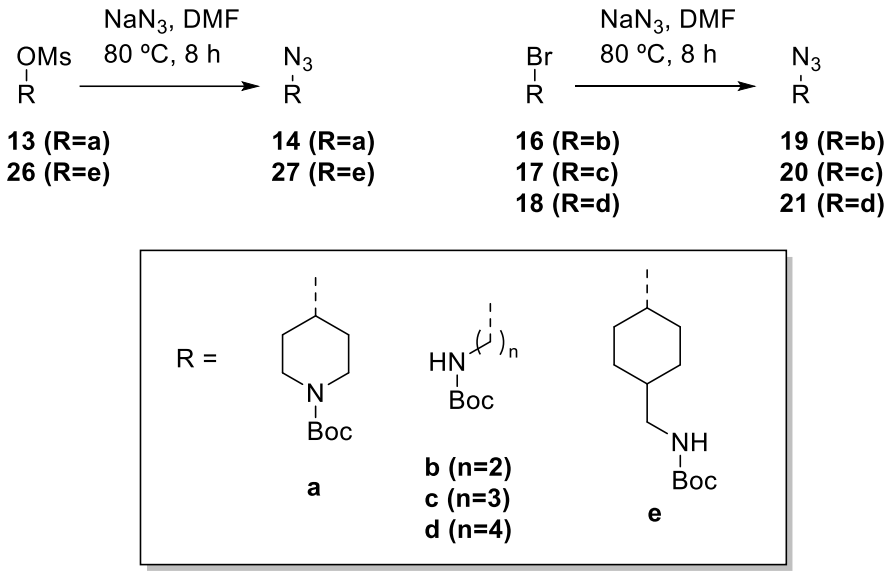

Scheme 5. Synthesis of azide derivatives through nucleophilic substitution.

Azide derivatives were obtained by nucleophilic substitution of two different leaving groups, a mesylate group or a bromide group. In both cases, the substitution was accomplished by refluxing the precursor in DMF at 80 °C for 8 hours[136]. Reaction completion was checked through ^{1}H-NMR. When substituting a mesylate group (Figure 29), the absence of its characteristic singlet (3H) was observed, proving that the leaving group was no longer present. When substituting bromide, the displacement of certain signals of the corresponding carbon chain was used to determine the reaction success (Figure 30). The reaction products were obtained in all cases with yields in the range of 85-95 %.

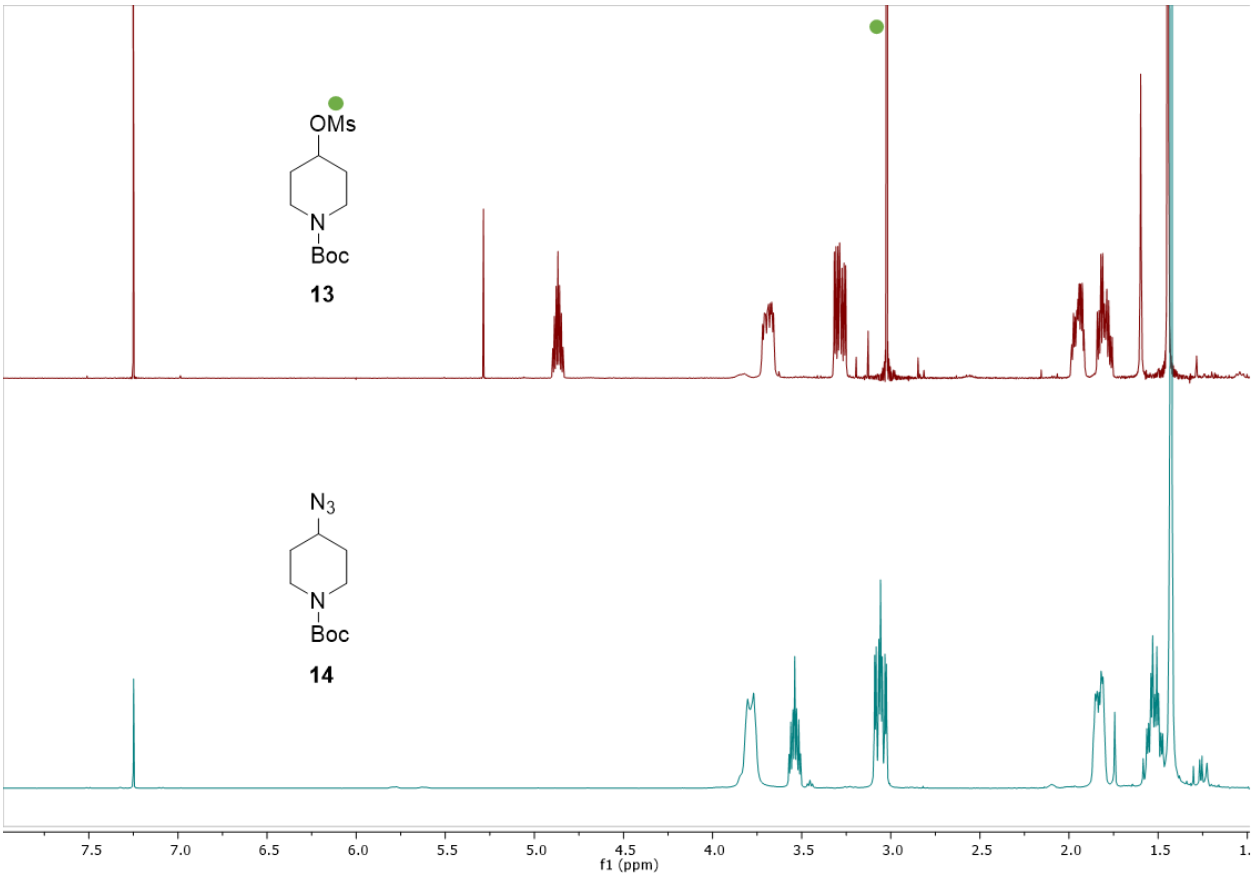

Figure 29. Mesylate group substitution into azide, validated through ^{1}H-NMR. A signal at approximately 3.0 ppm corresponding to the mesylate group disappeared, confirming its substitution.

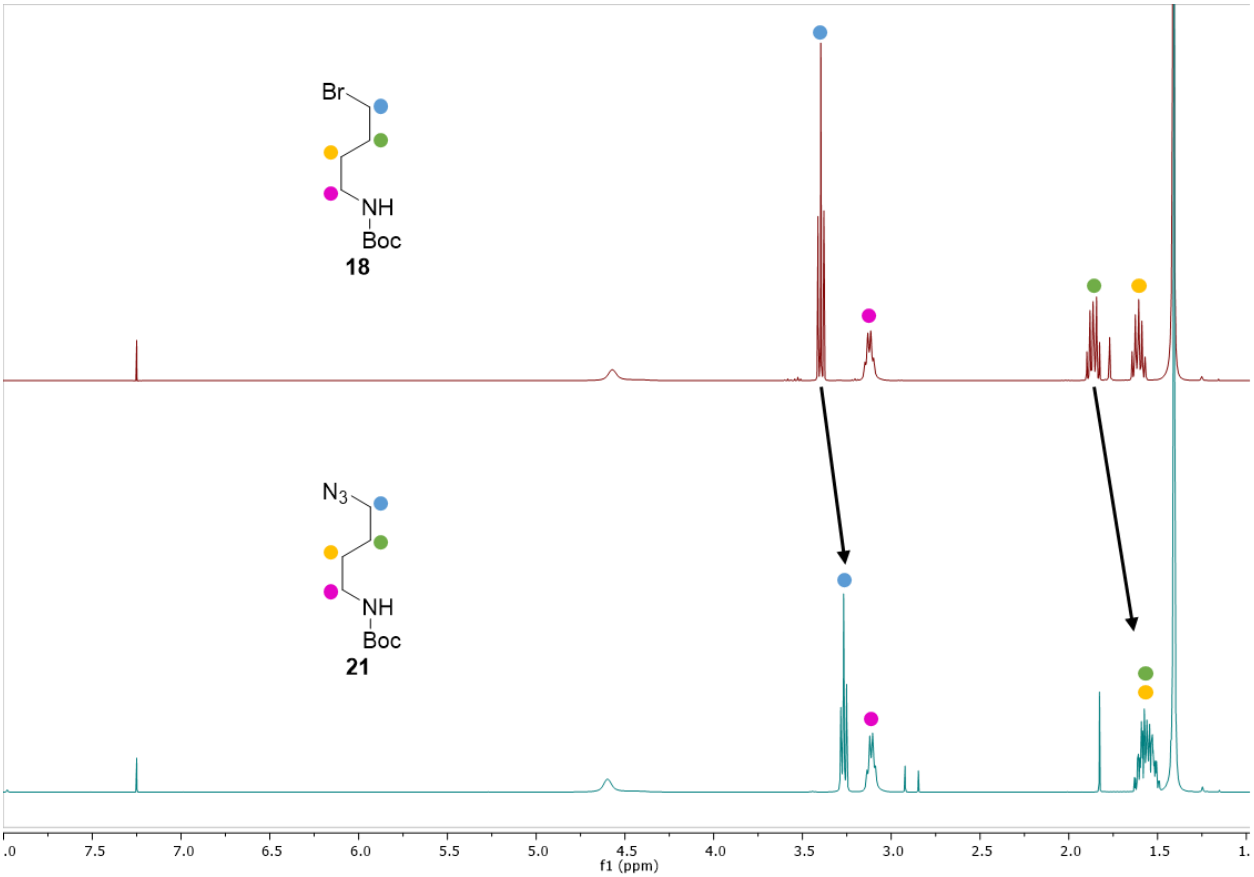

Figure 30. Bromide group substitution into azide. ^{1}H-NMR signals of one or more methylene groups of the linear chains were displaced due to the substitution.

3.4.2. Triazole (1,2,3) ring formation

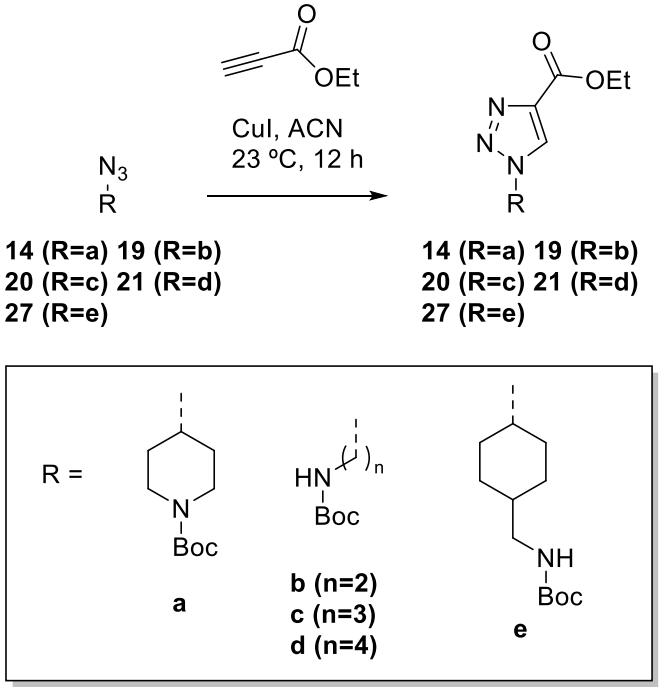

Scheme 6. Formation of the 1,2,3-triazole ring.

The azide group was transformed into 1,2,3-triazole ring by reaction with ethyl propiolate. This reaction was performed in all cases at room temperature for 12 hours, using ACN as solvent. A very important element of this reaction was Cu(I), which acted as catalyst. In our case, CuI was used as the source of Cu(I). Both the azide derivative and ethyl propiolate were added at an equimolar rate to avoid an excess of propiolate and therefore facilitate the subsequent product separation[136]. The formation of a 1,2,3-triazole ring was verified through 1H-NMR (Figure 31), which included the presence of a singlet (1H) at approximately 8.1 ppm. Additionally, the presence of a quadruplet (2H) and a triplet (3H), corresponding to the ethyl ester, also confirmed the success of the reaction.

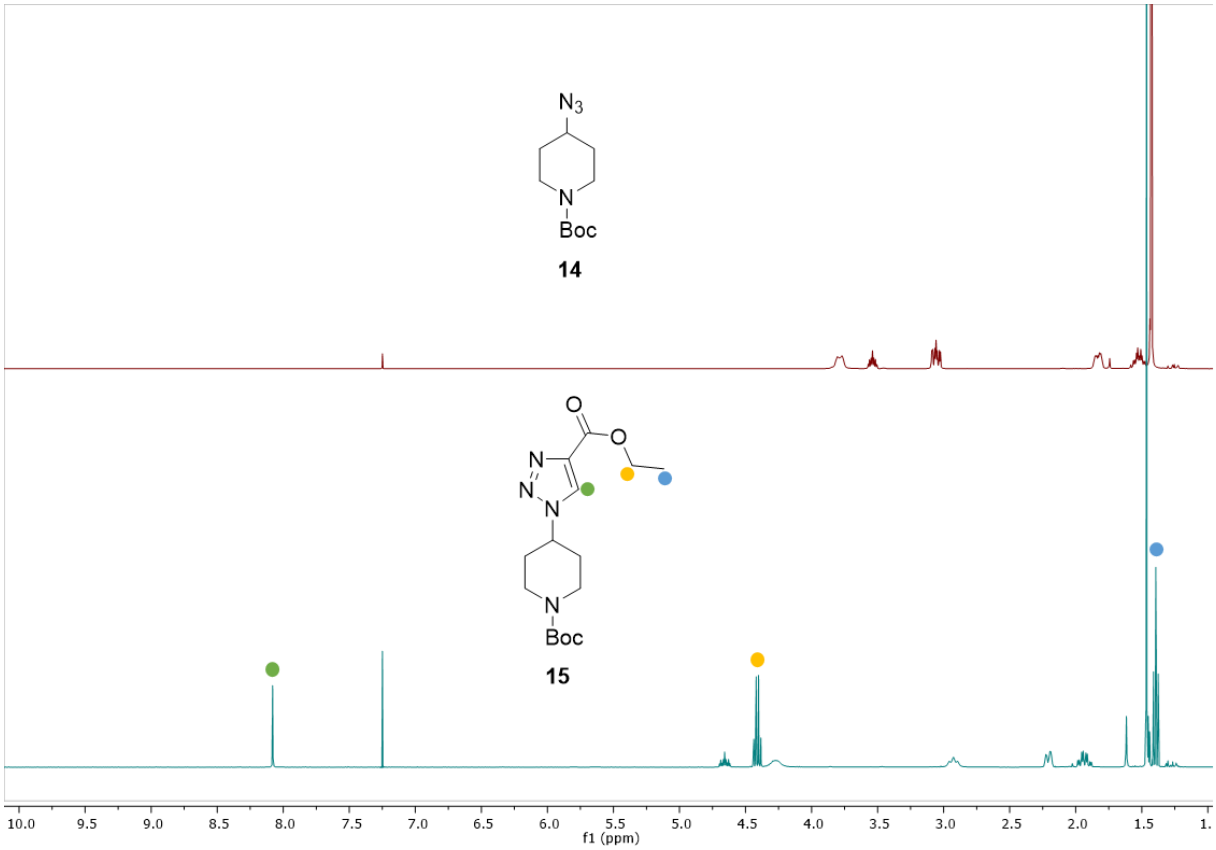

Figure 31. Formation of the 1,2,3-triazole ring was validated by ^{1}H-NMR, with $CDCl_3$ as solvent. The singlet (1H) at approximately 8.1 ppm corresponds to the only hydrogen atom present in the triazole moiety.

3.4.3. Ester-triazole (1,2,4) compound synthesis

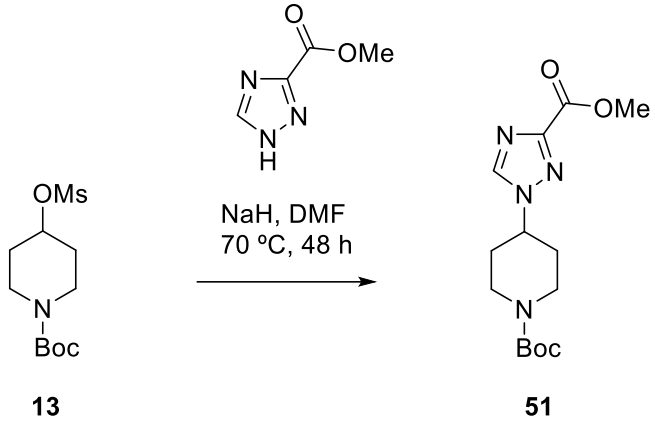

Scheme 7. Synthesis of 1,2,4-triazole derivative through alkylation.

To obtain the ester-triazole derivative in the case of 1,2,4-triazoles, the mesylate-activated piperidine compound was linked directly to the commercially available 1*H*-1,2,4-triazole-3-carboxylate, through an alkylation reaction. To do so, the triazole compound was first mixed in DMF with NaH, which acted as the base, during 1 h at 70 °C. The mesylate-piperidine compound was then added to the mixture at a 90% molar rate compared to the activated triazole. The reaction was then allowed to progress at 70 °C for 48 h. After the subsequent purification through chromatography, compound **51** was obtained in 25% yield.

Reaction completion was verified through ^{1}H-NMR (Figure 32). The identifying singlet (3H) of the mesylate group disappeared, while two new signals appeared: a singlet (1H) for the triazole hydrogen, and another singlet (3H) for the methyl ester.

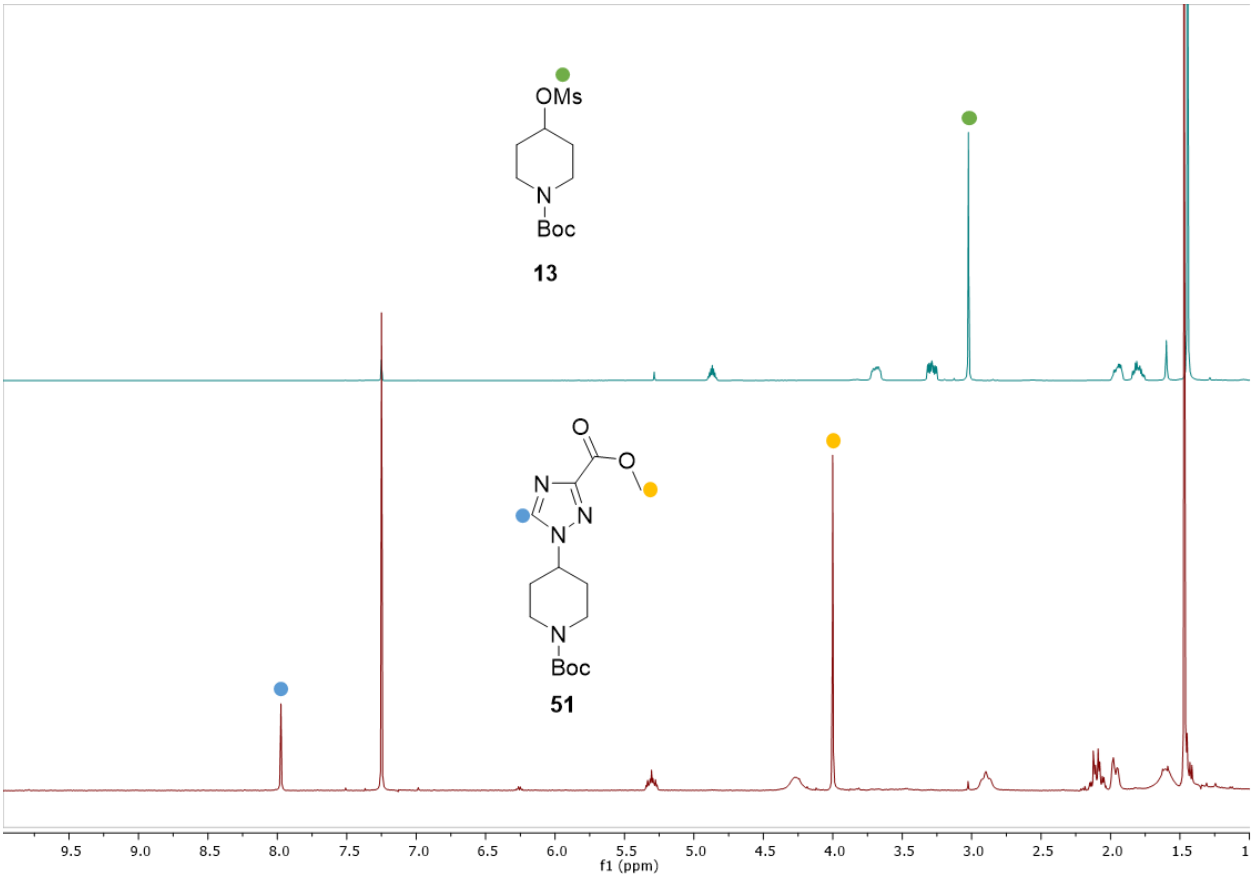

Figure 32. ^{1}H-NMR (in $CDCl_3$) of 1,2,4-triazole compound formation through alkylation. The singlet (3H) at 3.0 ppm, corresponding to the mesylate group, was not present for the triazole product. Additionally, a new singlet (1H) appeared at 8.0 ppm, which represented the hydrogen atom of the triazole ring. In addition, a singlet (3H) representing the methyl ester appeared at 4.0 ppm.

3.4.4. Hydrazide derivative synthesis

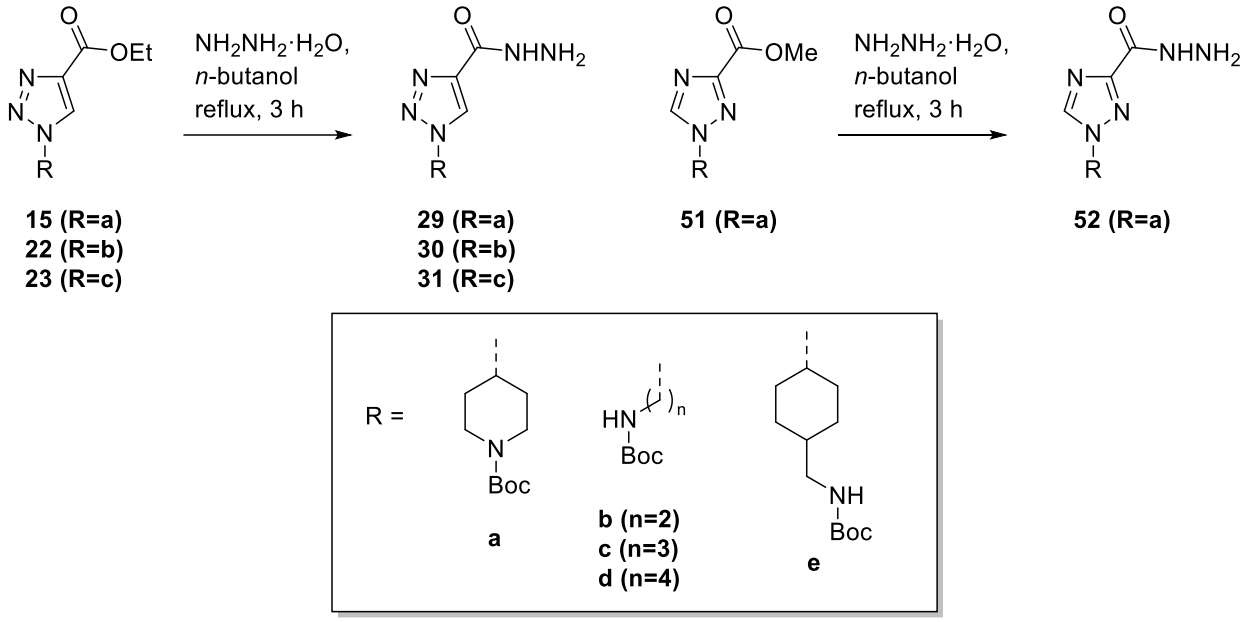

Scheme 8. Hydrazide derivative synthesis for all triazole compounds.

To obtain the hydrazide-triazole derivatives, the methyl or ethyl ester precursors we treated with hydrazine hydrate. The reaction was performed in *n*-butanol, and the mixture was refluxed (~118 °C) for 3 h. As a result, the ethoxy or methoxy group was substituted for a hydrazine moiety. After the solvent evaporation and further washing of the obtained product, reaction completion was monitored through ^{1}H-NMR. As a result of the reaction (Figure 33), the identifying quadruplet (2H) and triplet (3H) corresponding to the ethyl ester disappeared. The newly formed signals corresponding to the hydrazide hydrogen atoms were very broad, and often not easy to identify. However, the absence of ester moiety indicates the successful transformation into the corresponding hydrazide derivative.

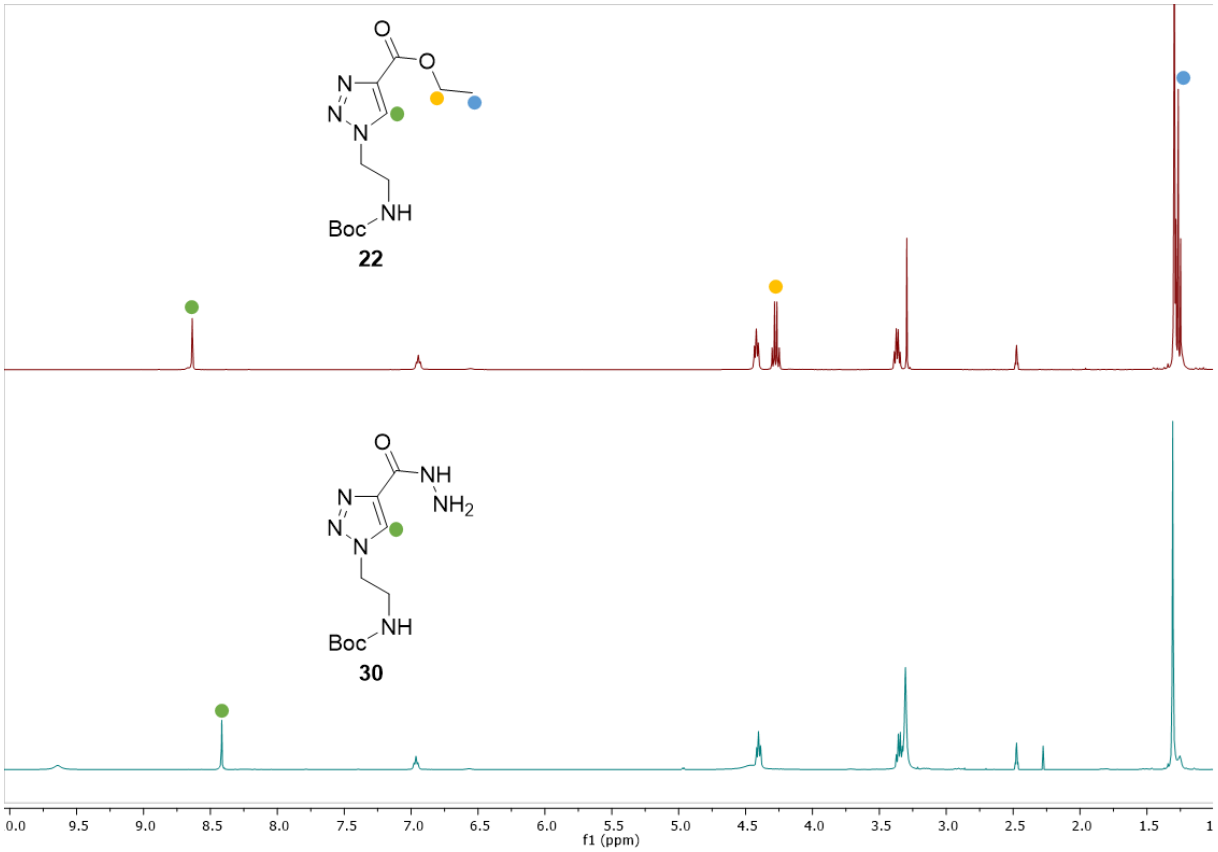

Figure 33. ^{1}H-NMR d_6-DMSO of an example of hydrazide formation from an ethyl ester precursor. The removal of the ethoxy moiety was visualized by the absence of its two identifying signals, a quadruplet (2H) for the methylene and a triplet (3H) for the methyl group.

3.4.5. Carboxamide derivative synthesis

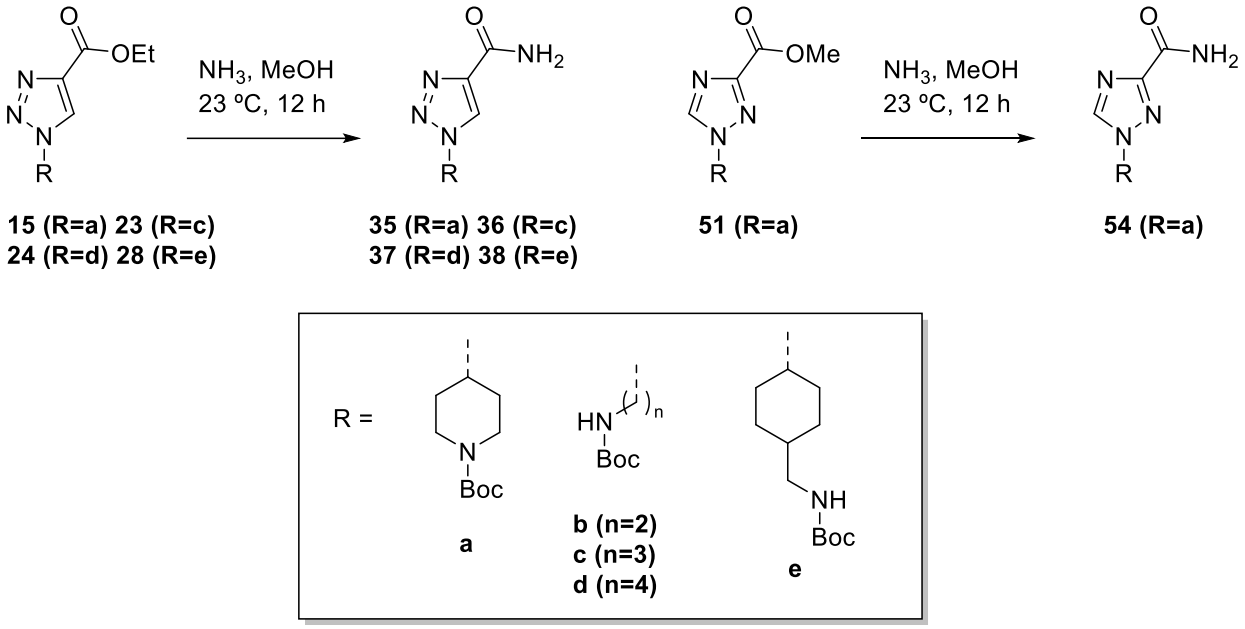

Scheme 9. Synthesis of carboxamide derivatives for triazole compounds.

To obtain the carboxamide-triazole derivatives, the ester precursors were treated with ammonia in methanol. The mixture was stirred for 12 hours at room temperature. Due to the reaction, the ethoxy or methoxy groups were substituted for an amino group. The removal of the ester group was validated, as in the hydrazide formation reaction, through ^{1}H-NMR (Figure 34). The newly formed signals corresponding to the amide hydrogen atoms were not always easy to identify. However, the absence of ester moiety indicates the adequate transformation into the corresponding carboxamide derivative.

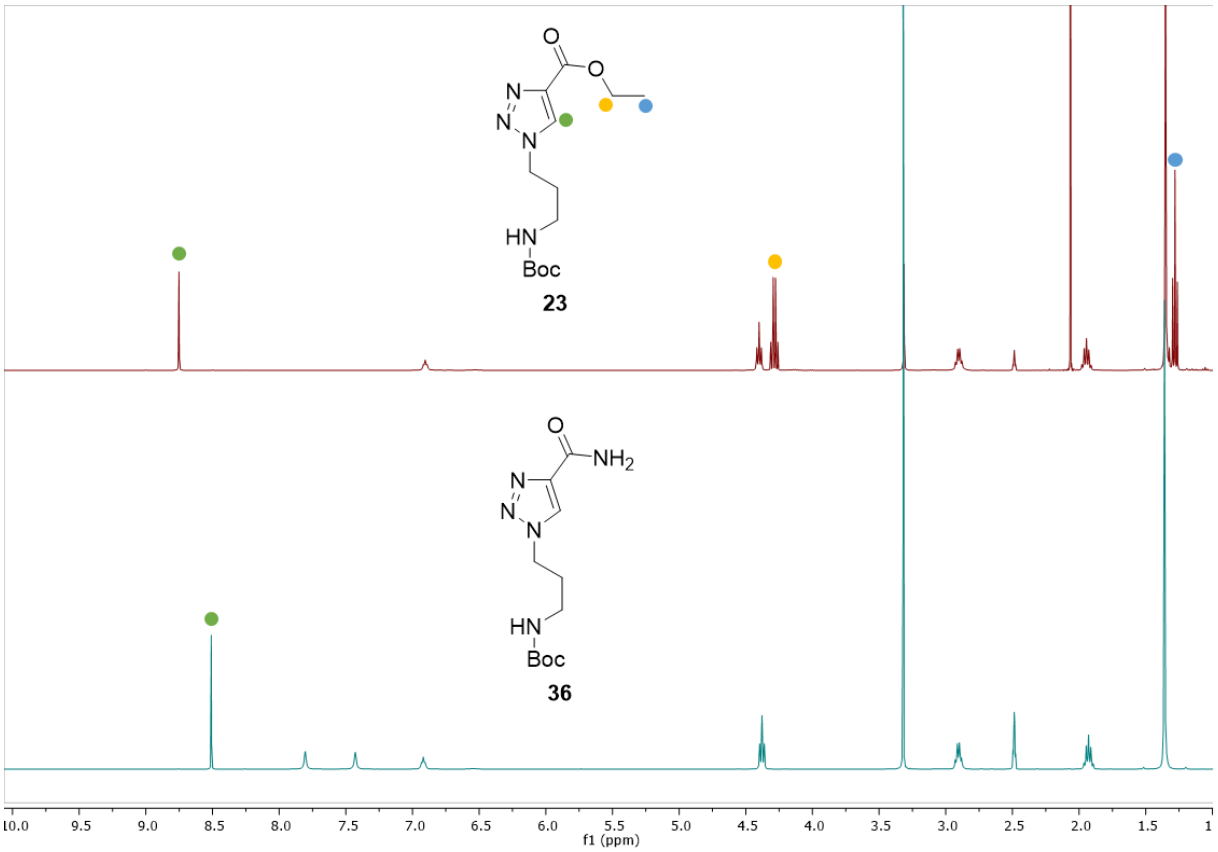

Figure 34. ^{1}H-NMR in d_6-DMSO of an example of amide formation from an ethyl ester precursor. The removal of the ethoxy moiety was visualized by the absence of its two specific signals, one for the methylene and another for the methyl group.

3.4.6. Nitrile derivative synthesis

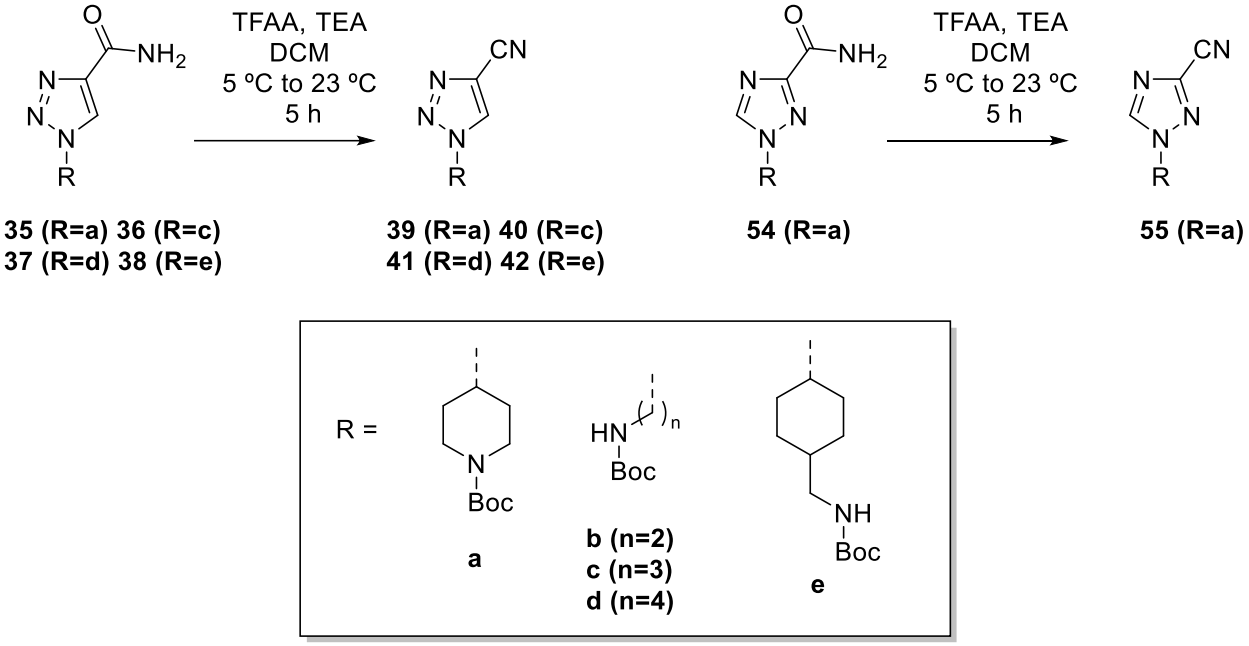

Scheme 10. Nitrile formation reaction by dehydration of amide.

The carboxamide precursors were transformed into nitrile derivatives through treatment with TFAA. After dissolving the precursor in DCM and adding TEA, the mixture was cooled at 0-5 °C. The TFAA, which acted as a dehydrating agent, was added dropwise and then the mixture was warmed to room temperature and then stirred for a total of 5 h. After the necessary extractions, the final product was obtained with a yield higher than 85% in all cases. The reaction progress was followed by ^{1}H-NMR and IR spectroscopy. ^{1}H-NMR (Figure 35) proved that the signal or signals corresponding to the carboxamide (when clearly identifiable) had disappeared. In addition, the singlet (1H) corresponding to the triazole ring was displaced when compared to the carboxamide precursor. However, the presence of a nitrile group was validated through IR spectroscopy (Figure 36). As seen in the spectra, the formation of the characteristic triple bond between C and N caused the presence of a band at approximately 2250 cm^{-1}.

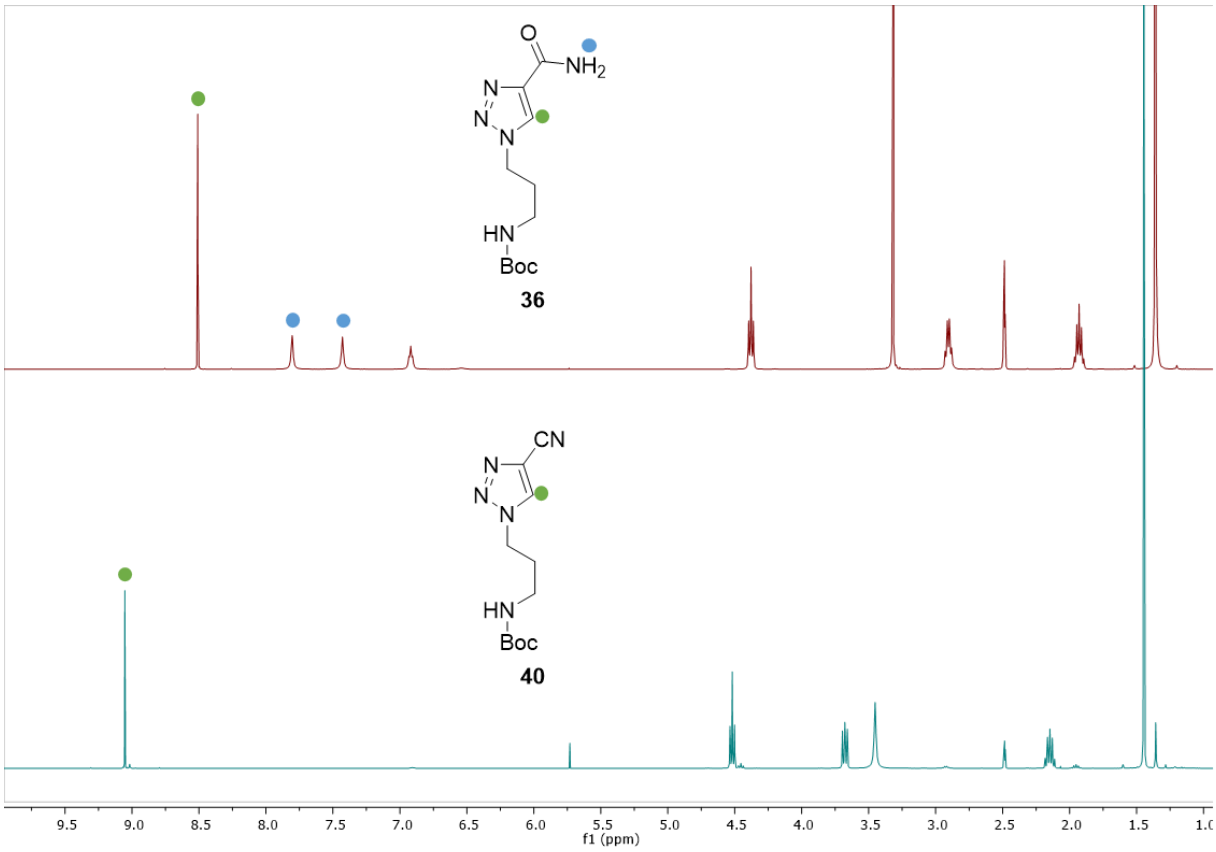

Figure 35. ^{1}H-NMR in d_6-DMSO of an example of amide dehydration into nitrile. ^{1}H-NMR revealed the absence of the amide protons, which were initially represented by two separate singlets (1H each).

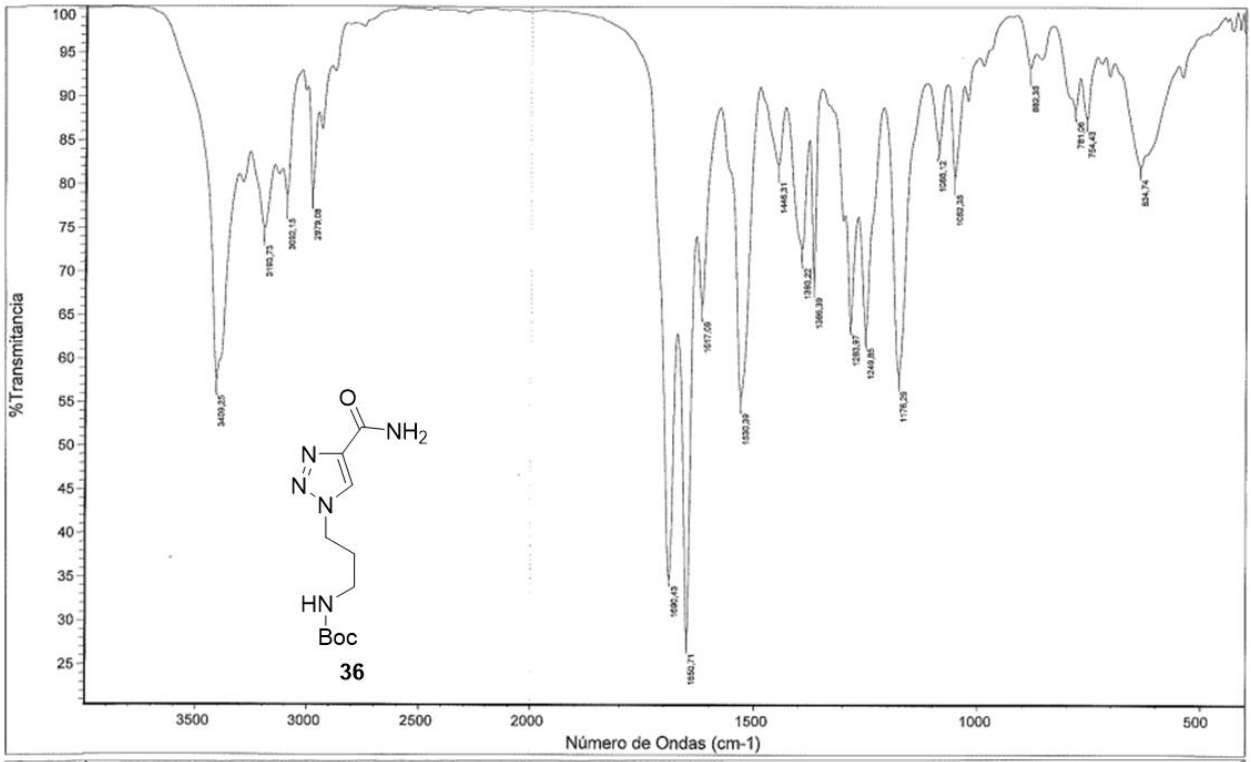
%Transmitancia
Número de Ondas (cm-1)
O
NH2
N
N
N
HN
Boc
36

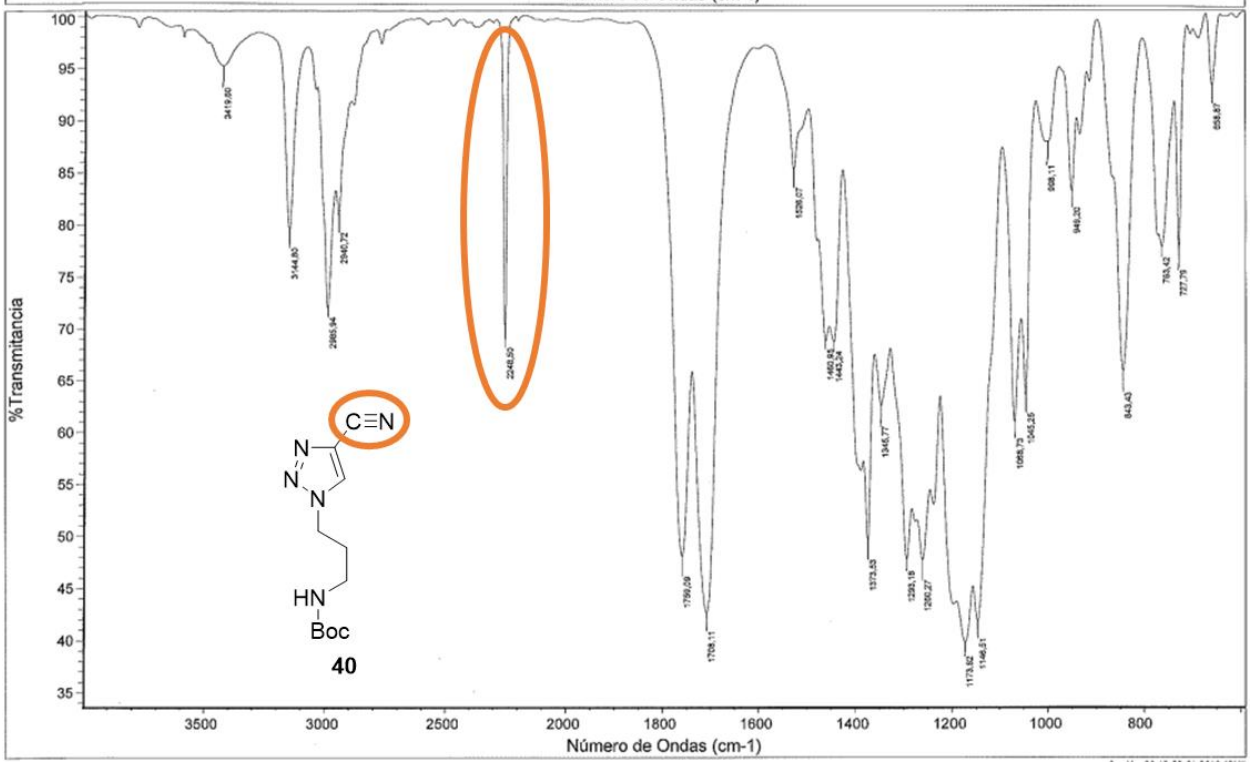
%Transmitancia
Número de Ondas (cm-1)
C≡N
N
N
N
HN
Boc
40

Figure 36. Infrared spectroscopy of an example of amide dehydration into nitrile. The spectra of the reaction product showed a band at approximately 2250 cm^{-1}, corresponding to a triple bond. This is consistent with the presence of a nitrile group.

3.4.7. Hydroxylamine derivative synthesis

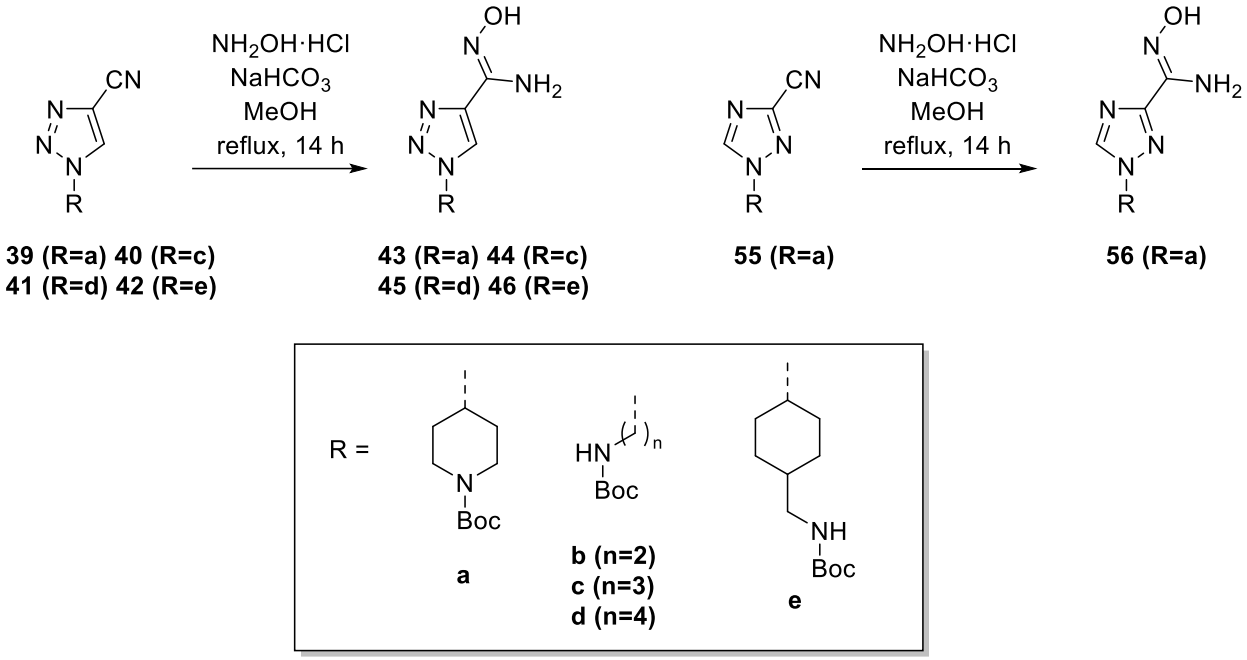

Scheme 11. Synthesis of hydroxylamine derivatives for triazole compounds.

Hydroxylamine derivatives were obtained by reacting their nitrile precursors with hydroxylamine hydrochloride. The reaction was performed in MeOH, using sodium bicarbonate as the base. The mixture was refluxed for 14 h, after which the solvent was evaporated. The resulting crude was then suspended in ethyl acetate and filtered. After the necessary washes and drying the product under vacuum, the yield afforded was in the range of 70-85%. Reaction progress was monitored through ^{1}H-NMR (Figure 37). The spectra of the products showed the presence of two new signals: a singlet (1H) corresponding to the hydroxy group, and another singlet (2H) corresponding to the amine.

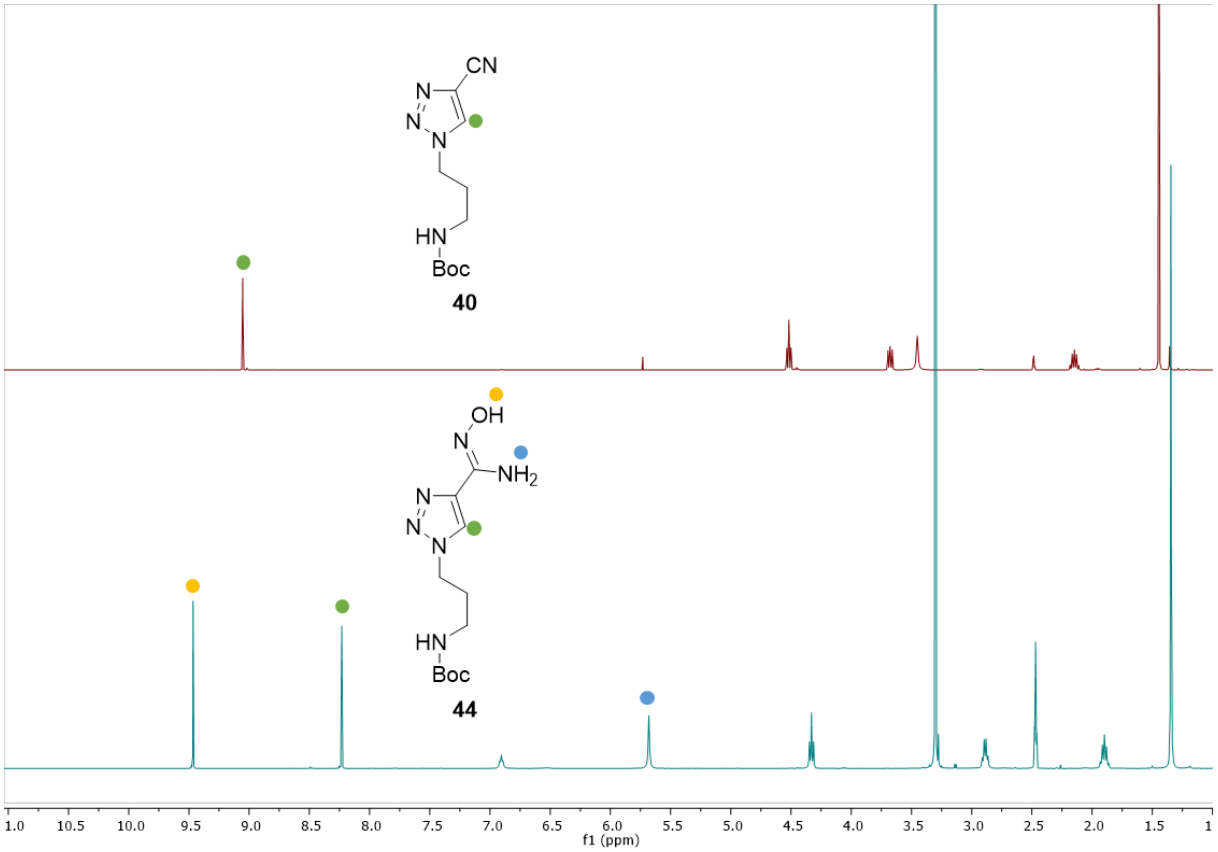

Figure 37. ^{1}H-NMR in d_6-DMSO of an example of the reaction between nitrile group and hydroxylamine hydrochloride. Two new signals appeared due to the reaction: a singlet (1H, yellow) corresponding to the hydroxyl group, and another singlet (2H, blue) corresponding to the new amine group.

3.4.8. Oxadiazolone ring formation

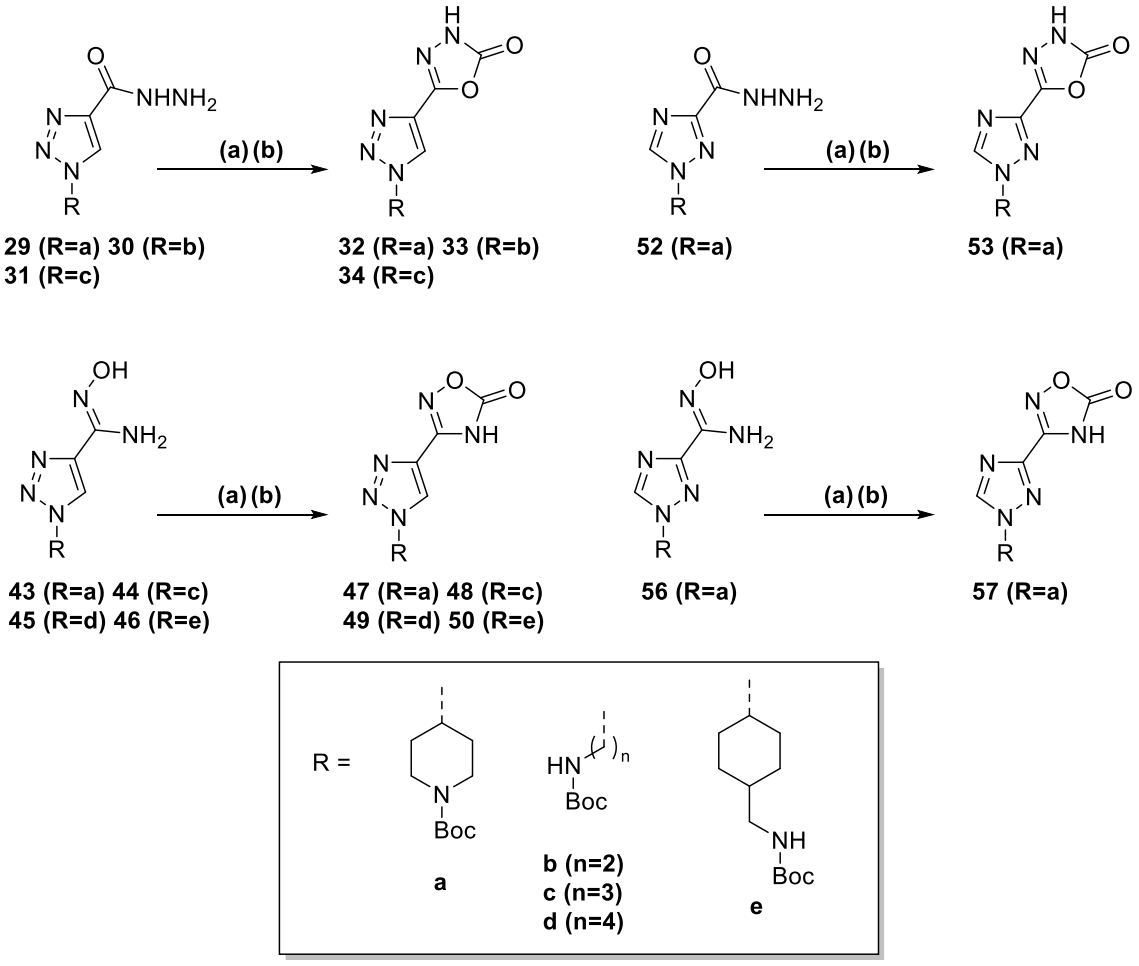

Scheme 12. Oxadiazolone ring formation for triazole derivatives. (a) CDI, TEA, THF-DMF 10:1, reflux 15 h. (b) CDI, DBU, ACN, reflux, 15 h.

The oxadiazolone ring formation (Scheme 12) was initially performed by reacting with CDI in a 10:1 mixture of THF and DMF using TEA as a base. The mixture was refluxed for 15 h in an inert atmosphere. After, the product was isolated and purified through column chromatography. These conditions afforded a good yield for the 1,3,4-oxadiazolone formation of **32**, as seen in Table 3. However, the equivalent reaction for the 1,2,4-oxadiazolone in **47** provided a noticeably lower

yield of 6%, which hinders the overall yield of compound **4**. Compound **34**, a 1,3,4-oxadiazolone with a propylamine as the primary amine, was also obtained with a rather low yield of 24%. In the case of it 1,2,4 counterpart, compound **48**, the amount produced was not detectable. The reaction did furnish a good yield in the synthesis of both 1,2,4-triazole derivatives (**53**, **57**).

Based on these results, the conditions were substituted by using DBU, a stronger base than TEA, and ACN, polar solvent with a higher boiling point than THF. These conditions clearly improved the yield of **34**, **47** and **48**, always staying above 50%. Consequently, all further oxadiazolone formation reactions were performed by refluxing in ACN with the presence of DBU as the base.

Table 3. Yields of oxadiazolone ring formation reaction for triazole derivatives with two different reaction conditions. (a) CDI, TEA, THF-DMF 10:1, reflux 15 h. (b) CDI, DBU, ACN, reflux, 15 h.

	Yield (%)	
Reaction Product	**(a)**	**(b)**
32	90	89
33	-	78
34	24	82
47	6	57
48	<1	53
49	-	75
50	-	81
53	95	-
57	95	-

The progress of the reaction was monitored mainly through ^{13}C-NMR, both in the case of 1,3,4- (Figure 38) and 1,2,4-oxadiazolone (Figure 39) formation. In both cases, the number of signals corresponding to aromatic carbon atoms increased from four to five. This occurred due to the addition of a carbonyl group to the molecule, which is part of the newly formed oxadiazolone ring.

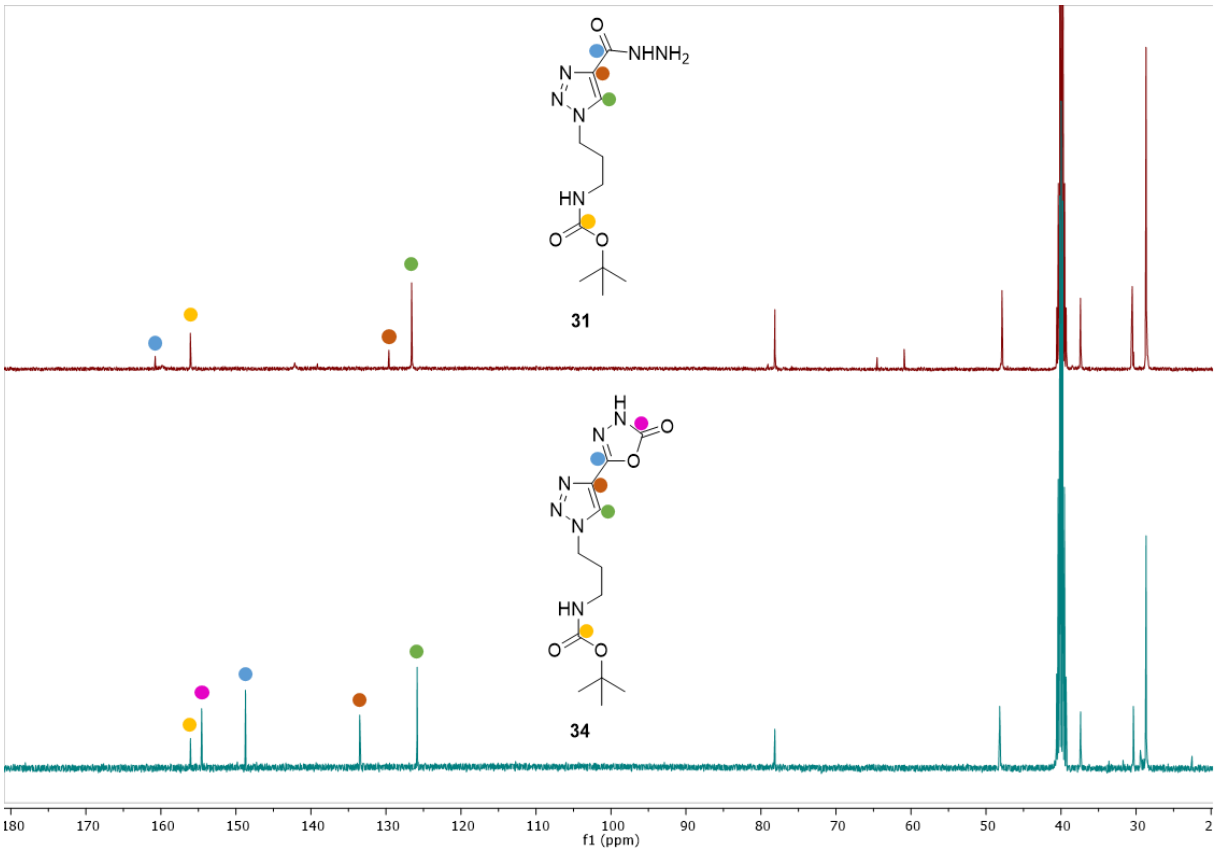

Figure 38. ^{13}C-NMR in *d*$_6$-DMSO of an example of 1,3,4-oxadiazolone ring formation from a hydrazone precursor. The hydrazone derivative (top) presented 4 aromatic carbon signals. The oxadiazolone compound (bottom) showed an additional signal, for a total of 5, corresponding to the additional carbonyl group present in the newly formed ring.

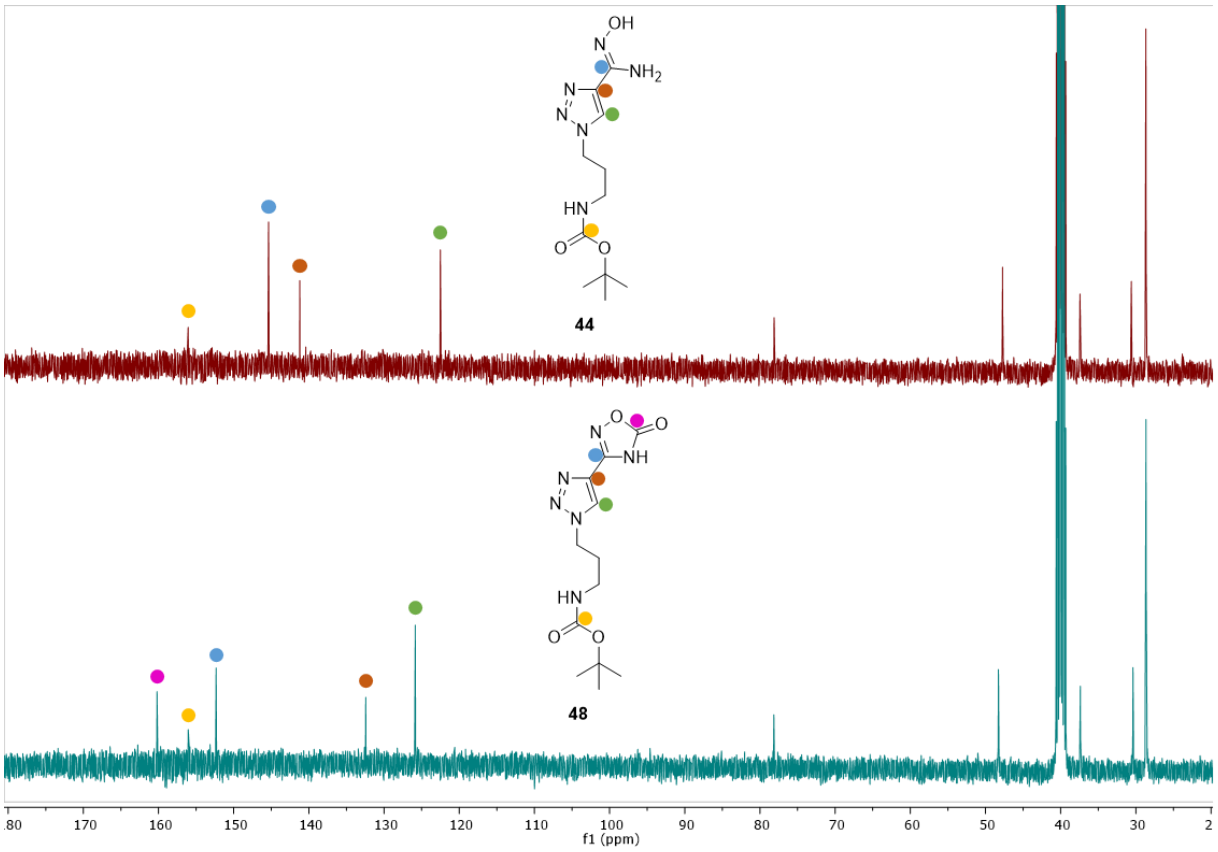

Figure 39. ^{13}C-NMR in d_6-DMSO of an example of 1,2,4-oxadiazolone ring formation from a hydroxylamine precursor. The hydroxylamine derivative (top) presented 4 aromatic carbon signals. The oxadiazolone compound (bottom) showed an additional signal, for a total of 5, corresponding to the additional carbonyl group present in the newly formed ring.

3.4.9. Tranexamic acid derivative reactions

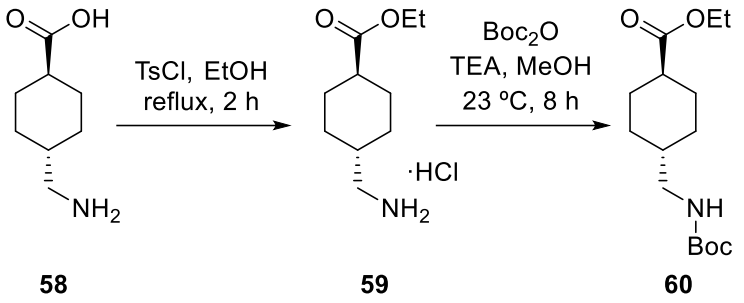

Scheme 13. Esterification and Boc protection reactions for tranexamic acid derivative compound (**11**).

The carboxy group in tranexamic acid was first transformed into an ethyl ester. To do so, the acid was treated with thionyl chloride in EtOH under reflux for 2 h. After, the solvent was evaporated and the hydrochloride was precipitated in ether, with a yield of 89 %. Subsequently, the free amine was protected with a Boc group. The compound was mixed in MeOH with TEA and di-*tert*-butyl dicarbonate. The mixture was then stirred at room temperature for 8 h. After completion, solvent was removed, the product was dissolved in DCM and washed with aqueous HCl 1 M. After isolation, the Boc derivative was obtained in 95 % yield.

The completion of both esterification and Boc protection reactions was followed through ^{1}H-NMR (Figure 40). Although the spectrum for tranexamic acid was not acquired due to lack of solubility in $CDCl_3$, the formation of an ethyl ester was monitored by the appearance of its identifying signals: quadruplet (2H) and triplet (3H). In addition, a signal consistent with a protonated terminal amine (singlet, 3H) was also present. After Boc group was introduced, its specific singlet (9H) at approximately 1.5 ppm was observed. The amine signal displays a singlet (1H) at 4.6 ppm, consistent with the product of the reaction.

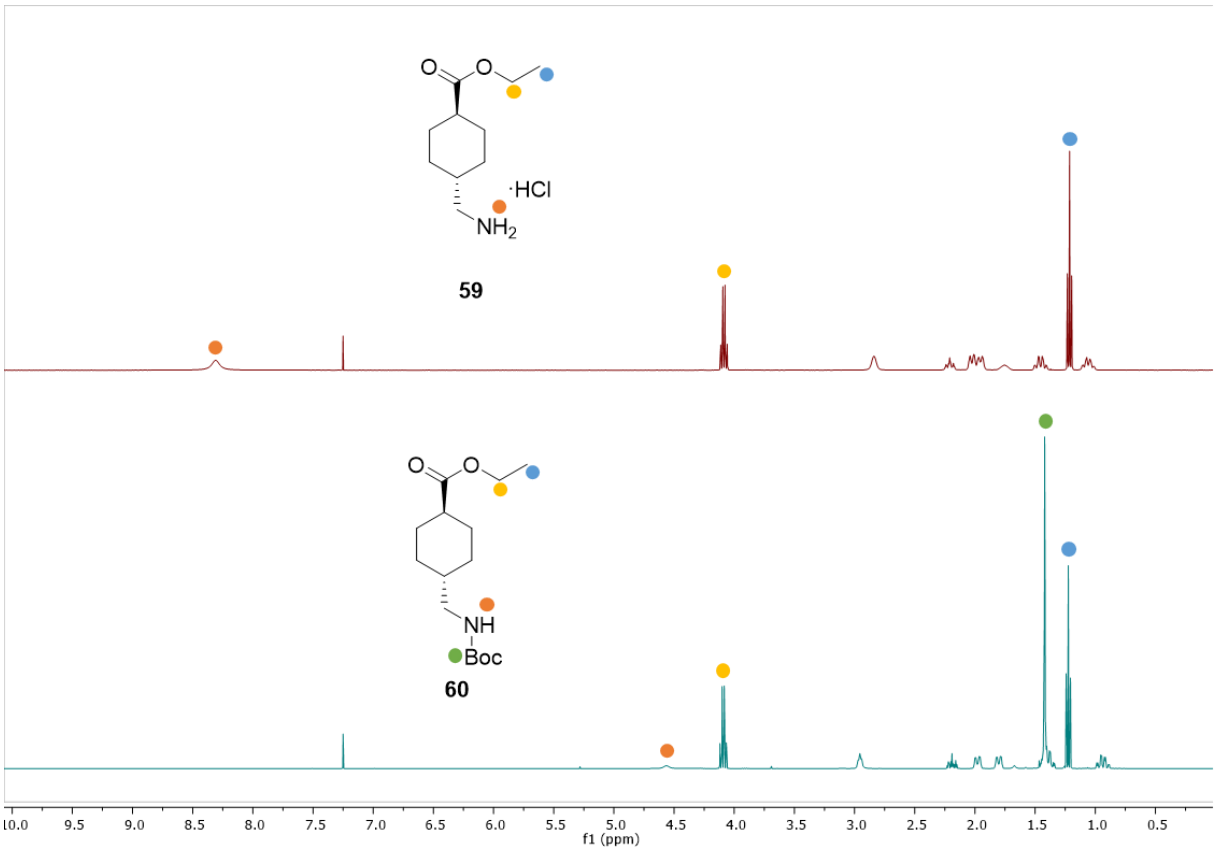

Figure 40. ^{1}H-NMR (in $CDCl_3$) of Boc protection reaction in the synthesis of the TXA derivative (**11**). A large singlet (9H) appeared at approximately 1.5 ppm, which corresponds to the specific Boc signal. The signal representing the amine group changed from a cationic amine signal (3H) at 8.3 ppm to a neutral amine (1H) at 4.6 ppm. The ethylic ester, introduced in the previous reaction in substitution of a carboxyl group, maintained the characteristic quadruplet (2H) and triplet (3H).

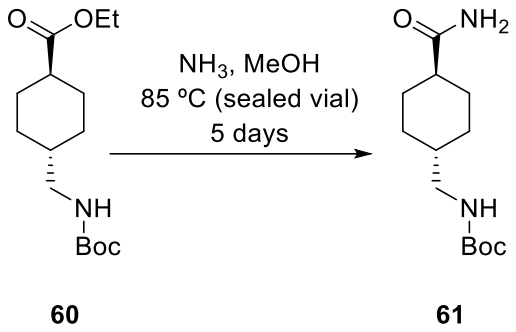

60 **61**

Scheme 14. Transformation from ethyl ester to amide for the tranexamic derivative (**11**).

The ethyl ester transformation into amide was performed under different conditions than for the previously explained triazole derivatives. The different chemical nature of the cyclohexane ring when compared to a triazole ring decreased the reactivity of the compound. Consequently, the reaction was accomplished at higher temperature and for a longer period of time. Specifically, the ester precursor was stirred in methanolic ammonia at 85 °C for 5 days. The reaction was performed inside a sealed vial to avoid the loss of ammonia. The remaining ester precursor was then eliminated through saponification by adding an amount of NaOH 1 M and heating at 40 °C for 4 h. After further isolation, the final amide was obtained with a yield of 25 %.

As for the previously explained triazole derivatives, the complete transformation of the ester group into a carboxamide was validated through ^{1}H-NMR (Figure 41). Both identifying signals of the ethyl ester disappeared due to the reaction. At the same time, a new signal consistent with the newly formed amide also appeared.

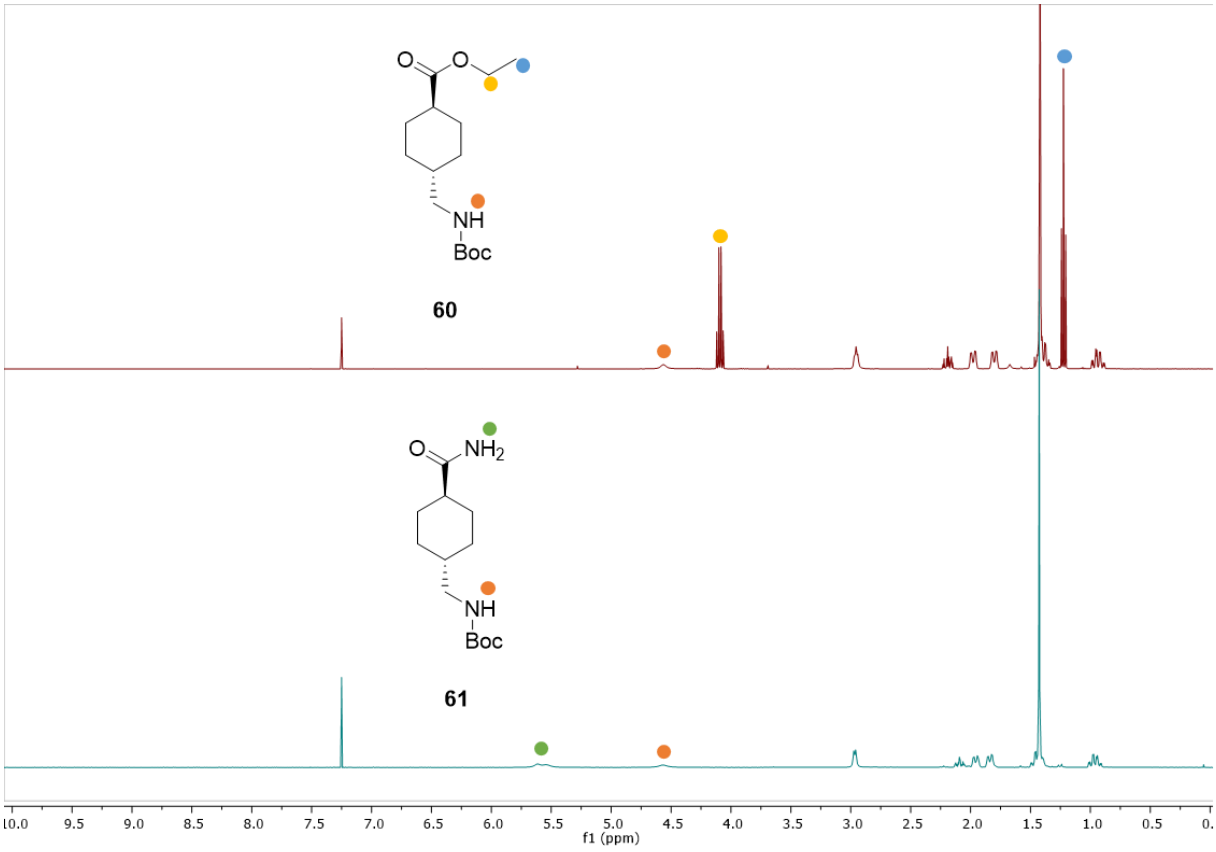

Figure 41. ^{1}H-NMR (in $CDCl_3$) of the conversion from ethyl ester to amide, for the synthesis of the TXA derivative (**11**). The characteristic signals from an ethyl ester, quadruplet (2H) and triplet (3H), disappeared. In addition, a broad signal (2H) corresponding the newly formed amide also appeared.

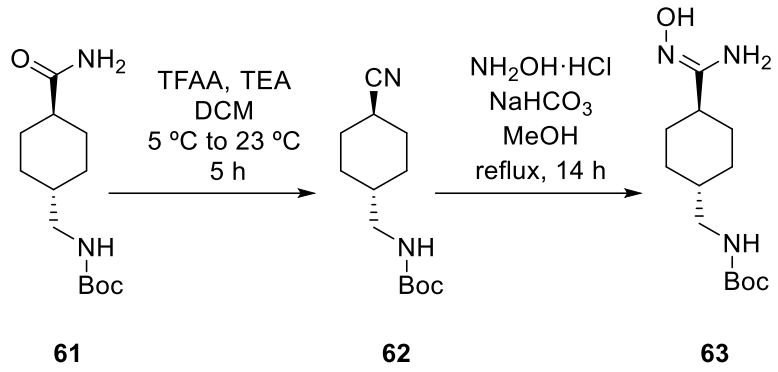

Scheme 15. Nitrile formation and subsequent hydroxylamine compound synthesis for the tranexamic derivative (**11**).

Amide dehydration into nitrile was performed by treatment with TFAA in DCM, in equivalent conditions to the triazole derivatives. The following hydroxylamine compound synthesis was also performed equally to the triazole derivatives. These reactions furnished compounds **62** and **63** in 91 % and 82 % yield, respectively. As seen in Figure 42, ^{1}H-NMR shows the absence of amide signal (2H) when transformed into nitrile (**62**). In addition, the subsequent transformation into hydroxylamine (**63**) caused the appearance of the hydroxy signal (1H) and the newly formed amine signal (2H).

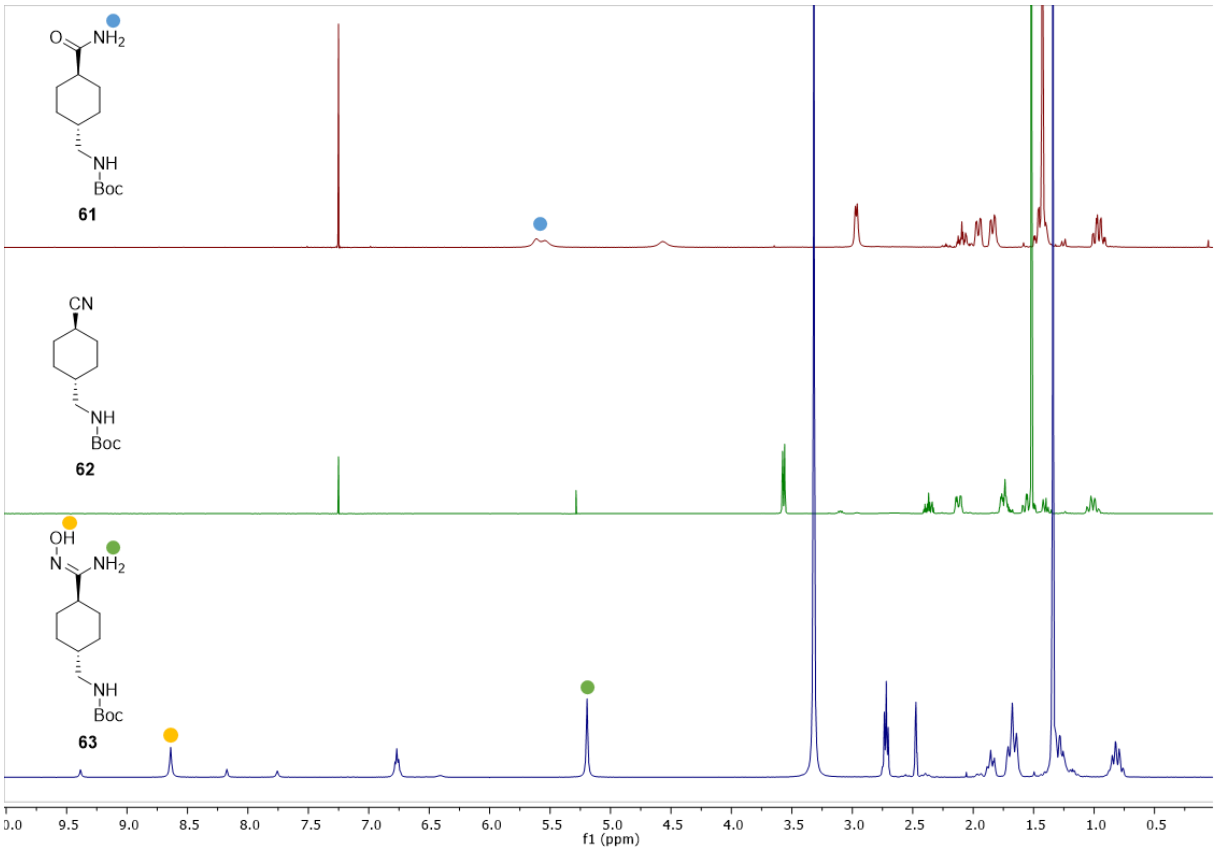

Figure 42. ^{1}H-NMR for carboxamide, nitrile and hydroxylamine derivatives for the synthesis of the TXA derivative. Compounds **61** and **62** were analyzed in $CDCl_3$, while **63** was analyzed in *d_6*-DMSO due to low solubility in $CDCl_3$.

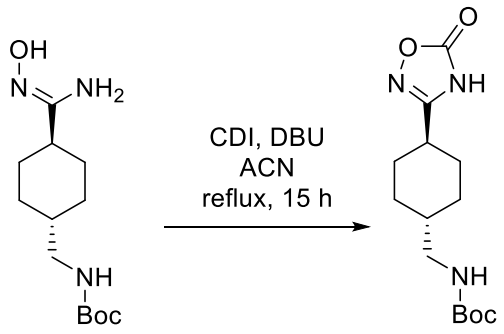

63 **64**

Scheme 16. 1,2,4-oxadiazolone ring formation for the tranexamic acid derivative (**11**).

The oxadiazolone ring formation was performed by refluxing the hydroxylamine precursor and CDI in ACN, using DBU as the base. The conditions were therefore not different from the ones used for the triazole derivatives. The furnished yield after further product isolation was 78 %. The reaction progress was monitored through ^{13}C-NMR. As shown by the spectra (Figure 43), a signal corresponding to the newly formed carbonyl group emerged, validating the formation of the oxadiazolone ring.

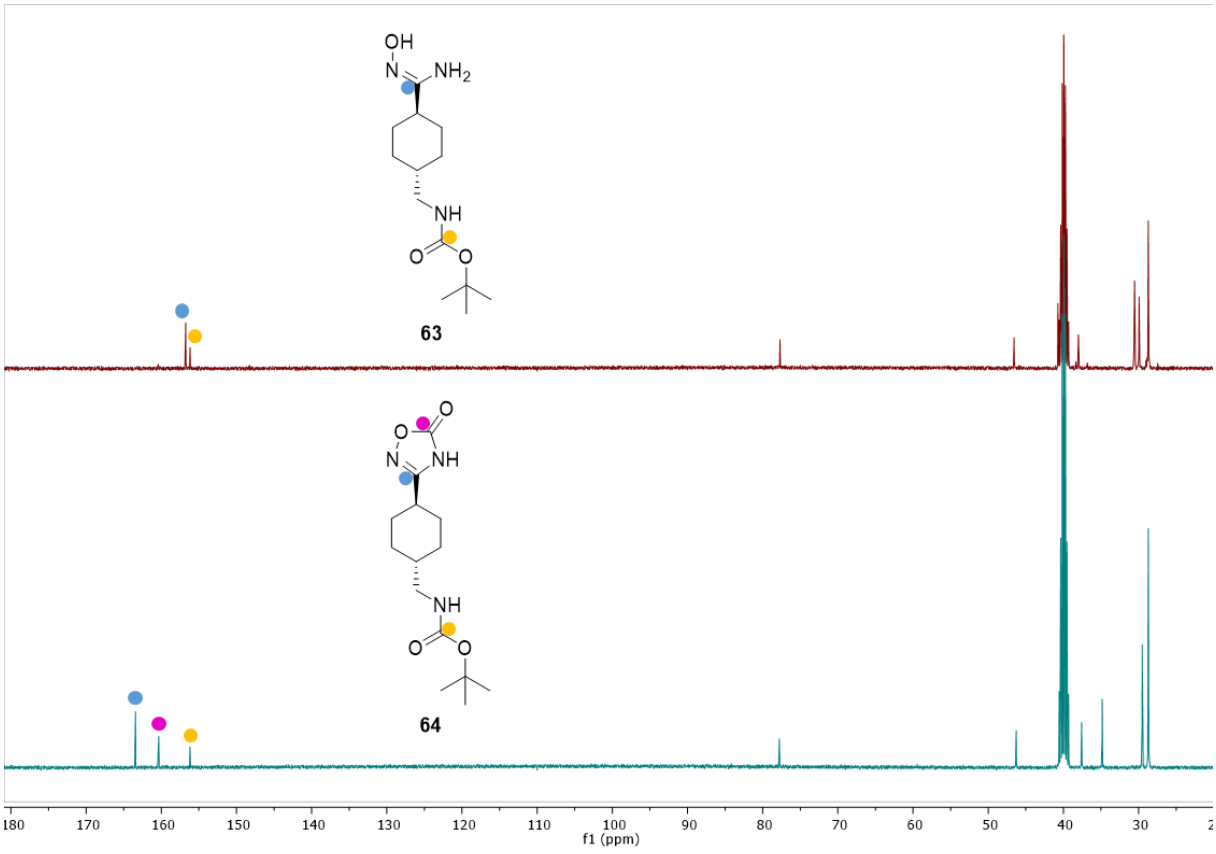

Figure 43. ^{13}C-NMR of oxadiazolone ring formation for the synthesis of the TXA derivative (**11**). The number of aromatic carbon signals varies from two to three, due to the carbonyl group present in the newly formed ring.

3.4.10. Boc group removal

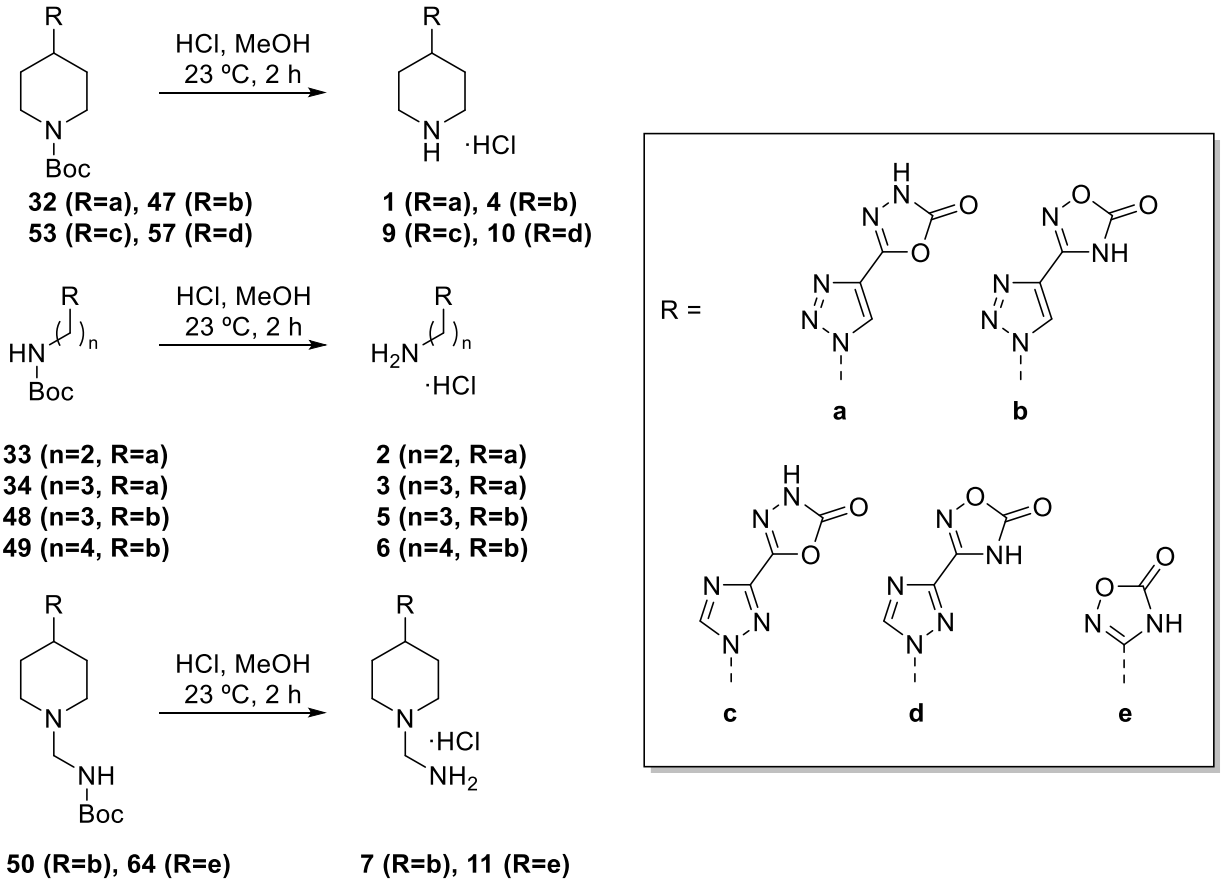

Scheme 17. Boc group removal reaction.

The removal of the Boc protecting group was accomplished by treating the corresponding Boc precursor in methanolic 3 M HCl at room temperature for 2 h. The product was consequently transformed into a hydrochloride salt, which was then washed with ethyl acetate. The yield in all cases was above 80 %. Complete removal of the Boc group was checked by both ^{1}H-NMR and ^{13}C-NMR. Proton resonance (Figure 44) showed the absence of the specific singlet (9H) corresponding to the Boc group. At the same time, the signal corresponding to the protonated amine was also visualized.

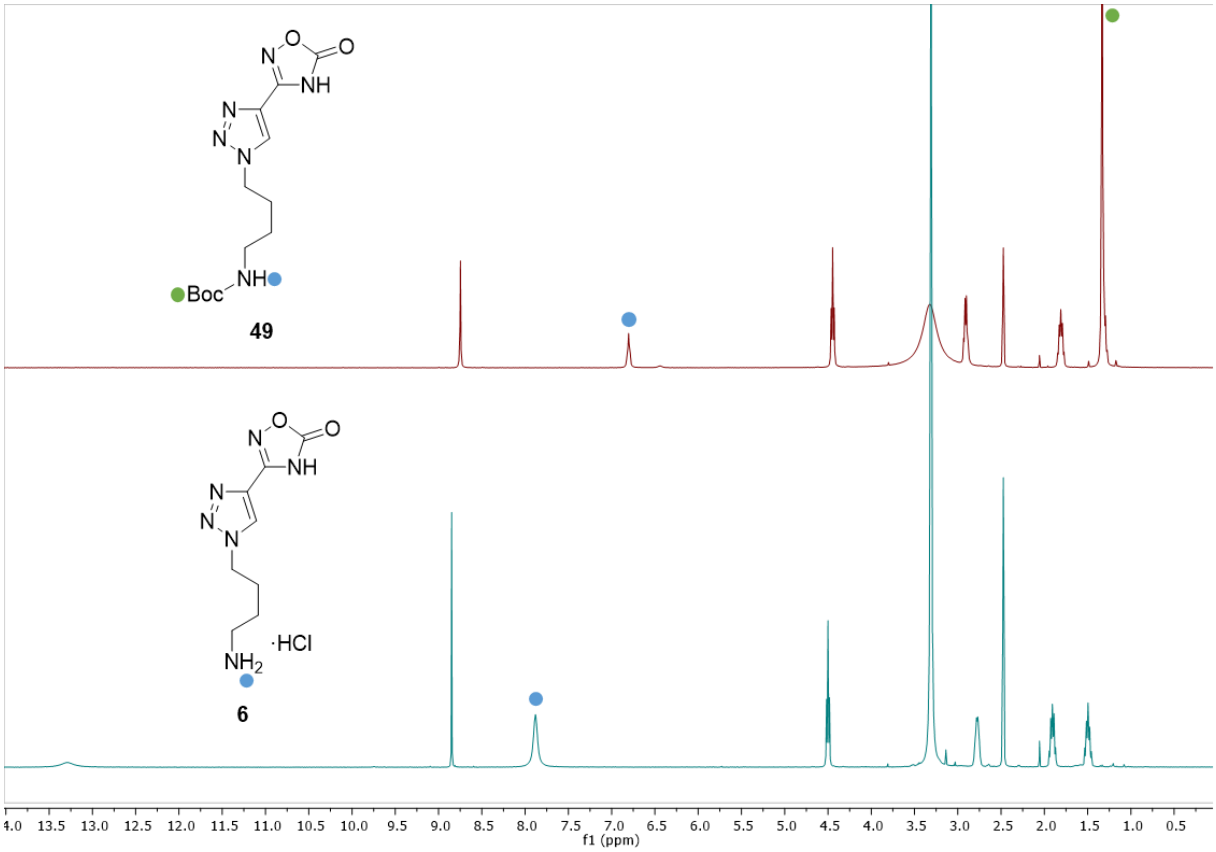

Figure 44. ^{1}H-NMR (d_6-DMSO) of example of Boc group removal reaction. The characteristic singlet (9H) of Boc disappeared. The Boc protected amine changed into a protonated free amine in the hydrochloride salt. Therefore, its signal changed from a 1H integral to a 3H integral.

3.5. Activity Quantification

As mentioned in chapter 1, the turbidimetric assay using preformed plasma clots offered highly accurate and repeatable results. In addition, it assured that only fibrinolysis was being studied, with no influence of the coagulation process. For these reasons, it was the selected assay to quantify the antifibrinolytic activity of each studied compound. Different concentrations of each compound of interest, including TXA and EACA, were studied. As explained in chapter 1, we calculated the fibrinolytic activity relative to the control for each condition. The dose-response curve (Figure 45) was then created for all molecules which presented inhibitory power at concentrations below 1000 µM. The IC_{50} values (Figure 46) for each active compound were also calculated from this data.

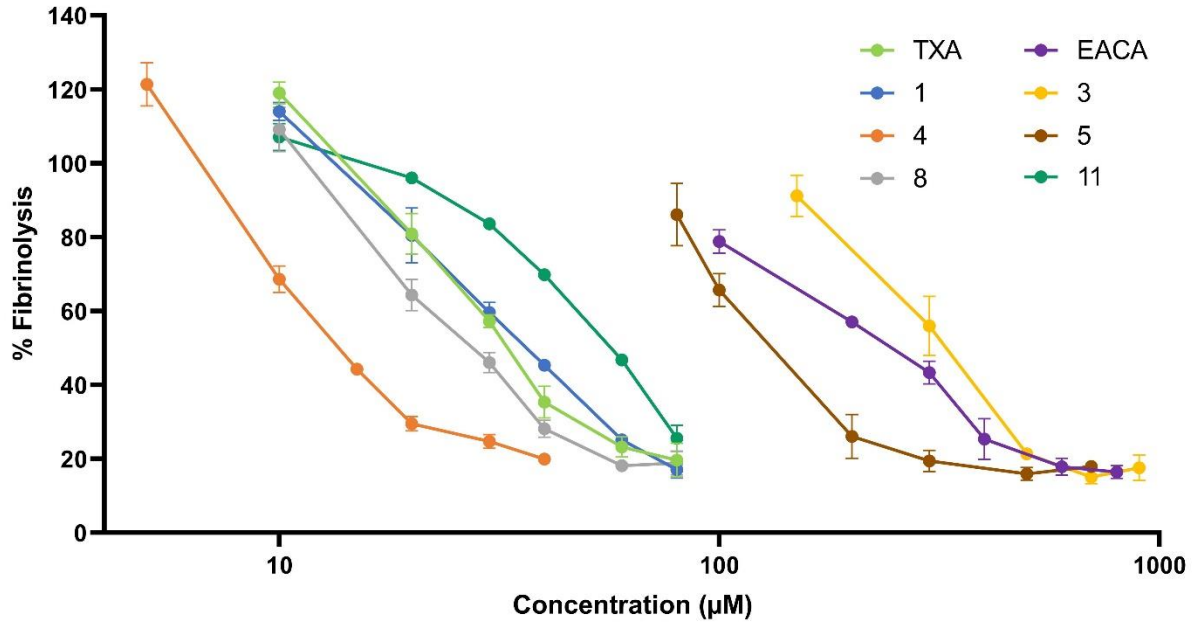

Figure 45. Dose-response curve for each molecule represented as % of fibrinolysis vs concentration (µM) of inhibitor measured in plasma clot lysis assays. Compounds not included in this graph showed undetectable activity below 1000 µM. Error bars indicate standard deviation. Each condition was tested in triplicate.

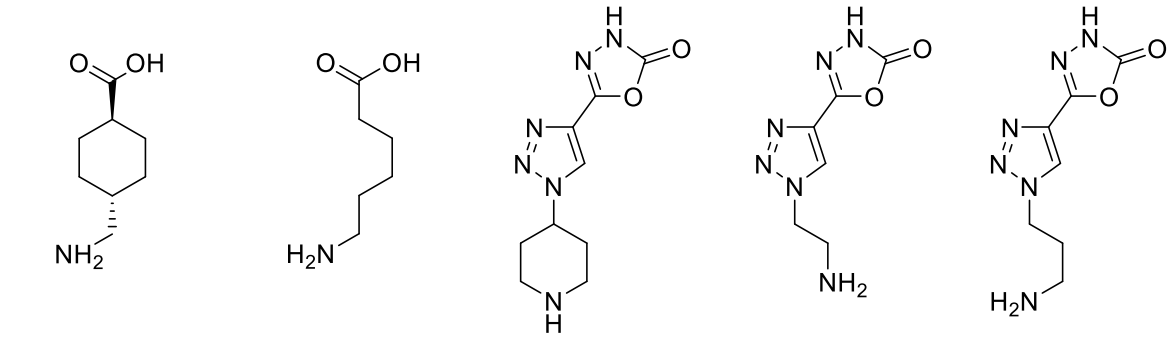

TXA IC_{50} = 33.3 μM

EACA IC_{50} = 263 μM

1 IC_{50} = 36.8 μM

2 IC_{50} >1000 μM

3 IC_{50} = 335 μM

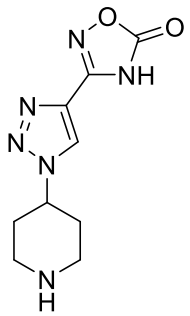

4 IC_{50} = 13.8 μM

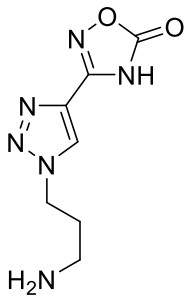

5 IC_{50} = 138 μM

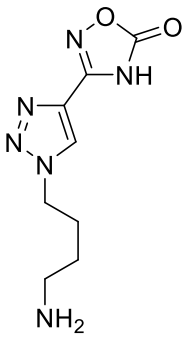

6 IC_{50} > 1000 μM

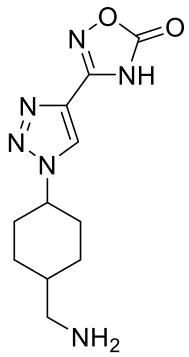

7 IC_{50} > 1000 μM

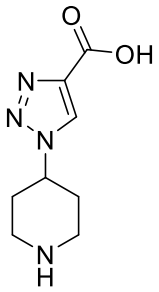

8 IC_{50} = 27.8 μM

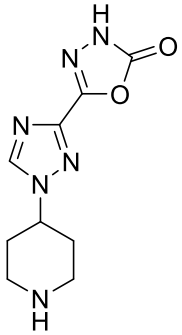

9 IC_{50} > 1000 μM

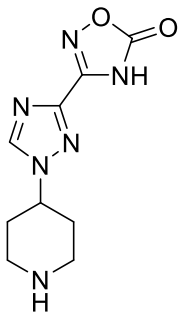

10 IC_{50} > 1000 μM

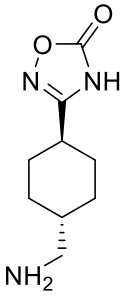

11 IC_{50} = 60.4 μM

Figure 46. Tested molecules and their IC_{50} values. IC_{50} was considered as the concentration at which each inhibitor reduced the fibrinolytic activity by 50 %.

The results reveal that among all molecules tested, compound **4** presents the highest antifibrinolytic activity. Specifically, it shows 2.5-fold reduction of the IC_{50} when compared to compound **1**, also known as LTI-6. In addition, it also shows such an improvement over TXA, the current gold standard of antifibrinolytic drugs. The chemical structure of compound **4** only contains a 1,2,4-oxadiazolone instead of the 1,3,4-oxadiazolone present in compound **1**. The difference in activity indicates a higher affinity for the 1,2,4 conformation of the oxadiazolone ring. Accordingly, compound **5** also provided a higher activity than **3**.

Compounds **2-3** and **5-6** all present the same structures as **1** and **4**, except for the presence of a piperidine ring. This moiety was replaced with linear amines of different lengths. In all cases, the presence of a linear amine severely decreased the activity. This observation highlights the importance of the bulkiness and rigidity of the piperidine ring compared to a linear chain. Compounds with a propylamine residue (**3**, **5**) showed a 10-fold increase in the IC_{50} when compared to their piperidine counterparts. For compounds with either shorter (**2**) or longer (**6**) linear chains, no activity could be measured below 1000 μM. In addition, a lack of activity was observed for compound **7**, which presents the structure of compound **4** with a cyclohexyl methanamine residue instead of propylamine.

The possibility of maintaining a carboxylic acid (present in TXA) instead of an oxadiazolone ring was also considered. Compound **8** presents the structure of **4**, with a carboxylic acid moiety instead of the 1,2,4-oxadiazolone. Results showed a 2-fold decrease in activity, although still conserving a slightly higher potency than compound **1**. In addition, compound **11** was synthesized as a derivative of TXA, having its carboxylic acid substituted for the 1,2,4-oxadiazolone ring present in compound **4**. The results showed that, although a noticeable activity was maintained, it was lower compared to that of TXA.

Regarding the central triazole ring, results showed that almost all activity was lost when substituting the 1,2,3-triazole (compounds **1** and **4**) for a 1,2,4-triazole (compounds **9** and **10**). This points toward the importance of having all three nitrogen atoms aligned on the same side of the molecule.

In summary, linear amines heavily decreased the activity compared to piperidine, 1,2,4-oxadiazolone provided an increase activity over the 1,3,4 conformation, and modifying the 1,2,3-triazole into a 1,2,4-triazole caused the loss of activity. To further understand the interaction of each part of the molecule with the target, a series of computational studies were performed with the Kringle 1 domain of plasminogen.

3.6. Computational Studies with Kringle 1 domain

Docking simulations were performed for all studied compounds, using the Kringle 1 domain of plasminogen as protein target. The protein file was extracted from a Protein Data Bank (PDB) file with code 1cea. This file contains the structure of Kringle 1 domain in complex with EACA, which was obtained through X-ray diffraction.

3.6.1. Lysine analogues

To validate the protein file and study the binding pocket, we first performed docking studies with the commonly used lysine analogues: EACA and TXA.

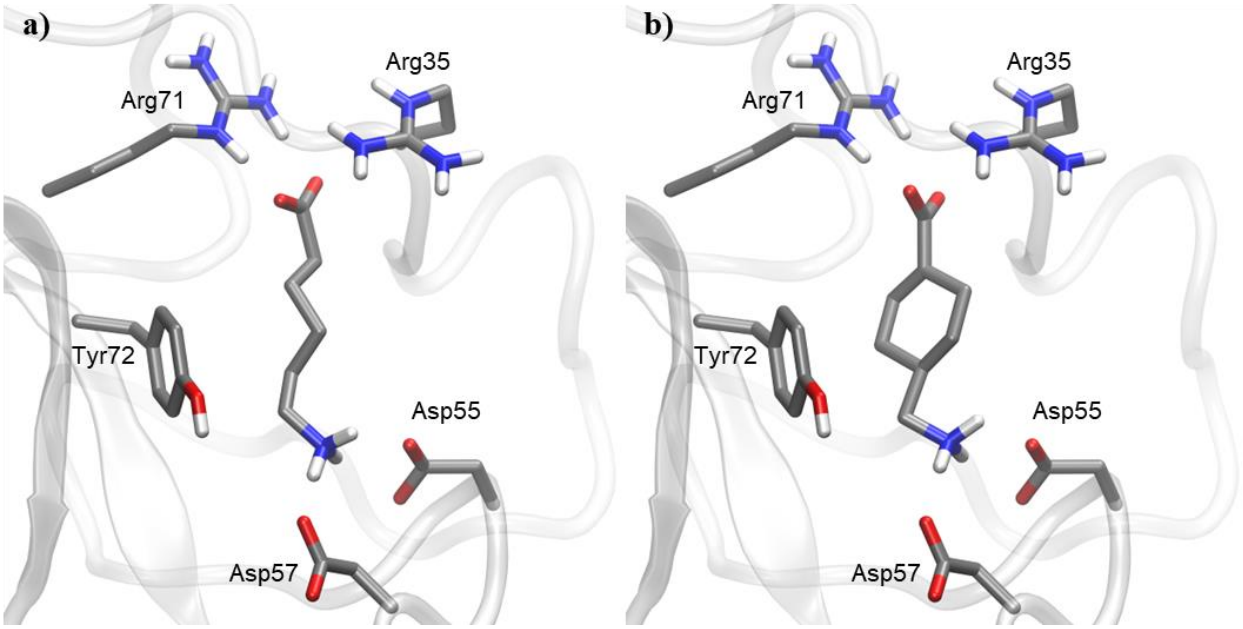

Figure 47. Docking of most representative poses for lysine analogues a) ε-aminocaproic acid (EACA) and b) tranexamic acid (TXA). Docking studies were performed with Kringle 1 lysine binding site (pdb code 1cea), using AutoDock 4.2.

The binding mode (Figure 47) for lysine analogues, EACA and TXA, is equivalent to what has been reported. Their most favorable target-ligand interactions are concentrated in two areas. On one side, the terminal amine can form salt bridges with Asp55 and Asp57. Simultaneously, the carboxylic acid moiety at the opposite end of the molecule can form other salt bridges with Arg35 and Arg71. These two very differentiated regions of the pocket, one acid (aspartic acid residues) and one basic (arginine residues) play a key role in all interactions with any potential ligands.

Therefore, it is very important to study the effect that the different chemical modifications have on the interactions with both regions.

3.6.2. Oxadiazolone and carboxyl group

The docking results of compounds with 1,3,4 and 1,2,4-oxadiazolone rings were compared. As seen in Figure 48, the oxadiazolone moiety interacts with the basic region of the pocket. Therefore, it plays a similar role as the carboxyl group plays in traditional lysine analogues (EACA, TXA). In this case no salt bridges can be formed, and therefore the electrostatic interactions are weaker. Instead, H-bonds can be formed. In the case of 1,3,4-oxadiazolone derivatives, an H-bond is observed between the carbonyl group and Arg71, while a certain electrostatic interaction with Arg35 can also be expected. In the case of 1,2,4-oxadiazolone derivatives, however, the oxygen atom from the ting enables the formation of an additional H-bond with Arg71. This additional polar interaction can explain the increased activity of 1,2,4-oxadiazolone derivatives over their 1,3,4-oxadiazolone counterparts.

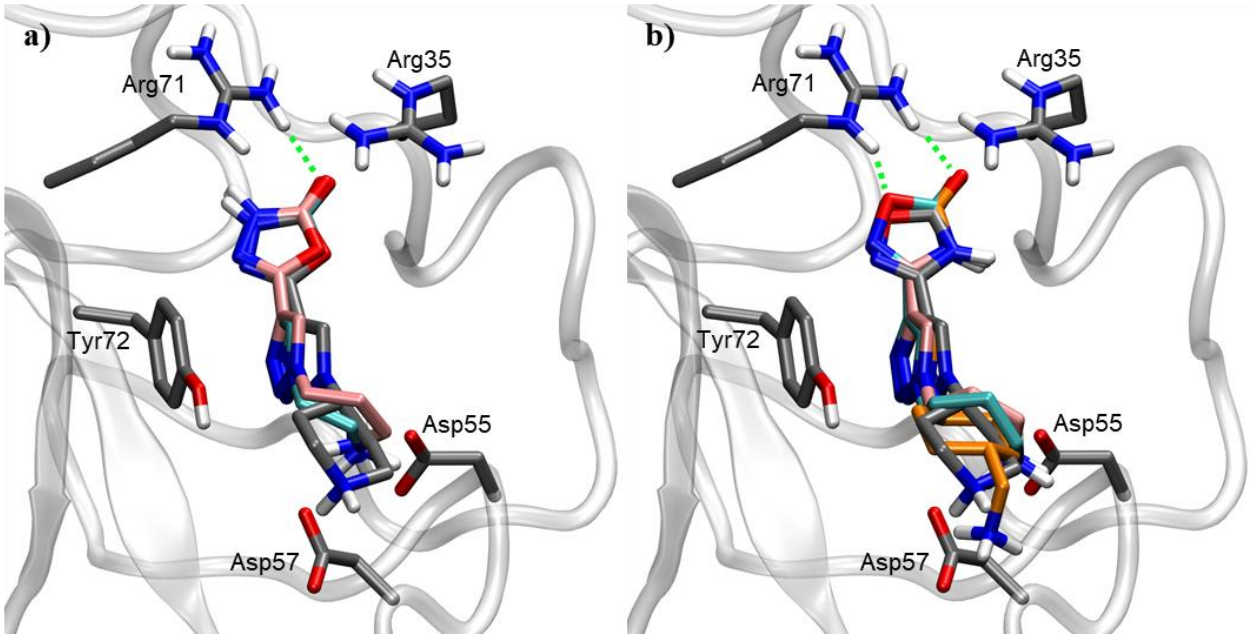

Figure 48. Docking of most representative poses for 1,2,3-triazole derivatives with different oxadiazolone rings. a) 1,3,4-oxadiazolone compounds: **1** (grey), **2** (cyan), **3** (pink). b) 1,2,4-oxadiazolone compounds: **4** (grey), **5** (pink), **6** (cyan), **7** (orange). Docking studies were performed with Kringle 1 lysine binding site (pdb code 1cea), using AutoDock 4.2. H-bonds interactions with the oxadiazolone ring are indicated as green dashed lines.

Figure 48 also shows that, as expected, the terminal amine in all studied compounds interacts with the acid region of the pocket, formed by Asp 55 and Asp57. In addition, the 1,2,3-triazole ring remains in a parallel orientation to Tyr72. Such orientation, together with the ring aromaticity, allows for certain pi-pi interaction to occur between the triazole moiety and the aromatic amino acid.

In the case of compound **8**, which includes a carboxyl group instead of an oxadiazolone ring, this parallel orientation between triazole and Tyr72 is lost (Figure 49). Presumably, reduced length of the compound displaces the position of the triazole moiety, hampering its ability to interact with Tyr72. Based on the ability to form salt bridges of the carboxyl group, one could expect compound

8 to show a higher potency than **4**. However, compound **8** presented an activity of around halve of **4** (Figure 46). The lack of pi-pi interactions, therefore, seems crucial to understand this behavior.

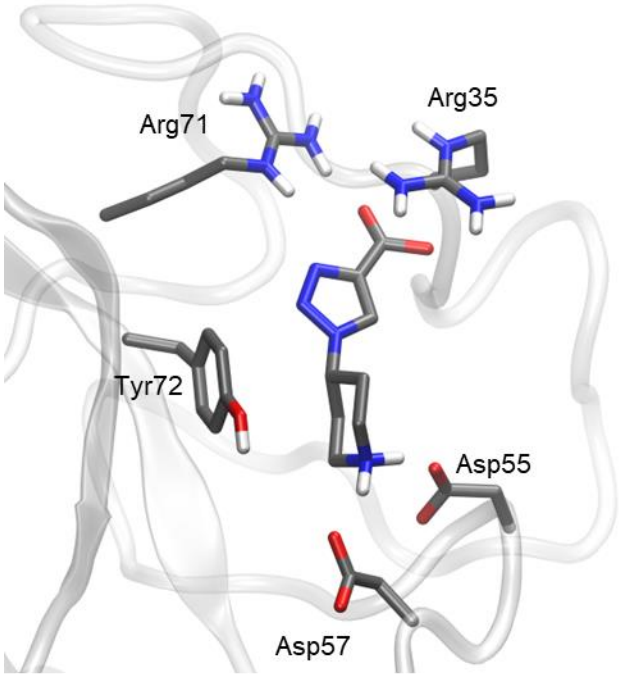

Figure 49. Docking of most representative pose for 1,2,3-triazole derivative combined with a carboxyl group (**8**). Docking studies were performed with Kringle 1 lysine binding site (pdb code 1cea), using AutoDock 4.2. H-bonds interactions with the oxadiazolone ring are indicated as green dashed lines.

3.6.3. Terminal amine

As previously mentioned, different terminal amine moieties were tested for the 1,2,3-triazole derivatives. In Figure 50, all 5 different amines are shown in their most representative docking pose. These docking results show a slight difference between linear amines and the two bulkier groups (piperidine and cyclohexyl methanamine). In the compounds with linear moieties, the terminal amine interacts with both Asp55 and Asp 57. However, in the case of bulkier groups, such interaction is only observed with Asp 57. This observation contradicts the activity results,

since piperidine was clearly the terminal amine which presented higher activity among all 1,2,3-triazole derivatives (compounds **1**, **4** and **8**). It is important to consider that docking studies were performed without considering any movement from the protein. Therefore, flexibility of the pocket was not included in the calculations. This flexibility could potentially be crucial for the adaptation of the pocket to each specific ligand.

Although not explicitly shown by the docking results, one must take into account than substituting a piperidine for linear amines reduces the rigidity of the molecule, therefore increasing the entropy and in consequence providing less stable interactions. In addition, the bulkiness of piperidine can also provide higher stability due to a higher number of weak interactions with the pocket. These factors seem to explain that even propylamine, the linear amine with higher potency (**3**, **5**), still reduces the overall activity of its piperidine counterpart (**1**, **4**) by 10-fold.

In the case of compound **7**, with a cyclohexyl methanamine group, the docking reflects that the increased size of the molecule highly hinders its interactions with the acid region of the pocket. This correlates well with the absence of activity at concentrations bellow 1000 μM, determined in our activity assays.

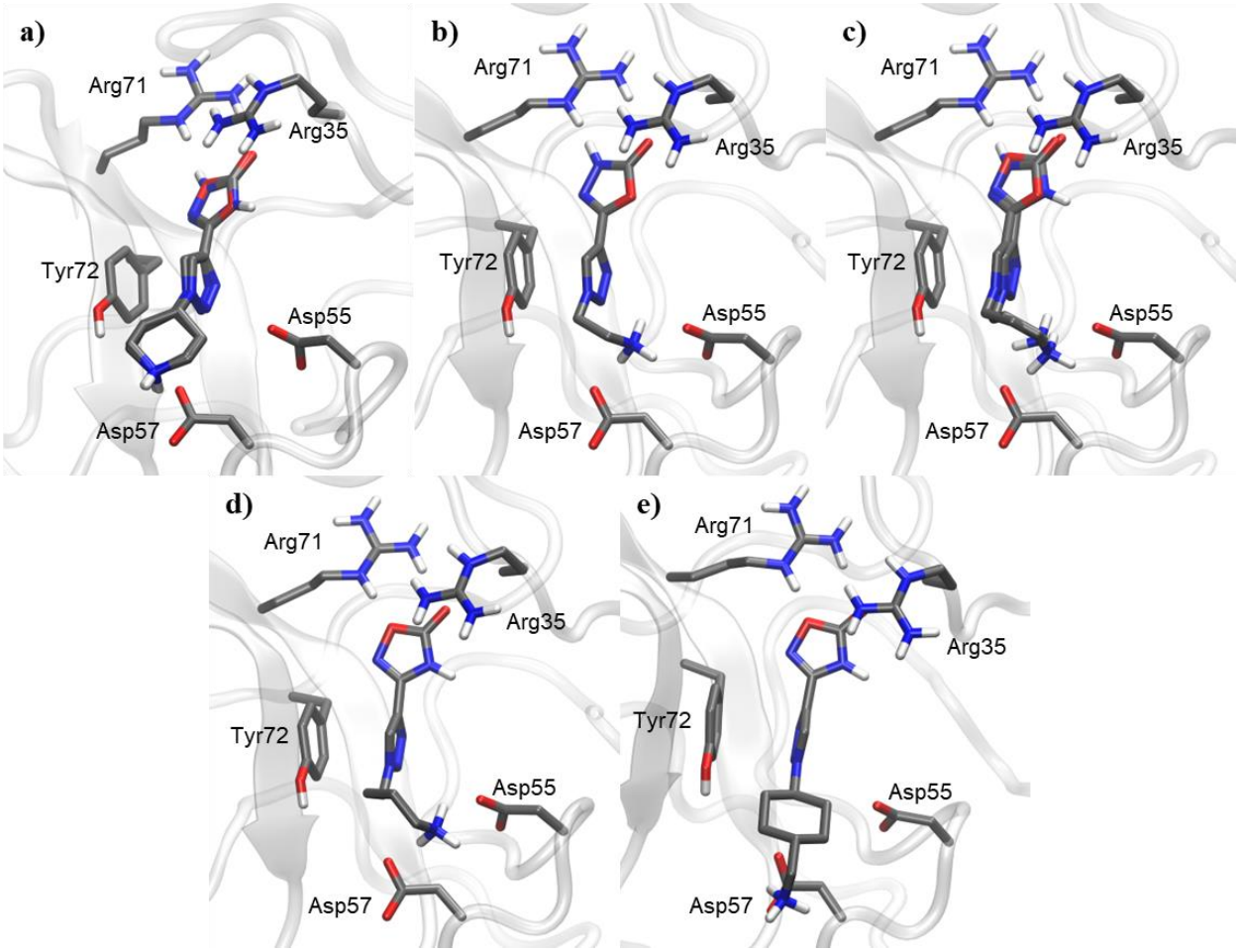

Figure 50. Docking of most representative poses for 1,2,3-triazole derivatives with different terminal piperidine groups: a) piperidine (**1**, **4**), b) ethylamine (**2**), c) propylamine (**3**, **5**), d) butylamine (**6**) and e) cyclohexyl methanamine (**7**). Docking studies were performed with Kringle 1 lysine binding site (pdb code 1cea), using AutoDock 4.2.

3.6.4. Triazole ring

As presented earlier, two derivatives of 1,2,4-triazole were also synthesized and tested. Their docking poses, compared in Figure 51, show no apparent differences. In both cases, the triazole ring can form pi-pi interactions with Ty72. However, no activity could be measured in the case of

the 1,2,4-triazole derivatives (compounds **9** and **10**). Therefore, docking studies were not able to explain our results, and further studies were necessary.

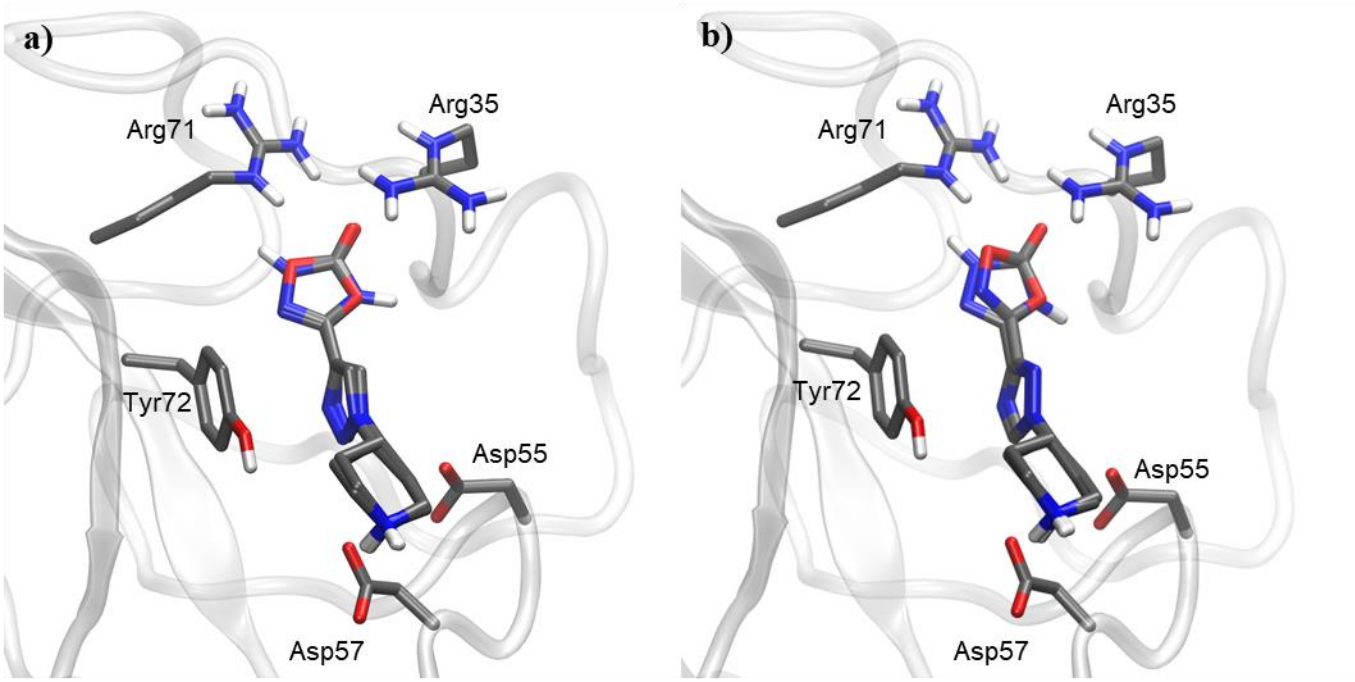

Figure 51. Docking of most representative poses for different triazole conformations, all with piperidine as the terminal amine: a) 1,2,3-triazole derivatives (**1**, **4**), b) 1,2,4-triazole derivatives (**9**, **10**). Docking studies were performed with Kringle 1 lysine binding site (pdb code 1cea), using AutoDock 4.2.

A compound with no presence of triazole ring was also synthesized and studied (**11**). This molecule was the result of substituting the carboxyl group in TXA for a 1,2,4-oxadiazolone. As seen in Figure 52, the interactions are similar to those of TXA (Figure 47). Piperidine is able to form salt bridges with both aspartic residues, while the carbonyl group of the oxadiazolone interacts with Arg71. As explained before, this carbonyl allows for H-bonds to be formed instead of the stronger salt bridges formed when a carboxyl group is present. This weaker interaction, in this case, cannot be compensated by pi-pi stacking due to the lack of an aromatic triazole ring.

Altogether, this explains that compound **11** was found to be almost halve as potent as TXA from our plasma clot lysis assays.

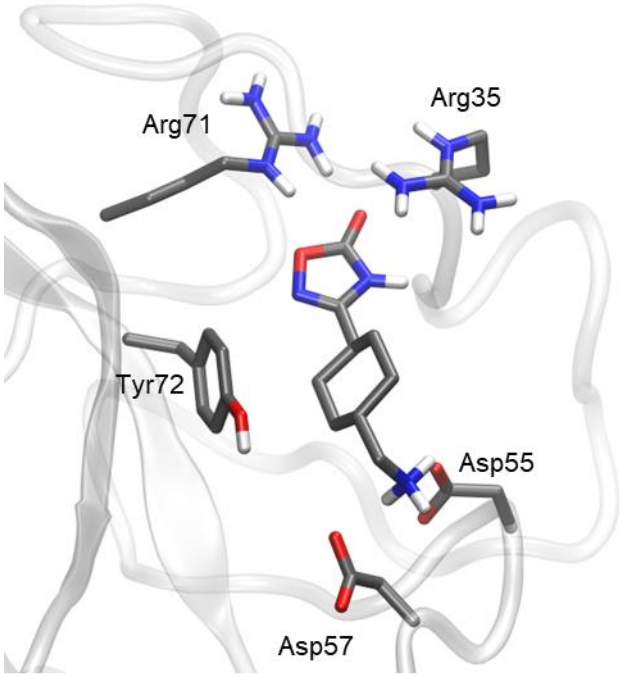

Figure 52. Docking of most representative pose for tranexamic acid derivative **11**. Docking studies were performed with Kringle 1 lysine binding site (pdb code 1cea), using AutoDock 4.2.

3.6.5. Molecular dynamics of different triazole rings

The complete loss of activity when changing the 1,2,3-triazole for a 1,2,4-triazole could not be explained through docking. Consequently, molecular dynamics simulations were performed.

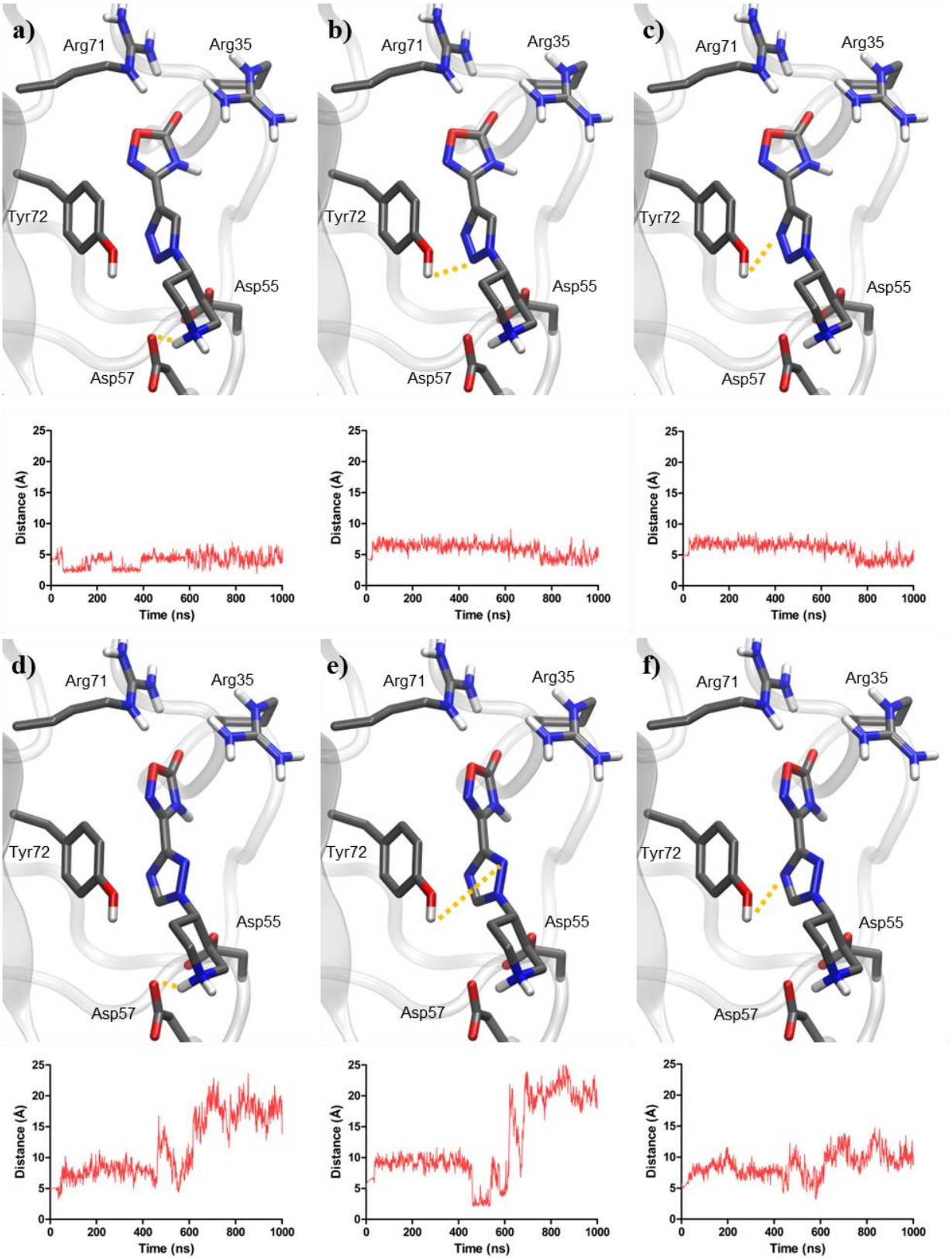
a)
Arg71
Arg35
Tyr72
Asp55
Asp57
b)
Arg71
Arg35
Tyr72
Asp55
Asp57
c)
Arg71
Arg35
Tyr72
Asp55
Asp57
Distance (A)
Time (ns)
0
200
400
600
800
1000
5
10
15
20
25
d)
Arg71
Arg35
Tyr72
Asp55
Asp57
e)
Arg71
Arg35
Tyr72
Asp55
Asp57
f)
Arg71
Arg35
Tyr72
Asp55
Asp57
Distance (A)
Time (ns)

Figure 53. Representation of the most important distances for molecular dynamics simulations of compounds **4** and **10**. Distances for compound **4**: a) piperidine and Asp57, b) triazole (nitrogen N2) and Tyr72, c) triazole (nitrogen N3) and Tyr72. Distances for compound **10**: d) piperidine and Asp57, e) triazole (nitrogen N2) and Tyr72, f) triazole (nitrogen N4) and Tyr72.

Molecular dynamics results (Figure 53) show a clearly different behavior for compounds **4** and **10**. Molecule **4** (1,2,3-triazole) remains inside the binding site throughout the entire simulation time (1000 ns), while molecule **10** (1,2,4-triazole) does not, abandoning it at 500-600 ns.

The distance between piperidine and Asp57 was the most stable throughout the simulations. In the case of compound **4**, it remained around 3 Å during the entire simulation, indicating the presence of an H-bond. For compound **10**, the interaction is weaker, with a distance around 7 Å, until the piperidine suddenly separates at 600 ns, indicating the exit of the molecule from the binding site.

Additionally, the distances between the nitrogen atoms in each triazole ring and Tyr72 (particularly its hydroxyl group) also provides key information. For compound **4**, these distances fluctuate between 3 and 6 Å, which allow for polar interactions including H-bonds. In the case of compound **10**, these distances are always above 7 Å, until the molecule finally exits the pocket. These results highlight the role of 1,2,3-triazole in providing anchoring to the binding site, mainly with Tyr72, that 1,2,4-triazole cannot provide.

3.7. Structure-Activity Relationship discussion

As seen in the docking results, the modified oxadiazolone ring interacts with the arginine residues of the LBS pocket, comparably to the carboxylic acid in traditional lysine analogues (EACA and TXA). Interestingly, the 1,2,4-oxadiazolone was more active than a carboxylic acid derivative. Given the basic nature of arginine, the affinity with an acidic moiety could be expected

to be higher than with an oxadiazolone. However, the additional bulkiness and rigidity of the ring when compared to a linear chain appears to positively impact the activity. The size of the oxadiazolone allows for H-bonds to form between the oxadiazolone and Arg71 and interestingly, docking studies show 2 potential bonds being formed in the presence of the 1,2,4-oxadiazolone moiety, giving it its highest activity.

The 1,2,3-triazole disposition has proven to be of critical importance. Against all odds, replacing such disposition for a 1,2,4-triazole made the drug totally inactive. Only molecular dynamic simulations were able to differentiate significantly both structures, pointing towards the idea of a more stable ligand-target binding. Although docking assays are a relevant tool to identify key interactions for each compound, dynamic simulations provide more complex information. This becomes more relevant in an external binding site, such as the studied K1 domain, which is therefore inherently flexible. Consequently, the different interactions of 1,2,3-triazole and 1,2,4-triazole derivatives with Tyr72 were only observed when studying their behavior in a dynamic system. 1,2,3-triazole demonstrated higher stabilizing capacity for the pocket, explaining the activity difference between **4** and **10**.

The presence of a terminal piperidine, instead of other amine residues, proved to be crucial for activity, in alignment with the literature. On the one hand, substituting the piperidine for a linear amine rendered inactive or less active molecules, confirming the importance of the bulkiness and rigidity of piperidine ring. Interestingly, however, substituting the piperidine with a cyclohexyl methanamine residue radically decreased the activity, indicating an excessive distance between terminal amine and oxadiazolone ring. On the other hand, when comparing linear amines, the propylamine residue showed higher activity than the ethylamine and butylamine residues. This is coherent with the adequacy of piperidine, since propylamine presents the same number of bonds

between the triazole ring and the amine group. Therefore, these results reinforce the unicity of piperidine in compounds interacting with LBS of the K1 domain of plasminogen.

3.8. Affinity towards $GABA_A$ receptor

Some of the documented secondary effects of TXA, such as the occurrence of seizures during cardiac surgery, have been linked in the past with its affinity for the $GABA_A$ receptor. $GABA_A$ is a ligand-gated receptor present mainly in neuronal tissue. Its main ligand is γ-aminobutyric acid (GABA), the major inhibitory neurotransmitter in the central nervous system. As mentioned in the introduction, other molecules containing piperidine rings have been documented in literature to provide antifibrinolytic effects. One of the most researched, 4-PIOL presented high activity values (IC_{50} around 1 μM). However, 4-PIOL was found to be a low affinity $GABA_A$ receptor antagonist. This raised concern since some side effects of high dose TXA treatments had been previously linked to its $GABA_A$ antagonistic properties. In order to examine the possible interaction of our most active compound (**4**) with the $GABA_A$ receptor, we performed a series of computational studies comparing the results to those of 4-PIOL and TXA, both known $GABA_A$ antagonists.

The molecular surface of all three molecules were calculated, and then compared to the size of the original ligand, GABA (Table 4). The results show that molecule **4** presents a size almost 50% larger than GABA in terms of molecular surface. In the case of TXA and 4-PIOL, this relative increase in molecular surface is 15% and 20%, respectively. These results reveal what is apparent by looking at the molecular structure of each molecule, that compound **4** is significantly larger than GABA, TXA and 4-PIOL.

Docking simulations were also performed with the GABA binding site of $GABA_A$ receptor. Figure 54 shows the docking poses of both TXA and 4-PIOL with the binding site. As expected, viable binding modes were found for both compounds, in alignment to their known affinity

towards the receptor. Although both TXA and 4-PIOL are larger than GABA in terms of molecular surface (Table 4), this increase in size does not preclude them from interacting with the GABA binding pocket. In case of compound **4**, however, no docking pose was found inside the binding site. This result strongly indicates that the size of molecule **4**, almost 50% more molecular surface than GABA, precludes it from entering the enclosed GABA binding site of $GABA_A$ receptor.

These results, therefore, suggest that compound **4** presents a very low chance of interacting with $GABA_A$ receptor *in vivo*, and therefore don't share this source of neurological secondary effects with TXA and 4-PIOL.

Table 4. Molecular surfaces calculated for GABA, TXA, 4-PIOL and compound **4**.

Ligand	**Molecular Surface ($Å^2$)**
GABA	256.4
TXA	293.7
4-PIOL	310.9
4	374.4

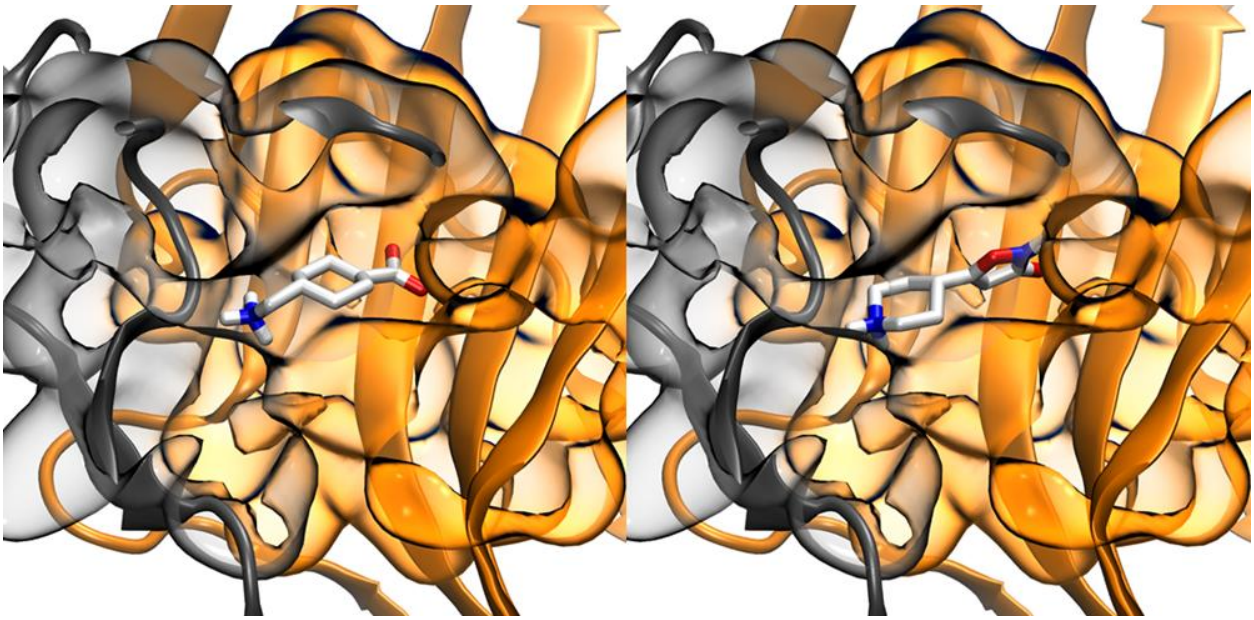

Figure 54. Binding poses with GABA binding pocket of $GABA_A$ receptor for tranexamic acid (left) and 4-PIOL (right). $GABA_A$ receptor file obtained from PDB code 6d6u. Docking performed using AutoDock 4.2.

3.9. Chapter conclusions

A number of chemical modifications were proposed based on LTI-6 (compound **1**), to further improve the activity of the molecule as well as to study the SAR of this family of compounds. After synthesizing and studying the described new molecules, both *in vitro* and *in silico*, a series of conclusions can be extracted.

Modifying the 1,3,4-oxadiazolone for a 1,2,4-oxadiazolone improved the activity of the compound, likely due to a larger number of H-bond interactions with Arg71 of the K1 pocket. Moreover, the 1,2,4-oxadiazolone derivative **4** showed the highest activity among all tested compounds, with an IC_{50} 2.5-fold lower than TXA and compound **1**.

The presence of linear amines instead of a piperidine ring clearly reduced the overall activity of the molecule. In the case of propylamine, compounds showed a 10-fold increase of IC_{50} over their

piperidine counterparts, while molecules with either ethylamine or butylamine showed no detectable activity. Therefore, the bulkiness and rigidity provided by the piperidine ring appears to be critical for the fibrinolytic activity of this family of compounds.

Substitution of the 1,2,3-triazole ring for a 1,2,4-triazole provided molecules (**9**, **10**) with no detectable activity. The results obtained with molecular dynamics suggest that 1,2,3-triazole provides anchoring to the binding site, mainly by interacting with Tyr72. In contraposition, 1,2,4-triazole is not able to provide such anchoring.

Finally, the interaction of the most active compound (**4**) and $GABA_A$ receptor was studied computationally. The results suggest a very low chance of this undesirable interaction, which is a known source of secondary effects for TXA.

4. Blood Brain Barrier Activity

4.1. Chapter introduction

In the previous chapter, an extensive study was performed to further understand the structure activity relationship (SAR) of the newly discovered family of compounds, as well as to develop a compound with improved activity over the original LTI-6 (compound **1**). The results of this extensive study provided a new candidate (compound **4**) with improved antifibrinolytic activity in plasma with an IC_{50} approximately 2.5 times lower than compound **1**.

As explained in the introduction, hyperfibrinolysis during traumatic brain injury (TBI) has been linked by numerous publications to an increase in blood brain barrier (BBB) permeability. Such increase in permeability is known to contribute to tissue damage, edema, inflammation and neural disfunction. In addition, it is associated with neurodegeneration and other comorbidities such as Alzheimer's disease and epilepsy.

The objective of this chapter is to test our most active compound **4** in a hyperfibrinolytic BBB *in vitro* model. Other antifibrinolytic compounds, such as TXA or compound **1** will also be assayed for comparison. The hypothesis is that BBB degradation occurs, at least partially, due to an excessive activation of Plg into Plm by tPA, caused by the mentioned hyperfibrinolytic state. If this hypothesis is true, compound **4** should offer a protective effect by reducing the rate of Plg activation *in vitro*. This effect should also be observed for other antifibrinolytic compounds.

To assess the effect caused by the different compounds evaluated, permeability studies will be performed. In addition, the effect over tight junction formation will also be studied.

4.2. Validation of hyperfibrinolytic BBB *in vitro* model

The first step to simulate a given condition *in vitro* is to choose which type of model is the most appropriate. In the case of the BBB, many different strategies have been developed over the years. The indispensable element forming the model are brain microvascular endothelial cells, which

conform the physical barrier. However, in many cases, BBB *in vitro* models also include astrocytes due to their documented relevance in the BBB phenotype. Other cell types such as pericytes have also been considered in some cases. It is important to highlight that increasing the number of cell types present in a model also dramatically increases its complexity, and therefore hinders reproducibility. Other physical properties can also be considered, such as the presence of a 3D environment to mimic the extracellular matrix, or the exposure to shear stress on the cells through fluid flow.

In this work, the choice was made to value simplicity over complexity to guarantee high reproducibility in the replicates of each condition assayed. Therefore, the chosen model was a 2D monolayer of human brain microvascular endothelial cells (HBMEC). In all permeability and Western blot assays, the conditions were always static, that is in the absence of shear stress forces. However, immunofluorescence staining was performed under both static and dynamic conditions, in order to evaluate the effect of shear stress on tight junctions.

Independently of the type of experiment, hyperfibrinolytic conditions were simulated by exposing the HBMECs to depleted medium containing certain concentrations of tPA and/or Plg. Prior to using the *in vitro* model to assay the effect of any external compound, the model was evaluated and optimized by determining permeability, as well as tight junction (TJ) formation and distribution.

4.2.1. Effect of tPA and Plg on permeability

Permeability was assessed for different concentrations of tPA and Plg. The ratio of tPA and Plg was kept at 1:2 following the conditions used by Niego et al[141]. As observed in Figure 55, permeability was not significantly different from the control group for tPA and Plg concentrations equal or lower than 0.5 and 1.0 µg/mL respectively. When exposed to 1.0 µg/mL tPA and 2.0

µg/mL Plg concentrations, however, permeability increased over 2-fold with respect to the control. This increase indicates damage to the cells and/or junctions of the BBB, which negatively impacts its ability to prevent the crossing of high molecular weight solutes. These results are in accordance with the literature which suggests that Plm, activated from Plg by the action of tPA, can induce BBB disruption.

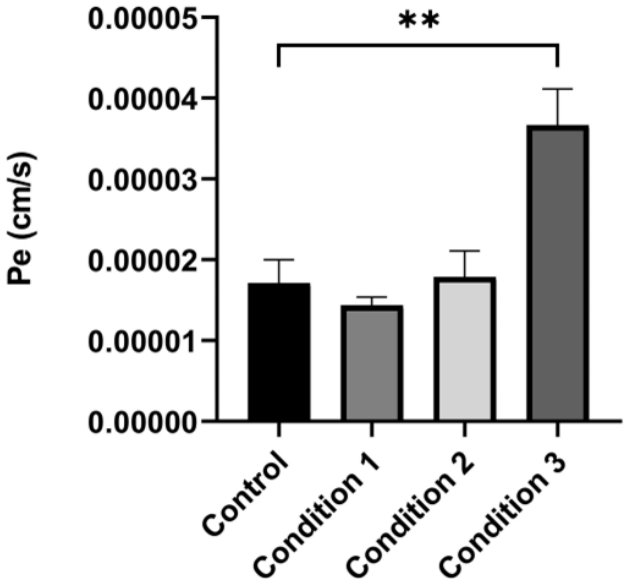

	tPA (µg/mL)	Plg (µg/mL)
Condition 1	0.1	0.2
Condition 2	0.5	1.0
Condition 3	1.0	2.0

Figure 55. BBB permeability under exposure to different concentrations of tPA and Plg for 24 hours. Each condition was assayed in triplicate. Error bars represent standard deviation. **P value < 0.01.

4.2.2. Effect of tPA and Plg on tight junctions

The expression of claudin-5, a tight junction protein of the claudin family, was quantified through western blot for different concentrations of tPA and Plg. The results (Figure 56) show that claudin-5 expression is highly sensitive to the combined presence of tPA and Plg. In fact, all three different conditions severely reduced the amount of claudin-5 present in the cell population

compared to the control group. The lower concentration tested (0.1 µg/mL tPA and 0.2 µg/mL Plg) reduced the claudin-5 content almost by half. Increased concentrations of tPA and Plg further reduced the protein expression.

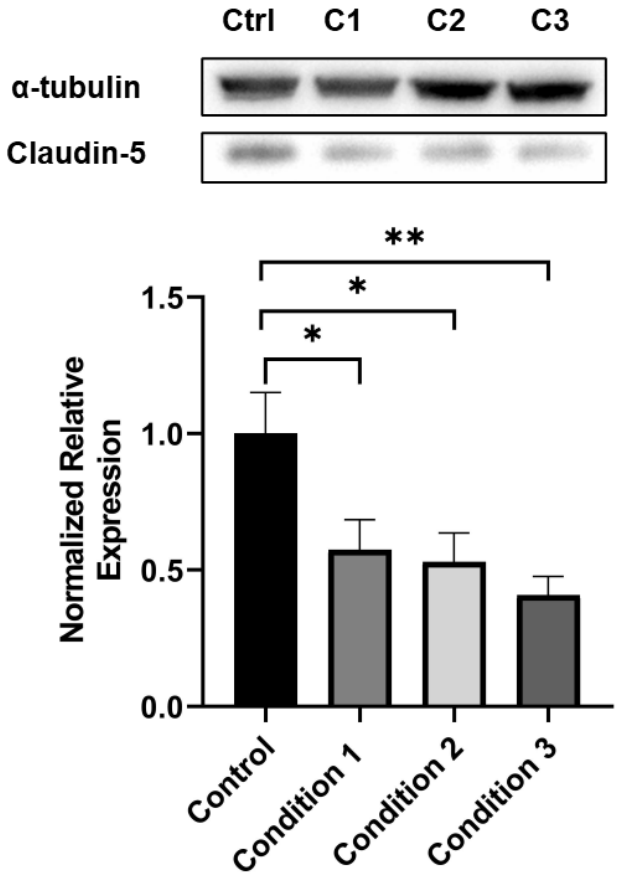

	tPA (µg/mL)	Plg (µg/mL)
Condition 1	0.1	0.2
Condition 2	0.25	0.5
Condition 3	0.5	1.0

Figure 56. Western blot determination of claudin-5 expression under different concentrations of tPA and Plg for 24 hours. α-tubulin was used as the loading control protein. The graph shows the expression of claudin-5 relative to that of α-tubulin. Image quantification performed with ImageJ software. **P value < 0.01. *P value < 0.05.

These results show a higher sensitivity towards tPA and Plg concentrations than the permeability assays. While the permeability was not significantly affected at concentrations of 0.5 µg/mL tPA and 1.0 µg/mL Plg or lower, the claudin-5 content was reduced by almost halve at much lower

concentrations (0.1 µg/mL tPA and 0.2 µg/mL Plg). Considering that in both assays the exposure was for 24 hours, this comparison indicates that claudin-5 degradation is probably not enough by itself to explain the increase in permeability.

Overall, the combined effect of tPA and Plg is proved to reduce the amount of claudin-5 present in a monolayer of HBMEC. Thereby, the presence of in situ activated Plm can cause the degradation of tight junctions (TJs).

4.3. Evaluation of antifibrinolytic compounds

4.3.1. Permeability assays

Both compound **4** and TXA were evaluated to study their effect on HBMEC under hyperfibrinolytic conditions. Compound **4** was the molecule with highest antifibrinolytic potency among the new family of compounds, while TXA remains the gold standard among antifibrinolytic drugs. As shown in Figure 57, both compounds presented a similar behavior. In both cases, permeability increased by approximately 50% in the presence of tPA and Plg. However, the presence of either compound **4** or TXA at a concentration of 100 µM successfully mitigated the negative impact on permeability, achieving values which were not significantly different from the control. These results reinforce the notion that the increase in permeability is caused by active plasmin, since both compound **4** (in this thesis) and TXA (in abundant literature) have been proven to inhibit the activation of Plg into Plm. Unexpectedly, increasing the concentration of either TXA or compound **4** to 1 mM did not improve their BBB protective function. In fact, permeability slightly increased at 1 mM when compared to 100 µM for both compounds. This could indicate a certain toxicity by both compounds when used at such high concentrations. In any case, it shows that increasing the concentration over 100 µM for these

two compounds is not necessary in order to mitigate the permeability increase caused by our hyperfibrinolytic BBB conditions.

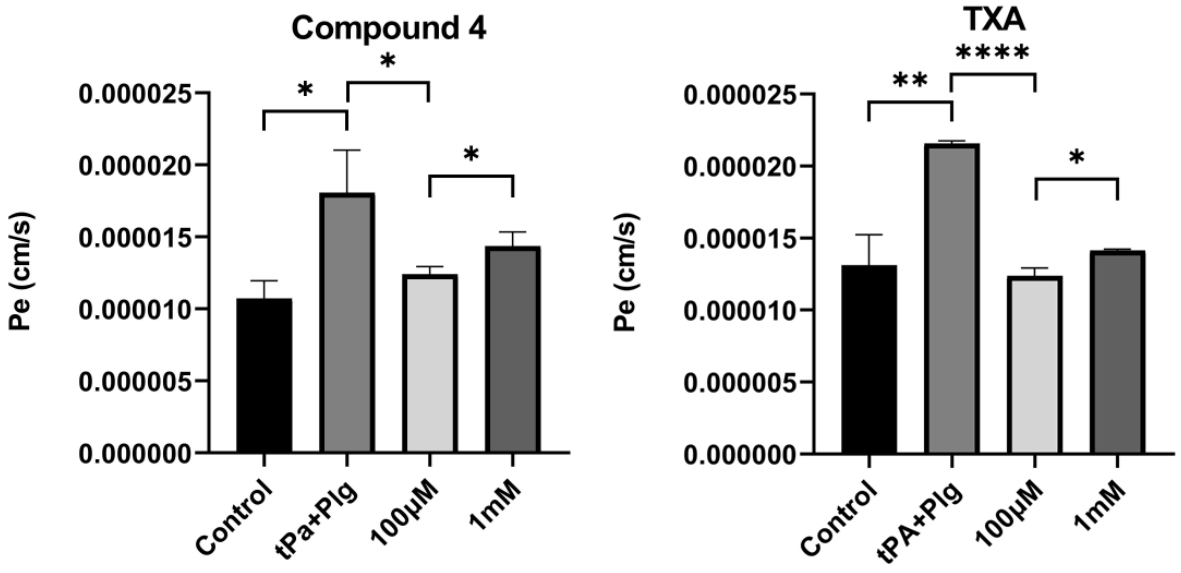

Figure 57. Permeability assays for compound **4** and TXA. Each sample was exposed to their corresponding condition for 24 hours before the permeability assay. All conditions, except for the control, included 1.0 µg/mL tPA and 2.0 µg/mL Plg. Two different compound concentrations were tested, 100 µM and 1 mM. Each condition was tested in triplicate. ****P value < 0.0001. **P value < 0.01. *P value < 0.05.

4.3.2. Claudin-5 expression

The effect of different compounds on the expression of claudin-5 was also studied through western blot assays. As expected, the results (Figure 58) show a clear reduction in claudin-5 protein content when exposed to tPA and Plg (1.0 µg/mL and 2.0 µg/mL respectively). In such hyperfibrinolytic conditions claudin-5 content was reduced by approximately half when compared to the control. Four different compounds were tested at 100 µM in the same hyperfibrinolytic conditions. Both compounds 4 and 1 exerted a complete inhibition of claudin-5 degradation,

showing protein levels which were not significantly different from the control. Both compounds are part of the newly discovered family of 1,2,3-triazole derivatives. TXA was also tested in this assay, as well as the piperidine derivative with high antifibrinolytic activity 4-PIOL. As seen in Figure 58, both compounds showed a small reduction in the degradation of claudin-5 when compared to the condition with only tPA and Plg, although not statistically significant. Therefore, compounds 4 and 1 showed a significantly higher inhibition of claudin-5 degradation than TXA or 4-PIOL. This indicates that both 1,2,3-triazole derivatives presented a higher inhibition of Plm activation than 4-PIOL or TXA in our hyperfibrinolytic BBB model.

These results are especially surprising in the case of 4-PIOL which is reported to present an IC_{50} in plasma of approximately 1 μM, and therefore significantly more potent than compounds **4** (13.8 μM) or **1** (36.8 μM). TXA also presented an IC_{50} in human plasma (33.3 μM) similar to that of compound **1**. These differences between results in plasma and in a cellular environment point towards the different levels of specificity of the different molecules. The environment of human plasma contains a limited number of potential receptors when compared to an environment containing cells. TXA and 4-PIOL are known to present some problems with specificity. Their small size facilitates their interaction with many other lysine residues besides the ones of interest, and their affinity towards other receptors such as $GABA_A$ have also been described. In contraposition, compounds **4** and **1** present a relatively larger size which potentially limits the number of receptors they can interact with. As an example, our docking studies with $GABA_A$ showed that compound **4** was not able to fit in the GABA pocket, therefore making it highly unlikely that such interaction could occur *in vivo*.

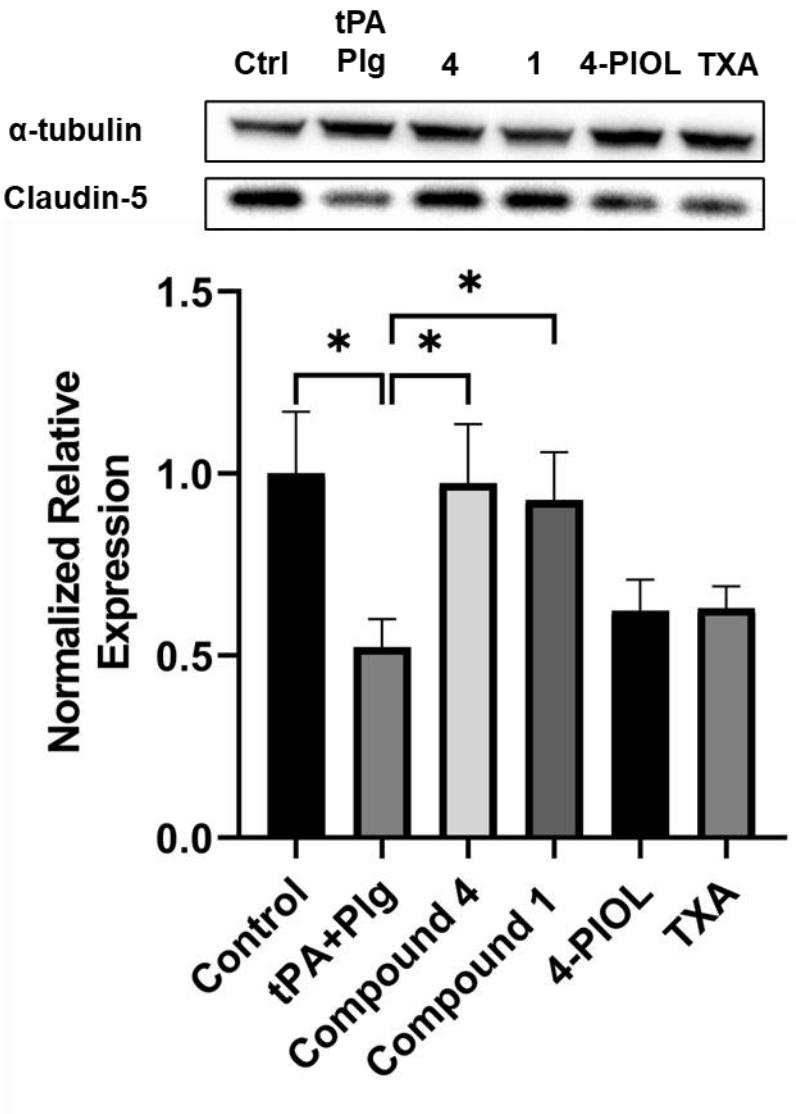

Figure 58. Western blot determination of claudin-5 expression in a hyperfibrinolytic BBB state for different antifibrinolytic compounds. All conditions, except for the control, included 1.0 µg/mL tPA and 2.0 µg/mL Plg. Compounds were tested at a concentration of 100 µM.

4.3.3. Morphology and tight junction localization in static conditions

The effect on morphology and tight junction localized intensity was studied through immunofluorescent staining. In this case, cells were cultured and exposed to the different

conditions on culture plates adapted for confocal microscopy. After 24 hours of exposure, cells were fixed, stained, and imaged using a confocal microscope.

First, the conditions were applied without the presence of flow shear stress. The control HBMEC (Figure 59) show a classic endothelial cell *in vitro* morphology, in which cells form a perfect monolayer with close contact among neighboring cells. The localized presence of ZO-1 at the intercellular connections is proof of healthy tight junction formation. In this experiment a condition with only Plg (and no additional tPA) was also included. In this case, some tight junctions were already weakened or lost. This can be explained due the capacity of endothelial cells to release tPA. Such concentration of tPA, although probably low, can trigger a certain Plm activation and therefore tight junction degradation. With the addition of both Plg and external tPA, such negative effect on TJs was exacerbated. In this case, the intensity of ZO-1 between most cells was lost or greatly weakened, indicating severe TJ degradation. The presence of these TJs was visibly recovered with the presence of each of the tested compounds: TXA, **4** and **1**.

The average intensity of junctions was quantified from all acquired images (Figure 60). The results show that under static conditions, both TXA and compound **4** were able to maintain a ZO-1 intercellular intensity similar to that of the control, although slightly lower. Compared to the hyperfibrinolytic condition with tPA and Plg, ZO-1 intensity was almost twice as high. In the case of compound **1**, such value was approximately 20% lower than for **4**. However, it was still significantly higher than that of tPA and Plg combined. The graph also shows that the difference in TJ intensity between only Plg and the combination of Plg and tPA was statistically significant. This is in line with the notion that active Plm is responsible for the degradation of TJs and consequently the increase in BBB permeability.

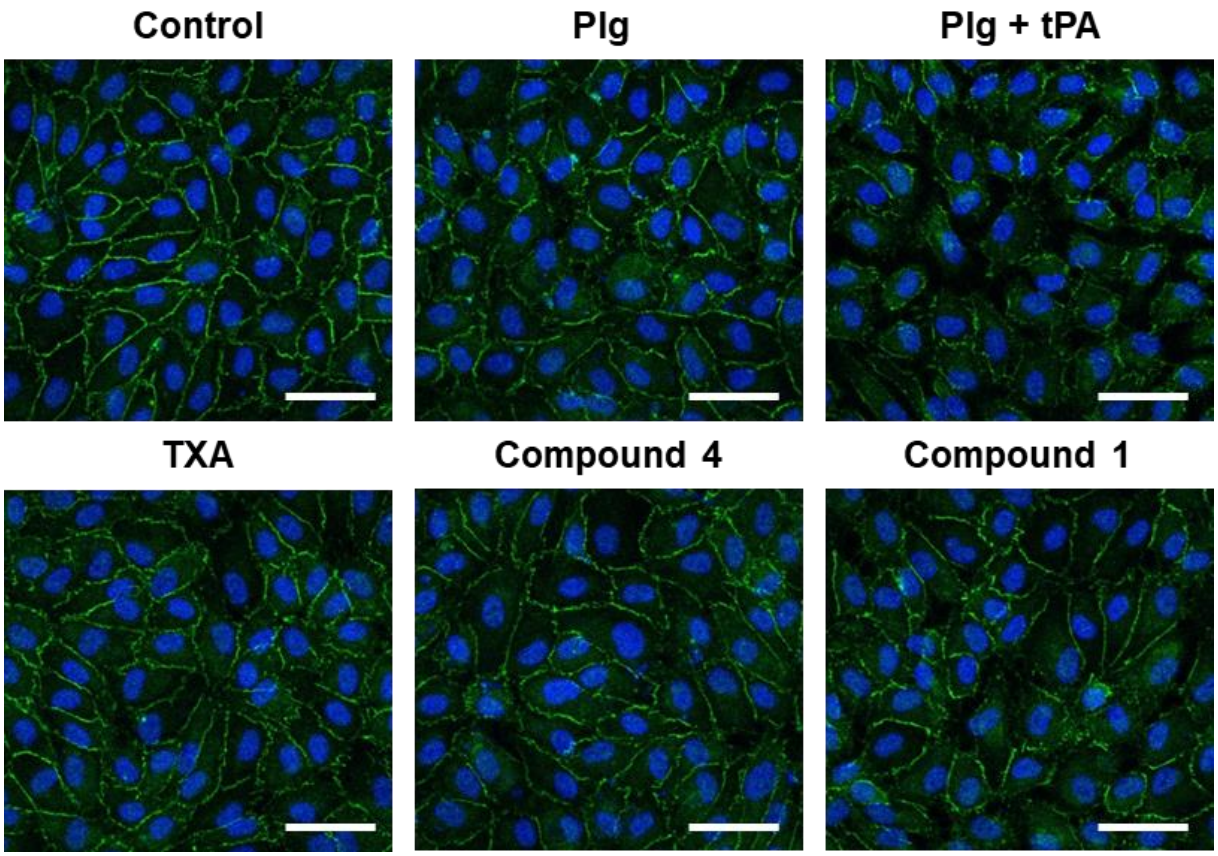

Figure 59. Confocal microscope images of HBMEC exposed to hyperfibrinolytic static conditions with or without the presence of different antifibrinolytic compounds. Concentrations used were 1.0 µg/mL for tPA, 2.0 µg/mL for Plg, and 100 µM for the three compounds tested. Cells were exposed to their corresponding condition for 24 hours. Tight junction protein ZO-1 is stained in green, and nuclei are stained in blue (DAPI). Scale bar indicates 50 µm.

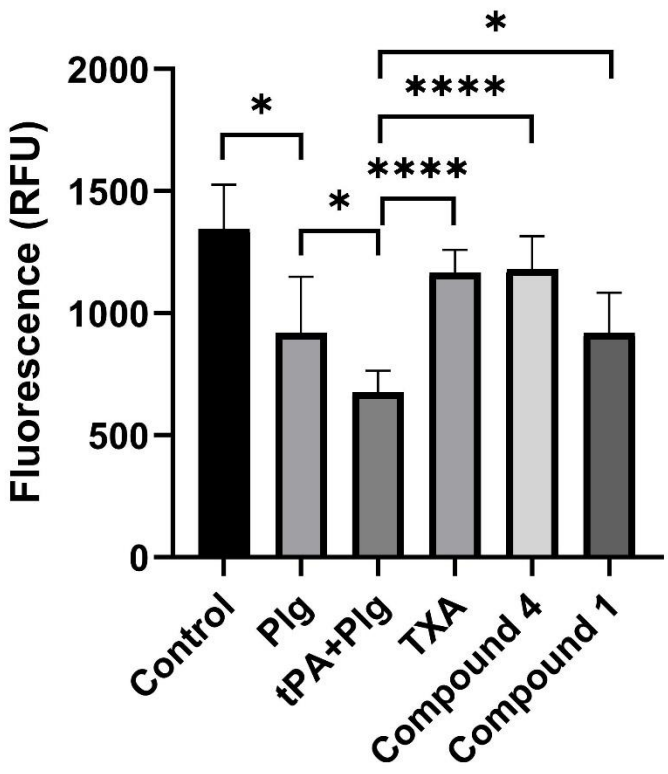

Figure 60. Average ZO-1 fluorescence intensity values under static conditions. Fluorescence at the junction areas between cells was quantified using ImageJ. ****P value < 0.0001. *P value < 0.05.

4.3.4. Morphology and tight junction localization in flow conditions

The above-described experimental set-up was replicated but under flow conditions, to introduce a very important mechanical stimuli, shear stress, in the *in vitro* model. In this case, commercially available flow chambers were used to seed the HBMEC. The chambers allowed for direct visualization using a confocal microscope following cell fixation and immune staining.

As seen in Figure 61, the morphology of endothelial cells was clearly different between flow and static conditions. When exposed to shear stress, cells adopted a more elongated morphology, aligned in the direction of flow, while maintaining the close interconnections between cells and "cobblestone" distribution. In this case, the negative effect of Plg and tPA combined caused

noticeable cell detachment, in addition to the loss of tight junctions. This indicates that active Plm possibly affects not only TJs, but other proteins responsible for cell adhesion, such as integrins. The intensity of TJs and the general *in vitro* BBB health state were visibly worsened under the combination of Plg and tPA, with a ZO-1 expression less than half than that of the control. The addition of TXA, **4** ,or **1** clearly inhibited, at least partially, the damaging effect of the hyperfibrinolytic state. In this case, however, the quantified TJ intensity was slightly higher for compound **1** compared to those of TXA and compound **4**. The first caused a 100% increase in ZO-1 intensity compared to the hyperfibrinolytic state (tPA + Plg), while the other two showed approximately a 50% increase. In all cases, the intensity levels remained lower than that of the healthy control. However, a visible reduction in the damaging effect of the hyperfibrinolytic conditions was observed.

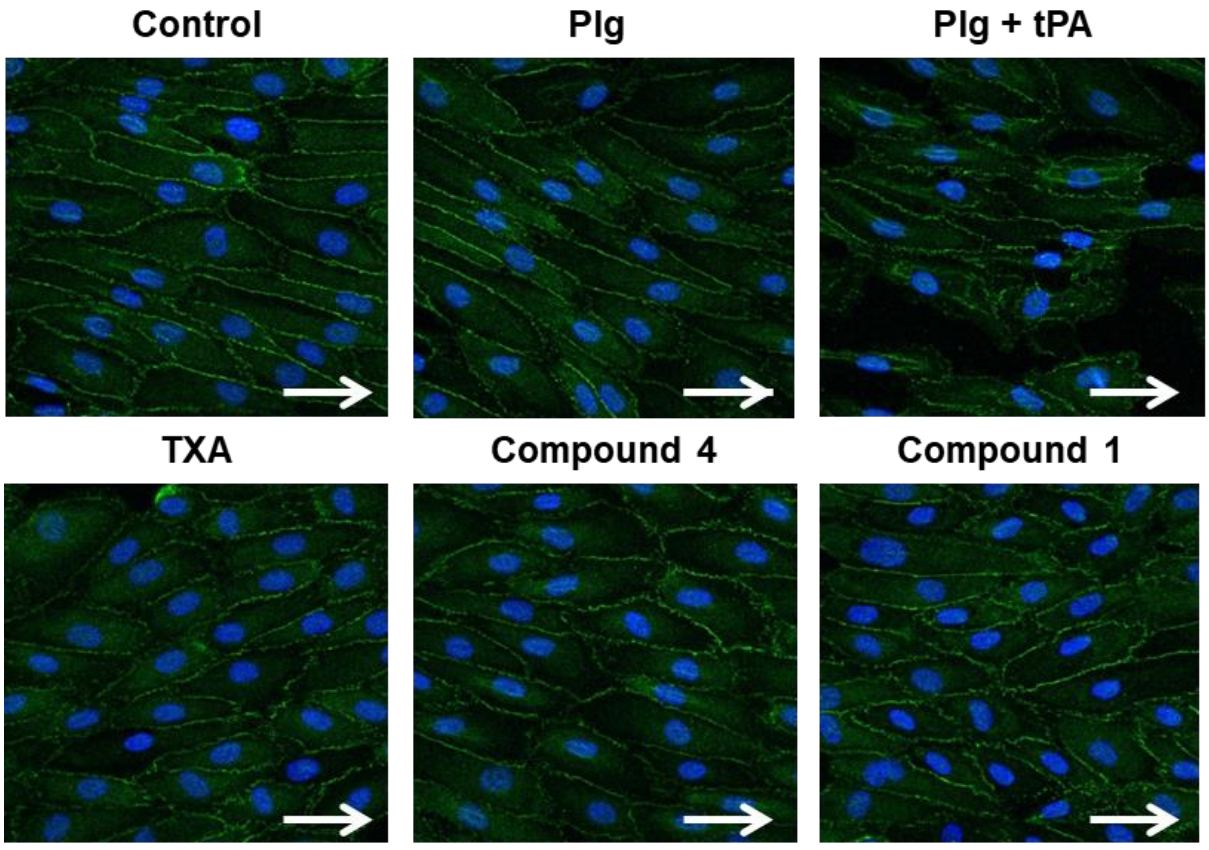

Figure 61. Confocal microscope images of HBMEC exposed to hyperfibrinolytic flow conditions (10 dyn/cm^2 shear stress) with or without the presence of different antifibrinolytic compounds. Concentrations used were 1.0 µg/mL for tPA, 2.0 µg/mL for Plg, and 100 µM for the three compounds tested. Cells were exposed to their corresponding condition for 24 hours. Tight junction protein ZO-1 is stained in green, and nuclei are stained in blue (DAPI). Arrow indicates scale bar of 50 µm and flow direction.

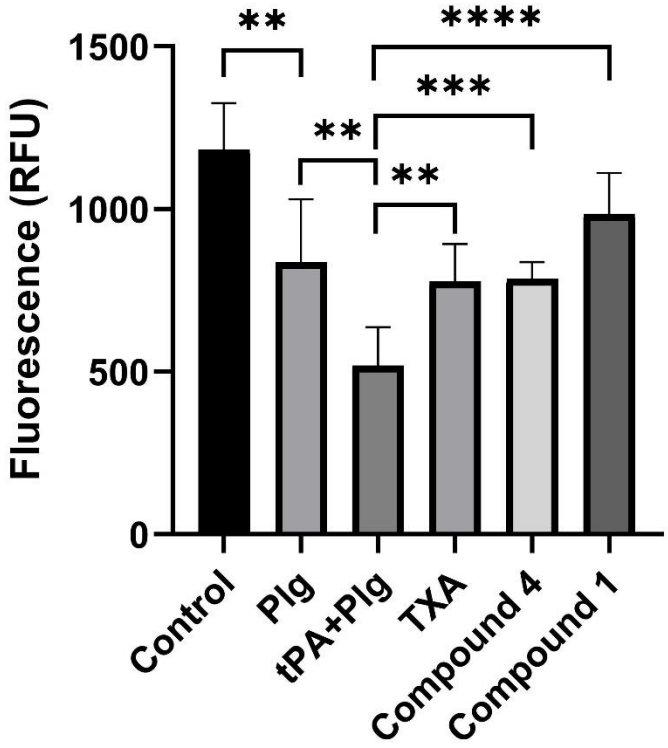

Figure 62. Average ZO-1 fluorescence intensity values under flow conditions (10 dyn/cm^2 shear stress). Fluorescence at the junction areas between cells was quantified using ImageJ. ****P value < 0.0001. ***P value < 0.001.**P value < 0.01.

4.4. Conclusions of the chapter

Several conclusions were extracted from the results presented in this chapter. The combined presence of Plg and tPA caused a measurable increase in permeability of the BBB *in vitro* model. Permeability under the hyperfibrinolytic conditions was approximately 2-fold higher than for the control. In addition, the hyperfibrinolytic conditions also had an effect on TJ protein expression. Both the total amount of claudin-5 and the localized expression of ZO-1 was reduced by approximately 50% in the presence of high Plg and tPA concentrations.

The addition of compound **4** or TXA at 100 μM both reduced the permeability increase, achieving values not significantly different than the control. Therefore, both antifibrinolytic compounds acted as protecting agents in the hyperfibrinolytic model.

With regards to TJ proteins, antifibrinolytics also proved to significantly reduce their degradation. The total expression of claudin-5 remained at the level of the control with the presence of compound 4 as well as of compound 1, both at 100 μM. Such effect was not significantly observed, however, for other antifibrinolytic agents such as TXA and 4-PIOL.

The localized expression of ZO-1 was also affected by the presence of different studied antifibrinolytic agents. TXA, compound **1** and **4** all showed a significantly increased intensity of junction-localized ZO-1 when compared with the hyperfibrinolytic condition (tPA + Plg), both under static and dynamic conditions.

Overall, the most active compounds of the newly discovered family, **1** and **4**, showed a protective effect on the BBB hyperfibrinolytic model. The results do not allow, however, to conclude that their performance in this regard is significantly better than TXA. Despite this, the work presented in this chapter confirms the hypothesis that an increased level of activated Plm causes increased BBB permeability. It also indicates that such hyperfibrinolytic conditions have a direct negative

impact on TJ expression, both globally and locally at the junction areas. And finally, the results show that the newly described family of compounds can be an effective tool to minimize such negative effect on the BBB when exposed to the hyperfibrinolytic conditions present during traumatic brain injury (TBI).

5. Materials and methods

5.1. Equipment

Incubator: Forma™ Steri-Cult™ CO_2 Incubator (ThermoFisher, 3307TS)

Centrifuge: Centrifuge 5702 (Eppendorf, 5702000329)

Biological hood: Class II Type A2 (NiuAire)

Cell counter: Cellometer Auto T4 Bright Field Cell Counter (Nexcelom Bioscience)

Refrigerated centrifuge: Symphony 2417R (VWR)

Varioskan™ LUX multimode microplate reader (ThermoFisher, VL0000D0)

Peristaltic pump: MCP ISM404B (Ismatec®)

Fluorescent inverted microscope Eclipse Ti-E (Nikkon)

Confocal microscope: Olympus FV1200

5.2. Materials and reagents

5.2.1. Blood and Plasma assays

Butterfly needle (BD Vacutainer, 1026367282)

Needle holder (BD Vacutainer, 1026364815)

Sodium citrate tubes 0,105 M (BD Vacutainer, 1026367714)

Non-silicone dry tubes (BD Vacutainer, 1026367624)

96-Well Microtiter Microplates (Thermo Scientific, AB0796)

TF: Recombinant Human Tissue Factor (Siemens, OUHP20)

tPA: Recombinant human Tissue Plasminogen Activator (abcam, ab92637)

Calcium chloride (Sigma-Aldrich, C8106)

Tris Hydrochloride 1M. pH = 7.5 solution (Fisher BioReagents, 10573145)

Tranexamic acid (Sigma-Aldrich, PHR1812)

ε-Aminocaproic acid (Sigma-Aldrich, A2504)

Plasmin Inhibitor Screening Assay Kit (Fluorometric) (abcam, ab204729)

Tissue Plasminogen Activator Activity Assay Kit (Colorimetric) (BioVision, K178-100)

Tissue type Plasminogen Activator Human Activity Assay Kit (Colorimetric) (abcam, ab108905)

5.2.2. Organic synthesis

1-(piperidin-4-yl)-1H-1,2,3-triazole-4-carboxylic acid hydrochloride (**8**, Enamine, EN300-261273)

tert-butyl 4-hydroxypiperidine-1-carboxylate (**12**, Sigma-Aldrich, 495484)

tert-butyl (2-bromoethyl)carbamate (**16**, Sigma-Aldrich, 17354)

tert-butyl (3-bromopropyl)carbamate (**17**, Sigma-Aldrich, 17356)

tert-butyl (4-bromobutyl)carbamate (**18**, Sigma-Aldrich, 90303)

tert-butyl ((4-hydroxycyclohexyl)methyl)carbamate (**25**, Fluorochem, 238420)

Tranexamic acid (**59**, Sigma-Aldrich, PHR1812)

Triethylamine (Sigma-Aldrich, 8083520100)

Methanesulfonyl chloride (Sigma-Aldrich, 471259)

Dichloromethane (Sigma-Aldrich, 270997)

Sodium azide (Sigma-Aldrich, S2002)

N,N-Dimethylformamide (Sigma-Aldrich, 227056)

Ethyl propiolate (Sigma-Aldrich, E46607)

Copper(I) iodide (Sigma-Aldrich, 205540)

Hydrazine hydrate (Sigma-Aldrich, 225819)

n-butanol (Sigma-Aldrich, 360465)

Acetonitrile (Sigma-Aldrich, 271004)

CDI: 1,1′-Carbonyldiimidazole (Sigma-Aldrich, 115533)

DBU: 1,8-Diazabicyclo[5.4.0]undec-7-ene (Sigma-Aldrich, 139009)

Methanolic ammonia 7 N (Sigma-Aldrich, 499145)

TFAA: Trifluoroacetic anhydride (Sigma-Aldrich, 106232)

Hydroxylamine hydrochloride (Sigma-Aldrich, 159417)

Sodium bicarbonate (Sigma-Aldrich, S6014)

Methanol (Sigma-Aldrich, 322415)

p-Toluenesulfonyl chloride (Sigma-Aldrich, T35955)

Ethanol (Sigma-Aldrich, 493546)

Di-tert-butyl dicarbonate (Sigma-Aldrich, 205249)

Tetrahydrofuran (Sigma-Aldrich, 401757)

Hydrogen chloride 3 M in methanol (Sigma-Aldrich, 90964)

methyl 1H,1,2,4-triazole-3-carboxylate (Sigma-Aldrich, 530352)

Sodium hydride (Sigma-Aldrich, 4529120)

5.2.3. Cell culture

HBMEC: Human Brain Microvascular Endothelial Cells (Pelobiotech, PB-CH-110-4011)

Endothelial Microvascular Growth Medium EGM-2MV (Lonza, CC-3202) supplemented with 5% FBS and PS 1%

Endothelial Microvascular Depleted Medium: Regular EGM-2MV medium depleted of Vascular Endothelial Growth Factor (VEGF), and supplemented with 2% FBS and PS 1%

FBS: Fetal Bovine Serum (ThermoFisher, 10437036)

PBS: Phosphate Buffered Saline (ThermoFisher, 10010023)

Trypsin: 0.05% Trypsin-EDTA (ThermoFisher, 25300054)

DMSO: Dimethyl Sulfoxide (Sigma-Aldrich, 276855)

PS: Penicillin 10000 units/ml penicillin G sodium with Streptomycin 10 mg/ml streptomicyn sulfate 0.85% NaCl (Life Technologies, 25030-081)

Freezing container: Mr. Frosty™ Freezing Container (Thermo Scientific, 5100- 0001)

T75 Culture Flasks (Fisher Scientific, 15350591)

P100 Culture dishes (Fisher Scientific, 08-772E)

5.2.4. Cell-based experiments

µ-Dish for static conditions: µ-Dish 35 mm, high (Ibidi, 81156)

µ-Slide for dynamic conditions: µ-Slide I Luer ibiTreat 0.8 mm (Ibidi, 80196)

Connectors for µ-Slide: Elbow Luer Connector Male (Ibidi, 10802)

Flow loop tubing: Silastic 2415526 Laboratory Tubing, .03" ID x .065" OD, 50' (Cole-Parmer, NC1044271)

Flow loop connectors: Masterflex Fitting, Polypropylene, Straight, Hose Barb Union, 1/16" (Cole-Parmer, 0636511)

Plasminogen: Native human Plasminogen protein (Active) (abcam, ab92924)

tPA: Recombinant human Tissue Plasminogen Activator (abcam, ab92637)

TXA (Sigma-Aldrich, PHR1812)

5.2.5. Permeability assays

Transwell inserts: Corning® Transwell® polycarbonate membrane cell culture inserts (Sigma-Aldrich, CLS3413)

24-well plates Corning® (Sigma-Aldrich, CLS3526)

Dextran-FITC: Fluorescein isothiocyanate–dextran 4,000 MW (Sigma-Aldrich, 46944)

384-well plates black: Nunc® MaxiSorp™ 384 well plates (Sigma-Aldrich, P6491)

5.2.6. Western Blot

RIPA buffer (ThermoFisher, 89900)

Protease inhibitor tablets (ThermoFisher, 88266)

4X Sample Buffer Reducing Agent (Fisher Scientific, AAJ60015AC)

NuPAGE™ 10 %, Bis-Tris, 1,0 mm, Mini protein gels (ThermoFisher, NP0301BOX)

NuPAGE™ MES SDS Processing Buffer (20X) (ThermoFisher, NP0002)

iBlot™ Transfer Stack, nitrocellulose, regular size (ThermoFisher, IB301031)

NuPAGE™ Transfer Buffer (20X) (ThermoFisher, NP00061)

Tween 20 (Sigma-Aldrich, P7949)

StartingBlock™ (PBS) Blocking Buffer (ThermoFisher, 37578)

5% non-fat dry milk (LabScientific)

Claudin 5 Monoclonal Antibody (4C3C2) (ThermoFisher, 35-2500)

Anti-alpha Tubulin antibody [DM1A] - Loading Control (Abcam, ab7291)

Goat anti-Mouse IgG (H+L) Poly-HRP Secondary Antibody, HRP (ThermoFisher, 32230)

Immobilon Forte Western HRP substrate (Sigma-Aldrich, WBLUF)

5.2.7. Immunofluorescence

PFA: Paraformaldehyde (Sigma-Aldrich, 158127)

Glycine (Sigma-Aldrich, 50046)

Triton™ X-100 (Sigma-Aldrich, X100)

PBS: Phosphate Buffered Saline (ThermoFisher, 10010023)

BSA: Bovine Serum Albumin (Sigma-Aldrich, 810664)

Goat serum (Sigma-Aldrich, G9023)

ZO-1 Polyclonal Antibody (ThermoFisher, 40-2200)

Anti-CD31(PECAM-1) antibody, Mouse monoclonal (Sigma-Aldrich, P8590)

Goat Anti-Rabbit IgG H&L (Alexa Fluor® 488) (Abcam, ab150077)

Goat Anti-Mouse IgG H&L (Alexa Fluor® 568) (Abcam, ab175473)

DAPI (Sigma-Aldrich, D9542)

5.3. Blood assays

5.3.1. Blood obtention

For experiments performed at IQS, blood was obtained from healthy donors, following the protocol approved by the ethics committee from Ramon Llull University (CER URL 2017_18_006, approved on March 19th of 2018). For experiments performed at MIT, human blood was obtained and manipulated under the MIT biological registration 401 for the Edelman Lab.

5.3.2. Whole blood coagulation assay

To determine the effect on clotting, compounds were assessed on a qualitative assay based on the visual observation of clot generation. The test was carried out without the addition of exogenous tPA to avoid the activation of fibrinolysis. Therefore, only clot formation was studied. Blood samples were allowed to clot in the presence of the studied compounds and the quality of generated clots was examined.

Compounds were first dissolved in deionized water, and then diluted in Tris HCl buffer to achieve a final assay concentration of 40 µM. The assay was performed in glass tubes. Previously to blood addition, 20 µL of the evaluated compounds in Tris HCl were added to the different tubes. Each tube was then filled with 800 µL of blood, and then incubated at 37 ºC to allow blood clotting. Shaking of the tubes was performed right after blood addition to ensure mixture of the compounds with blood. A positive control (PC) clot for the assay was performed with 20 µL of Tris HCl buffer, previously added to the tube.

Clots were continuously observed during their formation to detect differences in clot formation. Clot size, and integrity were monitored until clots were generated and photographs were taken during this period.

5.3.3. Whole blood dosage

A qualitative assay was performed to determine the *ex vivo* dose at which LTI-6 was able to inhibit clot degradation in whole blood. The results were compared to those of TXA. Therefore, whole blood was allowed to clot on tubes already containing fibrinolysis activators and the studied compounds. Once fibrinolysis was initiated, clots were monitored to detect the time at which each concentration of the compounds produced the lysis of the clot. The assay was performed following the model developed by Prasad et al. (2006).

Compounds were first dissolved in deionized water, and then diluted in Tris HCl buffer to achieve final assay concentrations of 10, 20, 40 and 60 µM. The source of tPA for the assay was stored at -20 ºC until used.

The assay was performed in glass tubes, which were previously prepared with 20 µL of a mixture of tPA (final concentration 10 µg/mL) and the evaluated compound in Tris HCl buffer. Following, 800 µL of blood were transferred to each tube and allowed to clot. Tubes were incubated at 37 ºC and clots were observed for 24 h or until the clots were completely lysed. The assay was performed with occasional shaking. A PC clot was performed with 20 µL of tPA (final concentration 10 µg/mL) in Tris HCl Buffer.

The effective dosage of each compound was determined by monitoring clot degradation over time. Photographs of the evolution of clots were taken during the 24 h of incubation.

5.3.4. Whole blood clot lysis

Fibrinolysis can be assessed quantitatively in whole blood by measurement of D-dimer concentration. D-dimer is the smallest proteolytic degradation product released by the lysis of a fibrin clot and serves as a specific fibrinolytic marker. The quantitation of D-dimer can be determined photometrically by an immunoturbidimetric assay.

Accordingly, whole blood clots were prepared following the method described by Elnager et al. (2014), optimized with small variations. Once fibrinolysis was initiated with the addition of tPA together with the studied compounds, changes in absorbance over time were measured. The quantity of D-dimer released from the clots reflected the thrombolytic activity of the fibrinolytic components and at the same time, the antifibrinolytic capacity of the studied compounds[142]. Hence, the ex vivo antifibrinolytic activity of LTI-6 and TXA in whole blood was determined through D-dimer quantification.

The Elisa Assay Kit was stored at 4 ºC. All reagents were brought to RT before use and prepared according to manufacturer's instructions. Wash Buffer Concentrate was mixed and diluted 1:20 with deionized water to prepare 1X Wash Buffer. Assay Diluent was diluted 5-fold with deionized water and the reconstituted biotin conjugate was diluted 80-fold with Assay Diluent. The Streptavidin-HRP solution was prepared within 15 min of usage, being diluted 900-fold with Assay Diluent. Standards for the assay were prepared from a 500 pg/mL reconstituted standard solution. 60 µL of the standard solution were added to 440 µL of Assay Diluent to prepare a 60 pg/mL standard solution, which was considered standard 1. To prepare standards 2 to 7, 400 µL of Assay Diluent were pipetted into Eppendorf tubes. The 60 pg/mL standard solution was used to produce a dilution series, from which 200 µL were taken to prepare the following standard. Before the next transfer, each tube was carefully mixed. The blank was constituted with 400 µL of Assay

Diluent. The source of tPA for the assay was stored at -20 ºC until used. Compounds were first dissolved in deionized water, and then diluted in Tris HCl buffer to achieve final assay concentration of 20 µM.

Directly after extraction, 500 µL of blood were transferred into glass tubes and allowed to clot for 10 min at RT. Tubes were incubated at 37 ºC for 1h to enable clot retraction from the walls of the glass tubes. 100 µL of a mixture of tPA and the studied compound in Tris HCl buffer were added on top of each clot. Each tube had a tPA concentration of 10.0 µg/mL in the final volume. Tubes were incubated at 37 ºC and samples were extracted at times 0, 2, 4, 7 and 24 h after the addition of tPA-compound mixture. After gentle shaking of the tubes, 5 µL of the supernatant from each tube were pipetted into Eppendorf tubes containing 100 µL of the Assay Diluent. Samples were diluted 500,000-fold and stored at -20 ºC until assayed. Each clot condition was performed in triplicate.

Following manufacturer's protocol, 100 µL of each standard and diluted samples were added to the wells of a 96-well microtiter plate from the ELISA kit. Each well had incorporated the primary antibody pre-coated, to which the samples and standards bound. The plate was covered and incubated for 2.5 hours at RT with gentle shaking. After, the solutions were discarded, and the plate was washed 4 times with Wash Buffer. After adding to each well 100 µL of the biotinylated antibody. the plate was incubated for 1 hour at RT with gentle shaking. The solutions were again discarded and the plate was washed 4 times with Wash Buffer. 100 µL of Streptavidin-HRP solution were added to each well and incubated for 45 min at RT with gentle shaking. The solutions were discarded and the plate was washed 4 times with Wash Buffer. 100 µL of 3,3′,5,5′-Tetramethylbenzidine (TMB) Substrate were added to each well, which generated measurable intensity signal. The plate was incubated for 30 min at RT in the dark with gentle shaking.

Ultimately, 50 µL of a Stop Solution were added to each well to end the reaction, causing a change of color to the solution. Absorbance was read at 450 and 550 nm within 30 min after the addition of the Stop Solution.

Absorbance values obtained from the higher wavelength (550 nm) were subtracted from the values from the lower wavelength (450 nm) to correct optical imperfections of the microplate.

$$\Delta OD = OD_{550} - OD_{450} \quad \text{(Eq. 1)}$$

Data from the standards were graphed to generate the standard curve. Using a four-parameter curve-fit, a polynomial of second order trendline was obtained for the standard curve. The absorbance values for each condition were translated into concentration values by use of the trendline. To the obtained values the Dilution Factor was applied to correct for the sample dilution.

5.4. Plasma clot lysis assay

The antifibrinolytic activity of all studied compounds was assessed through a turbidimetric assay in plasma. Specifically, changes in Optical Density (OD) were measured in plasma clots over time, after the sequential addition of tPA and the compound of interest.

Blood samples were centrifuged at 1,000 g for 15 min to obtain platelet-poor plasma. From each centrifugated tube, the supernatant was extracted and plasma was frozen and stored in aliquots at -20 °C immediately. Just before the assays, plasma was thawed at RT.

Coagulation was initiated in plasma samples by the addition of an activation mix, consisting of Tissue Factor (TF) and $CaCl_2$. Before application, TF flasks were reconstituted following manufacturer's instructions using deionized water and stored at 4ºC. A solution of $CaCl_2$ 100 mM was prepared dissolving 0.111 g of $CaCl_2$ into 10 mL of deionized water and preserved at RT until use. The source of tPA for the assay was stored as well at -20 ºC until used. A stock solution for each of the studied compounds was prepared with deionized water. From these stock solutions,

different volumes were taken to prepare various concentrations of the compounds with Tris HCl buffer.

Plasma clots were generated combining the protocols described by Stief (2008), Mutch et al. (2008) and Wu et al (2019). Hence, 20 µL of TF and 20 µL of $CaCl_2$ 100 mM were pipetted into a 96-well microtiter plate. After, 140 µL of plasma were added. The plate was sealed and incubated at 37 °C for 30 min allowing clot formation, which was closely monitored on a microplate reader at 405 nm to ensure proper clot generation. To initiate fibrinolysis, a mixture of tPA (final concentration 10 µg/mL) and different concentrations of the studied compounds were adjusted to a total volume of 20 µL with Tris HCl buffer and added on top of each clot. The plate was directly loaded into a Microplate reader and changes in OD were recorded every minute for 6 h at 37 °C at a wavelength of 405 nm.

Each assay was run independently for each molecule and clot conditions were performed in triplicate. Positive control (PC) clots were performed using 20 µL of tPA 10 µg/mL in Tris HCl buffer, which represented natural fibrinolysis without the presence of an antifibrinolytic compound inhibiting the process. Negative controls (NC) provided absorbance values for the natural dehydration of the clot over time and were performed with 20 µL of Tris HCl buffer.

Raw OD data obtained for each condition at each time point was represented as mean values plus and minus Standard Deviation (SD), from which key values were extracted. An example of the data obtained is presented in Figure 63, showing the decrease in OD over time as fibrinolysis occurs.

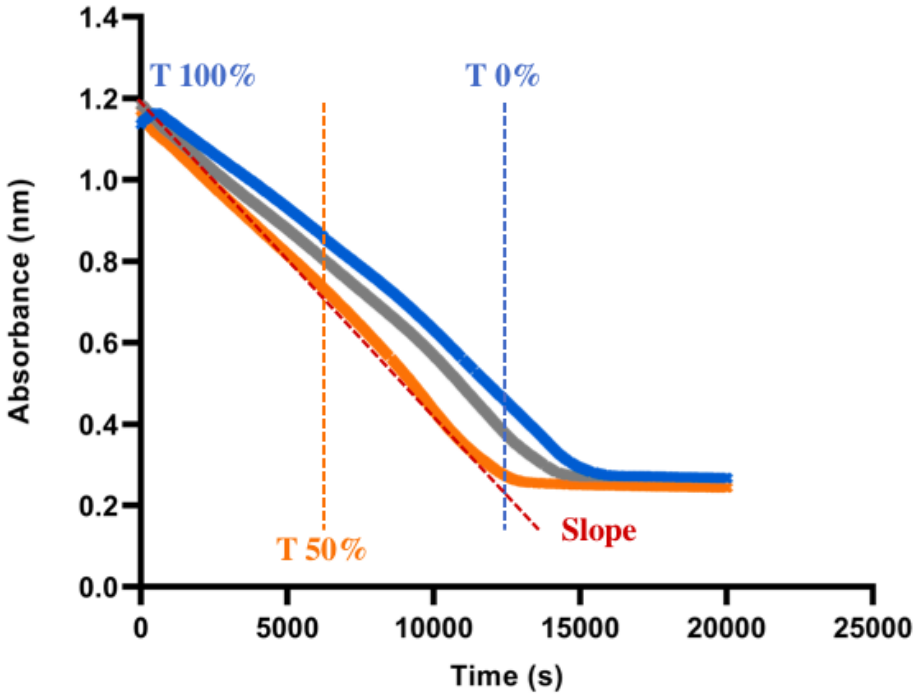

Figure 63. Fibrinolysis assay presented as changes in OD over time. Fibrin clots were formed (T100%) and lysis was monitored until clots were fully degraded (T0%). T50% represents the time at which lysis of the clots was 50%.

The rate of clot dissolution (RCD) was calculated from the slope of the graph, determined as the difference between maximum OD and minimum OD divided by the respective time between these two points. Minimum OD was taken as the absorbance value obtained after 6 h of measurement or the absorbance value at which the clot was completely lysed.

$$RCD = \frac{OD_{max} - OD_{min}}{t_{max} - t_{min}} \quad \text{(Eq. 2)}$$

The fibrinolysis rate for each compound was then obtained dividing the RCD value by the same value for the PC.

$$Fibrinolysis\ rate\ (\%) = \frac{RCD_{Compound}}{RCD_{PC}} \quad \text{(Eq. 3)}$$

The data obtained were presented as mean values ± SD, plotted into a dose-response curve. IC_{50} values for each compound were determined as the half-maximal fibrinolytic inhibitory concentration and thereby, the concentration associated with the 50% of the antifibrinolytic activity.

5.5. Isolated enzyme assays

5.5.1. Plasmin activity assay

One mechanism to block fibrinolysis is to inhibit the active site of plasmin (i.e. aprotinin). To assess whether LTI-6 was acting through this mechanism, its activity was evaluated on the active site of plasmin using a purified system. A fluorometric assay was performed, based on the capacity of plasmin to cleave a synthetic 7-amino-4-methylcoumarin-based (AMC) peptide substrate. The cleavage of the substrate releases AMC, which can be measured by fluorescence. The presence of plasmin inhibitors causes a reduction or even the completely abolition of the cleavage reaction and the resulting fluorescence intensity can be correlated to the quantity of inhibitor. The activity of LTI-6 was also compared to that of TXA and aprotinin.

The Assay Kit was stored at -20 ºC in the dark upon receipt. Before use, all reagents were equilibrated to RT. Plasmin Enzyme Solution and Plasmin Substrate Solution were prepared following manufacturer's instructions, diluting Plasmin Enzyme and Plasmin Substrate with Plasmin Assay Buffer. Stock solutions for each compound were prepared with deionized water. From these stock solutions, different volumes were taken to prepare various concentrations of the compounds with Tris HCl buffer.

10 µL of each tested compound in Tris HCl buffer were pipetted in a 96-well microtiter plate. Then, 50 µL of Plasmin Enzyme Solution were added to each well. The plate was incubated at RT for 15 min and 40 µL of Plasmin Substrate Solution were added. Fluorescence was measured at

an Ex/Em of 360/450 nm in a kinetic mode, with a reading interval of 1 min for 10 min or until the system reached saturation at 37 ºC.

Following manufacturer's instructions, a PC (or Enzyme Control) for the assay was performed adding 10 µL of Plasmin Assay Buffer. An aprotinin control (or Inhibitor Control) was run mixing 1 µL of Plasmin Inhibitor (aprotinin, 0.6 mM) and 9 µL of Plasmin Assay Buffer. Each condition was performed in duplicate.

Raw fluorescence data obtained at each time point was plotted into graphics. From the linear range of the plot, two time points (t_1 and t_2) were chosen and their corresponding fluorescence values were obtained (RFU_1 and RFU_2). The slope for each sample, Enzyme Control (EC) and Inhibition Control (IC) was calculated using equation 4:

$$Slope = \frac{RFU_2 - RFU_1}{t_2 - t_1} \quad \text{(Eq. 4)}$$

Relative Inhibition (RI) was calculated using equation 5.

$$RI\ (\%) = \frac{Slope\ of\ EC - Slope\ of\ Sample}{Slope\ of\ EC} \quad \text{(Eq. 5)}$$

5.5.2. Tissue Plasminogen Activator (tPA) activity assay

Active tPA has the ability to hydrolyze a synthetic substrate releasing the chromophore *para*-nitroaniline (*p*NA), whose absorbance can be measured. The presence of tPA inhibitors in the solution causes a decrease in the release of *p*NA, which can be quantified by OD. Therefore, a colorimetric assay was performed in a purified system, quantifying the activity of the studied compounds on the active site of tPA and comparing it to the activity of TXA.

The Assay Kit was stored at -20 ºC protected from light upon receipt. Before performing the assay, all reagents were brought to RT. Prior to use, a tPA Substrate solution was prepared following manufacturer's instructions. The tPA source was stored as well at -20 ºC until used. Stock solutions were prepared for each studied compounf with deionized water. From these stock

solutions, different volumes were taken to prepare various concentrations of the compounds with Tris HCl buffer.

10 µL of each sample, prepared with the assayed compounds in Tris HCl buffer, were pipetted into a 96-well microtiter plate. Following, 5 µL of tPA and 65 µL of tPA Assay Buffer were added to each well. The plate was incubated at 37 ºC for 10 min. After incubation, 20 µL of tPA Substrate solution were added to each well. The total volume in each well was 100 µL and the final concentration of tPA was 3.25 µg/mL. Absorbance was immediately measured on at 405 nm in a kinetic mode with a reading interval of 1 min at 37 ºC for 30 min or until the system reached saturation.

A PC was performed using 10 µL of tPA Assay Buffer as sample. A negative control was assayed with 80 µL of tPA Assay Buffer (without sample or tPA) and 20 µL of tPA Substrate. Each condition was performed in duplicate.

The data obtained at each time point were plotted into graphics, which allowed to identify the linear range of the activity of the compounds. From each condition, two time points (t_1 and t_2) in the linear range of the plot were chosen and their corresponding absorbance values were obtained (OD_1 and OD_2). The slope for each sample and PC was calculated as follows:

$$Slope = \frac{OD_2 - OD_1}{t_2 - t_1} \quad \text{(Eq. 6)}$$

RI was calculated using equation 5. Relative Activity (RA) for each condition was calculated subtracting from the total activity of the enzyme (100%), obtained with the PC, the RI of each concentration.

$$RA\ (\%) = RI_{PC} - RI_{Sample} \quad \text{(Eq. 7)}$$

5.5.3. Plasminogen activation assay

In the absence of fibrin, lysine analogues are able to induce a conformational change in plasminogen, accelerating its conversion to plasmin by tPA. This mechanism is opposed to the real outcome of lysine analogues in the presence of fibrin, which provide an antifibrinolytic effect inhibiting the formation of plasmin and its interaction with fibrin. The rate of plasminogen activation by tPA was assessed in the absence of fibrin, both for LTI-6 and for the known lysine analogue TXA.

A colorimetric assay was performed measuring the ability of tPA to activate plasminogen into plasmin in a solution containing a plasmin-specific synthetic substrate. The quantity of plasmin generated can be quantified through the chromophore *p*NA, released in the reaction. Changes in absorbance are directly proportional to the tPA activity and allow to measure the velocity of plasmin generation.

Human Plasminogen and Plasmin Substrate, components of the Assay Kit, were stored at -20 ºC upon arrival, while Assay Diluent was kept at 4 ºC. Reagents Human Plasminogen and Plasmin Substrate were prepared following manufacturer's instructions. The source of tPA source was stored at -20 ºC until used. The stock solutions for studied compounds were prepared with deionized water. From these stock solutions, different volumes were taken to prepare various concentrations of the compounds with Tris HCl buffer.

In a 96-well microtiter plate, 80 µL of the Assay Mix, previously prepared with the instructed volumes of Plasminogen and Plasmin Substrate, were added to each well. After, 20 µL of the samples were added to each well. The samples consisted in a mixture of different concentrations of the compound of interest, tPA (final concentration 6.8 µg/mL) and Tris HCl buffer. Absorbance

was immediately read at 405 nm in a kinetic mode every minute for 2 h or until the system reached saturation at 37 ºC.

PC for the assays were performed using 20 µL of tPA (final concentration 6.8 µg/mL) in Tris HCl buffer. Negative controls were obtained with 20 µL of Tris HCl buffer. Each condition was performed in duplicate.

The data obtained at each time point were plotted into graphics, which allowed to identify the linear range of the activity of the compounds. Two time points (t_1 and t_2) from the linear range of the plot were chosen for each condition and their corresponding absorbance values were obtained (OD_1 and OD_2). The slope for each sample and control was calculated as mentioned before (equation 6). Activity Rate (AR) was calculated dividing the slope of each concentration by the same slope for the PC (equation 8).

$$AR\ (\%) = \frac{Slope_{Sample}}{Slope_{PC}}\ x\ 100 \qquad \text{(Eq. 8)}$$

Following, RA, which represented the relative increased plasminogen conversion, was calculated subtracting from the Activity Rate of each concentration, the total activity of the enzyme (100%), obtained with the PC.

$$\%\ Relative\ Activity\ (RA) = AR_{Sample} - AR_{PC} \qquad \text{(Eq. 9)}$$

5.6. Synthetic methodologies

***tert*-butyl 4-((methylsulfonyl)oxy)piperidine-1-carboxylate (13)**

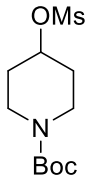

13

To a stirred solution of *tert*-butyl 4-hydroxypiperidine-1-carboxylate (**12**) (0.96 g, 4.8 mmol) in 10 mL dichloromethane was added triethylamine (1 mL) and stirred at room temperature for 5 minutes and then cooled to 0-5 °C. Methanesulfonyl chloride (0.67 g, 6.2 mmol) was added dropwise at 0-5 °C and after addition the reaction mixture was allowed to warm to room temperature and then stirred at room temperature for 2 h. After completion (monitored by TLC), the reaction was quenched by addition of distilled water, additional dichloromethane was added and the dichloromethane layer after extraction was separated, dried ($MgSO_4$) and concentrated *in vacuo* to yield 1.3 g of *tert*-butyl 4-((methylsulfonyl)oxy)piperidine-1-carboxylate (**13**) as a pale yellow solid. Yield: 97 %. ^{1}H-NMR (400 MHz, $CDCl_3$) δ (ppm): 4.84 – 4.90 (m, 1H), 3.66 – 3.72 (m, 2H), 3.25 – 3.32 (m, 2H), 3.02 (s, 3H), 1.91 – 1.99 (m, 2H), 1.76 – 1.84 (m, 2H), 1.44 (s, 9H).

***tert*-butyl 4-azidopiperidine-1-carboxylate (14)**

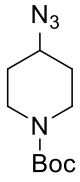

14

To a stirred solution of *tert*-butyl 4-((methylsulfonyl)oxy)piperidine-1-carboxylate (**13**) (2.48 g, 8.9 mmol) in 20 mL dimethyl formamide, sodium azide (1.74, 26.8 mmol) was added and the resulting suspension was stirred at 80 °C for 8 h. After completion (monitored by TLC), the

reaction was allowed to cool to room temperature and then poured into cold water with occasional stirring. The residue was extracted with ethyl acetate (3x10 mL). The combined organic layers were concentrated *in vacuo* and the residue was dissolved in hexane (50 mL) and an extraction with water (3x10 mL) was made. The combined organic layers were dried ($MgSO_4$) and concentrated *in vacuo* to yield 1.75 g of *tert*-butyl 4-azidopiperidine-1-carboxylate (**14**) as a yellow oil. Yield: 87%. ^{1}H-NMR (400 MHz, $CDCl_3$) δ (ppm): 3.81 – 3.76 (m, 2H), 3.51 – 3.56 (m, 1H), 3.02 – 3.09 (m, 2H), 1.79 – 1.86 (m, 2H), 1.49 – 1.56 (m, 2H), 1.44 (s, 9H).

***tert*-butyl 4-(4-(ethoxycarbonyl)-1*H*-1,2,3-triazol-1-yl)piperidine-1-carboxylate (15)**

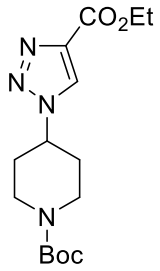

15

tert-butyl 4-azidopiperidine-1-carboxylate (**14**) (0.66 g, 2.9 mmol) was taken in acetonitrile (15 mL) and to it ethyl propiolate (0.29 g, 2.9 mmol) was added, followed by CuI (0.11 g, 0.6 mmol) and the resulting solution was stirred at room temperature for 12 h. After completion (monitored by TLC), solvent was removed *in vacuo* and distilled water was added to the residue and then extracted with 3 portions (3x10 mL) of ethyl acetate. The combined organic layers were dried ($MgSO_4$) and concentrated *in vacuo* to yield 0.79 g of the desired compound *tert*-butyl 4-(4-(ethoxycarbonyl)-1*H*-1,2,3-triazol-1-yl)piperidine-1-carboxylate (**15**) as a pale yellow solid. Yield: 84%. ^{1}H-NMR (400 MHz, $CDCl_3$) δ (ppm): 8.08 (s, 1H), 4.62 – 4.70 (m, 1H), 4.40 (q, *J*=7.1Hz, 2H), 4.23 – 4.31 (m, 2H), 2.89 – 2.93 (m, 2H), 2.18 – 2.23 (m, 2H), 1.88 – 1.98 (m, 2H), 1.46 (s, 9H), 1.39 (t, *J*=7.1Hz, 3H).

***tert*-butyl 4-(4-(hydrazinecarbonyl)-1*H*-1,2,3-triazol-1-yl)piperidine-1-carboxylate (29)**

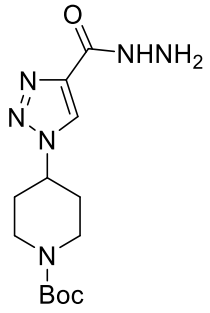

29

tert-butyl 4-(4-(ethoxycarbonyl)-1*H*-1,2,3-triazol-1-yl)piperidine-1-carboxylate (**15**) (1 g, 3.1 mmol) and hydrazine hydrate (0.5 g) in 20 mL of *n*-butanol were refluxed for 3 h. Then, the solvent was removed by evaporation under vacuum. The residue was treated with dichloromethane and washed with water. The organic phase was dried ($MgSO_4$) and the solvent removed under reduced pressure. The resulting pale-yellow solid was washed with cold ethanol. Yield 0.93 g, 97%. ^{1}H NMR (400 MHz, $CDCl_3$), δ (ppm): 8.08 (s, 1H), 4.63 (tt, *J* = 11.6, 3.6 Hz, 1H), 4.27 (s, 2H), 4.03 (s, 1H), 2.94 (t, *J* = 13.0 Hz, 2H), 2.21 (d, *J* = 12.8 Hz, 2H), 1.94 (qd, *J* = 12.0, 4.4 Hz, 2H), 1.47 (d, *J* = 0.6 Hz, 9H).

***tert*-butyl 4-(4-(5-oxo-4,5-dihydro-1,3,4-oxadiazol-2-yl)-1*H*-1,2,3-triazol-1-yl)piperidine-1-carboxylate (32)**

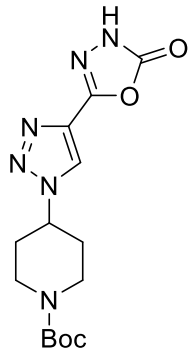

32

To a suspension *tert*-butyl 4-(4-(hydrazinecarbonyl)-1*H*-1,2,3-triazol-1-yl)piperidine-1-carboxylate (**29**) (0.15 g, 0.50 mmol) in anhydrous acetonitrile (5 mL) *N*,*N'*-carbonyldiimidazole (CDI) (0.10 g, 0.65 mmol) and DBU (0.1 mL) were added at room temperature. The mixture was stirred for 15 h under reflux. After completion (monitored by TLC), 10% (v/v) acetic acid (25 mL) was added, and the mixture was extracted with ethyl acetate (3x10 mL). The combined organic layers washed with distilled water (3x10 mL), dried ($MgSO_4$) and concentrated *in vacuo* to provide 0.15 g of compound **32** as a white solid. Yield: 89%. ^{1}H NMR (400 MHz, $CDCl_3$), δ (ppm): 9.52 (s, 1H), 8.05 (s, 1H), 4.70 (tt, *J* = 11.7, 4.1 Hz, 1H), 4.29 (d, *J* = 11.9 Hz, 2H), 2.96 (t, *J* = 12.7 Hz, 2H), 2.38 – 2.17 (m, 2H), 2.17 – 1.88 (m, 2H), 1.47 (s, 9H). ^{13}C NMR (100 MHz, *d*$_6$-DMSO), δ (ppm): 154.5, 154.1, 148.7, 133.6, 124.1, 79.4, 58.2, 42.2, 32.0, 28.50. IR (cm^{-1}): 3130.52, 2986.99, 1747.35, 1704.20, 1540.88, 1410.72, 1366.35, 1235.55, 1149.52, 999.32, 950.23, 728.20. HRMS (ESI-FIA-TOF): m/z calculated for $C_{14}H_{20}N_6NaO_4$ 359.1444, found 359.1438.

5-(1-(piperidin-4-yl)-1*H*-1,2,3-triazol-4-yl)-1,3,4-oxadiazol-2(3*H*)-one hydrochloride (1)

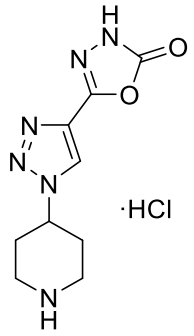

1

A mixture of *tert*-butyl 4-(4-(5-oxo-4,5-dihydro-1,3,4-oxadiazol-2-yl)-1*H*-1,2,3-triazol-1-yl)piperidine-1-carboxylate (**32**) (100 mg, 0.3 mmol) and 4N HCl in dioxane (2 mL) was stirred at room temperature for 2 h. The solvent was removed *in vacuo* and the resulting yellow solid was triturated with EtOAc to provide 74 mg of the hydrochloride of 5-(1-(piperidin-4-yl)-1*H*-1,2,3-triazol-4-yl)-1,3,4-oxadiazol-2(3*H*)-one as a white solid. Yield: 91%. ^{1}H NMR (400 MHz, *d*$_6$-

DMSO), δ (ppm): 13.24 (s, 1H), 9.26 (s, 1H), 9.10 (s, 1H), 8.24 (s, 1H), 5.28 – 5.02 (m, 1H), 3.38 (d, J = 12.7 Hz, 2H), 3.05 (q, J = 11.7 Hz, 2H), 2.40 – 1.99 (m, 4H). ^{13}C NMR (100 MHz, d_6-DMSO), δ (ppm): 154.0, 148.1, 133.1, 124.2, 54.9, 41.7, 28.2. Elemental analysis calculated (%) for $C_9H_{13}ClN_6O_2$: C 39.64, H 4.81, N 30.82. Found C 39.47, H 4.56, N 30.77. IR (cm^{-1}): 2939.70, 2802.84, 1808.57, 1770.15, 1657.33, 1397.35, 1397.35, 1213.28, 1048.40, 892.53. HRMS (ESI-FIA-TOF): m/z calculated for $C_9H_{13}N_6O_2$ 237.1095, found 237.1093.

***tert*-butyl 4-(4-carbamoyl-1*H*-1,2,3-triazol-1-yl)piperidine-1-carboxylate (35)**

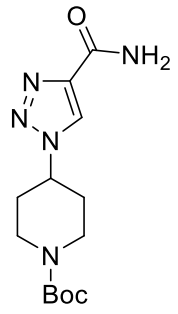

35

To a solution of *tert*-butyl 4-(4-(ethoxycarbonyl)-1*H*-1,2,3-triazol-1-yl)piperidine-1-carboxylate (**15**) (2.04 g, 6.3 mmol) in 20 mL of methanol, 40 mL of ammonia in methanolic solution was added and the resulting solution was stirred at room temperature for 12 h. After completion (monitored by TLC), solvent was removed *in vacuo* and distilled water was added to the residue. It was extracted with 3 portions (3x10 mL) of dichloromethane. The combined organic layers were dried ($MgSO_4$) and concentrated *in vacuo* to yield 1.69 g of *tert*-butyl 4-(4-carbamoyl-1*H*-1,2,3-triazol-1-yl)piperidine-1-carboxylate (**35**) as a white solid. Yield: 91 %. ^{1}H-NMR (400 MHz, $CDCl_3$) δ (ppm): 8.10 (s, 1H), 7.00 (s, 1H), 5.70 (s, 1H), 4.62 – 4.70 (m, 1H), 4.24 – 4.31 (m, 2H), 2.89 – 3.01 (m, 2H), 2.19 – 2.23 (m, 2H), 1.88 – 1.99 (m, 2H), 1.44 (s, 9H).

***tert*-butyl 4-(4-cyano-1*H*-1,2,3-triazol-1-yl)piperidine-1-carboxylate (39)**

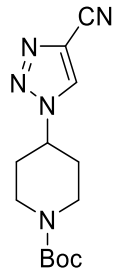

39

A solution of *tert*-butyl 4-(4-carbamoyl-1*H*-1,2,3-triazol-1-yl)piperidine-1-carboxylate (**35**) (0.21 g, 0.7 mmol) and 0.4 mL of triethylamine in 9 mL of dichloromethane was stirred at room temperature. The resulting solution was then cooled to 0-5 $^{\circ}$C in an ice bath. To this cooled solution, trifluoroacetic anhydride (0.30 g, 1.5 mmol) was added. The resulting solution was stirred for 5 h. After completion (monitored by TLC), solvent was removed *in vacuo* and distilled water added to the residue and then extracted with 3 portions (3x10mL) of dichloromethane. The organic layer was washed with saturated $NaHCO_3$ solution, dried ($MgSO_4$) and concentrated *in vacuo* to yield 0.19 g of *tert*-butyl 4-(4-cyano-1*H*-1,2,3-triazol-1-yl)piperidine-1-carboxylate (**39**) as a brown oil. Yield: 97%. ^{1}H-NMR (400 MHz, $CDCl_3$) δ (ppm): 8.12 (s, 1H), 4.61 – 4.72 (m, 1H), 4.25 – 4.30 (m, 2H), 2.89 – 3.03 (m, 2H), 2.20 – 2.26 (m, 2H), 1.92 – 2.04 (m, 2H), 1.48 (s, 9H).

***tert*-butyl (*Z*)-4-(4-(N'-hydroxycarbamimidoyl)-1*H*-1,2,3-triazol-1-yl)piperidine-1-carboxylate (43)**

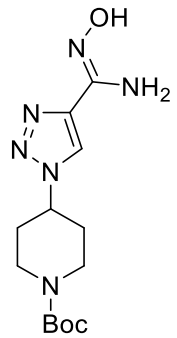

43

To a stirred solution of *tert*-butyl 4-(4-cyano-1*H*-1,2,3-triazol-1-yl)piperidine-1-carboxylate (**39**) (0.14 g, 0.5 mmol) in 10 mL methanol, hydroxylamine hydrochloride (0.07g, 1 mmol) and sodium bicarbonate (0.07 g, 0.9 mmol) was added. The resulting mixture was heated under reflux for 14 h. After completion (monitored by TLC), solvent was removed *in vacuo* and distilled water added to the residue and then extracted with 3 portions (3x10mL) of dichloromethane. The organic layer dried ($MgSO_4$) and concentrated *in vacuo*. A small portion of ethyl acetate was added and stirred at room temperature for 30 minutes. The resulting solid, *tert*-butyl (*Z*)-4-(4-(*N*'-hydroxycarbamimidoyl)-1*H*-1,2,3-triazol-1-yl)piperidine-1-carboxylate (**43**) was collected by filtration. After drying under vacuum, 0.04 g of **43** were obtained. Yield: 23%. ^{1}H-NMR (400 MHz, d_6-DMSO) δ (ppm): 9.50 (s, 1H), 8.35 (s, 1H), 5.71 (s, 2H), 4.69 – 4.77 (m, 1H), 4.03 – 4.07 (m, 2H), 2.95 (s, 2H), 2.05 – 2.09 (m, 2H), 1.82 – 1.93 (m, 2H), 1.42 (s, 9H).

***tert*-butyl 4-(4-(5-oxo-4,5-dihydro-1,2,4-oxadiazol-3-yl)-1*H*-1,2,3-triazol-1-yl)piperidine-1-carboxylate (47)**

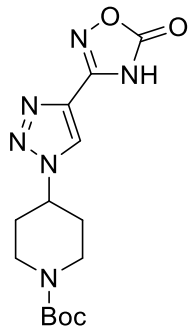

47

To a suspension *tert*-butyl (*Z*)-4-(4-(*N*'-hydroxycarbamimidoyl)-1*H*-1,2,3-triazol-1-yl)piperidine-1-carboxylate (**43**) (0.15 g, 0.50 mmol) in anhydrous acetonitrile (5 mL) *N*,*N'*-carbonyldiimidazole (CDI) (0.10 g, 0.65 mmol) and DBU (0.1 mL) were added at room temperature. The mixture was stirred for 15 h under reflux. After completion of the reaction (monitored by TLC), 10% (v/v) acetic acid (25 mL) was added, and the mixture was extracted

with ethyl acetate (3x10 mL). The combined organic layers washed with distilled water (3x10 mL), dried ($MgSO_4$) and concentrated *in vacuo* to furnish 96 mg of compound **47**. Yield: 57%. ^{1}H NMR (400 MHz, d_6-DMSO), δ (ppm): 8.57 (s, 1H), 6.92 (s, 1H), 4.71 – 4.77 (m, 1H), 4.00 – 4.03 (m, 2H), 2.82 – 3.01 (m, 2H), 2.03 – 2.08 (m, 2H), 1.81 – 1.89 (m, 2H), 1.38 (s, 9H). ^{13}C NMR (100 MHz, d_6-DMSO), δ (ppm): 159.6, 154.2, 151.9, 150.6, 139.8, 79.4, 57.5, 42.9, 31.6, 28.4. IR (cm^{-1}): 3301.13, 3127.81, 2973.45, 2848.88, 1788.44, 1679.12, 1530.05, 1400.15, 1365.24, 1243.75, 1166.05, 1052.23, 973.32, 930.96, 763.27. HRMS (ESI-FIA-TOF): m/z calculated for $C_{14}H_{21}N_6O_4$ 337.1624, found 337.1619.

hydrochloride of 3-(1-(piperidin-4-yl)-1*H*-1,2,3-triazol-4-yl)-1,2,4-oxadiazol-5(4*H*)-one (4)

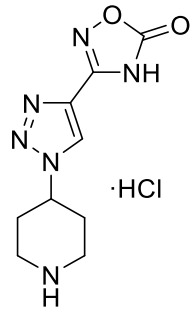

4

A mixture of *tert*-butyl 4-(4-(5-oxo-4,5-dihydro-1,2,4-oxadiazol-3-yl)-1*H*-1,2,3-triazol-1-yl)piperidine-1-carboxylate (**47**) (10 mg, 0.03 mmol) and 4N HCl in dioxane (2 mL) was stirred at 23 °C for 2 h. The solvent was removed *in vacuo* and the resulting yellow solid was triturated with EtOAc to provide 7 mg of the hydrochloride of 3-(1-(piperidin-4-yl)-1*H*-1,2,3-triazol-4-yl)-1,2,4-oxadiazol-5(4*H*)-one (**4**) as a white solid. Yield: 90%. ^{1}H NMR (400 MHz, d_6-DMSO), δ (ppm): 13.28 (s, 1H), 9.10 (s, 1H), 8.90 (s, 1H), 8.89 (s, 1H), 4.92 (m, 1H), 3.32 (m, 2H), 3.09 (m, 2H), 2.33 – 2.24 (m, 4H). ^{13}C NMR (100 MHz, d_6-DMSO), δ (ppm): 159.4, 151.5, 131.9, 124.4, 55.1, 41.7, 30.6, 28.3. Elemental analysis calculated (%) for $C_9H_{13}ClN_6O_2$: C 39.64, H 4.81, N 30.82. Found C 39.89, H 4.72, N 30.97. IR (cm^{-1}): 3030.32, 2824.51, 2518.49, 1765.15, 1610.26,

1560.46, 1436.31, 1213.61, 1056.13, 923.46, 888.00, 836.19, 760.76. HRMS (ESI-FIA-TOF): m/z calculated for $C_9H_{13}N_6O_2$ 237.1095, found 237.1092.

***tert*-butyl (2-azidoethyl)carbamate (19)**

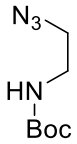

19

tert-butyl (2-bromoethyl)carbamate (**16**) (0.94 g, 4.2 mmol) and sodium azide (0.7 mg, 8.4 mmol) were dissolved in DMF (10 mL). The reaction mixture was refluxed overnight at 75 ºC with stirring. Subsequently, the solvent was evaporated and the reaction mixture was diluted with dichloromethane (50 mL) and washed with water (3x50 mL). Organic layer was collected, and solvent was evaporated, affording 0.74 g the compound **19** as pale-yellow oil. Yield: 94%. ^{1}H-NMR (400 MHz, $CDCl_3$) δ (ppm): 4.75 - 5.00 (s, 1H), 3.38 (t, J = 5.6 Hz, 2H), 3.28 (q, J = 5.8 Hz, 2H), 1.42 (s, 9H).

***tert*-butyl (3-azidopropyl)carbamate (20)**

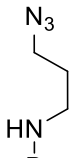

20

tert-butyl (3-bromopropyl)carbamate (**17**) (1.0 g, 4.2 mmol) and sodium azide (0.7 mg, 8.4 mmol) were dissolved in DMF (10 mL). The reaction mixture was refluxed overnight at 75 ºC with stirring. Subsequently, the solvent was evaporated and the reaction mixture was diluted with dichloromethane (50 mL) and washed with water (3x50 mL). Organic layer was collected, and solvent was evaporated, affording 0.80 g of compound **20** as pale-yellow oil. Yield: 95%. ^{1}H-NMR

(400 MHz, $CDCl_3$) δ (ppm): 4.45 - 4.90 (s, 1H), 3.32 (t, *J* = 6.7 Hz, 2H), 3.17 (t, *J* = 6.7 Hz, 2H), 1.74 (m, *J* = 6.7 Hz, 2H), 1.41 (s, 9H).

***tert*-butyl (4-azidobutyl)carbamate (21)**

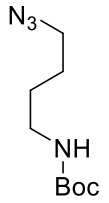

21

tert-butyl (4-bromobutyl)carbamate (**18**) (1.1 g, 4.2 mmol) and sodium azide (0.7 mg, 8.4 mmol) were dissolved in DMF (10 mL). The reaction mixture was refluxed overnight at 75 ºC with stirring. Subsequently, the solvent was evaporated and the reaction mixture was diluted with dichloromethane (50 mL) and washed with water (3x50 mL). Organic layer was collected, and solvent was evaporated, affording 0.86 g the product as pale-yellow oil. Yield: 96%. ^{1}H-NMR (400 MHz, $CDCl_3$) δ (ppm): 4.50 – 4.70 (s, 1H), 3.27 (t, *J* = 6.5 Hz, 2H), 3.10 (q, *J* = 6.5 Hz, 2H), 1.48-1.63 (m, 4H), 1.41 (s, 9H).

ethyl 1-(2-((*tert*-butoxycarbonyl)amino)ethyl)-1*H*-1,2,3-triazole-4-carboxylate (22)

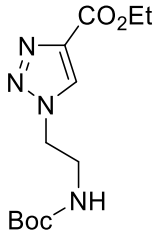

22

tert-butyl (2-azidoethyl)carbamate (**19**) (0.56 g, 3.0 mmol) was taken in acetonitrile (15 mL) and to it ethyl propiolate (0.33 g, 3.3 mmol) was added, followed by CuI (0.11 g, 0.6 mmol) and the resulting solution was stirred at room temperature for 15 h. After completion (monitored by TLC), solvent was removed *in vacuo* and distilled water was added to the residue and then extracted with

3 portions (3x10 mL) of ethyl acetate. The combined organic layers were dried ($MgSO_4$) and concentrated *in vacuo* to obtain 0.74 g the desired compound as a pale-yellow solid. Yield: 87%. ^{1}H-NMR (400 MHz, d_6-DMSO) δ (ppm): 8.66 (s, 1H), 6.97 (t, J = 5.9 Hz, 1H), 4.45 (t, 2H), 4.31 (q, J = 7.1 Hz, 2H), 3.40 (q, J = 6.4 Hz, 2H), 1.32 (s, 9H), 1.29 (t, J = 7.1 Hz, 3H).

ethyl 1-(3-((*tert*-butoxycarbonyl)amino)propyl)-1*H*-1,2,3-triazole-4-carboxylate (23)

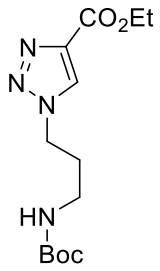

23

tert-butyl (3-azidopropyl)carbamate (**20**) (0.60 g, 3.0 mmol) was dissolved in acetonitrile (15 mL) and to it ethyl propiolate (0.33 g, 3.3 mmol) was added, followed by CuI (0.11 g, 0.6 mmol) and the resulting solution was stirred at room temperature for 15 h. After completion (monitored by TLC), solvent was removed *in vacuo* and distilled water was added to the residue and then extracted with 3 portions (3x10 mL) of ethyl acetate. The combined organic layers were dried ($MgSO_4$) and concentrated *in vacuo* to yield 0.79 g of the desired compound as a pale-yellow solid. Yield: 84%. ^{1}H-NMR (400 MHz, $CDCl_3$) δ (ppm): 8.31 (s, 1H), 4.78 (s, 1H), 4.49 (t, J = 6.5 Hz, 2H), 4.42 (q, J = 6.8 Hz, 2H), 3.12 (q, J = 6.1 Hz 2H), 2.09 (m, J = 6.5 Hz, 2H), 1.40 (s, 9H), 1.36 (t, 3H).

ethyl 1-(4-((*tert*-butoxycarbonyl)amino)butyl)-1*H*-1,2,3-triazole-4-carboxylate (24)

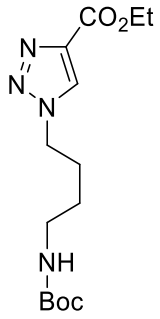

24

tert-butyl (4-azidobutyl)carbamate (**21**) (0.64 g, 3.0 mmol) was dissolved in acetonitrile (15 mL) and to it ethyl propiolate (0.33 g, 3.3 mmol) was added, followed by CuI (0.11 g, 0.6 mmol) and the resulting solution was stirred at room temperature for 15 h. After completion (monitored by TLC), solvent was removed *in vacuo* and distilled water was added to the residue and then extracted with 3 portions (3x10 mL) of ethyl acetate. The combined organic layers were dried ($MgSO_4$) and concentrated *in vacuo* to obtain 0.81 g the desired compound as a pale-yellow solid. Yield: 87%. ^{1}H-NMR (400 MHz, $CDCl_3$) δ (ppm): 8.08 (s, 1H) 4.62 (s, 1H), 4.43 (t, 2H), 4.38 (q, 2H), 3.13 (q, *J* = 6.7 Hz, 2H), 1.94 (m, 2H), 1.48 (m, 2H), 1.40 (s, 9H), 1.37 (t, *J* = 7.1 Hz, 3H).

***tert*-butyl (2-(4-(hydrazinecarbonyl)-1*H*-1,2,3-triazol-1-yl)ethyl)carbamate (30)**

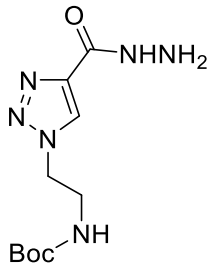

30

Ethyl 1-(2-((*tert*-butoxycarbonyl)amino)ethyl)-1*H*-1,2,3-triazole-4-carboxylate (**22**) (1.6 g, 5.7 mmol) and hydrazine hydrate (1.4 g, 28.7 mmol) in 15 mL of *n*-butanol were refluxed for 5 h. Then, the solvent was removed by evaporation under vacuum. The resulting solid was left drying

under vacuum in the presence of P_2O_5. 1.32 g of compound **30** were obtained. Yield: 86%. ^{1}H-NMR (400 MHz, d_6-DMSO) δ (ppm): 8.42 (s, 1H), 6.96 (t, J = 5.8 Hz, 1H), 4.39 (t, J = 5.9 Hz, 2H), 3.36 (q, J = 5.9 Hz, 2H), 1.31 (s, 9H).

***tert*-butyl (3-(4-(hydrazinecarbonyl)-1*H*-1,2,3-triazol-1-yl)propyl)carbamate (31)**

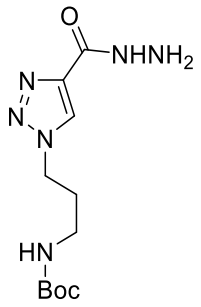

31

Ethyl 1-(3-((*tert*-butoxycarbonyl)amino)propyl)-1*H*-1,2,3-triazole-4-carboxylate (**23**) (1.7 g, 5.7 mmol) and hydrazine hydrate (1.4 g, 28.7 mmol) in 15 mL of *n*-butanol were refluxed for 5 h. Then, the solvent was removed by evaporation under vacuum. The resulting solid was left drying under vacuum in the presence of P_2O_5. 1.5 g of compound **31** were obtained. Yield: 94 %. ^{1}H-NMR (400 MHz, d_6-DMSO) δ (ppm): 8.52 (s, 1H), 6.92 (t, J = 5.7 Hz, 1H), 4.38 (t, J = 7.0 Hz, 2H), 2.90 (q, J = 6.5 Hz, 2H), 1.93 (m, J = 6.9 Hz, 2H), 1.35 (s, 9H).

***tert*-butyl (2-(4-(5-oxo-4,5-dihydro-1,3,4-oxadiazol-2-yl)-1*H*-1,2,3-triazol-1-yl)ethyl)carbamate (33)**

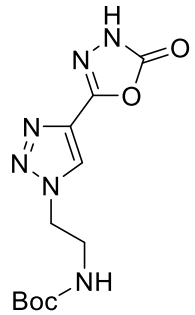

33

To a suspension of *tert*-butyl (3-(4-(hydrazinecarbonyl)-1*H*-1,2,3-triazol-1-yl)ethyl)carbamate (**30**) (0.50 mmol) in anhydrous acetonitrile (5 mL) *N*,*N'*-carbonyldiimidazole (CDI) (0.10 g, 0.65 mmol) and DBU (0.1 mL) were added at room temperature. The mixture was stirred for 4 h under reflux. After completion (monitored by TLC), 10% (v/v) acetic acid (25 mL) was added, and the mixture was extracted with ethyl acetate (3x10 mL). The combined organic layers were washed with distilled water (3x10 mL), dried ($MgSO_4$) and concentrated *in vacuo* to afford 0.11 g of compound **33**. Yield: 78%. ^{1}H-NMR (400 MHz, d_6-DMSO) δ (ppm): 12.59 (s, 1H), 8.70 (s, 1H), 6.97 (t, J = 5.9 Hz, 1H), 4.45 (t, J = 6.5 Hz, 2H), 3.39 (q, J = 5.9 Hz, 2H), 1.30 (s, 9H). ^{13}C-NMR (100 MHz, CD_3OD) δ (ppm): 156.8, 155.1, 148.7, 133.6, 124.9, 79.0, 50.2, 39.9, 27.2. IR (cm^{-1}): 3382.37, 3133.23, 2986.99, 1792.22, 1764.24, 1692.66, 1518.65, 1273.38, 1166.36, 1045.09, 861.15. HRMS (ESI-FIA-TOF): m/z calculated for $C_{11}H_{17}N_6O_4$ 297.1306, found 297.1306.

***tert*-butyl (3-(4-(5-oxo-4,5-dihydro-1,3,4-oxadiazol-2-yl)-1*H*-1,2,3-triazol-1-yl)propyl)carbamate 34)**

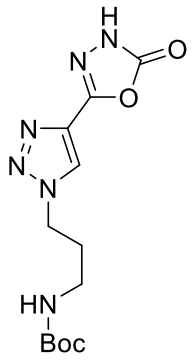

34

To a suspension of *tert*-butyl (3-(4-(hydrazinecarbonyl)-1*H*-1,2,3-triazol-1-yl)propyl)carbamate (**31**) (0.50 mmol) in anhydrous acetonitrile (5 mL) *N*,*N'*-carbonyldiimidazole (CDI) (0.10 g, 0.65 mmol) and DBU (0.1 mL) were added at room temperature. The mixture was stirred for 4 h under reflux. After completion (monitored by TLC), 10% (v/v) acetic acid (25 mL) was added, and the

mixture was extracted with ethyl acetate (3x10 mL). The combined organic layers washed with distilled water (3x10 mL), dried ($MgSO_4$) and concentrated *in vacuo* to afford 0.12 g of compound **34**. Yield: 82%. ^{1}H-NMR (400 MHz, d_6-DMSO) δ (ppm): 12.57 (s, 1H), 8.76 (s, 1H), 6.92 (t, J = 5.7 Hz, 1H), 4.33 (t, J = 7.0 Hz, 2H), 2.92 (q, J = 6.5 Hz, 2H), 1.95 (m, J = 6.9 Hz, 2H), 1.35 (s, 9H). ^{13}C-NMR (100 MHz, d_6-DMSO) δ (ppm): 156.0, 154.5, 148.7, 133.5, 125.8, 78.2, 48.2, 37.4, 30.4, 28.6. IR (cm^{-1}): 3341.75, 3127.81, 2986.99, 1766.73, 1690.71, 1518.53, 1363.91, 1239.24, 1172.27, 951.79, 722.10. HRMS (ESI-FIA-TOF): m/z calculated for $C_{12}H_{19}N_6O_4$ 311.1462, found 311.1459.

5-(1-(2-aminoethyl)-1*H*-1,2,3-triazol-4-yl)-1,3,4-oxadiazol-2(3*H*)-one hydrochloride (2)

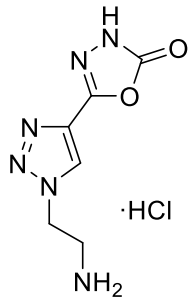

2

A mixture of *tert*-butyl (2-(4-(5-oxo-4,5-dihydro-1,3,4-oxadiazol-2-yl)-1*H*-1,2,3-triazol-1-yl)ethyl)carbamate (**33**) (100 mg, 0.3 mmol) and 3M HCl in methanol (5 mL) was stirred at room temperature for 2 h. The solvent was removed *in vacuo* and the resulting yellow solid was triturated with EtOAc to provide 60 mg of the corresponding hydrochloride as a white solid. Yield: 85%. ^{1}H-NMR (400 MHz, d_6-DMSO) δ (ppm): 12.67 (s, 1H), 8.84 (s, 1H), 8.13 (s, 3H), 4.73 (t, J = 6.5 Hz, 2H), 3.38 (t, J = 6.0 Hz, 2H). ^{13}C-NMR (100.0 MHz, d_6-DMSO) δ (ppm): 154.5, 148.6, 133.7, 126.5, 47.8, 36.7. IR (cm^{-1}): 3295.71, 3100.73, 2890.82, 1773.42, 1662.28, 1524.63, 1197.63, 1056.54, 950.37, 772.68, 698.62. HRMS (ESI-FIA-TOF): m/z calculated for $C_6H_9N_6O_2$ 197.0781, found 197.0779.

5-(1-(3-aminopropyl)-1*H*-1,2,3-triazol-4-yl)-1,3,4-oxadiazol-2(3*H*)-one hydrochloride (3)

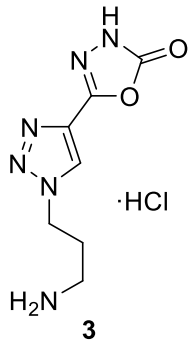

3

A mixture of *tert*-butyl (3-(4-(5-oxo-4,5-dihydro-1,3,4-oxadiazol-2-yl)-1*H*-1,2,3-triazol-1-yl)propyl)carbamate (**34**) (100 mg, 0.3 mmol) and 3M HCl in methanol (5 mL) was stirred at room temperature for 2 h. The solvent was removed *in vacuo* and the resulting yellow solid was triturated with EtOAc to provide 67 mg of the corresponding hydrochloride as a white solid. Yield: 81%. ^{1}H-NMR (400 MHz, *d*$_6$-DMSO) δ (ppm): 12.66 (s, 1H), 8.83 (s, 1H), 7.82 – 8.05 (s, 3H), 4.56 (t, *J* = 6.8 Hz, 2H), 2.79 (t, *J* = 7.6 Hz, 2H), 2.15 (m, 2H). ^{13}C-NMR (100 MHz, *d*$_6$-DMSO) δ (ppm): 154.5, 148.6, 133.6, 126.0, 47.6, 36.6, 28.0. IR (cm^{-1}): 3206.34, 3041.15, 2935.54, 1774.45, 1502.96, 1213.20, 946.02, 908.68, 756.25, 721.25. HRMS (ESI-FIA-TOF): m/z calculated for $C_7H_{11}N_6O_2$ 211.0938, found 211.0933.

***tert*-butyl (3-(4-carbamoyl-1*H*-1,2,3-triazol-1-yl)propyl)carbamate (36)**

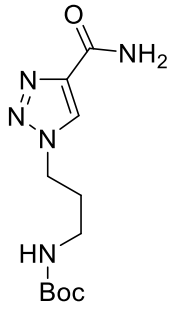

36

To a solution of ethyl 1-(3-((*tert*-butoxycarbonyl)amino)propyl)-1*H*-1,2,3-triazole-4-carboxylate (**23**) (2.48 g, 8.3 mmol) in 20 mL of ethanol, 30 mL of aqueous ammonia were added,

and the resulting solution was stirred at room temperature for 12 h. After completion (monitored by TLC), distilled water was added, and the mixture was filtrated under vacuum. The resulting white solid was washed with distilled water (3x10 mL) and dried under vacuum and in the presence of P_2O_5 overnight. 1.45 g of compound **36** were obtained. Yield: 65 %. ^{1}H-NMR (400 MHz, $CDCl_3$) δ (ppm): 8.32 (s, 1H), 7.07 (s, 1H), 5.90 (s, 1H), 5.07 (s, 1H), 4.48 (t, *J* = 6.8 Hz, 2H), 3.14 (q, *J* = 7.2 Hz, 2H), 2.18-2.07 (m, 2H), 1.44 (s, 9H). ^{13}C-NMR (100.0 MHz, *d*$_6$-DMSO) δ (ppm): 162.0, 156.1, 143.3, 127.1, 78.2, 47.9, 37.4, 30.5, 28.7.

***tert*-butyl (4-(4-carbamoyl-1*H*-1,2,3-triazol-1-yl)butyl)carbamate (37)**

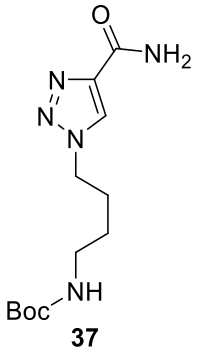

37

To a solution of ethyl 1-(4-((*tert*-butoxycarbonyl)amino)butyl)-1*H*-1,2,3-triazole-4-carboxylate (**24**) (2.48 g, 8.3 mmol) in 20 mL of ethanol, 30 mL of aqueous ammonia were added, and the resulting solution was stirred at room temperature for 12 h. After completion (monitored by TLC), distilled water was added, and the mixture was filtrated under vacuum. The resulting white solid was washed with distilled water (3x10 mL) and dried under vacuum and in the presence of P_2O_5 overnight. 1.62 g of compound **37** were obtained. Yield: 69 %. ^{1}H-NMR (400 MHz, $CDCl_3$) δ (ppm): 8.10 (s, 1H), 7.03 (s, 1H), 5.70 (s, 1H), 4.62 (s, 1H), 4.43 (t, *J* = 7.1 Hz, 2H), 3.15 (q, *J* = 6.6 Hz, 2H), 1.96 (m, 2H), 1.51 (m, 2H), 1.43 (s, 9H).

***tert*-butyl (3-(4-cyano-1*H*-1,2,3-triazol-1-yl)propyl)carbamate (40)**

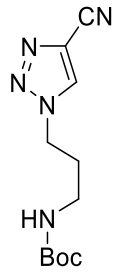

40

A solution of *tert*-butyl (3-(4-carbamoyl-1*H*-1,2,3-triazol-1-yl)propyl)carbamate (**36**) (1.46 g, 5.4 mmol) and 1.0 mL of triethylamine in 20 mL of dichloromethane was stirred at room temperature. The resulting solution was then cooled to 0-5 ^{o}C in an ice bath. To this cooled solution, trifluoroacetic anhydride (2.2 g, 10.8 mmol) was added. The resulting solution was stirred for 5 h. After completion (monitored by TLC), solvent was removed *in vacuo* and distilled water added to the residue and then extracted with 3 portions (3x10mL) of dichloromethane. The organic layer was washed with saturated $NaHCO_3$ solution, dried ($MgSO_4$) and concentrated *in vacuo* to yield 1.3 g of the desired compound. Yield: 96 %. ^{1}H-NMR (400 MHz, $CDCl_3$) δ (ppm): 8.19 (s, 1H), 4.48 (t, *J* = 6.7 Hz, 2H), 3.77 (t, *J* = 6.6 Hz, 2H), 2.30 (m, 2H), 1.52 (s, 9H).

***tert*-butyl (4-(4-cyano-1*H*-1,2,3-triazol-1-yl)butyl)carbamate (41)**

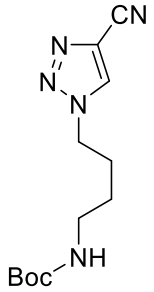

41

A solution of *tert*-butyl (4-(4-carbamoyl-1*H*-1,2,3-triazol-1-yl)butyl)carbamate (**37**) (1.46 g, 5.4 mmol) and 1.0 mL of triethylamine in 20 mL of dichloromethane was stirred at room temperature.

The resulting solution was then cooled to 0-5 ºC in an ice bath. To this cooled solution, trifluoroacetic anhydride (2.2 g, 10.8 mmol) was added. The resulting solution was stirred for 5 h. After completion (monitored by TLC), solvent was removed *in vacuo* and distilled water added to the residue and then extracted with 3 portions (3x10mL) of dichloromethane. The organic layer was washed with saturated $NaHCO_3$ solution, dried ($MgSO_4$) and concentrated *in vacuo* to yield 1.31 g of the desired compound. Yield: 92%. ^{1}H-NMR (400 MHz, $CDCl_3$) δ (ppm): 8.08 (s, 1H), 4.48 (t, *J* = 7.1 Hz, 2H), 3.74 (t, 2H), 1.96 (m, 2H), 1.62 (m, 2H), 1.51 (s, 9H).

***tert*-butyl (*Z*)-(3-(4-(*N'*-hydroxycarbamimidoyl)-1*H*-1,2,3-triazol-1-yl)propyl)carbamate (44)**

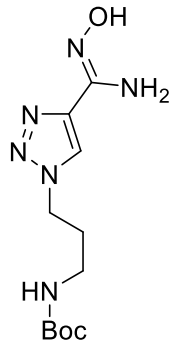

44

To a stirred solution of *tert*-butyl (3-(4-cyano-1*H*-1,2,3-triazol-1-yl)propyl)carbamate (**40**) (1.3 g, 5.1 mmol) in 20 mL methanol, hydroxylamine hydrochloride (0.72g, 10.3 mmol) and sodium bicarbonate (0.85 g, 10.1 mmol) was added. The resulting mixture was heated under reflux for 14 h. After completion (monitored by TLC), solvent was removed *in vacuo* and distilled water added to the residue. The mixture was filtrated under vacuum, and the white solid was washed with distilled water (2x10 mL) and ethyl acetate (2x10 mL) and dried overnight in the presence of P_2O_5. 1.04 g of compound **44** were obtained. Yield: 72 %. ^{1}H-NMR (400 MHz, d_6-DMSO) δ (ppm): 9.47 (s, 1H), 8.24 (s, 1H), 6.91 (t, *J* = 5.7 Hz, 1H), 5.69 (s, 2H), 4.34 (t, *J* = 7.0 Hz, 2H), 2.89 (q, *J* = 6.5 Hz, 2H), 1.90 (m, 2H), 1.35 (s, 9H).

***tert*-butyl (*Z*)-(4-(4-(*N'*-hydroxycarbamimidoyl)-1*H*-1,2,3-triazol-1-yl)butyl)carbamate (45)**

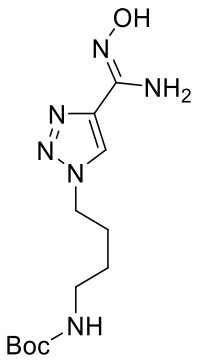

45

To a stirred solution of *tert*-butyl (4-(4-cyano-1*H*-1,2,3-triazol-1-yl)butyl)carbamate (**41**) (1.3 g, 5.1 mmol) in 20 mL methanol, hydroxylamine hydrochloride (0.72g, 10.3 mmol) and sodium bicarbonate (0.85 g, 10.1 mmol) was added. The resulting mixture was heated under reflux for 14 h. After completion (Monitored by TLC), solvent was removed *in vacuo* and distilled water added to the residue. The mixture was filtrated under vacuum, and the white solid was washed with distilled water (2x10 mL) and ethyl acetate (2x10 mL) and dried overnight in the presence of P_2O_5. 1.09 g of compound **45** were obtained. Yield: 72 %. ^{1}H-NMR (400 MHz, d_6-DMSO) δ (ppm): 9.59 (s, 1H), 8.27 (s, 1H), 6.81 (t, J = 6.7 Hz, 1H), 5.87 (s, 2H), 4.34 (t, J = 7.1 Hz, 2H), 2.89 (q, J = 6.7 Hz, 2H), 1.76 (m, 2H), 1.33 (s, 9H), 1.29 (m, 2H). ^{13}C-NMR (100 MHz, d_6-DMSO) δ (ppm): 156.0, 145.8, 140.6, 122.7, 77.9, 49.7, 41.6, 27.5, 26.8, 11.3.

***tert*-butyl (3-(4-(5-oxo-4,5-dihydro-1,2,4-oxadiazol-3-yl)-1*H*-1,2,3-triazol-1-yl)propyl)carbamate (48)**

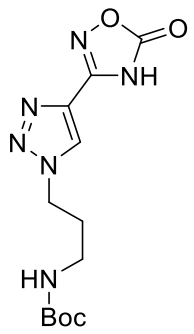

48

To a suspension of *tert*-butyl (*Z*)-(3-(4-(N'-hydroxycarbamimidoyl)-1*H*-1,2,3-triazol-1-yl)propyl)carbamate (**44**) (0.15 g, 0.50 mmol) in anhydrous acetonitrile (5 mL) *N*,*N'*-carbonyldiimidazole (CDI) (0.10 g, 0.65 mmol) and DBU (0.1 mL) were added at room temperature. The mixture was stirred for 4 h under reflux. After completion (Monitored by TLC), 10% (v/v) acetic acid (25 mL) was added, and the mixture was extracted with ethyl acetate (3x10 mL). The combined organic layers washed with distilled water (3x10 mL), dried ($MgSO_4$) and concentrated *in vacuo* to afford 82 mg of **48**. Yield: 53 %. ^{1}H-NMR (400 MHz, d_6-DMSO) δ (ppm): 13.21 (s, 1H), 8.76 (s, 1H), 6.92 (t, J = 5.7 Hz, 1H), 4.45, (t, J = 7.0 Hz, 2H), 2.91 (q, J = 6.4 Hz, 2H), 1.95 (m, 2H), 1.34 (s, 9H). ^{13}C-NMR (100 MHz, d_6-DMSO) δ (ppm): 160.2, 156.1, 152.3,132.4, 125.8, 78.2, 48.3, 37.4, 30.4, 28.6. IR (cm^{-1}): 3336.33, 3133.23, 2981.57, 2783.88, 1787.26, 1661.54, 1562.54, 1338.59, 1155.09, 1088.63, 924.13, 891.55, 758.80. HRMS (ESI-FIA-TOF): m/z calculated for $C_{12}H_{19}N_6O_4$ 311.1462, found 311.1462.

***tert*-butyl (4-(4-(5-oxo-4,5-dihydro-1,2,4-oxadiazol-3-yl)-1H-1,2,3-triazol-1-yl)butyl)carbamate (49)**

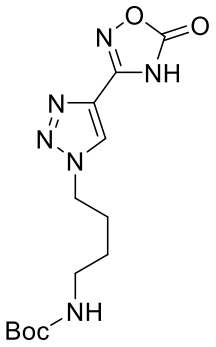

49

To a suspension of *tert*-butyl (Z)-(4-(4-(*N*'-hydroxycarbamimidoyl)-1*H*-1,2,3-triazol-1-yl)butyl)carbamate (**45**) (0.15 g, 0.50 mmol) in anhydrous acetonitrile (5 mL) *N*,*N'*-carbonyldiimidazole (CDI) (0.10 g, 0.65 mmol) and DBU (0.1 mL) were added at room temperature. The mixture was stirred for 4 h under reflux. After completion (monitored by TLC), 10% (v/v) acetic acid (25 mL) was added, and the mixture was extracted with ethyl acetate (3x10 mL). The combined organic layers washed with distilled water (3x10 mL), dried ($MgSO_4$) and concentrated *in vacuo*. to afford 121 mg of **49**. Yield: 75 %. ^{1}H-NMR (400 MHz, d_6-DMSO) δ (ppm): 8.78 (s, 1H), 6.80 (t, J = 5.8 Hz, 1H), 4.45 (t, J = 7.0 Hz, 2H), 2.90 (q, J = 6.6 Hz, 2H), 1.81 (m, 2H), 1.33 (s, 9H), 1.31 (m, 2H). ^{13}C-NMR (100 MHz, d_6-DMSO) δ (ppm): 160.0, 156.0, 152.1, 132.3, 125.6, 77.9, 50.1, 39.6, 28.6, 27.4, 26.7. HRMS (ESI-FIA-TOF): m/z calculated for $C_{13}H_{21}N_6O_4$ 325.1619, found 325.1619.

3-(1-(3-aminopropyl)-1*H*-1,2,3-triazol-4-yl)-1,2,4-oxadiazol-5(4*H*)-one hydrochloride (5)

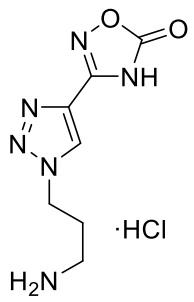

5

A mixture of *tert*-butyl (3-(4-(5-oxo-4,5-dihydro-1,2,4-oxadiazol-3-yl)-1*H*-1,2,3-triazol-1-yl)propyl)carbamate (**48**) (60 mg, 0.2 mmol) and 3M HCl in methanol (5 mL) was stirred at room temperature for 2 h. The solvent was removed *in vacuo* and the resulting yellow solid was triturated with ethyl acetate to provide 41 mg of the hydrochloride as a white solid. Yield: 86%. ^{1}H-NMR (400 MHz, d_6-DMSO) δ (ppm): 13.29 (s, 1H), 8.85 (s, 1H), 7.99 (s, 3H), 4.58 (t, J = 6.8 Hz, 2H), 2.78 (q, J = 7.5, 7.0 Hz, 2H), 2.15 (m, 2H). ^{13}C-NMR (100 MHz, d_6-DMSO) δ (ppm): 159.9, 152.0, 132.4, 126.1, 47.7, 36.5, 28.0. IR (cm^{-1}): 3165.72, 2870.49, 1797.92, 1558.51, 1208.58, 1043.91, 931.82, 783.92, 710.18. HRMS (ESI-FIA-TOF): m/z calculated for $C_7H_{11}N_6O_2$ 211.0938, found 211.0938.

3-(1-(4-aminobutyl)-1*H*-1,2,3-triazol-4-yl)-1,2,4-oxadiazol-5(4*H*)-one hydrochloride (6)

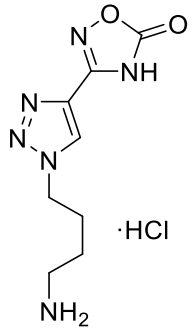

6

A mixture of *tert*-butyl (4-(4-(5-oxo-4,5-dihydro-1,2,4-oxadiazol-3-yl)-1*H*-1,2,3-triazol-1-yl)butyl)carbamate (**49**) (60 mg, 0.2 mmol) and 3M HCl in methanol (5 mL) was stirred at room temperature for 2 h. The solvent was removed *in vacuo* and the resulting yellow solid was triturated with ethyl acetate to provide 41 mg of the corresponding hydrochloride as a white solid. Yield: 86%. ^{1}H-NMR (400 MHz, d_6-DMSO) δ (ppm): 13.30 (s, 1H), 8.85 (s, 1H), 7.88 (s, 3H), 4.50 (t, J = 6.9 Hz, 2H), 2.78 (m, 2H), 1.91 (m, 2H), 1.49 (m, 2H). ^{13}C-NMR (100 MHz, d_6-DMSO) δ (ppm): 159.9, 152.1, 132.4, 125.9, 49.8, 38.5, 26.8, 24.3. IR (cm^{-1}): 3160.31, 2846.17, 1797.79, 1557.51, 1205.08, 930.61, 893.92, 706.24. HRMS (ESI-FIA-TOF): m/z calculated for $C_8H_{13}N_6O_2$ 225.1095, found 225.1091.

4-(((*tert*-butoxycarbonyl)amino)methyl)cyclohexyl methanesulfonate (26)

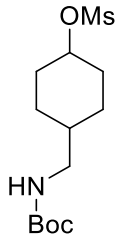

26

To a stirred solution of *tert*-butyl ((4-hydroxycyclohexyl)methyl)carbamate (**25**) (4.8 mmol) in 10 mL dichloromethane was added triethylamine (1 mL) and stirred at room temperature for 5 minutes and then cooled to 0-5 °C. Methanesulfonyl chloride (0.67 g, 6.2 mmol) was added dropwise at 0-5 °C and after addition the reaction mixture was allowed to warm to room temperature and then stirred at room temperature for 2 h. After completion (monitored by TLC), the reaction was quenched by addition of distilled water, additional dichloromethane was added and the dichloromethane layer after extraction was separated, dried ($MgSO_4$) and concentrated *in vacuo* to afford 1.40 g of compound **26**. Yield: 95%. ^{1}H-NMR (400 MHz, $CDCl_3$) δ (ppm): 4.62

(s, 1H), 4.54 (m, 1H), 2.97 (s, 3H), 2.94 (t, J = 6.5 Hz, 2H), 2.13 (m, 2H), 1.80 (m, 2H), 1.53 (m, 2H), 1.40 (s, 9H), 1.37 (m, 1H), 1.03 (m, 2H).

***tert*-butyl ((4-azidocyclohexyl)methyl)carbamate (27)**

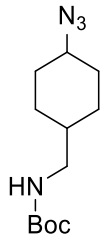

27

To a stirred solution of 4-(((*tert*-butoxycarbonyl)amino)methyl)cyclohexyl methanesulfonate (**26**) (8.9 mmol) in 20 mL dimethyl formamide, sodium azide (1.74, 26.8 mmol) was added and the resulting suspension was stirred at 80 °C for 8 h. After completion (monitored by TLC), the reaction was allowed to cool to room temperature and then poured into cold water with occasional stirring. The residue was extracted with ethyl acetate (3x10 mL). The combined organic layers were concentrated *in vacuo* and the residue was dissolved in hexane (50 mL) and an extraction with water (3x10 mL) was made. The combined organic layers were dried ($MgSO_4$) and concentrated *in vacuo* to afford 2.01g of **27**. Yield: 89%. ^{1}H-NMR (400 MHz, $CDCl_3$) δ (ppm): 4.62 (s, 1H), 3.79 (m, 1H), 2.97 (t, J = 6.4 Hz, 2H), 1.77 (m, 2H), 1.52 (m, 3H), 1.41 (s, 11H), 1.28 (m, 2H).

ethyl 1-(4-(((*tert*-butoxycarbonyl)amino)methyl)cyclohexyl)-1*H*-1,2,3-triazole-4-carboxylate (28)

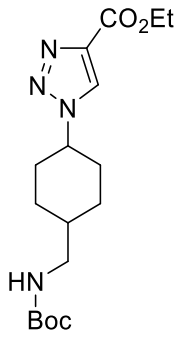

28

tert-butyl ((4-azidocyclohexyl)methyl)carbamate (**27**) (3.0 mmol) was taken in acetonitrile (15 mL) and to it ethyl propiolate (0.33 g, 3.3 mmol) was added, followed by CuI (0.11 g, 0.6 mmol) and the resulting solution was stirred at room temperature for 15 h. After completion (monitored by TLC), solvent was removed *in vacuo* and distilled water was added to the residue and then extracted with 3 portions (3x10 mL) of ethyl acetate. The combined organic layers were dried ($MgSO_4$) and concentrated *in vacuo* to obtain 0.84 g the desired compound as a pale yellow solid. Yield: 89%. ^{1}H-NMR (400 MHz, $CDCl_3$) δ (ppm): 8.12 (s, 1H), 4.62 (m, 1H), 4.59 (m, 1H), 4.39 (q, J = 7.1 Hz, 2H), 3.09 (t, J = 6.8 Hz, 2H), 2.17 (m, 2H), 2.00 (m, 2H), 1.68 (m, 2H), 1.52 (m, 2H), 1.41 (s, 10H), 1.38 (m, 3H).

***tert*-butyl ((4-(4-carbamoyl-1*H*-1,2,3-triazol-1-yl)cyclohexyl)methyl)carbamate (38)**

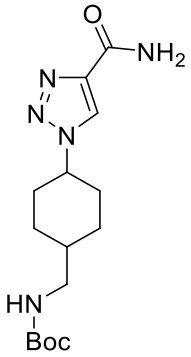

38

To a solution of ethyl 1-(4-(((*tert*-butoxycarbonyl)amino)methyl)cyclohexyl)-1*H*-1,2,3-triazole-4-carboxylate (**28**) (8.3 mmol) in 20 mL of ethanol, 30 mL of aqueous ammonia were added, and the resulting solution was stirred at room temperature for 12 h. After completion (Monitored by TLC), distilled water was added, and the mixture was filtrated under vacuum. The resulting white solid was washed with distilled water (3x10 mL) and dried under vacuum and in the presence of P_2O_5 overnight to provide 1.95 g of compound **38**. Yield. 73%. ^{1}H-NMR (400 MHz, $CDCl_3$) δ (ppm): 8.23 (s, 1H), 7.08 (s, 1H), 5.84 (s, 1H), 4.63 (t, *J* = 6.1 Hz, 1H), 4.58 (m, 1H), 3.09 (t, *J* = 6.8 Hz, 2H), 2.23 (m, 2H), 1.99 (m, 2H), 1.78 (m, 1H), 1.68 (m, 1H), 1.51 (m, 3H), 1.42 (s, 9H).

***tert*-butyl ((4-(4-cyano-1*H*-1,2,3-triazol-1-yl)cyclohexyl)methyl)carbamate (42)**

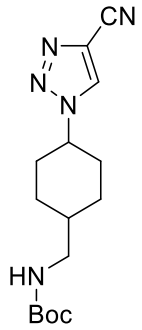

42

A solution of *tert*-butyl ((4-(4-carbamoyl-1*H*-1,2,3-triazol-1-yl)cyclohexyl)methyl)carbamate (**38**) (5.4 mmol) and 1.0 mL of triethylamine in 20 mL of dichloromethane was stirred at room temperature. The resulting solution was then cooled to 0-5 °C in an ice bath. To this cooled solution, trifluoroacetic anhydride (2.2 g, 10.8 mmol) was added. The resulting solution was stirred for 5 h. After completion (monitored by TLC), solvent was removed *in vacuo* and distilled water added to the residue and then extracted with 3 portions (3x10mL) of dichloromethane. The organic layer was washed with saturated $NaHCO_3$ solution, dried ($MgSO_4$) and concentrated *in vacuo* to yield 1.58 g of the desired compound. Yield: 96%. ^{1}H-NMR (400 MHz) δ (ppm): 8.23 (s, 1H),

4.60 (m, 1H), 3.71 (d, *J* = 7.5 Hz, 2H), 3.09 (m, 1H), 2.20 (m, 2H), 2.03 (m, 4H), 1.68 (m, 2H), 1.51 (s, 10H).

***tert*-butyl (*Z*)-((4-(4-(N'-hydroxycarbamimidoyl)-1*H*-1,2,3-triazol-1-yl)cyclohexyl)methyl)carbamate (46)**

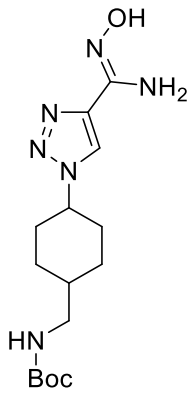

46

To a stirred solution of *tert*-butyl ((4-(4-cyano-1*H*-1,2,3-triazol-1-yl)cyclohexyl)methyl)carbamate (**42**) (1.3 g, 5.1 mmol) in 20 mL methanol, hydroxylamine hydrochloride (0.72g, 10.3 mmol) and sodium bicarbonate (0.85 g, 10.1 mmol) was added. The resulting mixture was heated under reflux for 14 h. After completion (monitored by TLC), solvent was removed *in vacuo* and distilled water added to the residue. The mixture was filtrated under vacuum, and the white solid was washed with distilled water (2x10 mL) and ethyl acetate (2x10 mL). After drying overnight in the presence of P_2O_5, 1.46 g of compound **46** were obtained. Yield: 85 %. ^{1}H-NMR (400 MHz, d_6-DMSO) δ (ppm): 9.44 (s, 1H), 8.28 (s, 1H), 6.83 (t, *J* = 6.0 Hz, 1H), 5.68 (s, 2H), 4.51 (m, 1H), 2.91 (t, *J* = 6.7 Hz, 2H), 2.10 (m, 2H), 1.81 (m, 2H), 1.65 (m, 1H), 1.55 (m, 2H), 1.41 (m, 2H), 1.34 (s, 9H).

***tert*-butyl ((4-(4-(5-oxo-4,5-dihydro-1,2,4-oxadiazol-3-yl)-1*H*-1,2,3-triazol-1-yl)cyclohexyl)methyl)carbamate (50)**

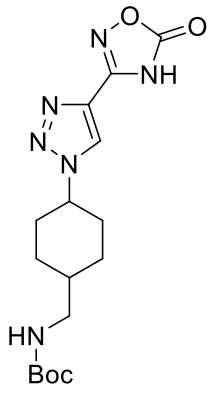

50

To a suspension *tert*-butyl (Z)-((4-(4-(*N'*-hydroxycarbamimidoyl)-1*H*-1,2,3-triazol-1-yl)cyclohexyl)methyl)carbamate (**46**) (0.50 mmol) in anhydrous acetonitrile (5 mL) *N*,*N'*-carbonyldiimidazole (CDI) (0.10 g, 0.65 mmol) and DBU (0.1 mL) were added at room temperature. The mixture was stirred for 15 h under reflux. After completion of the reaction (monitored by TLC), 10% (v/v) acetic acid (25 mL) was added, and the mixture was extracted with ethyl acetate (3x10 mL). The combined organic layers washed with distilled water (3x10 mL), dried ($MgSO_4$) and concentrated *in vacuo* to provide 0.15 g of **50**. Yield: 81%. ^{1}H-NMR (400 MHz, d_6-DMSO) δ (ppm): 8.85 (s, 1H), 6.84 (t, J = 6.0 Hz, 1H), 4.63 (m, 1H), 2.91 (t, J = 7.3 Hz, 2H), 2.13 (m, 2H), 1.85 (m, 2H), 1.66 (m, 1H), 1.57 (m, 2H), 1.41 (m, 2H), 1.34 (s, 9H). ^{13}C-NMR (100 MHz, d_6-DMSO) δ (ppm): 160.5, 156.2, 152.6, 132.5, 124.5, 77.8, 58.8, 43.2, 34.2, 28.7, 28.4, 25.8. IR (cm^{-1}): 3371.35, 3219.88, 2930.12, 1805.71, 1688.31, 1509.09, 1244.27, 1168.71, 930.82, 899.20, 668.88. HRMS (ESI-FIA-TOF): m/z calculated for $C_{16}H_{25}N_6O_4$ 365.1932, found 365.1932.

3-(1-(4-(aminomethyl)cyclohexyl)-1*H*-1,2,3-triazol-4-yl)-1,2,4-oxadiazol-5(4*H*)-one hydrochloride (7)

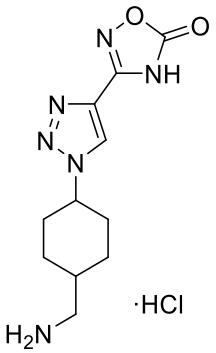

7

A mixture of *tert*-butyl ((4-(4-(5-oxo-4,5-dihydro-1,2,4-oxadiazol-3-yl)-1*H*-1,2,3-triazol-1-yl)cyclohexyl)methyl)carbamate (**50**) (0.2 mmol) and 3M HCl in methanol (5 mL) was stirred at room temperature for 2 h. The solvent was removed *in vacuo* and the resulting yellow solid was triturated with ethyl acetate to provide 41 mg of hydrochloride **7** as a white solid. Yield: 91%. ^{1}H-NMR (400 MHz, d_6-DMSO) δ (ppm): 13.28 (s, 1H), 9.00 (s, 1H), 8.05 (s, 3H), 4.69 (m, 1H), 2.84 (m, 2H), 2.13 (m, 2H), 1.90 (m, 3H), 1.67 (m, 2H), 1.54 (m, 2H). ^{13}C-NMR (100 MHz, d_6-DMSO) δ (ppm): 159.9, 152.2, 132.3, 124.7, 58.4, 41.7, 32.0, 28.7, 28.0, 25.5. IR (cm^{-1}): 3051.98, 2935.54, 1786.12, 1612.98, 1463.24, 1433.63, 926.44, 894.03, 753.45. HRMS (ESI-FIA-TOF): m/z calculated for $C_{11}H_{17}N_6O_2$ 265.1408, found 265.1410.

***tert*-butyl 4-(3-(methoxycarbonyl)-1H-1,2,4-triazol-1-yl)piperidine-1-carboxylate (51)**

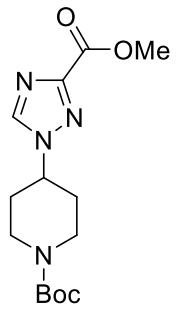

51

NaH (1 g; 41.7 mmol) was added to a solution of methyl 1*H*-1,2,4-triazole-3-carboxylate (2.8 g; 22 mmol) in DMF (130 mL). The reaction mixture was stirred at 25 °C for 20 minutes followed by 1 h at 70 °C. *tert*-butyl 4-(3-(methoxycarbonyl)-1H-1,2,4-triazol-1-yl)piperidine-1-carboxylate (**13**) (6 g, 19.3 mmol) was added and the reaction mixture was heated at 70 °C for 48 h. The solution was cooled to 0 °C and the insoluble material was removed by filtration. The filtrate was diluted with DCM and washed with water, brine, dried over Na_2SO_4, filtered, and evaporated to dryness. The residue was purified by chromatography over silica gel (mobile phase: petroleum ether/ethyl acetate 1/5) to render 1.50 g of compound **51**. Yield: 25%. ^{1}H-NMR (400 MHz, $CDCl_3$) δ (ppm): 7.98 (d, J = 0.6 Hz, 1H), 5.32 (s, 1H), 4.24 (t, J = 16.7 Hz, 2H), 4.01 (s, 3H), 2.91 (s, 2H), 2.17 – 2.05 (m, 2H), 1.99 (s, 2H), 1.48 (s, 9H).

***tert*-butyl 4-(3-(hydrazinecarbonyl)-1*H*-1,2,4-triazol-1-yl)piperidine-1-carboxylate (52)**

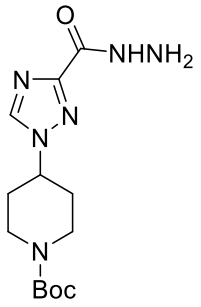

52

tert-butyl 4-(3-(methoxycarbonyl)-1*H*-1,2,4-triazol-1-yl)piperidine-1-carboxylate (**51**) (0.5 g, 1.6 mmol) and hydrazine hydrate (0.25 g) in 20 mL of *n*-butanol were refluxed for 3 h. Then, the solvent was removed by evaporation under vacuum. The residue was dissolved in dichloromethane and washed with water. The organic phase was dried ($MgSO_4$) and the solvent removed under reduced pressure. The resulting solid was washed with cold ethanol to afford 0.50 g of compound **52**. Yield: 95%. ^{1}H-NMR (400 MHz, $CDCl_3$) δ (ppm): δ 8.53 (s, 1H), 7.86 (s, 1H), 5.51 (tt, J =

11.4, 4.2 Hz, 1H), 4.27 (s, 2H), 4.03 (s, 2H), 2.90 (s, 2H), 2.16 – 2.02 (m, 2H), 1.96 (d, *J* = 11.8 Hz, 2H), 1.47 (s, 9H).

***tert*-butyl 4-(3-(5-oxo-4,5-dihydro-1,3,4-oxadiazol-2-yl)-1*H*-1,2,4-triazol-1-yl)piperidine-1-carboxylate (53)**

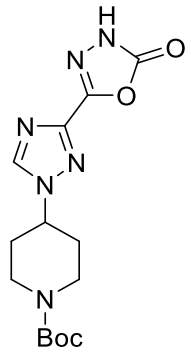

53

To a suspension of *tert*-butyl 4-(3-(hydrazinecarbonyl)-1*H*-1,2,4-triazol-1-yl)piperidine-1-carboxylate (**52**) (0.15 g, 0.50 mmol) in anhydrous acetonitrile (5 mL) *N*,*N*'-carbonyldiimidazole (CDI) (0.10 g, 0.65 mmol) and DBU (0.1 mL) were added at room temperature. The mixture was stirred for 15 h under reflux. After completion (monitored by TLC), 10% (v/v) acetic acid (25 mL) was added, and the mixture was extracted with ethyl acetate (3x10 mL). The combined organic layers washed with distilled water (3x10 mL), dried ($MgSO_4$) and concentrated *in vacuo* to render 0.15 g of compound **53**. Yield: 90%. ^{1}H-NMR (400 MHz, $CDCl_3$) δ (ppm): 8.04 (s, 1H), 5.00 (d, *J* = 11.3 Hz, 1H), 4.29 (s, 2H), 2.90 (s, 2H), 2.24 – 1.92 (m, 4H), 1.49 (s, 9H). ^{13}C-NMR (100 MHz, d_6-DMSO) δ (ppm): 153.9, 153.7, 151.2, 145.6, 139.7, 78.9, 56.6, 54.9, 31.1, 28.04. IR (cm^{-1}): 3083.51, 2972.69, 2867.28, 1818.87, 1780.92, 1638.91, 1434.60, 1367, 1268.44, 1164.10, 1133.93, 1046.99, 1006.74, 902.33, 675.17. HRMS (ESI-FIA-TOF): m/z calcd for $C_{14}H_{21}N_6O_4$ 337.1619, found 337.1621.

5-(1-(piperidin-4-yl)-1*H*-1,2,4-triazol-3-yl)-1,3,4-oxadiazol-2(3*H*)-one hydrochloride (9)

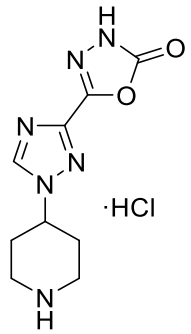

9

A mixture of *tert*-butyl 4-(3-(5-oxo-4,5-dihydro-1,3,4-oxadiazol-2-yl)-1*H*-1,2,4-triazol-1-yl)piperidine-1-carboxylate (**53**) (100 mg, 0.3 mmol) and 4N HCl in dioxane (2 mL) was stirred at room temperature for 2 h. The solvent was removed *in vacuo* and the resulting yellow solid was triturated with ethyl acetate to provide 77 mg of hydrochloride **9** as a white solid. Yield: 95%. ^{1}H-NMR (400 MHz, d_6-DMSO) δ (ppm): 13.24 (s, 1H), 9.25 (s, 1H), 9.10 (s, 1H), 8.24 (d, J = 0.6 Hz, 1H), 5.18 – 5.03 (m, 1H), 3.38 (d, J = 12.7 Hz, 2H), 3.05 (q, J = 11.7 Hz, 2H), 2.33 – 2.08 (m, 4H). ^{13}C-NMR (100 MHz, d_6-DMSO) δ (ppm): 153.5, 151.3, 145.4, 139.9, 54.0, 41.8, 27.9. IR (cm^{-1}): 2908.46, 2786.59, 2705.99, 2494.12, 1810.53, 1774.29, 1487.00, 1401.30, 1285.47, 1045.03, 904.69, 773.68, 724.76. HRMS (ESI-FIA-TOF): m/z calcd for $C_9H_{13}N_6O_2$ 237.1095, found 237.1094.

***tert*-butyl 4-(3-carbamoyl-1*H*-1,2,4-triazol-1-yl)piperidine-1-carboxylate (54)**

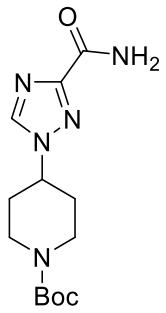

54

To a solution of *tert*-butyl 4-(3-(methoxycarbonyl)-1*H*-1,2,4-triazol-1-yl)piperidine-1-carboxylate (**51**) (0.85 g, 2.6 mmol) in 10 mL of methanol, 20 mL of ammonia in methanolic solution was added and the resulting solution was stirred at room temperature for 12 h. After completion (monitored by TLC), solvent was removed *in vacuo* and distilled water was added to the residue. It was extracted with 3 portions (3x10 mL) of dichloromethane. The combined organic layers were dried ($MgSO_4$) and concentrated *in vacuo* to render 0.75 g of the desired compound *tert*-butyl 4-(3-carbamoyl-1*H*-1,2,4-triazol-1-yl)piperidine-1-carboxylate (**54**) as a white solid. Yield: 96 %. ^{1}H-NMR (400 MHz, d_6-DMSO) δ (ppm): 13.08 (s, 2H), 8.20 (s, 1H), 5.19 – 4.89 (m, 1H), 4.19 – 3.82 (m, 2H), 2.80 (m, 2H), 1.95 (s, 2H), 1.88 – 1.69 (m, 2H), 1.39 (s, 9H).

***tert*-butyl 4-(3-cyano-1*H*-1,2,4-triazol-1-yl)piperidine-1-carboxylate (55)**

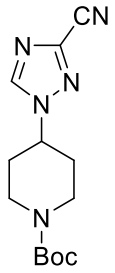

55

A solution of *tert*-butyl 4-(3-carbamoyl-1*H*-1,2,4-triazol-1-yl)piperidine-1-carboxylate (**54**) (0.9 g, 3.0 mmol) and 1.7 mL of triethylamine in 80 mL of dichloromethane was stirred at room temperature. The resulting solution was then cooled to 0-5 $^{\circ}$C in an ice bath. To this cooled solution, trifluoroacetic anhydride (1.3 g, 6.2 mmol) was added in 20 mL of dichloromethane. The resulting solution was stirred for 5 h. After completion (monitored by TLC), solvent was removed *in vacuo* and distilled water added to the residue and then extracted with 3 portions (3x10mL) of dichloromethane. The organic layer was washed with saturated $NaHCO_3$ solution, dried ($MgSO_4$) and concentrated *in vacuo* to render 0.70 g the desired compound **55** as a brown oil. Yield: 91%.

^{1}H-NMR (400 MHz, $CDCl_3$) δ (ppm): 8.04 (s, 1H), 4.62 (tt, *J* = 11.4, 4.3 Hz, 1H), 4.29 (s, 2H), 2.92 (t, *J* = 13.1 Hz, 2H), 2.13 (dddd, *J* = 13.1, 12.0, 11.3, 4.5 Hz, 2H), 2.00 (m, 2H), 1.47 (s, 9H).

***tert*-butyl (*Z*)-4-(3-(*N*'-hydroxycarbamimidoyl)-1*H*-1,2,4-triazol-1-yl)piperidine-1-carboxylate (56)**

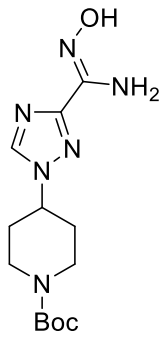

56

To a stirred solution of *tert*-butyl 4-(3-cyano-1*H*-1,2,4-triazol-1-yl)piperidine-1-carboxylate (**55**) (0.38 g, 1.3 mmol) in 10 mL methanol, hydroxylamine hydrochloride (0.47g, 6.8 mmol) and sodium bicarbonate (0.93 g, 6.8 mmol) was added. The resulting mixture was heated under reflux for 14 h. After completion (monitored by TLC), solvent was removed *in vacuo* and distilled water added to the residue and then extracted with 3 portions (3x10mL) of dichloromethane. The organic layer dried ($MgSO_4$) and concentrated *in vacuo*. A small portion of ethyl acetate was added and stirred at room temperature for 30 minutes. The resulting solid was collected by filtration and dried in vacuum to afford 0.33 g of compound **56**. Yield: 82%. ^{1}H-NMR (400 MHz, d_6-DMSO) δ (ppm): 10.21 (s, 1H), 7.99 (s, 1H), 5.93 (s, 2H), 5.25 – 5.08 (m, 1H), 4.02 (s, 2H), 2.79 (s, 2H), 1.95 – 1.72 (m, 4H), 1.39 (s, 9H).

***tert*-butyl 4-(3-(5-oxo-4,5-dihydro-1,2,4-oxadiazol-3-yl)-1*H*-1,2,4-triazol-1-yl)piperidine-1-carboxylate (57)**

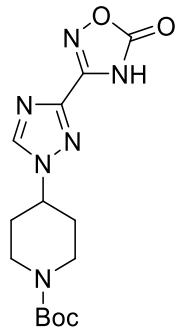

57

To a suspension of *tert*-butyl (*Z*)-4-(3-(*N*'-hydroxycarbamimidoyl)-1*H*-1,2,4-triazol-1-yl)piperidine-1-carboxylate (**56**) (0.15 g, 0.50 mmol) in anhydrous acetonitrile (5 mL) *N*,*N*'-carbonyldiimidazole (CDI) (0.10 g, 0.65 mmol) and DBU (0.1 mL) were added at room temperature. The mixture was stirred for 15 h under reflux. After completion (monitored by TLC), 10% (v/v) acetic acid (25 mL) was added, and the mixture was extracted with ethyl acetate (3x10 mL). The combined organic layers washed with distilled water (3x10 mL), dried ($MgSO_4$) and concentrated *in vacuo* to give 0.13 g of compound **57**. Yield: 78%. ^{1}H-NMR (400 MHz, d_6-DMSO) δ (ppm): 9.47 (s, 1H), 7.95 (s, 1H), 5.54 – 5.30 (m, 1H), 4.02 (d, J = 13.5 Hz, 2H), 2.84 (s, 2H), 1.95 – 1.70 (m, 2H), 1.70 – 1.49 (m, 2H), 1.39 (s, 9H). ^{13}C-NMR (100 MHz, d_6-DMSO) δ (ppm): 159.8, 153.7, 151.9, 132.1, 123.7, 79.0, 57.8, 42.3, 31.6, 28.0. IR (cm^{-1}): 3121.35, 2975.39, 2853.76, 1819.07, 1788.93, 1687.45, 1419.42, 1361.69, 1274.22, 1166.18, 948.42, 907.18, 733.88. HRMS (ESI-FIA-TOF): m/z calcd for $C_{14}H_21N_6O_4$ 337.1619, found 337.1619.

3-(1-(piperidin-4-yl)-1*H*-1,2,4-triazol-3-yl)-1,2,4-oxadiazol-5(4*H*)-one hydrochloride (10)

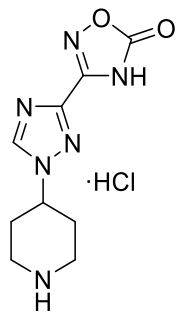

10

A mixture of *tert*-butyl 4-(3-(5-oxo-4,5-dihydro-1,2,4-oxadiazol-3-yl)-1*H*-1,2,4-triazol-1-yl)piperidine-1-carboxylate (**57**) (100 mg, 0.3 mmol) and 4N HCl in dioxane (2 mL) was stirred at room temperature for 2 h. The solvent was removed *in vacuo* and the resulting yellow solid was triturated with EtOAc to provide 77 mg of compound **10** as a yellow solid. Yield: 95%. ^{1}H-NMR (400 MHz, d_6-DMSO) δ (ppm): 9.09 (s, 2H), 8.90 (d, J = 4.5 Hz, 1H), 7.67 (s, 2H), 4.93 (s, 1H), 3.13 – 3.03 (m, 2H), 2.38 – 2.29 (m, 2H), 2.24 (s, 2H). ^{13}C-NMR (100.0 MHz, d_6-DMSO) δ (ppm): 153.5, 151.3, 145.4, 139.9, 54.0, 41.8, 27.9. IR (cm^{-1}): 3213.25, 2707.80, 1754.73, 1422.42, 1068.24, 944.82, 906.40, 762.39, 742.79, 677.38. HRMS (ESI-FIA-TOF): m/z calcd for $C_9H_{13}N_6O_2$ 237.1095, found 237.1094.

ethyl 4-(aminomethyl)cyclohexane-1-carboxylate hydrochloride (59)

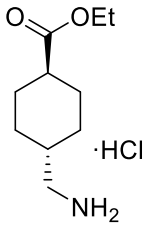

59

A solution of tranexamic acid (**58**) (4.0 g, 25.6 mmol) in ethanol (150 mL) was stirred at room temperature. The solution was then cooled to 0-5 ºC in an ice bath. To this cooled solution, thionyl chloride (9.1 g, 77 mmol) was added dropwise. The mixture was refluxed for 2 hours. After

completion, solvent was removed by evaporation and dichloromethane was added. The solution was washed with a saturated Na_2CO_3 solution and brine, dried ($MgSO_4$) and concentrated *in vacuo* to render 5.05 g of compound **59**. Yield: 89% yield. ^{1}H-NMR (400 MHz, $CDCl_3$) δ (ppm): 8.32 (s, 3H), 4.09 (q, *J* = 7.1 Hz, 2H), 2.84 (m, 2H), 2.21 (m, 1H), 2.01 (m, 4H), 1.75 (m, 1H), 1.47 (m, 2H), 1.21 (t, *J* = 7.1 Hz, 3H), 1.06 (m, 2H).

ethyl 4-(((*tert*-butoxycarbonyl)amino)methyl)cyclohexane-1-carboxylate (60)

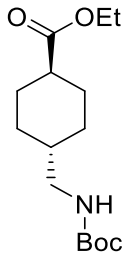

60

A mixture of ethyl 4-(aminomethyl)cyclohexane-1-carboxylate hydrochloride (**59**) (2.9 g, 13 mmol) and triethylamine (3.6 mL, 26 mmol) was dissolved in methanol (20 mL). After the addition of di-*tert*-butyl decarbonate (3.1 g, 14 mmol) the solution was stirred at room temperature for 8 hours. After completion, solvent was removed *in vacuo* and dichloromethane was added. The solution was then washed with 1M HCl solution and brine. The organic phase was dried ($MgSO_4$) and the solvent evaporated to obtain 3.52 g of compound **60**. Yield: 95%. ^{1}H-NMR (400 MHz, $CDCl_3$) δ (ppm): 4.56 (s, 1H), 4.09 (q, *J* = 7.1 Hz, 2H), 2.96 (t, 2H), 2.19 (m, 1H), 1.99 (m, 2H), 1.79 (m, 2H), 1.42 (s, 10H), 1.40 (m, 2H), 1.22 (t, *J* = 7.1 Hz, 3H), 0.95 (m, 2H).

***tert*-butyl ((4-carbamoylcyclohexyl)methyl)carbamate (61)**

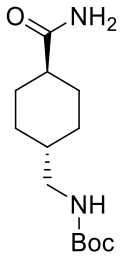

61

A solution of ethyl (4-(((*tert*-butoxycarbonyl)amino)methyl)cyclohexane-1-carboxylate (**60**) (2.6 g, 9.1 mmol) in 7N methanolic ammonia (20 mL) was stirred inside a pressurized vessel at 85 ºC for 5 days. After the addition of NaOH 1M (10 mL), the mixture was stirred at 40 ºC for 4 hours. The solvent was removed *in vacuo*, and water was added. The desired amide was extracted with ethyl acetate, dried ($MgSO_4$) and concentrated under vacuum to afford 0.58 g of compound **61**. Yield: 25%. ^{1}H-NMR (400 MHz, $CDCl_3$) δ (ppm): 5.58 (s, 2H), 4.56 (s, 1H), 2.96 (d, J = 6.6 Hz, 2H), 2.09 (m, 1H), 1.96 (m, 2H), 1.85 (m, 2H), 1.46 (m, 2H), 1.43 (s, 10H), 0.97 (m, 2H).

***tert*-butyl ((4-cyanocyclohexyl)methyl)carbamate (62)**

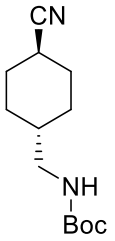

62

A solution of *tert*-butyl ((4-carbamoylcyclohexyl)methyl)carbamate (**61**) (3.0 mmol) and 1.7 mL of triethylamine in 80 mL of dichloromethane was stirred at room temperature. The resulting solution was then cooled to 0-5 °C in an ice bath. To this cooled solution, trifluoroacetic anhydride (6.2 mmol) was added in 20 mL of dichloromethane. The resulting solution was stirred for 5 h. After completion of the reaction (monitored by TLC), solvent was removed *in vacuo* and distilled

water added to the residue and then extracted with 3 portions (3x10mL) of dichloromethane. The organic layer was washed with saturated $NaHCO_3$ solution, dried ($MgSO_4$) and concentrated *in vacuo* to render 0.65 g of the desired product as a brown oil. Yield: 91%. ^{1}H-NMR (400 MHz, $CDCl_3$) δ (ppm): 3.58 (d, J = 6.8 Hz, 2H), 2.37 (m, 1H), 2.12 (m, 2H), 1.74 (m, 3H), 1.56 (m, 2H), 1.52 (s, 9H), 1.02 (m, 2H).

***tert*-butyl ((4-((*Z*)-*N*'-hydroxycarbamimidoyl)cyclohexyl)methyl)carbamate (63)**

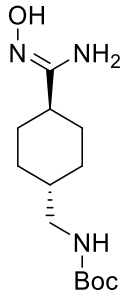

63

To a stirred solution of *tert*-butyl ((4-cyanocyclohexyl)methyl)carbamate (**62**) (1.3 mmol) in 10 mL methanol, hydroxylamine hydrochloride (6.8 mmol) and sodium bicarbonate (6.8 mmol) was added. The resulting mixture was heated under reflux for 14 h. After completion (monitored by TLC), solvent was removed *in vacuo* and distilled water added to the residue and then extracted with 3 portions (3x10mL) of dichloromethane. The organic layer dried ($MgSO_4$) and concentrated *in vacuo*. A small portion of ethyl acetate was added and stirred at room temperature for 30 minutes. The solid was collected by filtration and dried under vacuum to afford 0.29 g of compound **63**. Yield: 82%. ^{1}H-NMR (400 MHz, d_6-DMSO) δ (ppm): 8.64 (s, 1H), 6.77 (t, J = 6.1 Hz, 1H), 5.19 (s, 2H), 2.72 (q, J = 6.2 Hz, 2H), 1.86 (m, 1H), 1.68 (m, 4H), 1.34 (s, 10H), 1.28 (m, 2H), 0.82 (m, 2H).

***tert*-butyl ((4-(5-oxo-4,5-dihydro-1,2,4-oxadiazol-3-yl)cyclohexyl)methyl)carbamate (64)**

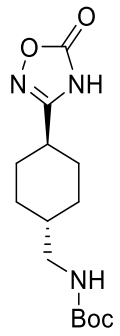

64

To a suspension of *tert*-butyl ((4-((*Z*)-*N*'-hydroxycarbamimidoyl)cyclohexyl)methyl)carbamate (**63**) (0.50 mmol) in anhydrous acetonitrile (5 mL) *N*,*N*'-carbonyldiimidazole (CDI) (0.10 g, 0.65 mmol) and DBU (0.1 mL) were added at room temperature. The mixture was stirred for 15 h under reflux. After completion (monitored by TLC), 10% (v/v) acetic acid (25 mL) was added, and the mixture was extracted with ethyl acetate (3x10 mL). The combined organic layers washed with distilled water (3x10 mL), dried ($MgSO_4$) and concentrated *in vacuo* to provide 115 mg of compound **64**. Yield: 78%. ^{1}H-NMR (400 MHz, d_6-DMSO) δ (ppm): 12.09 (s, 1H), 6.80 (t, J = 5.9 Hz, 1H), 2.75 (t, J = 6.3 Hz, 2H), 2.46 (m, 1H), 1.90 (m, 2H), 1.72 (m, 2H), 1.34 (s, 10H), 1.31 (m, 2H), 0.93 (m, 2H). ^{13}C-NMR (100 MHz, d_6-DMSO) δ (ppm): 163.4, 160.3, 156.2, 77.8, 46.8, 37.6, 34.8, 29.5, 28.7. IR (cm^{-1}): 3363.41, 2984.28, 2924.70, 1782.73, 1687.06, 1530.88, 1248.35, 1166.58, 953.70, 758.24. HRMS (ESI-FIA-TOF): m/z calculated for $C_{14}H_{24}N_3O_4$ 298.1761, found 298.1757.

3-(4-(aminomethyl)cyclohexyl)-1,2,4-oxadiazol-5(4*H*)-one hydrochloride (11)

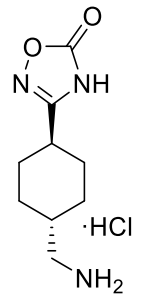

11

A mixture of *tert*-butyl ((4-(5-oxo-4,5-dihydro-1,2,4-oxadiazol-3-yl)cyclohexyl)methyl)carbamate (**64**) (0.2 mmol) and 3M HCl in methanol (5 mL) was stirred at room temperature for 2 h. The solvent was removed *in vacuo* and the resulting yellow solid was triturated with ethyl acetate to provide41 mg of hydrochloride **11** as a white solid. Yield: 88%. ^{1}H-NMR (400 MHz, d_6-DMSO) δ (ppm): 8.37 (s, 3H), 2.63 (d, J = 6.8 Hz, 2H), 2.52 (m, 1H), 1.93 (m, 2H), 1.84 (m, 2H), 1.56 (m 1H), 1.40 (m, 2H), 1.03 (m, 2H). ^{13}C-NMR (100 MHz, d_6-DMSO) δ (ppm): 165.8, 162.8, 46.7, 37.3, 36.7, 31.2, 30.5. IR (cm^{-1}): 3030.32, 2945.68, 1770.02, 1605.87, 1492.20, 1221.33, 959.10, 713.56. HRMS (ESI-FIA-TOF): m/z calculated for $C_9H_{16}N_3O_2$ 198.1237, found 198.1235.

5.7. Computational studies

5.7.1. Docking studies

The 3D structures of the enzyme-ligand complexes were modelled with AutoDock 4.2. Protein structure of the Kringle 1 domain of plasminogen was taken from the Protein Data Bank with PDB accession code 1CEA. Ligand structures for EACA and TXA were extracted from protein structures with pdb codes 1CEA (EACA) and 1CEB (TXA). The structures for all ligands were generated with AVOGADRO. Both protein and ligand structures were first parametrized with AutoDockTools: polar hydrogens were added, AutoDock 4.2 atom typing was used, and Gasteiger partial charges were computed. All rotatable bonds of the ligands were considered free during the docking calculations, whereas the whole protein structure was kept fixed.

Dockings for all ligands were performed with AutoDock 4.2. A grid-box of 38.25x37.5x33.75 Å with a grid point spacing of 0.375 Å, centered at the point (33.96, -1.477, -47.335), was used as the search space for docking. For each ligand docking, 1000 rounds of the genetic algorithm implemented in AutoDock 4.2 were performed. For each round, an initial population of 150 members was considered, with randomized initial position and orientation coordinates, and randomized conformations of the substrate flexible bonds. The genetic algorithm was extended up to 27000 offspring generations, with a maximum of 2500000 energy evaluations. Only low energy and repetitive binding poses were considered for analysis. Distances were measured and pictures of the complexes were generated using VMD [143].

5.7.2. Molecular dynamics simulations

The protein was inserted into a cubic box of water molecules, ensuring that the solvent shell would extend for at least 0.8 nm around the system. Three sodium counterions were added. The GROMOS 54a7 force field was used for both the protein and ligands. The water molecules were

described by the SPC/E model. Parameters for the ligands were generated with PRODRG webserver [144]. The system was minimized imposing harmonic position restraints of 1000 $kJ \cdot mol^{-1} \cdot nm^{-2}$ on solute atoms, allowing the equilibration of the solvent without distorting the solute structure. After an energy minimization of the solvent and the solute without harmonic restraints, the temperature was gradually increased from 0 to 298 K. This was performed by increasing the temperature from 0 to 298 K in 12 steps in which the temperature was increased by 25 K in 100 ps of MD.

Constant temperature−pressure (T = 298 K, P = 1 bar) 20-ns dynamics was then performed through the Nosé-Hoover and Andersen-Parrinello-Rahman coupling schemes. Periodic boundary conditions were applied. The final simulation box equilibrated at around 5.61×5.61×5.61 nm. Long-range electrostatic interactions were treated with the particle mesh Ewald (PME) method, using a grid with a spacing of 0.12 nm combined with a fourth-order B-spline interpolation to compute the potential and forces in between grid points. The cutoff radius for the Lenard-Jones interactions as well as for the real part of PME calculations was set to 0.9.

The simulations were performed under the Constant temperature−pressure scheme for 1000 ns for each compound, with a time step of 2 fs. Analysis of the simulated trajectories were performed with VMD [143].

5.7.3. Molecular surface calculations

Molecular surfaces were computed as described in Varshney et al. [145]. A probe radius of 1.4 Å was used to measure the solvent accessible surface area. 100 different conformations of each ligand were evaluated. Molecular surface values correspond to the average of this ensemble.

5.8. Cell culture

5.8.1. Seeding

Cryopreserved cells were thawed, seeded, grown, and passaged onto 75 cm2 tissue culture polystyrene plates (T75). Prior to thawing the cells, 10 ml of the specific medium were pre-warmed in a water bath at 37ºC and introduced into the T75. The 1 ml cryopreserved vial containing 1 million cells was thawed in the water bath at 37ºC for less than 2 minutes, and then its content was poured into the T75. The plate was then placed in the incubator. After 1-2 hours, the cells were - completely attached to the surface. After confirming the attachment visually using a light microscope, the culture medium was replaced for 10 ml of fresh medium.

5.8.2. Culture

Cells were cultured in an incubator at 37ºC, 5% CO_2 and 80% relative humidity. For all cell types, old medium was replaced with fresh medium every 2-3 days. The health condition of the cells, as well as their morphology, were checked daily using a bright field inverted microscope.

5.8.3. Sub-culture

To passage cells cultured on a T75, supernatant was aspirated off and cells were quickly rinsed with 10 ml of PBS, previously warmed in a bath at 37ºC. After removing the PBS, 3 ml of trypsin were pipetted into the plates. Trypsinization of adherent cells was carried out for 5 min at 37ºC and 5% CO_2. Cell detachment was visually checked under the bright field microscope, and then 7 ml of medium were added to the plate to neutralize the effect of trypsin. The content of the plate was gently aspirated, poured 2-3 times to mechanically detach cells and finally introduced in a falcon tube. Cell number was quantified using a cell counter. The cell suspension was centrifuged for 5 min at 1400 rpm and then the supernatant medium was carefully aspirated off. Cells were then resuspended in the amount of medium necessary to achieve the desired cell concentration.

Cells were then seeded into a T75 or any other required surface, depending on the type of experiment.

5.8.4. Cryopreservation

In order to cryopreserve the cells, one T75 was rinsed with PBS, trypsinized with 3 ml of Trypsin for 5 minutes and centrifuged for 5 minutes at 1400 rpm after adding 7 ml of medium. Cells were then resuspended in 1 ml of a mixture of 60% medium, 30% FBS and 10% DMSO. The suspension was transferred to a 1 ml cryovial and quickly introduced in a freezing container, which was then placed inside a -80ºC freezer. This freezing container, filled with isopropyl alcohol, guarantees a cooling rate of 1ºC/min. After 24-48 h, the vials were transferred to a -150ºC freezer for long-term storage and the cell inventory was updated accordingly.

5.9. Permeability assays

5.9.1. Cell culture on Transwell inserts

Permeability assays were performed on HBMEC cultured in 24-well plate Transwell inserts. Before seeding the endothelial cells, the Transwell membrane was coated with 5 µg/mL of Fn in PBS for 2 hours at 37 °C. Fn solution was aspirated, and the membranes were quickly rinsed with PBS. Meanwhile, a suspension of HBMEC in growth medium was prepared and 100 µL aliquots, with 60,000 cells each, were added on the upper side of each insert. Each well, or bottom compartment, was filled with 600 µL of growth medium.

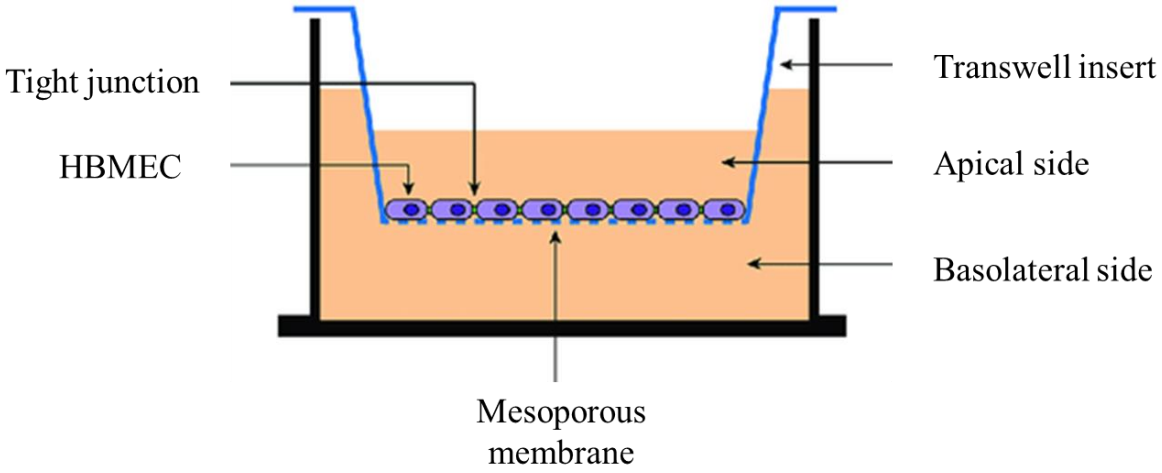

Figure 64. Different parts of a BBB *in vitro* model based on HBMECs seeded on a Transwell insert.

After allowing the cells to attach for 24 hours, the medium was switched into depleted medium on both sides of the membrane, which was left for an additional 48 hours before beginning the permeability assay.

5.9.2. Permeability assay

Stock solutions (1 mg/mL) of fluorescent-labeled 4 kDa dextran (FITC-Dextran) were prepared, dissolving it in PBS. This was further diluted in depleted medium to achieve a concentration of 100µg/mL. Prior to the assay, media was changed from the bottom compartment of the inserts for 0.6 mL of fresh non-fluorescent depleted medium. Then, apical medium was aspirated and 100 µL of fluorescent medium were poured so that fluorescent dyes diffused from the apical to the basolateral side. Samples of 50 µL were taken from the basolateral side every 30 minutes for 2.5 hours and added to black 384-well plates where fluorescence was measured (excitation: 492 nm / emission: 520 nm). Permeability coefficients (Pe) were calculated from the slope of the linear

regression between the amount of solute diffusing across the membrane and diffusion time, according to equation 10.

$$\frac{B}{T} \cdot V_B = P_e \cdot A \cdot t \quad \text{(Eq. 10)}$$

Where B and T are the raw fluorescence units from the bottom and top compartments, VB is the bottom compartment volume, A is the cross-sectional area of the membrane and t is time.

5.10. Western Blot

HBMEC were first cultured in P100 plates using growth medium until they reached confluency. At that point, the medium was switched for depleted medium and left for 48 hours. Cells were then exposed to the different conditions studied in the experiment, all diluted in depleted medium, for 24 hours.

Cells were then washed twice with ice-cold PBS and were lysed with radioimmunoprecipitation assay (RIPA) buffer containing 50 mM Tris-HCl, pH 7.4, 150 mM NaCl, 1% NP-40, 0.5% deoxycholate, 0.1% SDS and 5mM EDTA. The buffer was supplemented with protease inhibitor cocktail containing 2 mM AEBSF, 1mM EDTA, 130 µM bestatin, 14 µM E-64, 1 µM leupeptin and 0.3 µM aprotinin. Lysates were centrifuged at 8,000 g for 30 minutes at 4°C and supernatants were stored at -80°C until use. Protein concentration was determined using the Pierce BCA Protein Assay Kit. Samples were diluted to a protein concentration of 1µg/µL with 1:4 v/v of 4X Sample Buffer Reducing Agent, and the necessary volume of purified water. For protein separation, 20 µL (20 µg of protein) were loaded in each well of 10% Bis-Tris polyacrylamide gels. Gels were transferred to nitrocellulose membranes using the iBlot transfer system from Thermo Fisher. Membranes were blocked for 60 minutes with 5% non-fat dry milk solution in PBS-T (PBS with 0.05% Tween-20) and incubated overnight at 4°C and gentle rocking with primary antibody of interest diluted at their optimal concentration in PBS-T and 10% blocking buffer. After washing

twice with PBS-T, membranes were incubated for 1 hour at room temperature and gentle rocking with appropriate HRP-conjugated secondary antibodies at their optimal concentration in PBS-T and 10% blocking buffer. Then, membranes were washed twice with PBS-T, and protein bands were detected after membrane incubation in Immobilon Forte Western HRP substrate with a chemiluminescent image analyzer ChemiDoc XRS+ System (BioRad, USA). Blots were quantified using Fiji imaging software (NIH). α-tubulin was used as loading controls for all assays.

5.11. Experiments for confocal microscopy

Different experiments were performed with cultures of HBMEC to evaluate tight junction proteins through immunofluorescence. In order to visualize the results in a confocal microscope, special culture systems were use, both for static and for dynamic conditions.

5.11.1. Static conditions

When studying static conditions, endothelial cells were seeded on 35 mm µ-Dishes (Ibidi). A total of 100,000 cells in 2 mL of growth medium were deployed in each dish. After reaching confluency (2-3 days), the medium was switched into depleted medium for 48 hours. After that period, cells were exposed to the different conditions of the experiment, diluted in 2 mL of depleted medium, for 24 hours. At the conclusion of the experiment, cells were quickly washed with pre-warmed PBS, and then fixed with 3.7% PFA in PBS for 10 min. The following steps of the immunofluorescence staining protocol were then followed.

5.11.2. Dynamic conditions

When studying dynamic conditions, endothelial cells were seeded in special µ-Slides (Ibidi) with a central channel of 50x5x0.8 mm. This channel was first coated with 100 µg/mL Fn in PBS for 2 hours at 37 °C. After that, the channel was quickly rinsed with PBS, and a total of 200,000 HBMECs were introduced in the channel (200 µL of a 1 M/mL cells suspension), suspended in

growth medium. After 1 hour attachment of cells was checked visually through light microscopy, and then 120 µL of additional growth medium were added.

After 48 hours, the µ-Slide was connected to a previously sterilized flow loop (Figure 65). In this loop, depleted medium was circulated from a glass reservoir through the pump tubes, where the fluid was propelled by a 12-channel peristaltic pump. The medium flowed then through the µ-Slide which contained a monolayer of HBMECs, and finally returned to the reservoir. The whole loop was kept inside a bioreactor for the duration of the experiment. This bioreactor allowed to maintain 37 °C and 100% humidity while being connected to a peristaltic pump.

In our experiments, cells were exposed to a healthy flowrate to cause 10 dyn/cm^2 of shear stress. Initially, 10 mL of depleted medium were circulated for 72 hours to maximize tight junction formation. After this period, the different experimental conditions were introduced in each reservoir, and left during an additional period of 24 hours. At the conclusion of the experiment, the flow loop was disconnected inside the sterile biological hood. Cells were then quickly washed with pre-warmed PBS, before fixing them with 3.7% PFA in PBS for 10 min. The following steps of the immunofluorescence staining protocol were then followed.

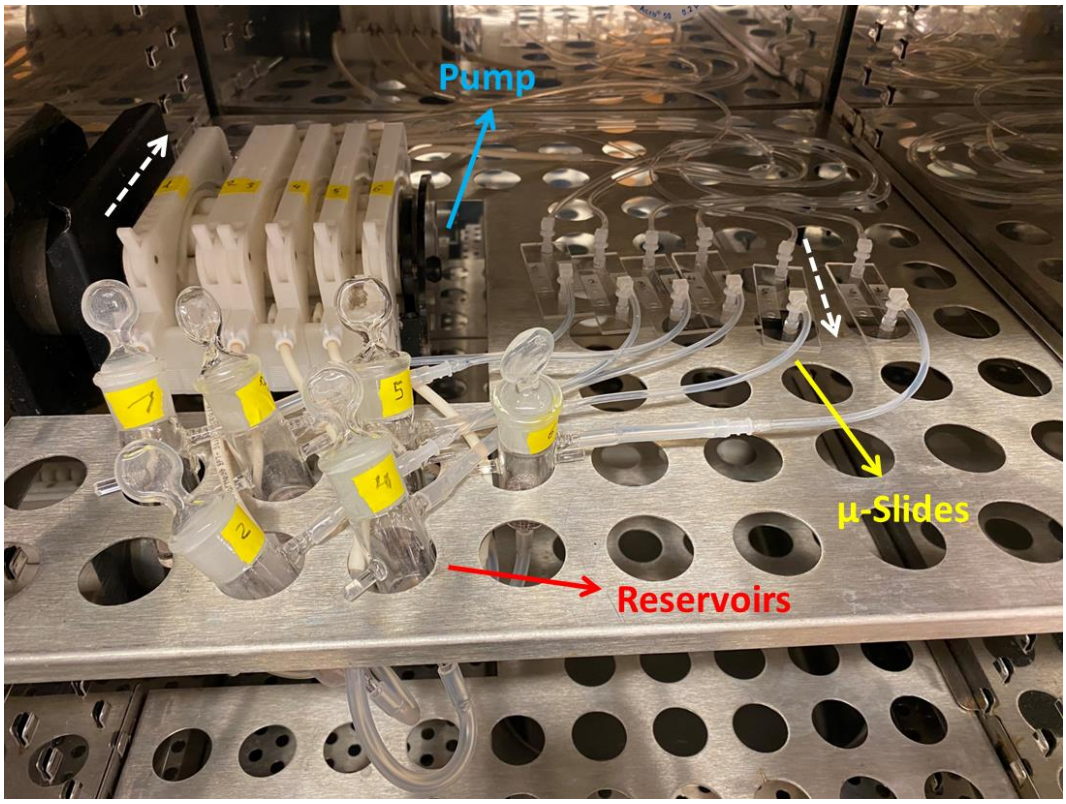

Figure 65. Picture of a connected flow loop inside the flow bioreactor. Medium flow from the reservoirs, through the pump tubes, through the µ-Slides and finally back to the reservoirs. Flow direction is indicated by the dashed white arrows.

5.12. Immunofluorescent staining

The goal with this procedure was always to stain one or more specific intra- and extracellular proteins. The first step was always to fix the cells. To do so, a 1 min wash with PBS was done, and the cells were fixed with PFA 3.7% in PBS for 10 min. PFA was then washed with PBS twice for 5 min. Cell membrane permeabilization was then performed to allow antibodies to penetrate inside the cell cytoplasm. This was done using a solution with 0.2% Triton X-100 in PBS for 20 min. Afterward, an additional wash with PBS was performed twice for 5 min. Then, samples were blocked for 1h at RT with 5% goat serum in PBS-BSA (1% BSA in PBS) to minimize unspecific

binding of the antibody. After blocking, the primary antibody solution was applied. To prepare it, the primary antibodies corresponding to the proteins of interest (maximum two, always from different host species) were diluted in PBS-BSA at a 1:100 ratio. This solution was left on the cells overnight at 4ºC while shaking. The next day, samples were washed twice for 10 min with PBS-BSA. Then the secondary fluorescent antibodies corresponding to the species of the primary antibodies used (usually rabbit and mouse) were diluted 1:200 in PBS-BSA. In the secondary antibody solution, DAPI was also added at 1 µg/ml to stain the nuclei of the cells. This whole mixture was applied to the cells at RT for 2 h. Before imaging, two final washes of 10 min with PBS were carried out. Samples were then imaged at a normal fluorescent microscope or a confocal microscope, depending on the precision requirements.

5.13. Statistical analysis

All *in vitro* quantitative experiments were performed at least in triplicate or quadruplicate specimens (n=3-4). Error bars for all experiments indicate standard deviation. Statistical differences were analyzed using GraphPad Prism 9 software. Difference between two measurements was tested using unpaired Student's t-test. Difference between sets of measurements was tested using one-way analysis of variance (ANOVA). Values of $P < 0.05$ were considered statistically significant and are represented with an asterisk symbol (*) in graphical representations. Furthermore, $P < 0.01$ was indicated by (**), $P < 0.001$ by (***) and $P < 0.0001$ by (****).

6. Conclusions

Conclusions

This work describes an extensive study of a new family of compounds with high antifibrinolytic activity, and its application as a protective agent of the BBB during TBI. The compounds are based on the originally discovered LTI-6 (**1**), which combines a piperidine, a 1,2,3-triazole ring and 1,3,4-oxadiazolone moiety.

Coagulation assays with plasma and whole blood confirmed that LTI-6 acts as a fibrinolysis inhibitor, with no noticeable effect on coagulation. The potency of LTI-6 as an antifibrinolytic was equivalent to that of TXA in plasma, but 1.5 times higher in whole blood.

The different studies with isolated enzymes allowed to propose that LTI-6 inhibits fibrinolysis by interacting with the LBS of plasminogen, in an analogous mechanism to lysine analogues. At micromolar range, LTI-6 increased the rate of activation of plasminogen to plasmin in the absence of fibrin. The enhancement of plasminogen activation was around 40-fold higher than that of TXA. A certain inhibition of the active site of plasmin was observed for LTI-6, as well as for TXA. However, this inhibition occurs at the millimolar range for both compounds, at concentrations around 500-fold higher than their therapeutic doses in plasma.

Modifying the 1,3,4-oxadiazolone for a 1,2,4-oxadiazolone improved the activity of the compound, likely due to a larger number of H-bond interactions with Arg71 of the K1 pocket. Moreover, the 1,2,4-oxadiazolone derivative **4** showed the highest activity among all tested compounds, with an IC_{50} 2.5-fold lower than TXA and compound **1**.

The presence of linear primary amines instead of a piperidine ring clearly reduced the overall activity of the molecule. In the case of propylamine, compounds showed a 10-fold increase of IC_{50} over their piperidine counterparts, while molecules with either ethylamine or butylamine showed

no detectable activity. Therefore, the bulkiness and rigidity provided by the piperidine ring appears to be critical for the fibrinolytic activity of this family of compounds.

Substitution of the 1,2,3-triazole ring for a 1,2,4-triazole provided molecules (**9**, **10**) with no detectable activity. The results obtained with molecular dynamics suggest that 1,2,3-triazole provides anchoring to the binding site, mainly by interacting with Tyr72. In contraposition, 1,2,4-triazole is not able to provide such anchoring.

The interaction of the most active compound (**4**) and $GABA_A$ receptor was studied computationally. The results suggest a very low chance of this undesirable interaction, which is a known source of secondary effects for TXA.

The combined presence of Plg and tPA caused a measurable increase in permeability of the BBB *in vitro* model. Permeability under the hyperfibrinolytic conditions was approximately 2-fold higher than for the control. In addition, the hyperfibrinolytic conditions also had an effect on TJ protein expression. Both the total amount of claudin-5 and the localized expression of ZO-1 was reduced by approximately 50% in the presence of high Plg and tPA concentrations.

The most active compounds of the newly discovered family, **1** and **4**, showed a protective effect on the BBB hyperfibrinolytic model. The results do not allow, however, to conclude that their performance in this regard is significantly better than TXA. Despite this, the work presented in this chapter confirms the hypothesis that an increased level of activated Plm causes increased BBB permeability. It also indicates that such hyperfibrinolytic conditions have a direct negative impact on TJ expression, both globally and locally at the junction areas.

Finally, the results presented in this thesis open the door to develop future drugs based on these 1,2,3-triazole derivatives for two purposes: as a novel antifibrinolytic agent to substitute TXA, and as a potential BBB protective agent during TBI.

7. References

1. Gale, A. J. Continuing Education Course #2: Current Understanding of Hemostasis. *Toxicol Pathol* **39**, 273–280 (2011).

2. Broos, K., Feys, H. B., de Meyer, S. F., Vanhoorelbeke, K. & Deckmyn, H. Platelets at work in primary hemostasis. *Blood Rev* **25**, 155–167 (2011).

3. Palta, S., Saroa, R. & Palta, A. Overview of the coagulation system. *Indian J Anaesth* **58**, 515–523 (2014).

4. Coagulation, clotting mechanisms. https://jackwestin.com/resources/mcat-content/circulatory-system/coagulation-clotting-mechanisms.

5. Johari, V. & Loke, C. Brief overview of the coagulation cascade. *Dis Mon* **58**, 421–423 (2012).

6. Smith, S. A., Travers, R. J. & Morrissey, J. H. How it all starts: Initiation of the clotting cascade. *Crit Rev Biochem Mol Biol* **50**, 326–336 (2015).

7. Grover, S. P. & Mackman, N. Intrinsic Pathway of Coagulation and Thrombosis. *Arterioscler Thromb Vasc Biol* **39**, 331–338 (2019).

8. de Witt, S. M., Verdoold, R., Cosemans, J. M. E. M. & Heemskerk, J. W. M. Insights into platelet-based control of coagulation. *Thromb Res* **133 Suppl**, S139-48 (2014).

9. Furie, B. Pathogenesis of thrombosis. *Hematology Am Soc Hematol Educ Program* 255–258 (2009) doi:10.1182/asheducation-2009.1.255.

10. Bagoly, Z., Koncz, Z., Hársfalvi, J. & Muszbek, L. Factor XIII, clot structure, thrombosis. *Thromb Res* **129**, 382–387 (2012).

11. The Revised Coagulation Cascade. https://www.learnhaem.com/courses/coagulation/lessons/normal-haemostasis/topic/the-revised-coagulation-cascade/.

12. Chapin, J. C. & Hajjar, K. A. Fibrinolysis and the control of blood coagulation. *Blood Rev* **29**, 17–24 (2015).

13. Hajjar, K. A. Molecular Basis of Fibrinolysis. in *Nathan and Oski's Hematology and Oncology of Infancy and Childhood* 984–998 (Saunders/Elsavier).

14. Bu, G., Warshawsky, I. & Schwartz, A. L. Cellular receptors for the plasminogen activators. *Blood* **83**, 3427–3436 (1994).

15. Wu, G. *et al.* Structural studies of plasmin inhibition. *Biochem Soc Trans* **47**, 541–557 (2019).

16. Schaller, J. & Gerber, S. S. The plasmin-antiplasmin system: structural and functional aspects. *Cell Mol Life Sci* **68**, 785–801 (2011).

17. Cederholm-Williams, S. A. Concentration of plasminogen and antiplasmin in plasma and serum. *J Clin Pathol* **34**, 979–981 (1981).

18. Al-Horani, R. A. & Desai, U. R. Recent advances on plasmin inhibitors for the treatment of fibrinolysis-related disorders. *Med Res Rev* **34**, 1168–1216 (2014).

19. Law, R. H. P. *et al.* The X-ray crystal structure of full-length human plasminogen. *Cell Rep* **1**, 185—190 (2012).

20. Xue, Y., Bodin, C. & Olsson, K. Crystal structure of the native plasminogen reveals an activation-resistant compact conformation. *Journal of Thrombosis and Haemostasis* **10**, 1385–1396 (2012).

21. Steinmetzer, T., Pilgram, O., Wenzel, B. M. & Wiedemeyer, S. J. A. Fibrinolysis Inhibitors: Potential Drugs for the Treatment and Prevention of Bleeding. *Journal of Medicinal Chemistry* vol. 63 1445–1472 (2020).

22. Swedberg, J. E. & Harris, J. M. Natural and engineered plasmin inhibitors: applications and design strategies. *Chembiochem* **13**, 336–348 (2012).

23. Stubbs, M. T., Renatus, M. & Bode, W. An active zymogen: unravelling the mystery of tissue-type plasminogen activator. *Biol Chem* **379**, 95–103 (1998).

24. Tate, K. M. *et al.* Functional role of proteolytic cleavage at arginine-275 of human tissue plasminogen activator as assessed by site-directed mutagenesis. *Biochemistry* **26**, 338–343 (1987).

25. van Zonneveld, A. J., Veerman, H. & Pannekoek, H. On the interaction of the finger and the kringle-2 domain of tissue-type plasminogen activator with fibrin. Inhibition of kringle-2 binding to fibrin by epsilon-amino caproic acid. *J Biol Chem* **261**, 14214–14218 (1986).

26. Hoylaerts, M., Rijken, D. C., Lijnen, H. R. & Collen, D. Kinetics of the activation of plasminogen by human tissue plasminogen activator. Role of fibrin. *J Biol Chem* **257**, 2912–2919 (1982).

27. Cesarman-Maus, G. & Hajjar, K. A. Molecular mechanisms of fibrinolysis. *Br J Haematol* **129**, 307–321 (2005).

28. Tissue Plasminogen Activator (tPA). https://diapharma.com/tissue-plasminogen-activator-tpa/.

29. Travis, J. & Salvesen, G. S. Human plasma proteinase inhibitors. *Annu Rev Biochem* **52**, 655–709 (1983).

30. Schneider, M. & Nesheim, M. A study of the protection of plasmin from antiplasmin inhibition within an intact fibrin clot during the course of clot lysis. *J Biol Chem* **279**, 13333–13339 (2004).

31. Sprengers, E. D. & Kluft, C. Plasminogen activator inhibitors. *Blood* **69**, 381–387 (1987).

32. Coolman, M. *et al.* Concentrations of plasminogen activators and their inhibitors in blood preconceptionally, during and after pregnancy. *Eur J Obstet Gynecol Reprod Biol* **128**, 22–28 (2006).

33. Coolman, M. *et al.* Angiogenic and fibrinolytic factors in blood during the first half of pregnancy and adverse pregnancy outcomes. *Obstetrics and gynecology* **119**, 1190–1200 (2012).

34. Broze, G. J. J. & Higuchi, D. A. Coagulation-dependent inhibition of fibrinolysis: role of carboxypeptidase-U and the premature lysis of clots from hemophilic plasma. *Blood* **88**, 3815–3823 (1996).

35. Chen, Z. *et al.* Intravenous Hemostats: Foundation, Targeting, and Controlled-Release. *Bioconjug Chem* (2022) doi:10.1021/acs.bioconjchem.2c00492.

36. U.S. Food and Drug Administration. Lysteda - Prescribing Information. http://www.ferringusa.com/wp-content/uploads/2016/07/LystedaPI_3.2016.pdf (2016).

37. Forbes, C. D. *et al.* Tranexamic Acid in Control of Haemorrhage after Dental Extraction in Haemophilia and Christmas Disease. *Br Med J* **2**, 311–313 (1972).

38. Hibbs, S. P., Roberts, I., Shakur-Still, H. & Hunt, B. J. Post-partum haemorrhage and tranexamic acid: a global issue. *British Journal of Haematology* vol. 180 799–807 Preprint at https://doi.org/10.1111/bjh.15073 (2018).

39. Benoni, G., Lethagen, S. & Fredin, H. The effect of tranexamic acid on local and plasma fibrinolysis during total knee arthroplasty. *Thromb Res* **85**, 195–206 (1997).

40. Veien, M., Sørensen, J. v., Madsen, F. & Juelsgaard, P. Tranexamic acid given intraoperatively reduces blood loss after total knee replacement: A randomized, controlled study. *Acta Anaesthesiol Scand* **46**, 1206–1211 (2002).

41. Edmunds, L. H. J. Managing fibrinolysis without aprotinin. *Ann Thorac Surg* **89**, 324–331 (2010).

42. Bayissa, B. B. & Alemu, S. Pattern of trauma admission and outcome among patients presented to Jimma University Specialized Hospital, south-western Ethiopia. *Trauma Surg Acute Care Open* **6**, e000609 (2021).

43. Hunt, B. J. Bleeding and coagulopathies in critical care. *The New England journal of medicine* vol. 370 2153 Preprint at https://doi.org/10.1056/NEJMc1403768 (2014).

44. Davis, J. S. *et al.* An analysis of prehospital deaths: Who can we save? in *Journal of Trauma and Acute Care Surgery* vol. 77 213–218 (2014).

45. Sauaia, A. *et al.* Early predictors of postinjury multiple organ failure. *Arch Surg* **129**, 39–45 (1994).

46. MacLeod, J. B. A., Lynn, M., McKenney, M. G., Cohn, S. M. & Murtha, M. Early coagulopathy predicts mortality in trauma. *J Trauma* **55**, 39–44 (2003).

47. Maegele, M. *et al.* Early coagulopathy in multiple injury: an analysis from the German Trauma Registry on 8724 patients. *Injury* **38**, 298–304 (2007).

48. Hrafnkelsdóttir, T., Erlinge, D. & Jern, S. Extracellular nucleotides ATP and UTP induce a marked acute release of tissue-type plasminogen activator in vivo in man. *Thromb Haemost* **85**, 875–881 (2001).

49. Rezaie, A. R. Vitronectin functions as a cofactor for rapid inhibition of activated protein C by plasminogen activator inhibitor-1. Implications for the mechanism of profibrinolytic action of activated protein C. *J Biol Chem* **276**, 15567–15570 (2001).

50. Brohi, K. *et al.* Acute traumatic coagulopathy: initiated by hypoperfusion: modulated through the protein C pathway? *Ann Surg* **245**, 812–818 (2007).

51. Hess, J. R. *et al.* The coagulopathy of trauma: a review of mechanisms. *J Trauma* **65**, 748–754 (2008).

52. Olldashi, F. *et al.* Effects of tranexamic acid on death, vascular occlusive events, and blood transfusion in trauma patients with significant haemorrhage (CRASH-2): A randomised, placebo-controlled trial. *The Lancet* **376**, 23–32 (2010).

53. Olldashi, F. *et al.* The importance of early treatment with tranexamic acid in bleeding trauma patients: An exploratory analysis of the CRASH-2 randomised controlled trial. *The Lancet* **377**, (2011).

54. Rossaint, R. *et al.* The European guideline on management of major bleeding and coagulopathy following trauma: Fourth edition. *Crit Care* **20**, (2016).

55. Begley, D. J. & Brightman, M. W. Structural and functional aspects of the blood-brain barrier. *Prog Drug Res* **61**, 39–78 (2003).

56. Abbott, N. J., Patabendige, A. A. K., Dolman, D. E. M., Yusof, S. R. & Begley, D. J. Structure and function of the blood-brain barrier. *Neurobiol Dis* **37**, 13–25 (2010).

57. Gawdi, R., Shumway, K. R. & Emmady, P. D. Physiology, Blood Brain Barrier. in (2022).

58. Furuse, M. *et al.* Occludin: A novel integral membrane protein localizing at tight junctions. *Journal of Cell Biology* **123**, 1777–1788 (1993).

59. Furuse, M., Fujita, K., Hiragi, T., Fujomoto, K. & Tsukita, S. Claudin-1 and -2: novel integral membrane proteins localizing at tight junctions with no sequence homology to occludin. *J Cell Biol* **141**, 1539–1550 (1998).

60. Stevenson, B. R., Siliciano, J. D., Mooseker, M. S. & Goodenough, D. A. Identification of Z0-1: a high molecular weight polypeptide associated with tight junction (zonula occludens) in a. *J. Cell Biol* **103**, 755–766 (1986).

61. Abbott, N. J. The Bipolar Astrocyte: Polarized Features of Astrocytic Glia Underlying Physiology, with Particular Reference to the Blood-Brain Barrier. in *Blood-Brain Barriers* 189–208 (John Wiley & Sons, Ltd, 2006). doi:https://doi.org/10.1002/9783527611225.ch8.

62. Bicker, J., Alves, G., Fortuna, A. & Falcão, A. Blood-brain barrier models and their relevance for a successful development of CNS drug delivery systems: a review. *Eur J Pharm Biopharm* **87**, 409–432 (2014).

63. Wolff, A., Antfolk, M., Brodin, B. & Tenje, M. In Vitro Blood-Brain Barrier Models-An Overview of Established Models and New Microfluidic Approaches. *J Pharm Sci* **104**, 2727–2746 (2015).

64. Schober, P., Loer, S. A. & Schwarte, L. A. Antifibrinolytics in the treatment of traumatic brain injury. *Curr Opin Anaesthesiol* **35**, 583–592 (2022).

65. Harhangi, B. S., Kompanje, E. J. O., Leebeek, F. W. G. & Maas, A. I. R. Coagulation disorders after traumatic brain injury. *Acta Neurochir (Wien)* **150**, 165–75; discussion 175 (2008).

66. Wada, T. *et al.* Disseminated intravascular coagulation with increased fibrinolysis during the early phase of isolated traumatic brain injury. *Crit Care* **21**, 219 (2017).

67. Shlosberg, D., Benifla, M., Kaufer, D. & Friedman, A. Blood-brain barrier breakdown as a therapeutic target in traumatic brain injury. *Nat Rev Neurol* **6**, 393–403 (2010).

68. Kwaan, H. C. The Central Role of Fibrinolytic Response in Trauma-Induced Coagulopathy: A Hematologist's Perspective. *Semin Thromb Hemost* **46**, 116–124 (2020).

69. Annegers, J. F., Hauser, W. A., Coan, S. P. & Rocca, W. A. A population-based study of seizures after traumatic brain injuries. *N Engl J Med* **338**, 20–24 (1998).

70. Ruttan, L., Martin, K., Liu, A., Colella, B. & Green, R. E. Long-term cognitive outcome in moderate to severe traumatic brain injury: a meta-analysis examining timed and untimed tests at 1 and 4.5 or more years after injury. *Arch Phys Med Rehabil* **89**, S69-76 (2008).

71. Zlokovic, B. v. The blood-brain barrier in health and chronic neurodegenerative disorders. *Neuron* **57**, 178–201 (2008).

72. Herman, S. T. Epilepsy after brain insult: targeting epileptogenesis. *Neurology* **59**, S21-6 (2002).

73. Laroche, M., Kutcher, M. E., Huang, M. C., Cohen, M. J. & Manley, G. T. Coagulopathy after traumatic brain injury. *Neurosurgery* **70**, 1334–1345 (2012).

74. Nicole, O. *et al.* The proteolytic activity of tissue-plasminogen activator enhances NMDA receptor-mediated signaling. *Nat Med* **7**, 59–64 (2001).

75. Liberatore, G. T., Samson, A., Bladin, C., Schleuning, W.-D. & Medcalf, R. L. Vampire bat salivary plasminogen activator (desmoteplase): a unique fibrinolytic enzyme that does not promote neurodegeneration. *Stroke* **34**, 537–543 (2003).

76. Yepes, M. *et al.* Tissue-type plasminogen activator induces opening of the blood-brain barrier via the LDL receptor-related protein. *J Clin Invest* **112**, 1533–1540 (2003).

77. Benchenane, K. *et al.* Tissue-type plasminogen activator crosses the intact blood-brain barrier by low-density lipoprotein receptor-related protein-mediated transcytosis. *Circulation* **111**, 2241–2249 (2005).

78. Su, E. J. *et al.* Activation of PDGF-CC by tissue plasminogen activator impairs blood-brain barrier integrity during ischemic stroke. *Nat Med* **14**, 731–737 (2008).

79. Yao, Y. & Tsirka, S. E. Truncation of monocyte chemoattractant protein 1 by plasmin promotes blood-brain barrier disruption. *J Cell Sci* **124**, 1486–1495 (2011).

80. Suzuki, Y., Nagai, N., Umemura, K., Collen, D. & Lijnen, H. R. Stromelysin-1 (MMP-3) is critical for intracranial bleeding after t-PA treatment of stroke in mice. *J Thromb Haemost* **5**, 1732–1739 (2007).

81. Marcos-Contreras, O. A. *et al.* Hyperfibrinolysis increases blood-brain barrier permeability by a plasmin- and bradykinin-dependent mechanism. *Blood* **128**, 2423–2434 (2016).

82. Watts, G. Utako Okamoto. *Lancet* **387**, 2286 (2016).

83. Weeks, A. The prevention and treatment of postpartum haemorrhage: what do we know, and where do we go to next? *BJOG* **122**, 202–210 (2015).

84. Okamoto, S. Plasmin and antiplasmin. *Keio j med* **8**, 211–217 (1959).

85. Abe, T., Sato, A. Reaction mechanism between ε-aminocaproic acid and plasmin, tissue activator and trypsin. *Keio j med* **8**, 219–224 (1959).

86. Okamoto, S., Okamoto, U. Amino-methyl-cyclohexane-carboxylic acid: amcha. *Keio j med* **11**, 105–115 (1962).

87. Markwardt, F., Landmann, H., Klöcking, H. P. *Fibrinolytics and antifibrinolytics*. (veb gustav fischer verlag, 1972).

88. Okamoto, S., Sato, S., Takada, Y., Okamoto, U. An active stereo-isomer (trans-form) of amcha and its antifibrinolytic (antiplasminic) action in vitro and in vivo. *Keio j med* **13**, 177–185 (1964).

89. Kavita, J., Onkar, S. *Antifibrinolytic drug market*. https://www.alliedmarketresearch.com/antifibrinolytic-drugs-market (2019).

90. Markwardt, F., Richter, M. [on the anti-fibrinolytic effect of derivatives of p-aminomethylbenzoid acid (pamba)]. *Acta biol med ger* **13**, 719–724 (1964).

91. Markwardt, F., Haustein, K. O., Kloecking, H. P. [the pharmacologic properties of a new antifibrinolytic, para-aminomethylbenzoic acid]. *Arch Int Pharmacodyn Ther* **152**, 223–233 (1964).

92. Westlund, L. E., Lundén, R. & Wallén, P. Effect of EACA, PAMBA, AMCA and AMBOCA on fibrinolysis induced by streptokinase, urokinase and tissue activator. *Haemostasis* **11**, 235–241 (1982).

93. Baumgarten, W. *et al.* 4-aminomethylbicyclo[2.2.2]-octane-1-carboxylic acid a new potent antifibrinolytic agent. Its evaluation by in vitro assay procedures. *Thromb Diath Haemorrh* **22**, 263–272 (1969).

94. Mathews, I. I., Vanderhoff-Hanaver, P., Castellino, F. J. & Tulinsky, A. Crystal structures of the recombinant kringle 1 domain of human plasminogen in complexes with the ligands ε-aminocaproic acid and trans-4-(aminomethyl)cyclohexane-1-carboxylic acid. *Biochemistry* **35**, 2567–2576 (1996).

95. Markus, G., DePasquale, J. L. & Wissler, F. C. Quantitative determination of the binding of epsilon-aminocaproic acid to native plasminogen. *J Biol Chem* **253**, 727–732 (1978).

96. Markus, G., Priore, R. L. & Wissler, F. C. The binding of tranexamic acid to native (Glu) and modified (Lys) human plasminogen and its effect on conformation. *Journal of Biological Chemistry* **254**, 1211–1216 (1979).

97. Marti, D. N. *et al.* Ligand preferences of kringle 2 and homologous domains of human plasminogen: canvassing weak, intermediate, and high-affinity binding sites by 1H-NMR. *Biochemistry* **36**, 11591–11604 (1997).

98. Wu, T. P., Padmanabhan, K., Tulinsky, A. & Mulichak, A. M. The refined structure of the epsilon-aminocaproic acid complex of human plasminogen kringle 4. *Biochemistry* **30**, 10589–10594 (1991).

99. Nilsson, I. M. Clinical pharmacology of aminocaproic and tranexamic acids. *J Clin Pathol Suppl (R Coll Pathol)* **14**, 41–47 (1980).

100. Royston, D. Blood-sparing drugs: aprotinin, tranexamic acid, and epsilon-aminocaproic acid. *Int Anesthesiol Clin* **33**, 155–179 (1995).

101. Phillips, P. Antifibrinolytics (lysine analogues) for the prevention of bleeding in people with haematological disorders. *Nurs Stand* **32**, 41–43 (2017).

102. Ker, K. & Roberts, I. Tranexamic acid for surgical bleeding. *BMJ (Clinical research ed.)* vol. 349 g4934 Preprint at https://doi.org/10.1136/bmj.g4934 (2014).

103. Breau, R. H. *et al.* The effects of lysine analogs during pelvic surgery: a systematic review and meta-analysis. *Transfus Med Rev* **28**, 145–155 (2014).

104. Sander, M. *et al.* Mortality associated with administration of high-dose tranexamic acid and aprotinin in primary open-heart procedures: a retrospective analysis. *Crit Care* **14**, R148 (2010).

105. Murkin, J. M. *et al.* High-dose tranexamic Acid is associated with nonischemic clinical seizures in cardiac surgical patients. *Anesth Analg* **110**, 350–353 (2010).

106. Furtmüller, R. *et al.* Tranexamic acid, a widely used antifibrinolytic agent, causes convulsions by a gamma-aminobutyric acid(A) receptor antagonistic effect. *J Pharmacol Exp Ther* **301**, 168–173 (2002).

107. Nilsson, I. M., Andersson, L. & Björkman, S. E. Epsilon-aminocaproic acid (E-ACA) as a therapeutic agent based on 5 year's clinical experience. *Acta Medica Scandinavica, Supplement* **448**, 1–46 (1966).

108. Andersson, L. *et al.* Experimental and Clinical Studies on AMCA, the Antifibrinolytically Active Isomer of p-Aminomethyl Cyclohexane Carboxylic Acid. *Scand J Haematol* **2**, 230–247 (1965).

109. Tranexamic acid side effects. https://www.drugs.com/sfx/tranexamic-acid-side-effects.html.

110. Tranexamic Acid 100mg/ml Solution for Injection. *Advanz Pharma* 1 https://www.medicines.org.uk/emc/product/1220/smpc (2018).

111. Boström, J., Grant, J. A., Fjellström, O., Thelin, A. & Gustafsson, D. Potent fibrinolysis inhibitor discovered by shape and electrostatic complementarity to the drug tranexamic acid. *J Med Chem* **56**, 3273–3280 (2013).

112. Jansen, M. *et al.* Synthesis of GABAA receptor agonists and evaluation of their α-subunit selectivity and orientation in the GABA binding site. *J Med Chem* **51**, 4430–4448 (2008).

113. Cheng, L. *et al.* Discovery of the fibrinolysis inhibitor AZD6564, acting via interference of a protein-protein interaction. *ACS Med Chem Lett* **5**, 538–543 (2014).

114. Ellermann, M.; Valot, G.; Cancho Grande, Y.; Hassfeld, J.; Kinzel, T.; Koebberling, J.; Beyer, K.; Roehrig, S.; Sperzel, M.; Stampfuss, J.; Meyer, I.; Koellnberger, M.; Burkhardt, N.; Schlemmer, K.-H.; Stegmann, C.; Schuhmacher, J.; Werner, M. Indazolopyrimidinones as fibrinolysis inhibitors. (2016).

115. Ellermann, M.; Valot, G.; Cancho Grande, Y.; Hassfeld, J.; Kinzel, T.; Koebberling, J.; Beyer, K.; Roehrig, S.; Sperzel, M.; Stampfuss, J.; Meyer, I.; Koellnberger, M.; Burkhardt, N.; Schlemmer, K.-H.; Stegmann, C.; Schuhmacher, J.; Werner, M.; Heiermann, W. J. Piperidinylpyrazolopyrimidinones as Plasminogen Inhibitors and Their Preparation. (2016).

116. Okada, Y. *et al.* Development of plasmin and plasma kallikrein selective inhibitors and their effect on M1 (melanoma) and HT29 cell lines. *Bioorg Med Chem Lett* **10**, 2217–2221 (2000).

117. Hidaka, K., Gohda, K., Teno, N., Wanaka, K. & Tsuda, Y. Active site-directed plasmin inhibitors: Extension on the P2 residue. *Bioorg Med Chem* **24**, 545–553 (2016).

118. Law, R. H. P. *et al.* X-ray crystal structure of plasmin with tranexamic acid-derived active site inhibitors. *Blood Adv* **1**, 766–771 (2017).

119. Sanders, T. C. & Seto, C. T. 4-Heterocyclohexanone-based inhibitors of the serine protease plasmin. *J Med Chem* **42**, 2969–2976 (1999).

120. Teno, N., Gohda, K., Wanaka, K., Sueda, T. & Tsuda, Y. Identification of novel plasmin inhibitors possessing nitrile moiety as warhead. *Bioorg Med Chem Lett* **21**, 6305–6309 (2011).

121. Saupe, S. M. & Steinmetzer, T. A new strategy for the development of highly potent and selective plasmin inhibitors. *J Med Chem* **55**, 1171–1180 (2012).

122. Swedberg, J. E. & Harris, J. M. Plasmin substrate binding site cooperativity guides the design of potent peptide aldehyde inhibitors. *Biochemistry* **50**, 8454–8462 (2011).

123. Zakharova, E., Horvath, M. P. & Goldenberg, D. P. Structure of a serine protease poised to resynthesize a peptide bond. *Proc Natl Acad Sci U S A* **106**, 11034–11039 (2009).

124. Ascenzi, P. *et al.* The bovine basic pancreatic trypsin inhibitor (Kunitz inhibitor): a milestone protein. *Curr Protein Pept Sci* **4**, 231–251 (2003).

125. Fritz, H. & Wunderer, G. Biochemistry and applications of aprotinin, the kallikrein inhibitor from bovine organs. *Arzneimittelforschung* **33**, 479–494 (1983).

126. Levy, J. H. Pharmacologic methods to reduce perioperative bleeding. *Transfusion (Paris)* **48**, 31S-38S (2008).

127. Trudell, J. & McMurdy, N. Current antifibrinolytic therapy for coronary artery revascularization. *AANA J* **76**, 121–124 (2008).

128. Dhir, A. Antifibrinolytics in cardiac surgery. *Ann Card Anaesth* **16**, 117–125 (2013).

129. Ortmann, E., Besser, M. W. & Klein, A. A. Antifibrinolytic agents in current anaesthetic practice. *Br J Anaesth* **111**, 549–563 (2013).

130. Schneeweiss, S., Seeger, J. D., Landon, J. & Walker, A. M. Aprotinin during coronary-artery bypass grafting and risk of death. *N Engl J Med* **358**, 771–783 (2008).

131. Mangano, D. T., Tudor, I. C. & Dietzel, C. The risk associated with aprotinin in cardiac surgery. *N Engl J Med* **354**, 353–365 (2006).

132. Fergusson, D. A. *et al.* A comparison of aprotinin and lysine analogues in high-risk cardiac surgery. *N Engl J Med* **358**, 2319–2331 (2008).

133. Filippovich, I. *et al.* A family of textilinin genes, two of which encode proteins with antihaemorrhagic properties. *Br J Haematol* **119**, 376–384 (2002).

134. Masci, P. P. *et al.* Textilinins from Pseudonaja textilis textilis. Characterization of two plasmin inhibitors that reduce bleeding in an animal model. *Blood Coagul Fibrinolysis* **11**, 385–393 (2000).

135. Flight, S. *et al.* Comparison of textilinin-1 with aprotinin as serine protease inhibitors and as antifibrinolytic agents. *Pathophysiol Haemost Thromb* **34**, 188–193 (2005).

136. Sangshetti, J. N., Nagawade, R. R. & Shinde, D. B. Synthesis of novel 3-(1-(1-substituted piperidin-4-yl)-1H-1,2,3-triazol-4-yl)-1,2,4-oxadiazol-5(4H)-one as antifungal agents. *Bioorg Med Chem Lett* **19**, 3564–3567 (2009).

137. Mølgaard, L., Ponting, C. P. & Christensen, U. Glycosylation at Asn-289 facilitates the ligand-induced conformational changes of human Glu-plasminogen. *FEBS Lett* **405**, 363–368 (1997).

138. Sasaoka, M., Wada, Y. & Hasumi, K. Stachybotrydial selectively enhances fibrin binding and activation of Glu-plasminogen. *J Antibiot (Tokyo)* **60**, 674–681 (2007).

139. Ohyama, S., Harada, T., Chikanishi, T., Miura, Y. & Hasumi, K. Nonlysine-analog plasminogen modulators promote autoproteolytic generation of plasmin(ogen) fragments with angiostatin-like activity. *Eur J Biochem* **271**, 809–820 (2004).

140. Worrell, B. T., Malik, J. A. & Fokin, V. v. Direct evidence of a dinuclear copper intermediate in Cu(I)-catalyzed azide-alkyne cycloadditions. *Science* **340**, 457–460 (2013).

141. Niego, B., Freeman, R., Puschmann, T. B., Turnley, A. M. & Medcalf, R. L. t-PA-specific modulation of a human blood-brain barrier model involves plasmin-mediated activation of the Rho kinase pathway in astrocytes. *Blood* **119**, 4752–4761 (2012).

142. Wang, X. *et al.* Alteration of blood clot structures by interleukin-1 beta in association with bone defects healing. *Scientific Reports* **6**, 1–11 (2016).

143. Humphrey, W., Dalke, A. & Schulten, K. VMD: visual molecular dynamics. *J Mol Graph* **14**, 27-28,33-38 (1996).

144. Schüttelkopf, A. W. & van Aalten, D. M. F. PRODRG: a tool for high-throughput crystallography of protein-ligand complexes. *Acta Crystallogr D Biol Crystallogr* **60**, 1355–1363 (2004).

145. Varshney, A., Brooks, F. P. & Wright, W. v. Linearly Scalable Computation of Smooth Molecular Surfaces. *IEEE Comp. Graphics and Applications* **14**, 19–25 (1994).

8. Annexes

8.1. NMR spectra

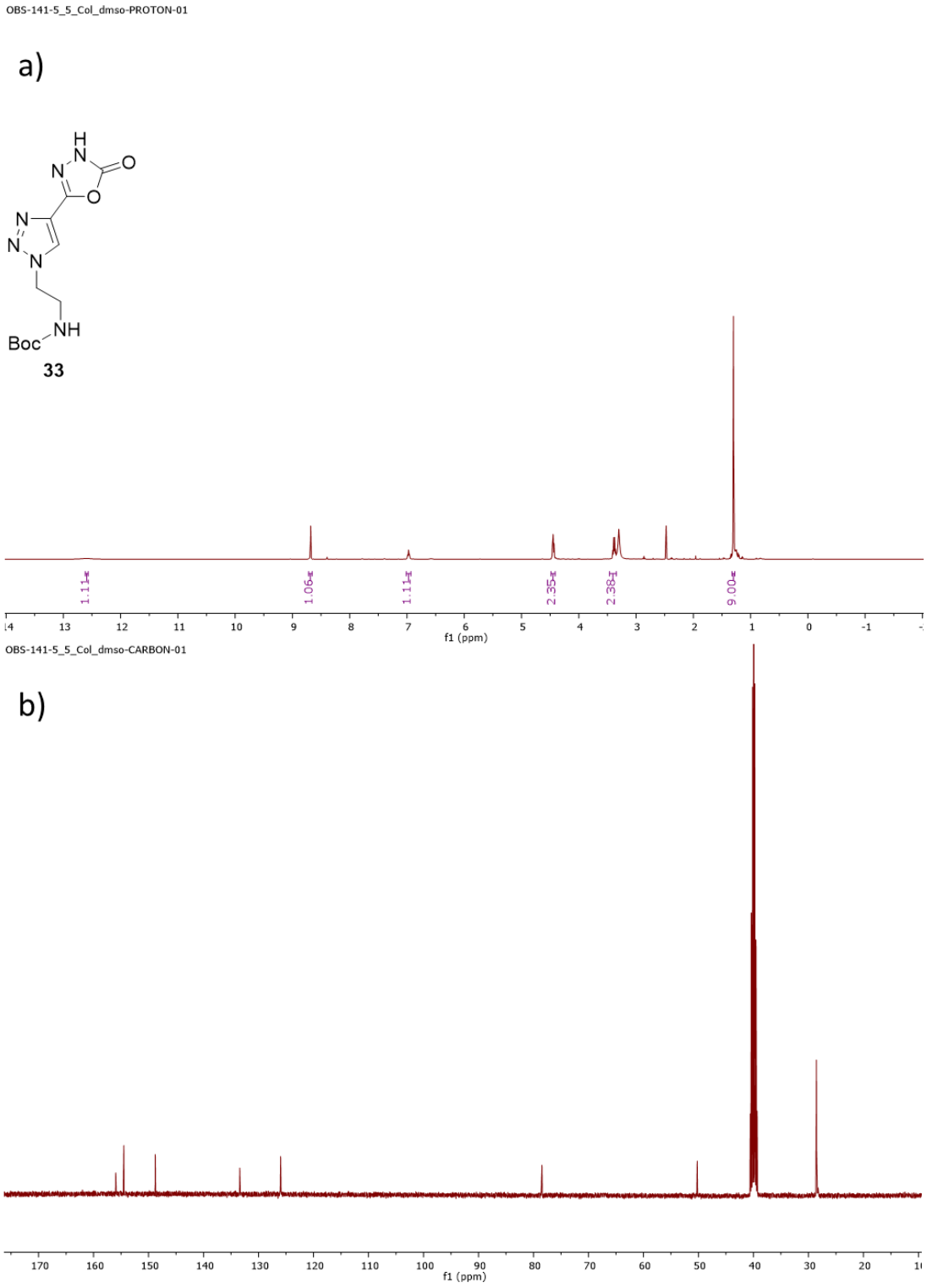

Figure S66. ^{1}H-NMR (a) and ^{13}C-NMR (b) spectra of **33** in *d*$_6$-DMSO.

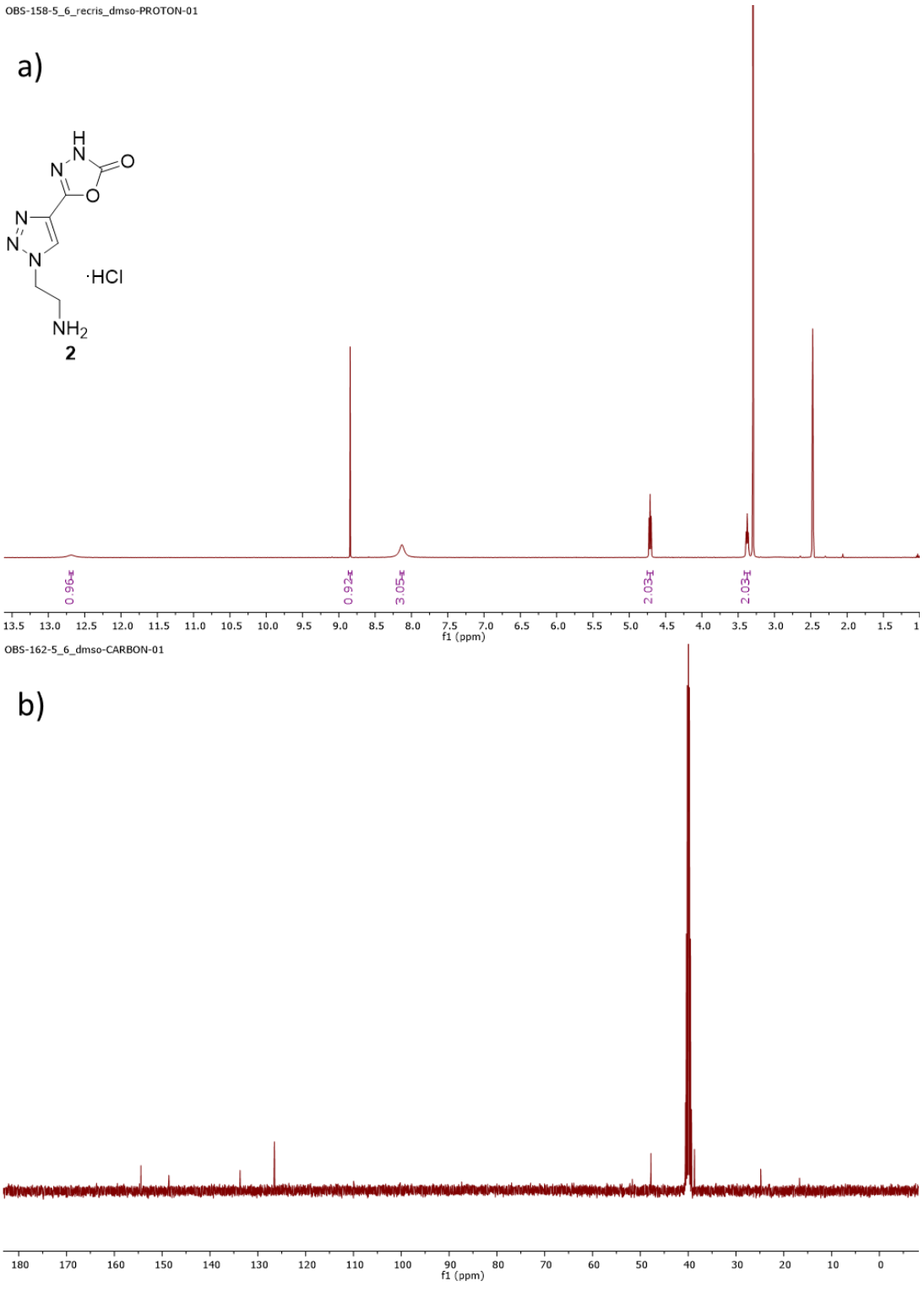

Figure S67. ^{1}H-NMR (a) and ^{13}C-NMR (b) spectra of **2** in d_6-DMSO.

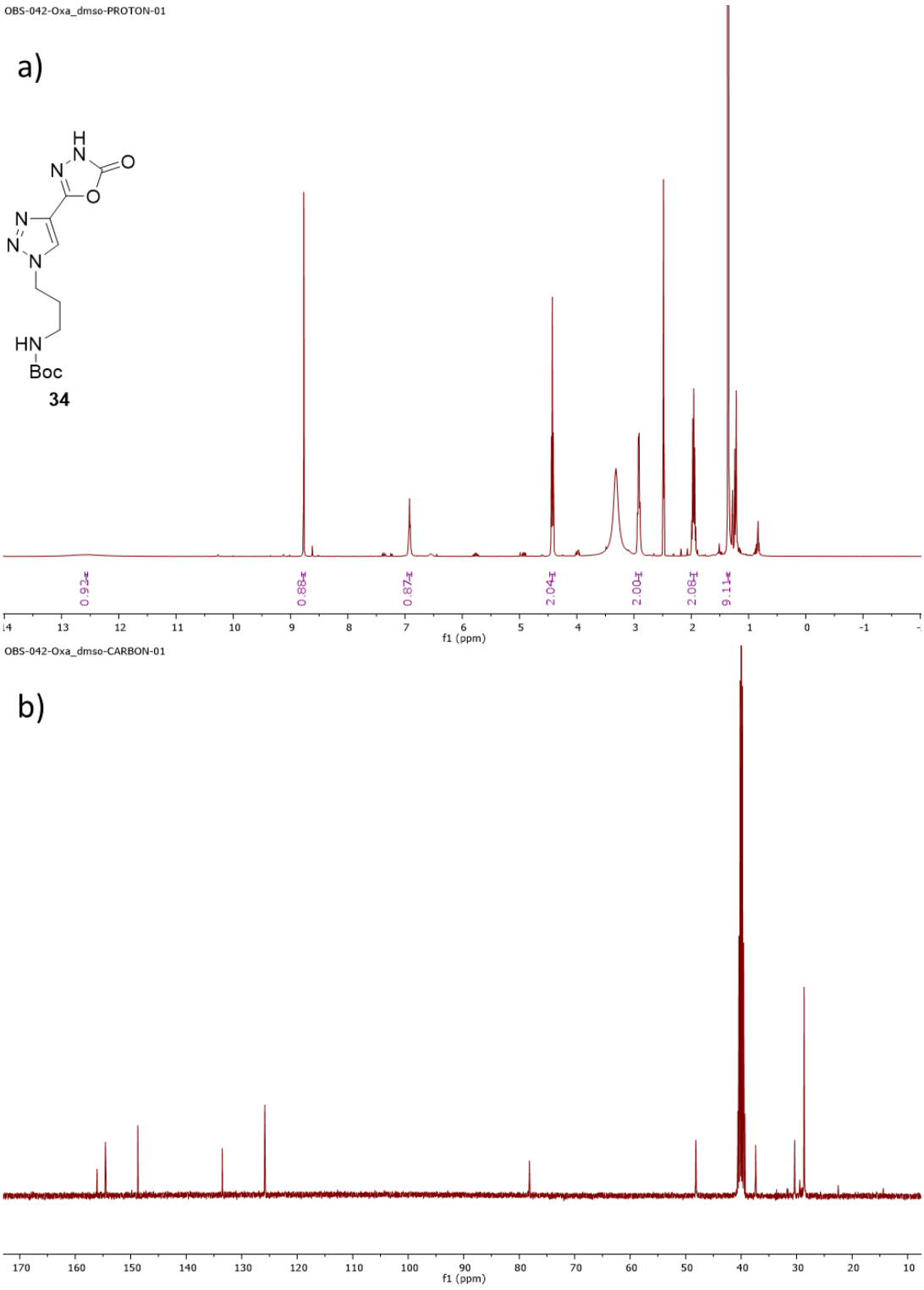

Figure S68. ^{1}H-NMR (a) and ^{13}C-NMR (b) spectra of **34** in d_6-DMSO.

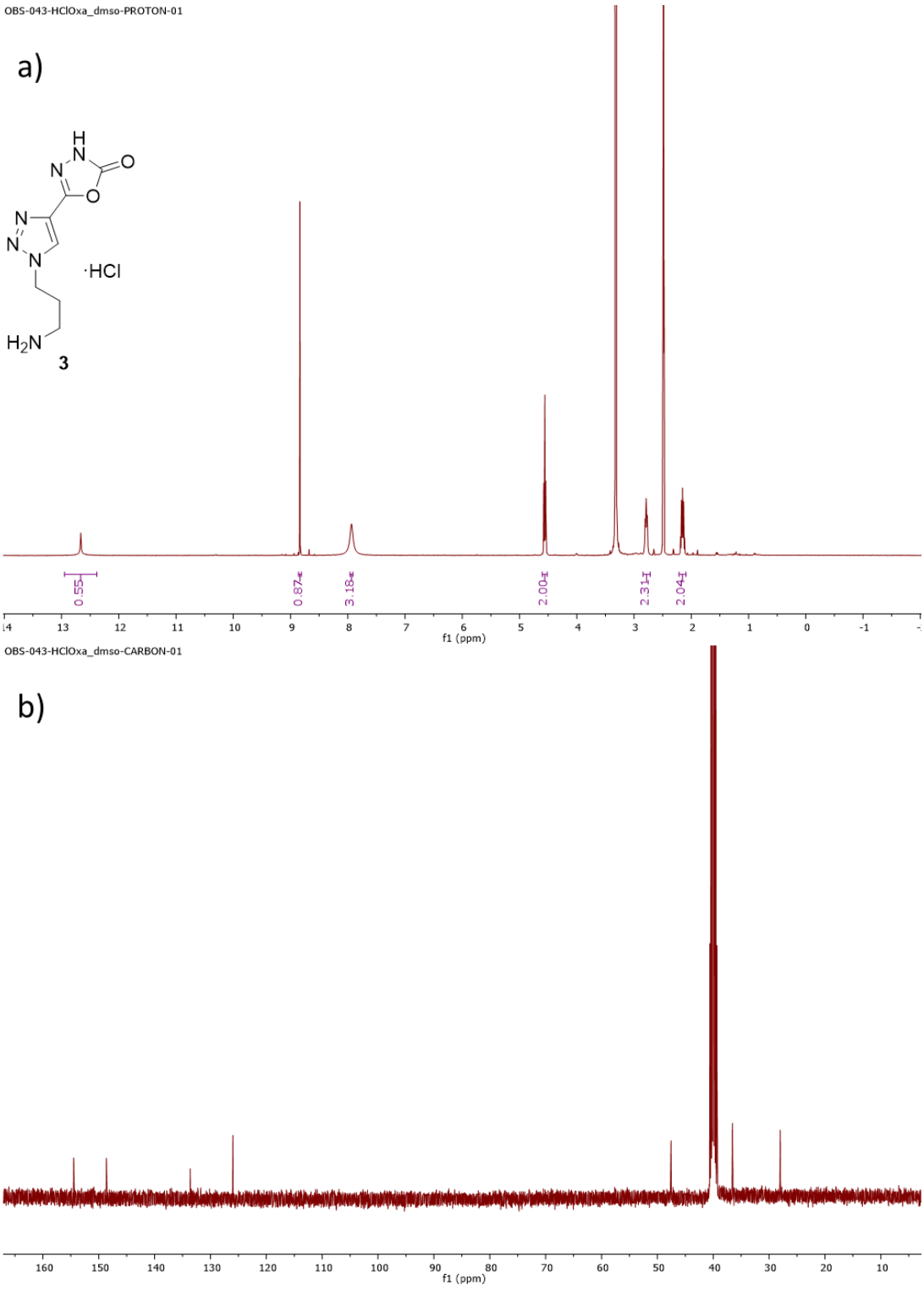

Figure S69. ^{1}H-NMR (a) and ^{13}C-NMR (b) spectra of **7** in d_6-DMSO.

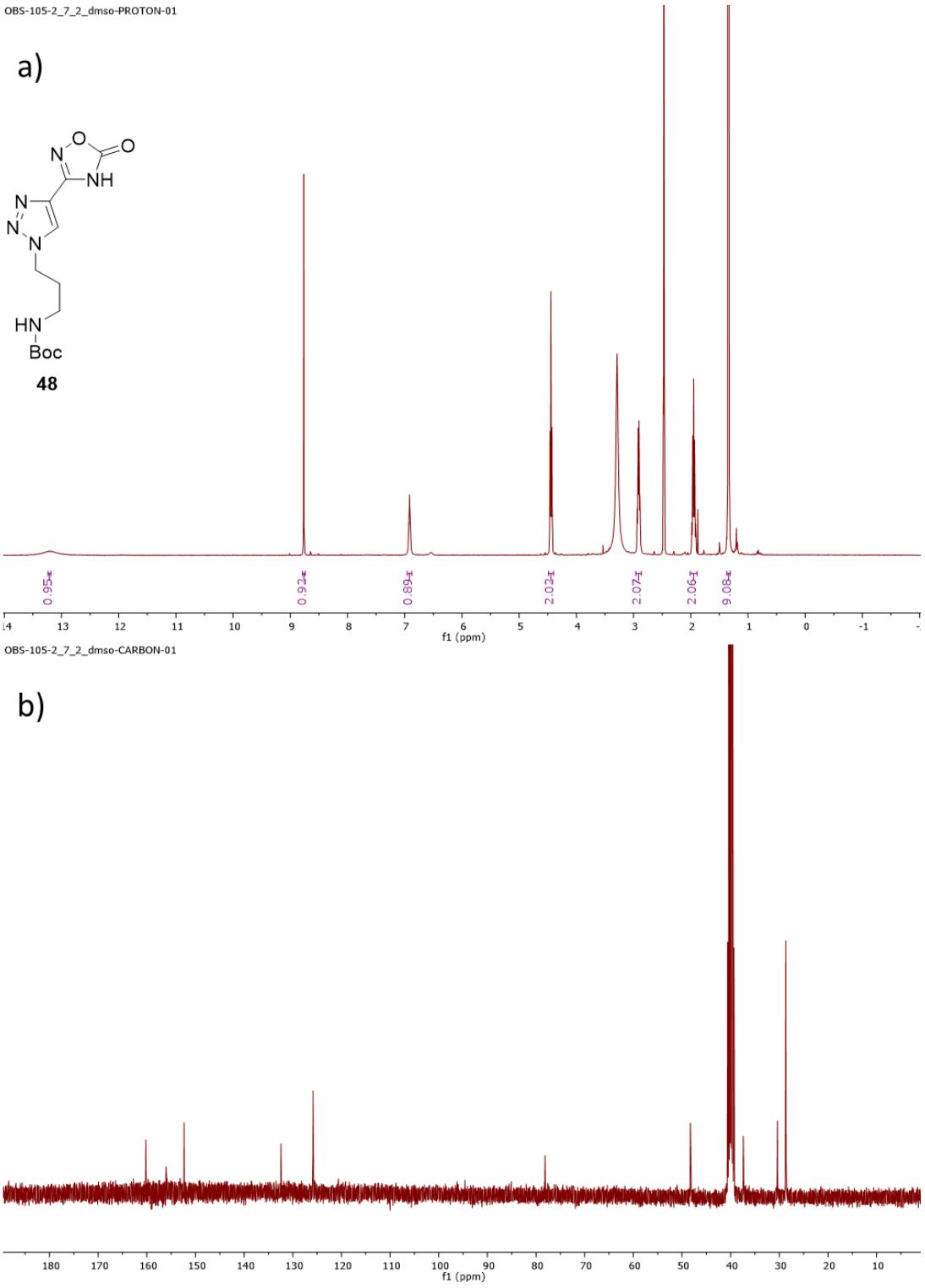

Figure S70. ^{1}H-NMR (a) and ^{13}C-NMR (b) spectra of **48** in d_6-DMSO.

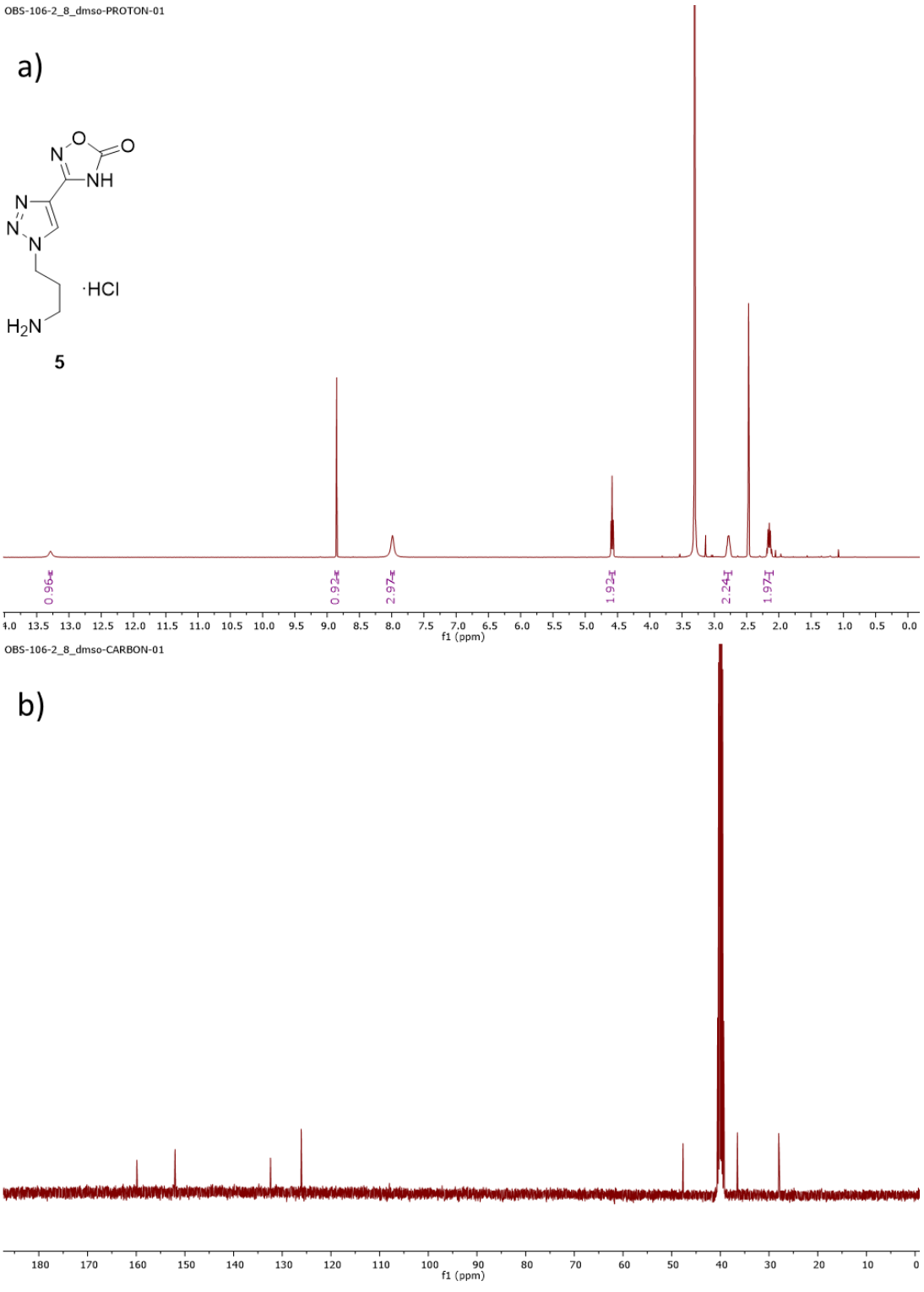

Figure S71. ^{1}H-NMR (a) and ^{13}C-NMR (b) spectra of **5** in d_6-DMSO.

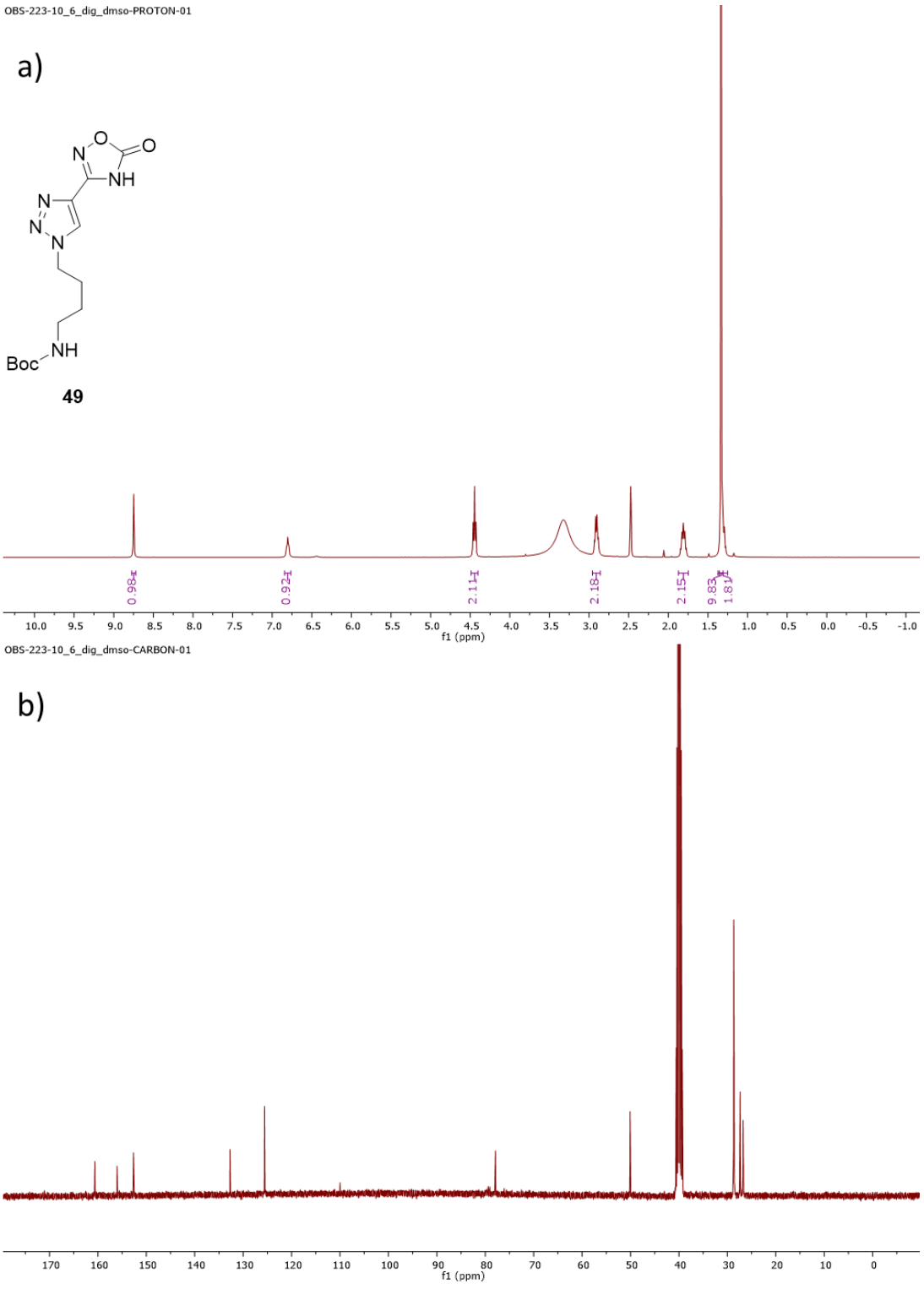

Figure S72. ^{1}H-NMR (a) and ^{13}C-NMR (b) spectra of **49** in d_6-DMSO.

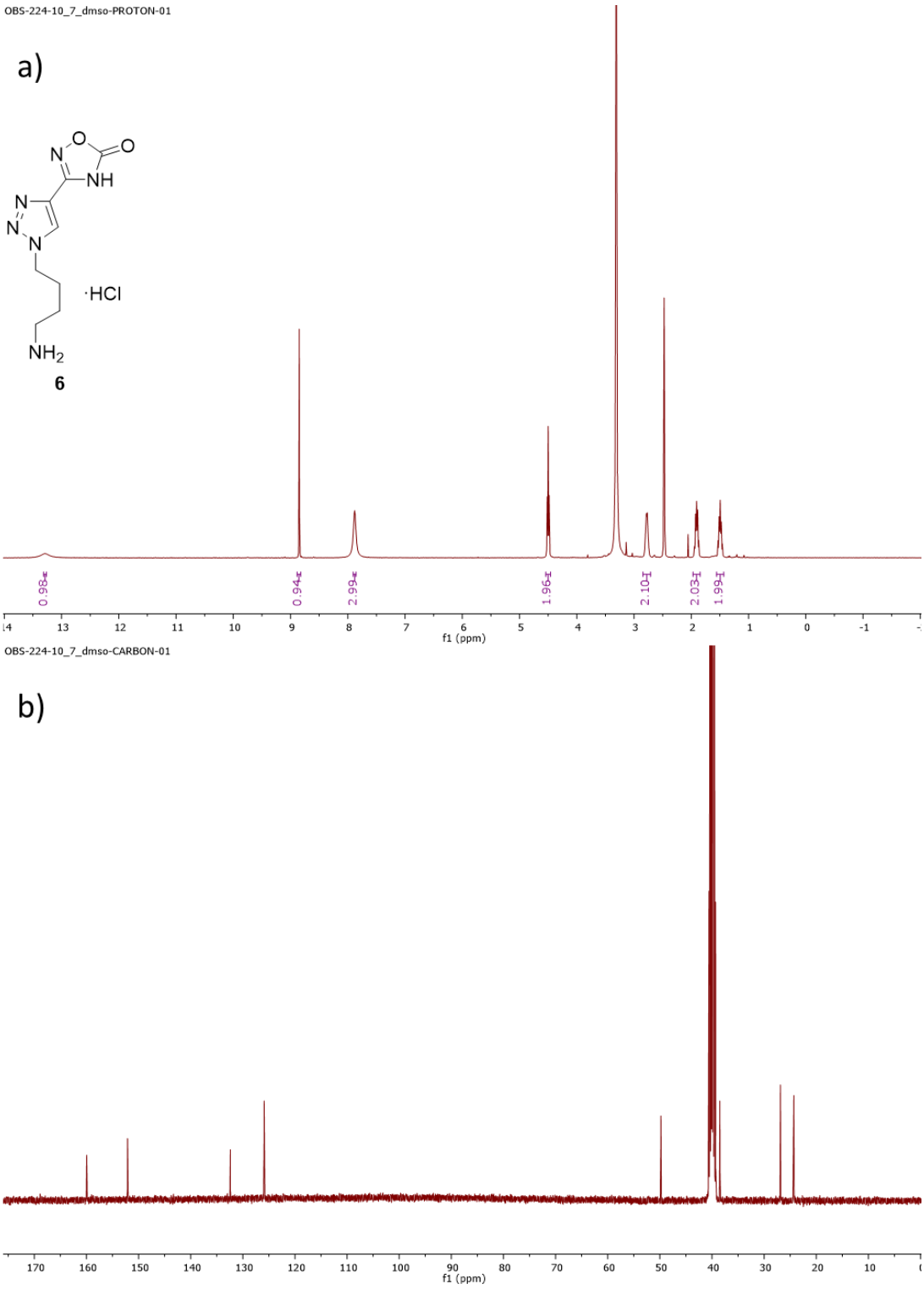

Figure S73. ^{1}H-NMR (a) and ^{13}C-NMR (b) spectra of **6** in d_6-DMSO.

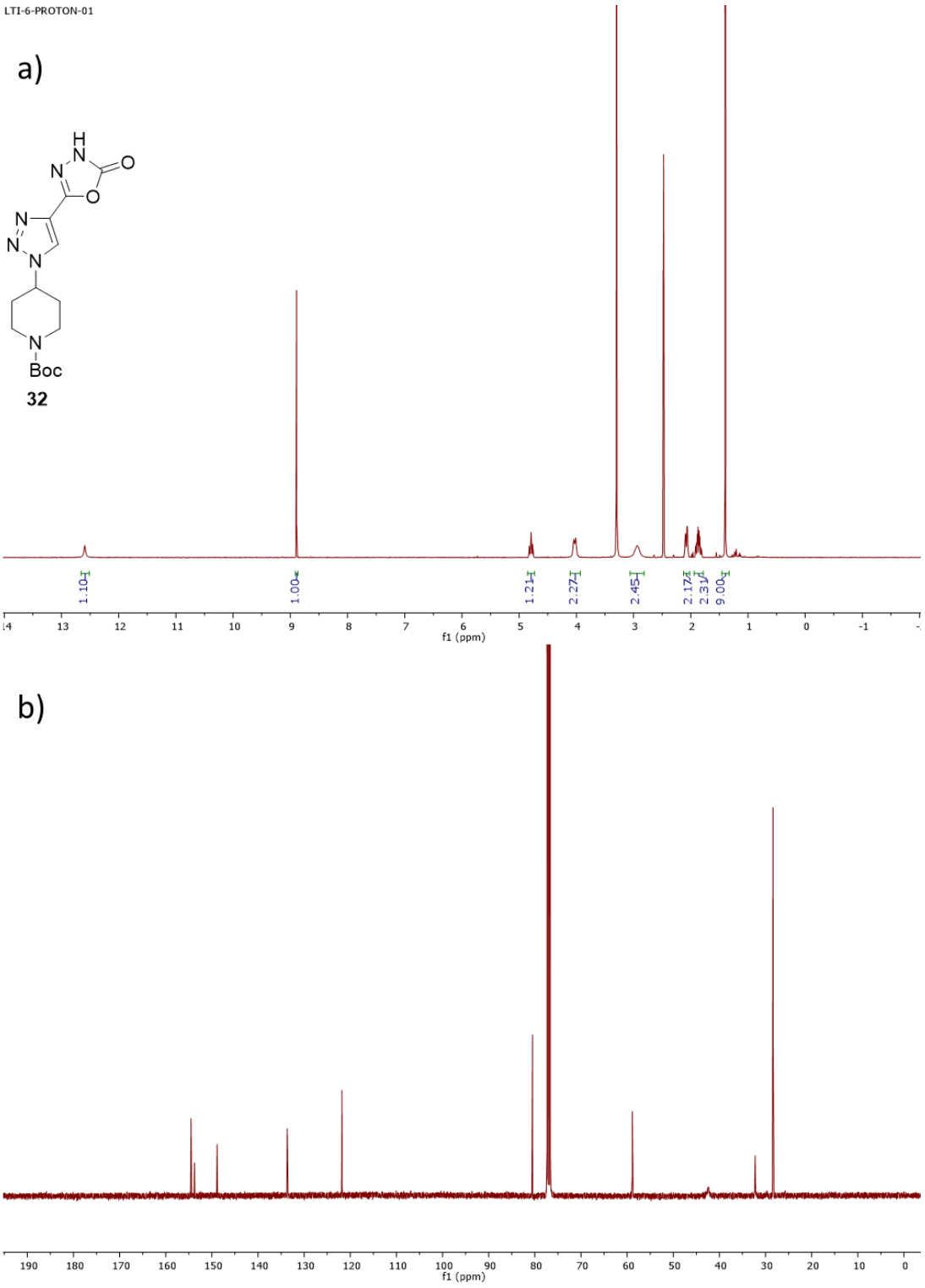

Figure S74. ^{1}H-NMR (a) and ^{13}C-NMR (b) spectra of **32** in d_6-DMSO.

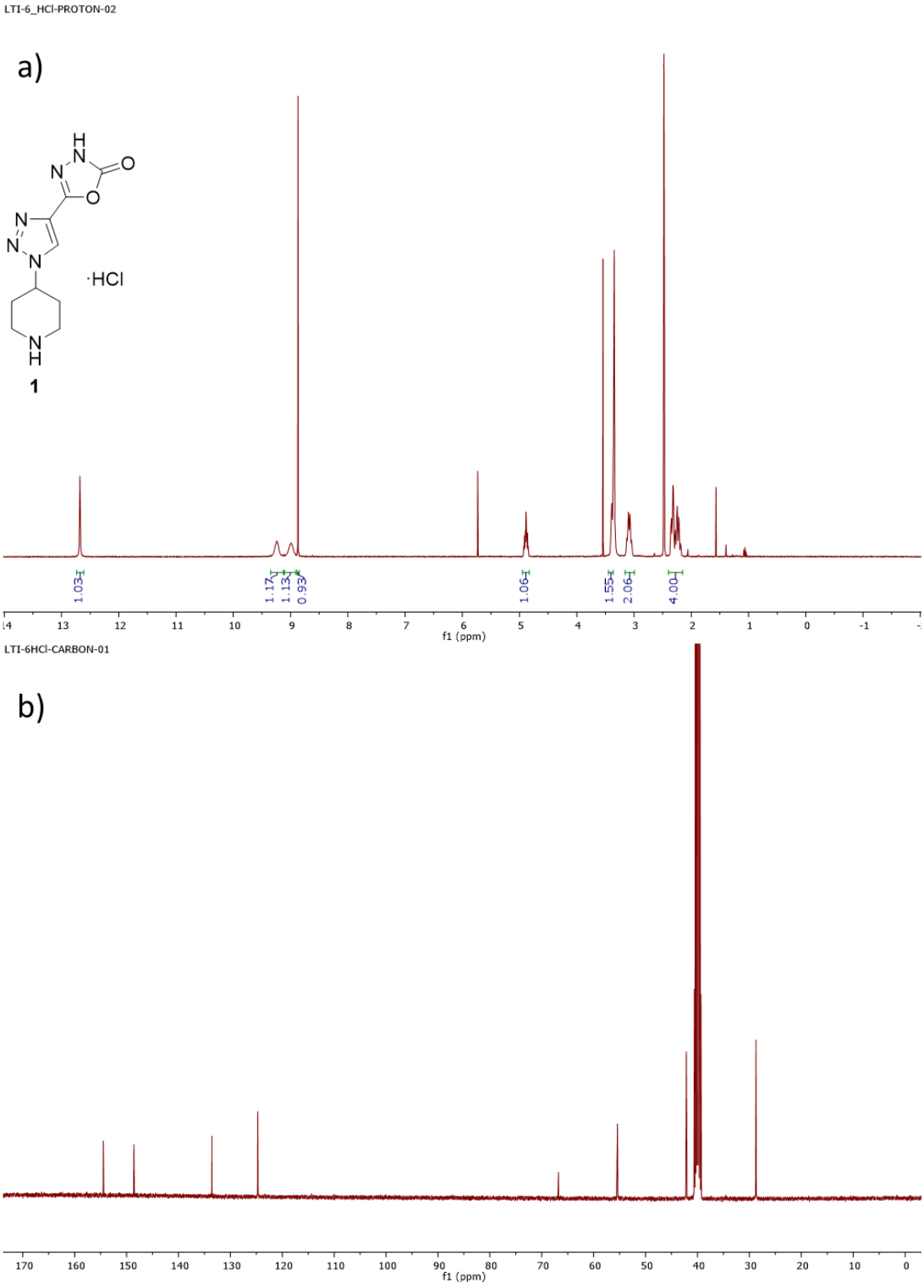

Figure S75. ^{1}H-NMR (a) and ^{13}C-NMR (b) spectra of **1** in d_6-DMSO.

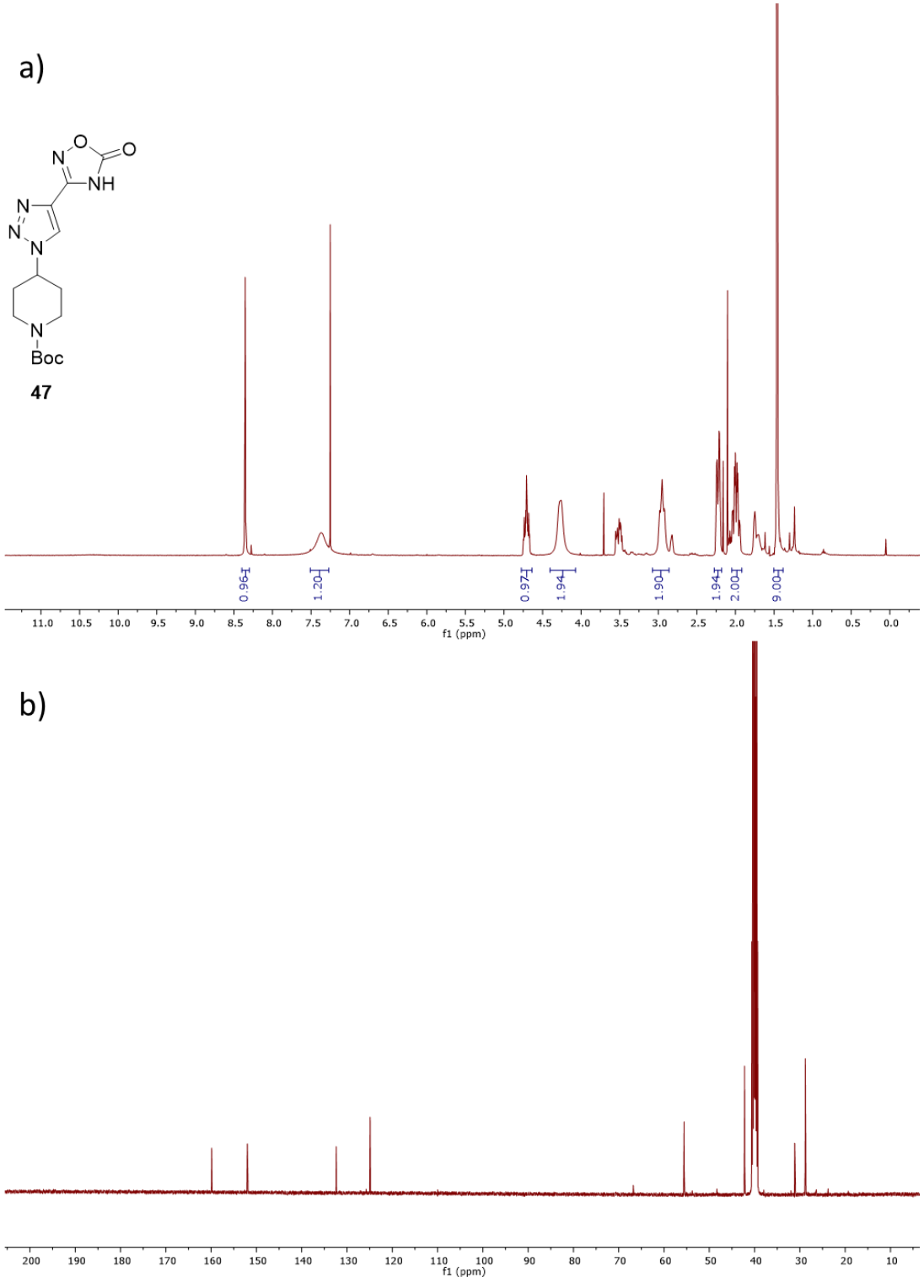

Figure S76. ^{1}H-NMR (a) and ^{13}C-NMR (b) spectra of **47** in d_6-DMSO.

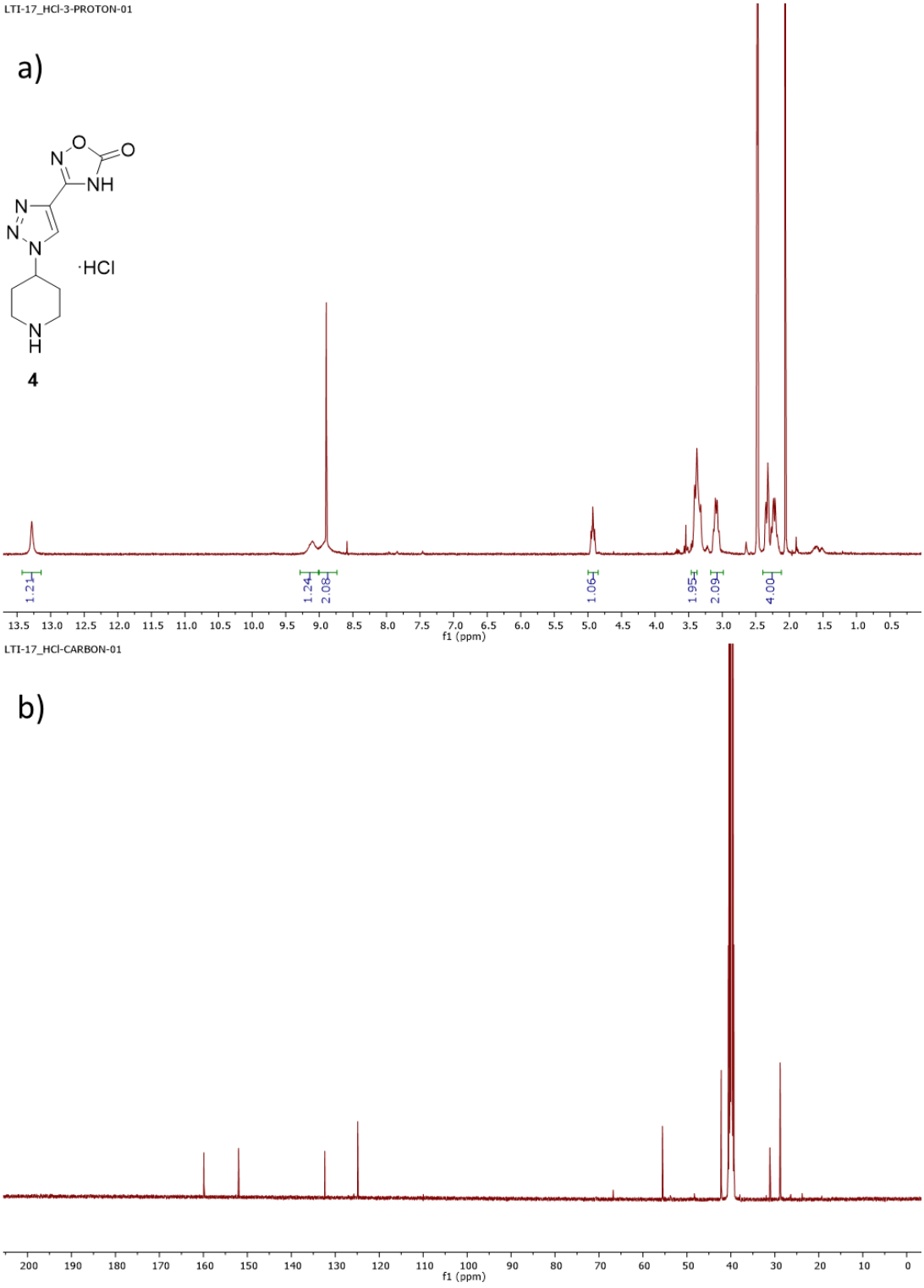

Figure S77. ^{1}H-NMR (a) and ^{13}C-NMR (b) spectra of **4** in d_6-DMSO.

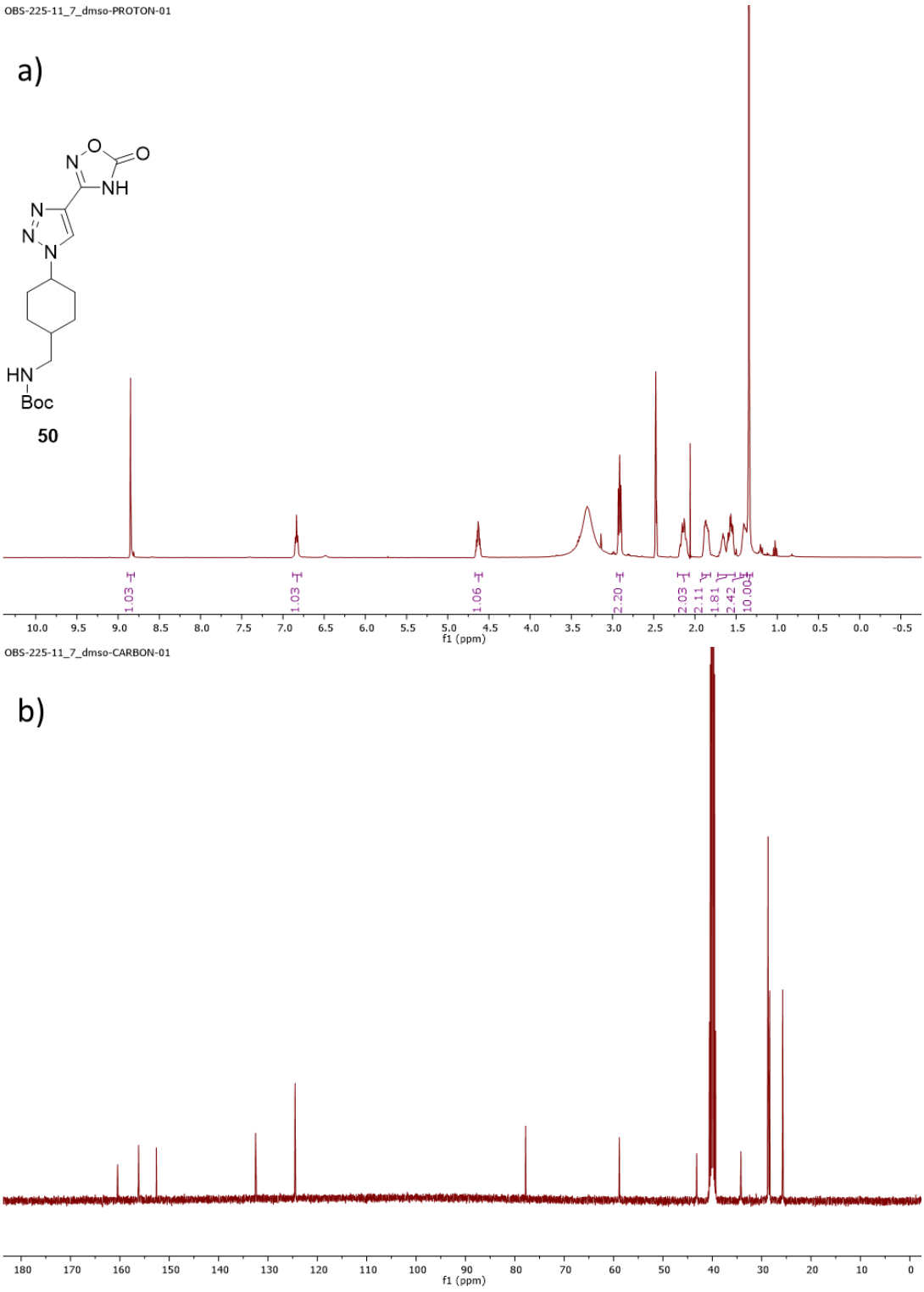

Figure S78. ^{1}H-NMR (a) and ^{13}C-NMR (b) spectra of **50** in d_6-DMSO.

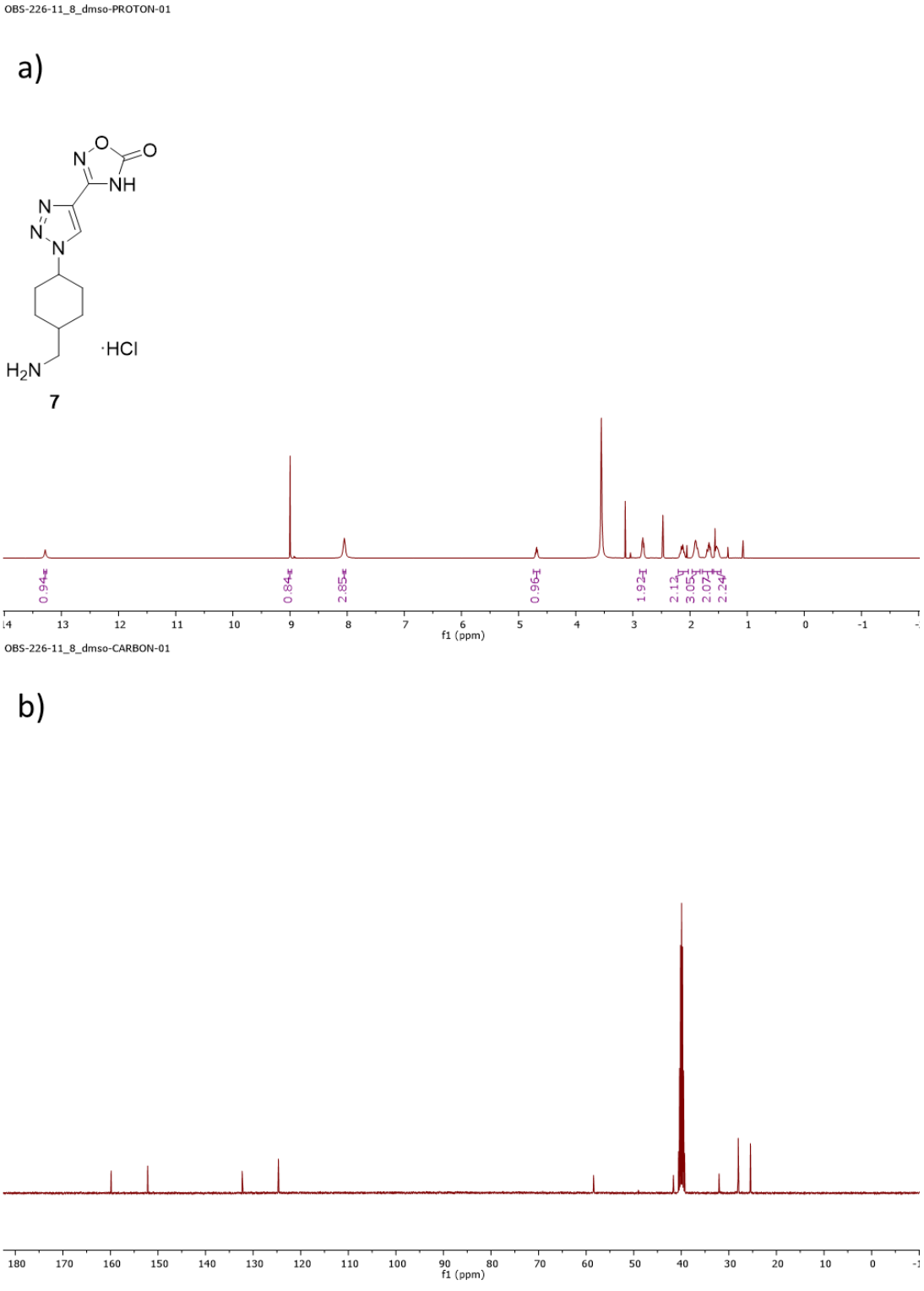

Figure S79. ^{1}H-NMR (a) and ^{13}C-NMR (b) spectra of **7** in d_6-DMSO.

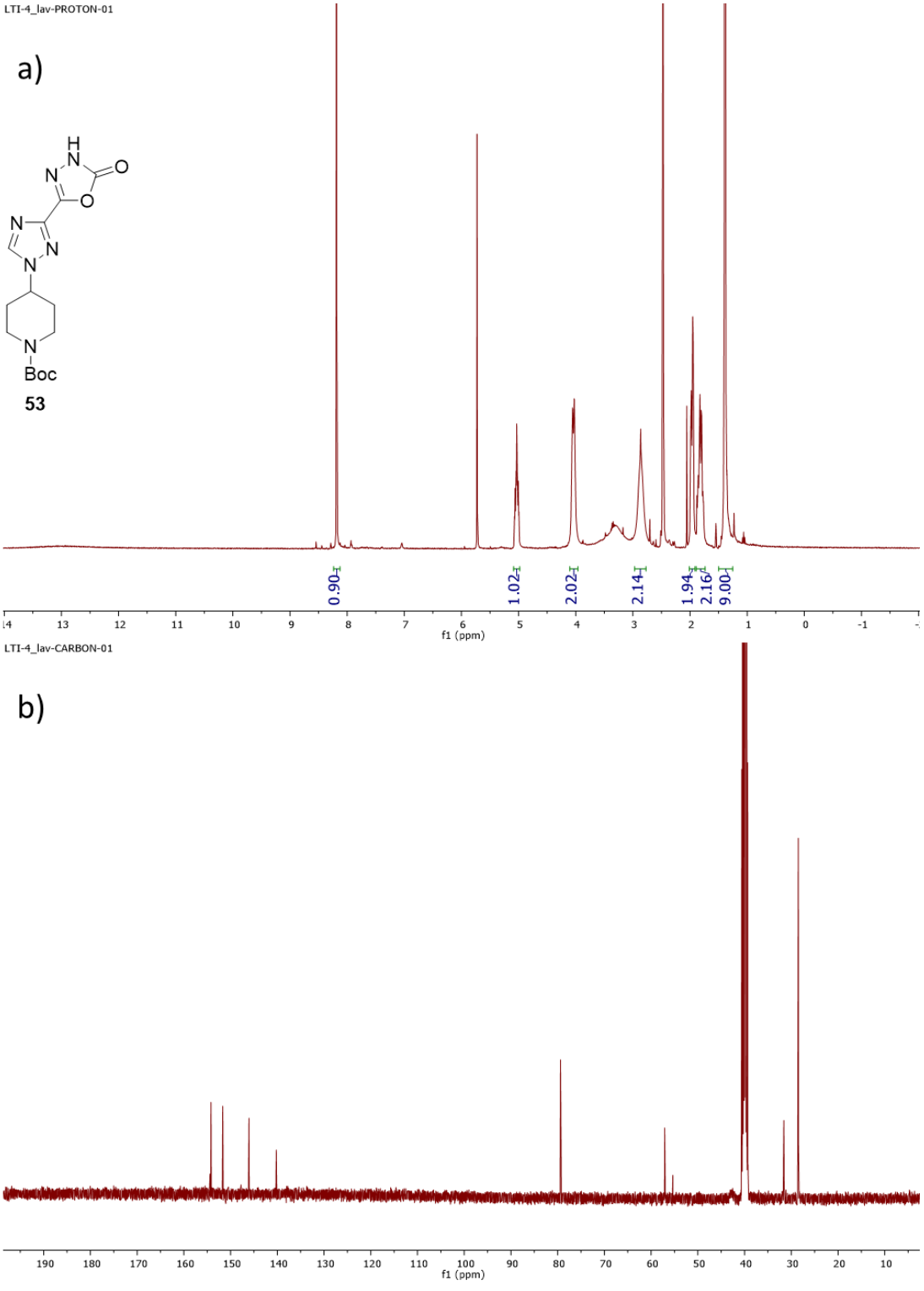

Figure S80. ^{1}H-NMR (a) and ^{13}C-NMR (b) spectra of **53** in d_6-DMSO.

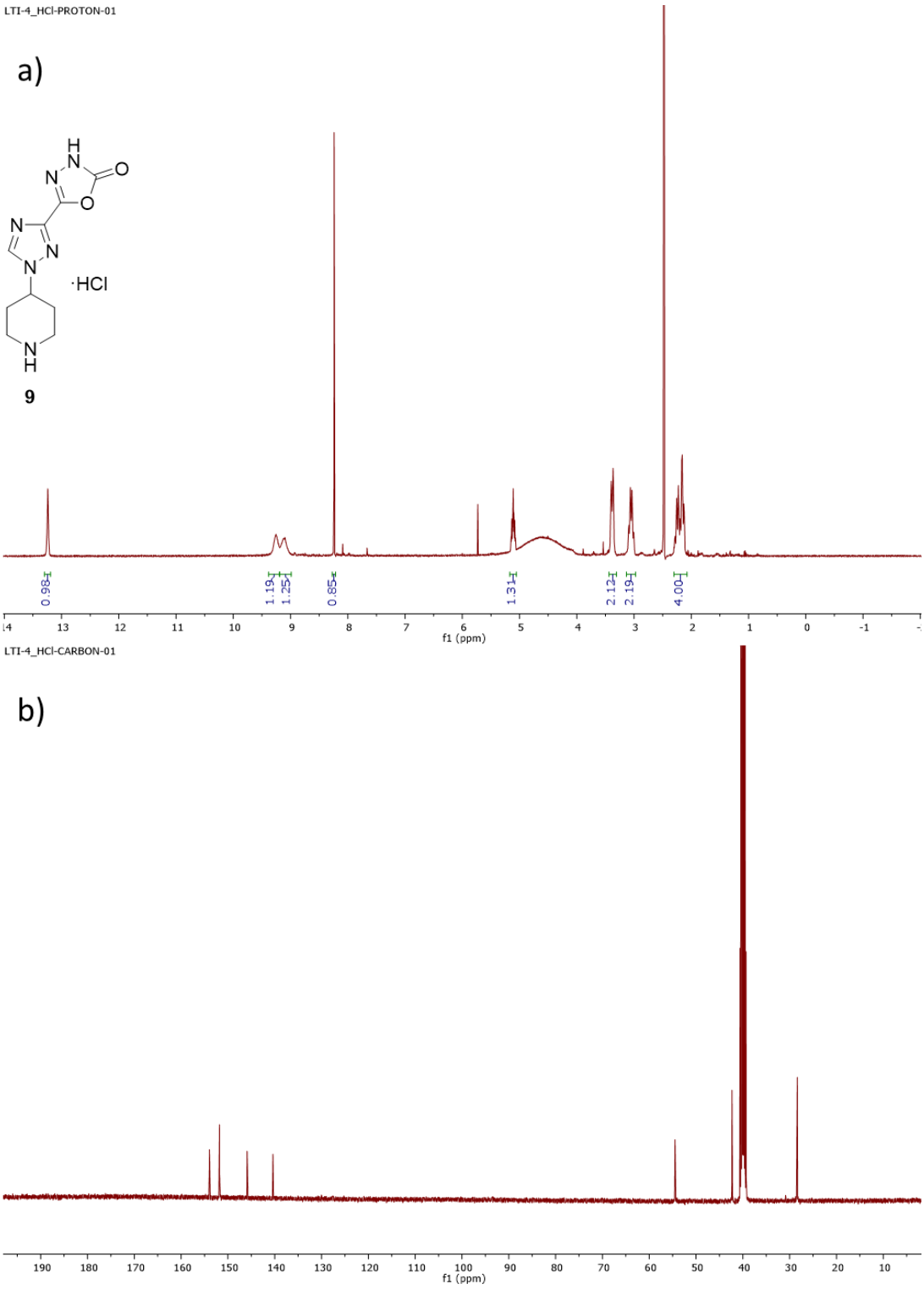

Figure S81. ^{1}H-NMR (a) and ^{13}C-NMR (b) spectra of **9** in d_6-DMSO.

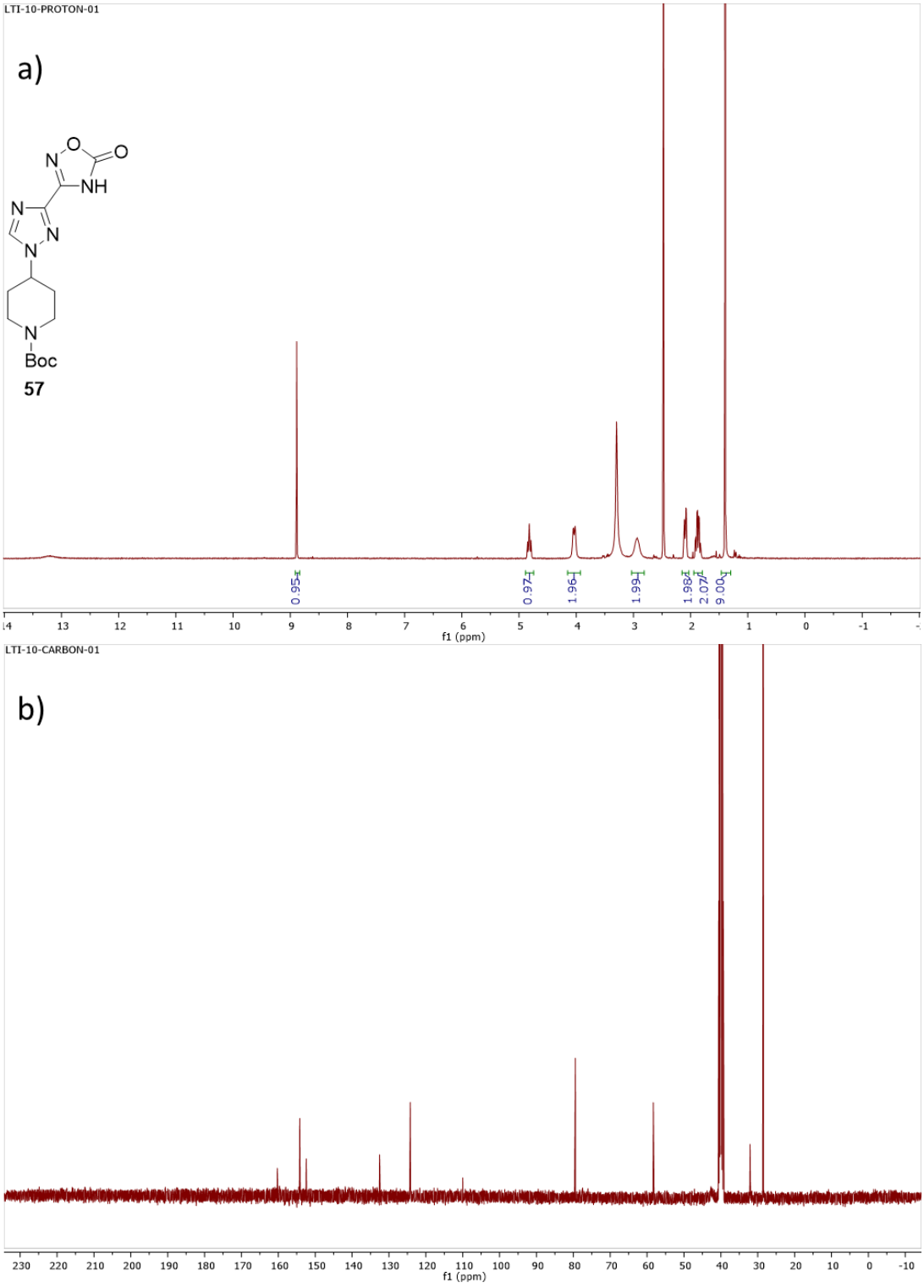

Figure S82. ^{1}H-NMR (a) and ^{13}C-NMR (b) spectra of **57** in d_6-DMSO.

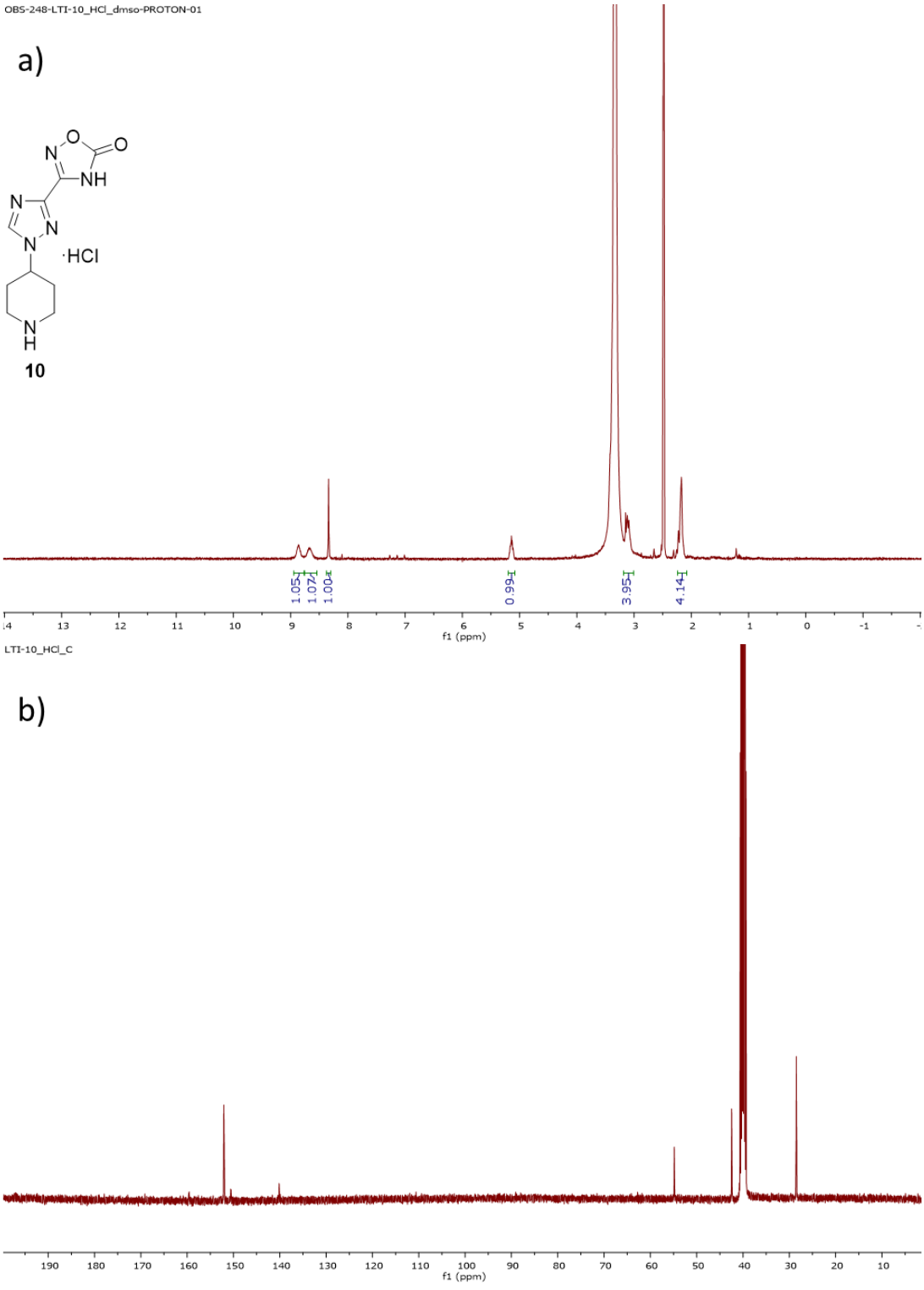

Figure S83. ^{1}H-NMR (a) and ^{13}C-NMR (b) spectra of **10** in d_6-DMSO.

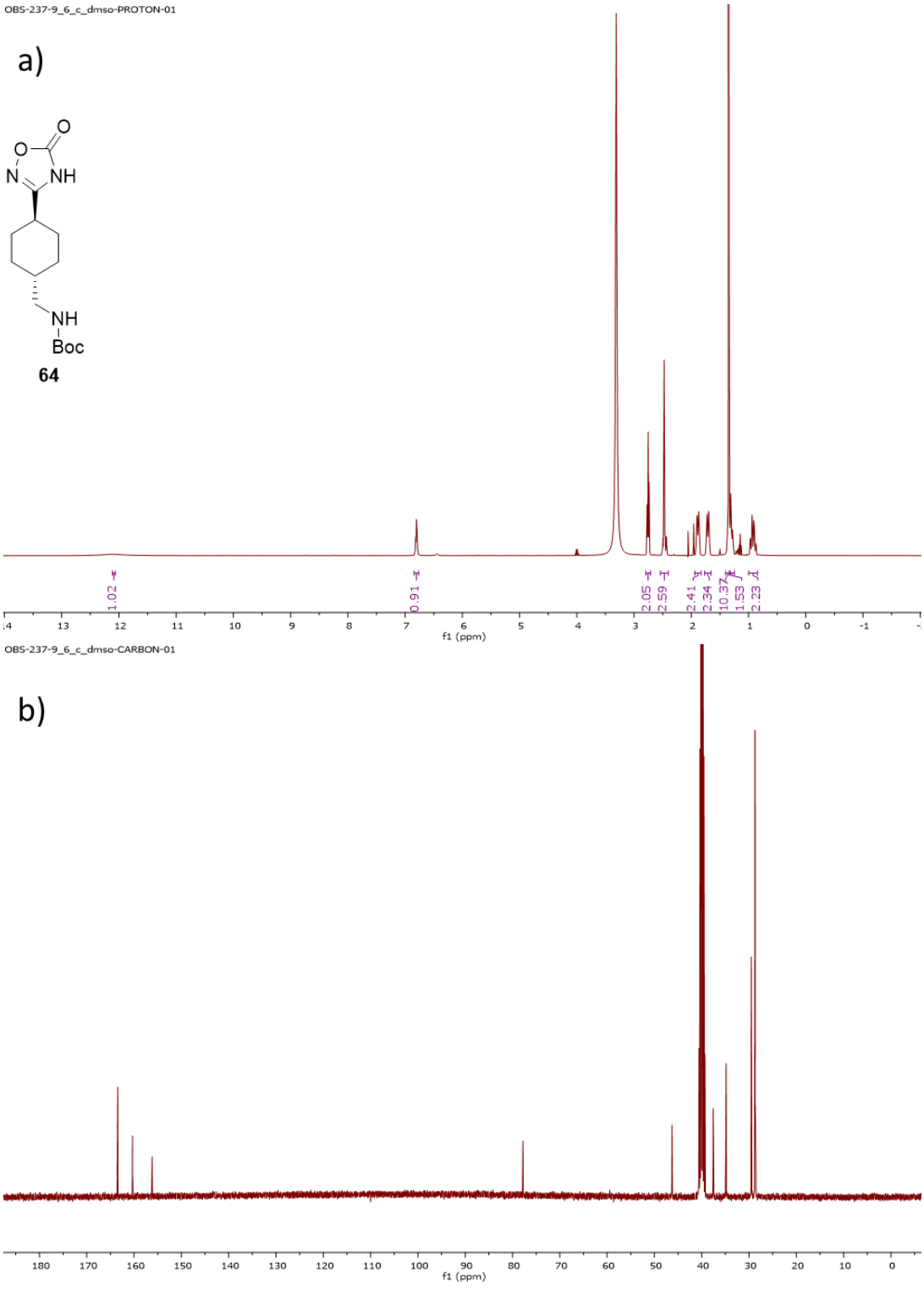

Figure S84. ^{1}H-NMR (a) and ^{13}C-NMR (b) spectra of **64** in d_6-DMSO.

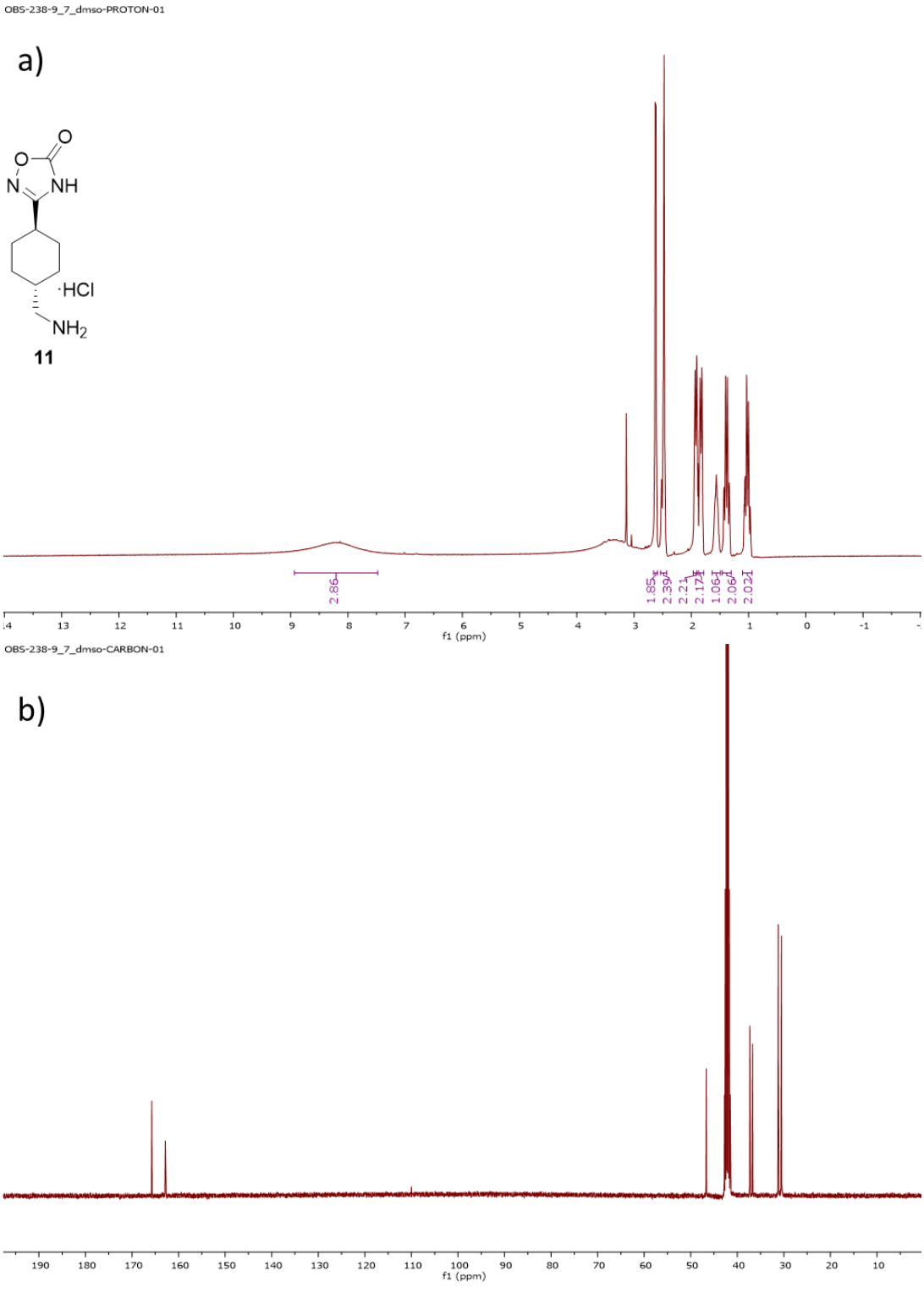

Figure S85. ^{1}H-NMR (a) and ^{13}C-NMR (b) spectra of **11** in d_6-DMSO.

Publications and conference abstracts

Publications

Bosch-Sanz, O.; Rabadà, Y.; Biarnés, X.; Pedreño, J.; Caveda, L.; Balcells, M.; Martorell, J.; Sánchez-García, D. 1,2,3-Triazole Derivatives as Novel Antifibrinolytic Drugs. Int. J. Mol. Sci. 2022, 23, 14942.

Conference abstracts

The 2nd Molecules Medicinal Chemistry Symposium. Barcelona, May 2019. Sanz, O.B.; Palasí, N.B.; Fontal, X.B.; Camps, M.B.; López, J.M.; Egea, F.J.P.; García, D.S. 1,2,3-triazole-oxazolidinone Derivatives as Inhibitors of the Plasminogen System.